

**Optical and thermal characterization of
dye intercalated montmorillonites and
rare earth doped materials**

Lyjo K. Joseph

International School of Photonics
Cochin University of Science and Technology
Kochi- 682022, Kerala, India

Ph. D. Thesis submitted to
Cochin University of Science and Technology
in partial fulfillment of the requirements for the
Degree of Doctor of Philosophy

November 2009

**Optical and thermal characterization of dye intercalated montmorillonites
and rare earth doped materials**

Ph. D. Thesis in the field of Photonics

Author:

Lyjo K. Joseph

Research Fellow, International School of Photonics

Cochin University of Science and Technology

Kochi – 682 022, India

Email: lyjokjoseph@yahoo.co.in, lyjok.joseph@gmail.com

Research Advisors:

Dr. P Radhakrishnan

Professor, International School of Photonics

Cochin University of Science and Technology

Kochi – 682 022, India

Email: radhak@cusat.ac.in

Dr. V P N Nampoori

Professor, International School of Photonics

Cochin University of Science and Technology

Kochi – 682 022, India

Email: vpnnampoori@cusat.ac.in

International School of Photonics,

Cochin University of Science and Technology

Kochi – 682 022, India

URL: www.photonics.cusat.edu

November 2009.

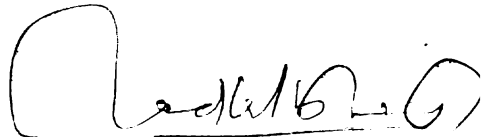
Cover design: Manu Balakrishnan

CERTIFICATE

Certified that the work presented in the thesis entitled “**Optical and thermal characterization of dye intercalated montmorillonites and rare earth doped materials**” is based on the original work done by Mr. Lyjo K Joseph under my guidance and supervision at the International School of Photonics, Cochin University of Science and Technology, Kochi-22, India and has not been included in any other thesis submitted previously for the award of any degree.

Kochi – 682022

20th November 2009.



Prof. P. Radhakrishnan

(Supervising Guide)

DECLARATION

Certified that the work presented in the thesis entitled “**Optical and thermal characterization of dye intercalated montmorillonites and rare earth doped materials**” is based on the original work done by me under the guidance of Dr. P Radhakrishnan, Professor, International School of Photonics, Cochin University of Science and Technology, Kochi-22, India and the co-guidance of Dr. V P N Nampoori, Professor, International School of Photonics, Cochin University of Science and Technology, Kochi-22, India and it has not been included in any other thesis submitted previously for the award of any degree.

Kochi – 682 022

20th November 2009.



Lyjo K Joseph

Contents

Acknowledgements	xix
General remarks regarding the thesis	xx
Preface	xxi
List of publications	xxv
List of abbreviations	xxix
Chapter 1: Materials, Methods and Measurements- An Overview	1
Abstract	1
1.1. Section I –Materials	3
1.1.1. Part A: Clay minerals	3
A1. Introduction	3
A2. Clay mineral properties	3
A3. Structures and mineralogy of clay minerals	5
A3.1. Tetrahedral sheet	5
A3.2. Octahedral sheet	6
A3.3. Subdivision of layer lattice silicates	7
A4. Montmorillonite	9
A5. Clay-water interactions	11
1.1.2. Part B: Dyes	12
B1. Introduction	12
B2. Methylene blue	12
B3. Malachite green	12
B4. Rhodamine B	13
B5. Auramine O	13
B6. Concluding remarks	14
1.1.3. Part C: Dye intercalated clay minerals	15
C1. Introduction	15
C2. Organisation of molecules at clay mineral surfaces	15
C3. Dye aggregation in clay dispersions	16
1.1.4. Part D: Rare earth doped materials	18

Contents

D1. Rare earth elements	18
D2. Optical properties of rare earth ions	19
D3. General properties of lanthanides	19
D3.1. Lanthanide contraction	19
D3.2. Radiative transitions in rare earth ions	20
D3.3. Magnetism of lanthanides	23
D3.4. Non-radiative transitions in rare earth ions	23
D4. Applications of rare earth elements	24
D5. Rare earth titanates	24
D6. Rare earth doped glasses	25
1.2. Section II –Methods	26
1.2.1. Part A: Self propagated high temperature synthesis (SHS)	26
E1. Introduction	26
E2. Advanced ceramics	26
E3. Basics of reactions	27
E4. Advantages	29
E5. Features	30
E6. Drawback	31
E7. Applications	31
1.2.2. Part B: Sol gel	31
F1. Introduction	31
F2. Sol and gel	32
F3. The silicon alkoxide sol gel process	32
F4. Advantages of sol gel synthesis	32
F5. Limitations of sol gel synthesis	33
F6. Silica sol gels- Reaction mechanisms and chemical control of reactions	34
F6.1. Hydrolysis- Acid and base catalysis	34
F6.2. Condensation	35
F6.3. Gelation	36
F6.4. Ageing	36
F6.4.1. Significance of ageing	37
F6.5. Drying	38
F6.5.1. Consequences of drying	38
F6.5.2. Avoiding cracks	38

F6.6. Densification	38
F7. Additives for structuring and processing	39
F7.1. Drying and control additives	39
F8. Entrapment of functional materials- Efficiency of entrapment	40
F9. The characterization of sol gel materials	40
F10. Application of sol gel silicates	40
1.2.3. Part C: Photothermal phenomena	42
G1. Introduction	42
G2. Photothermal detection and applications	44
H. Photoacoustics	45
H1. Introduction	45
H2. Photothermal spectroscopy	46
H2.1. Photoacoustic spectroscopy	47
H2.2. Principle of photoacoustic spectroscopy	47
H3. Historical perspective	49
H4. Instrumentation aspects of photoacoustics	50
H4.1. The light source	50
H4.2. Modulation techniques	50
H4.3. Detection schemes	51
H4.4. Signal processing	51
H5. Advantages of photoacoustics	51
H6. Limitations of photoacoustics	53
H7. Applications of photoacoustics	53
I. Rosencwaig- Gersho (RG) theory	54
I1. Introduction	54
I2. The thermal diffusion equations	55
I3. Temperature distribution in the cell	57
I4. Production of the acoustic signal	58
I5. Special cases	59
I6. Importance of RG theory	61
J. Photothermal deflection (PTD)	61
J1. Introduction	61
J2. Limitations	62

Contents

J3. Advantages	62
K. Thermal property determination by photothermal techniques	62
K1. Introduction	62
K2. Thermal diffusivity (TD)	63
K3. Thermal effusivity (TE)	64
1.2.4. Part D: Fluorescence and absorption	65
L1. Introduction	65
L2. Absorption spectroscopy	65
L3. Fluorescence	65
L4. Fluorescence excitation spectroscopy	66
L5. Laser induced fluorescence (LIF)	66
1.3. Section III –Measurements	67
1.3.1. Part A: Light sources	67
M1. Argon ion laser	67
M2. Pulsed Nd: YAG laser	67
M3. Xenon arc lamp	67
M4. Mode-locked Ti: sapphire laser	67
M5. Diode pumped solid state (DPSS) laser	68
M6. He- Ne laser	68
1.3.2. Part B: Photoacoustic cell (PAC)	68
N1. Introduction	68
N2. Standard photoacoustic cell	68
N3. Designing aspects of photoacoustic cell	68
N4. Photoacoustic cell design	69
1.3.3. Part C: Measuring instruments	71
O1. Spectrophotometer	71
O1.1. Specifications	71
O1.2. Reflectance measurement	71
O2. Fluorescence spectrophotometer	71
O3. Monochromator	72
O4. Monochromator CCD assembly	72
O5. Chopper	72

O6. Lock- in amplifier	73
O7. Preamplifier	73
O8. Micrometer	73
1.4. Scope of the thesis	73
1.5. References	74
Chapter 2: Thermal and optical characterization of dye intercalated montmorillonites	93
Abstract	93
2.1. Prologue	95
2.2. Sample details	96
2.2.1. Commercial clay samples: KSF and K-10	96
2.2.2. Sample preparation- Dye adsorption from solution	96
2.3. Dye molecular aggregates –Molecular exciton coupling theory	96
2.3.1. The exciton model	97
2.3.2. Angle of slippage (α)	98
2.3.3. H and J aggregates	98
2.4. Section I - Thermal characterization of dye intercalated montmorillonites using photoacoustics	101
2.4.1. Preamble	101
2.4.2. Thermal diffusivity measurement - photoacoustic theory	102
2.4.3. Experimental setup	103
2.4.4. Sample details	103
2.4.5. Part A: Thermal diffusivity dependence on host montmorillonite	104
A1. Introduction	104
A2. Materials and methods	104
A2.1. Sample details	104
A2.2. Reflectance spectra measurement	104
A2.3. Specific surface area and porosity measurement	105
A2.4. TG/DTA measurement	105
A3. Results and discussions	105
A3.1. Optical reflectance study	105
A3.2. Photoacoustic study	106

Contents

A3.3. Effect of pore volume on thermal diffusivity	108
A3.4. Effect of repeated adsorption on K-10	109
A3.5. Pore volume effect on the thermal diffusivity of dye adsorbed KSF	110
A3.6. Effect of repeated adsorption on KSF	110
A3.7. Thermal diffusivity of methylene blue adsorbed K-10 and KSF – A comparison	111
A4. Conclusions	111
2.4.6. Part B: Thermal diffusivity dependence on sintering temperature	111
B1. Introduction	111
B2. Experimental details	112
B3. Sample details	112
B4. Results and discussion	112
B4.1. Samples sintered at 300 °C	112
B4.2. TGA analysis of methylene blue intercalated K-10	113
B4.3. Samples sintered at 500 °C	113
B5. Conclusions	114
2.4.7. Part C: Thermal diffusivity dependence on dye	114
C1. Introduction	114
C2. Experimental setup	114
C3. Sample details	114
C4. Results and discussions	115
C4.1. Absorption studies on dye intercalated samples	115
C4.2. Photoacoustic study	117
C4.3. Anomalous behaviour of repeatedly adsorbed MG-X sample	119
C4.4. Thermal diffusivity of rhodamine B intercalated K-10 samples	120
C4.5. Ultrasonicated dye adsorbed sample	120
C4.5.1. Sample preparation	120
C4.5.2. Thermal diffusivity of the sample	121
C5. Conclusions	121

2.5. Section II - Spectroscopic studies of dye intercalated	
K-10 montmorillonite aqueous dispersions	122
2.5.1. Preamble	122
2.5.2. Dispersions of dye intercalated montmorillonite	123
2.5.3. Optical characterization	123
2.5.4. Part A: Rhodamine B intercalated K-10	123
D1. Introduction	123
D2. Experimental- Materials and methods	124
D2.1. Dye adsorption from solution	124
D2.2. Ultrasonicated dye adsorption	124
D3. Results	124
D3.1. Optical absorption studies	124
D3.2. Fluorescence studies	125
D4. Discussions	128
D4.1. Optical absorption studies	128
D4.2. Fluorescence studies	129
D5. Conclusions	130
2.5.5. Part B: Malachite green intercalated K-10	131
E1. Introduction	131
E2. Dispersions of malachite green intercalated K-10 montmorillonite	131
E3. Results	131
E3.1. Optical absorption studies	131
E3.2. Fluorescence studies	132
E4. Discussions	133
E5. Conclusions	134
2.5.6. Part C: Dispersions of KSF and K-10	134
F1. Introduction	134
F2. Materials and methods	135
F3. Results and discussions	135
F3.1. Optical absorption studies	135
F3.2. Fluorescence studies	135
F4. Conclusions	136
2.6. Summary	136
2.7. References	137

Chapter 3: Photoluminescence and photothermal studies on rare earth titanates prepared by self propagating high temperature synthesis method	151
Abstract	151
3.1. Prologue	153
3.2. Sample preparation	154
3.3. Experimental details	155
3.3.1. Instrumental	155
3.3.2. XRD and SEM measurements	156
3.4. Section I- Optical studies of rare earth titanates	158
3.4.1. Part A: Photoluminescence (PL) studies	158
A1. Laser induced fluorescence (LIF)	159
A2. Experimental details	160
A3. Results and discussions	160
A3.1. $\text{La}_2\text{Ti}_2\text{O}_7$	161
A3.2. $\text{Gd}_2\text{Ti}_2\text{O}_7$	162
A3.3. $\text{Nd}_2\text{Ti}_2\text{O}_7$	163
A3.4. $\text{Pr}_2\text{Ti}_2\text{O}_7$	164
A3.5. $\text{Dy}_2\text{Ti}_2\text{O}_7$	165
A3.6. $\text{Sm}_2\text{Ti}_2\text{O}_7$	166
A3.7. $\text{Y}_2\text{Ti}_2\text{O}_7$	167
A4. Conclusions	168
3.4.2. Part B: Photoacoustic spectroscopy (PAS)	168
B1. Experimental setup	169
B2. Results and discussions	169
B3. Conclusions	172
3.4.3. Part C: Frequency up-conversion studies on lanthanum titanate	172
C1. Experimental setup	173
C2. Results and discussions	173
C3. Conclusions	174
3.5. Section II- Photothermal studies of rare earth titanates	175
3.5.1. Part A: Thermal characterization using photothermal deflection	175

D1. Theory	176
D2. Experimental	178
D3. Results and discussions	179
D4. Conclusions	181
3.5.2. Part B: Photoacoustic thermal characterization – Fractal approach	181
E1. Theoretical background	182
E2. Experimental setup	182
E3. Results and discussions	183
E4. Conclusions	185
3.5.3. Part C: Thermal effusivity measurement using photoacoustics	185
F1. Theory	185
F2. Experimental setup	186
F3. Results and discussions	186
F4. Conclusions	187
3.6. Summary	187
3.7. References	188
Chapter 4: Optical and thermal characterization of rare earth doped sol gel silica glasses	197
Abstract	197
4.1. Prologue	199
4.2. Theoretical background	203
4.2.1. Crystalline field theory of rare earth ions	204
4.2.2. Weak crystalline field	204
4.3. Rare earth doped sol gel glasses- preparation	205
4.3.1. General trends	205
4.3.2. Sample preparation details	208
4.4. Section I- Optical studies	209
4.4.1. Preamble	209
4.4.2. Energy level diagram of the rare earth ions	209
4.4.3. Absorption studies	210
4.4.4. Excitation and emission studies	211

Contents

4.4.5. Results and discussions	212
4.4.5.1. La ³⁺ and Y ³⁺	213
4.4.5.2. Yb ³⁺	214
4.4.5.3. Tb ³⁺	214
4.4.5.4. Er ³⁺	215
4.4.5.5. Nd ³⁺	215
4.4.5.6. Dy ³⁺	215
4.4.6. Concluding remarks	216
4.5. Section II- Thermal characterization using photoacoustics	216
4.5.1. Preamble	216
4.5.2. Part A: Thermal effusivity (TE) measurement	217
4.5.2.1. Experimental	217
4.5.2.2. Results and discussions	217
4.5.3. Part B: Thermal diffusivity (TD) of erbium doped glasses	220
4.5.3.1. Experimental	220
4.5.3.2. Results and discussions	220
4.5.4. Conclusions	224
4.6. Summary	224
4.7. References	224
Chapter 5: Conclusions and future prospects in a nutshell	231
5.1. Major findings	231
5.2. Scenario for future	232
5.2.1. Dye intercalated clay minerals	232
5.2.2. Sol gel	233
5.2.3. Rare earth doped materials	233

Dedicated to
My parents and the Almighty God

Remembering my teachers

Late Dr. G V Vijayagovindan
(School of Pure and Applied Physics, M G University, Kottayam),

Late Smt. Susan John K
(Physics Department, Baselius College, Kottayam),
& Late H G Markose Mor Coorilose Metropolitan

Acknowledgements

First of all, I would like to express my sincere gratitude to my research supervisors Dr. P Radhakrishnan, Professor, ISP and Dr V P N Nampoori, the Director of ISP for their guidance, suggestions and support given to me in completing the thesis. Their timely help and motivation are also remembered.

I also thank Dr V M Nandakumaran and Dr C P Girijavallabhan for their constant support. Thanks to all other teachers of both ISP and CELOS.

I am grateful to Dr Sanjay G and Dr Suja H of Department of Applied Chemistry, CUSAT for providing me dye intercalated montmorillonite samples and to the suggestions regarding the experimental results.

Dr K R Dayas, Director, C-MET, Thrissur is also thanked for providing me rare earth titanates and giving me necessary ideas for interpreting the experimental results.

I am obliged to my colleagues and friends, especially Sudeesh, Thomas, Linesh, Murali, Bindu and Annieta for helping me with my experimental works and to Sajan, Sriram, Tamilarasan, Sheeba, Prabhath and Sajeev for providing me the necessary reference papers. The encouragement given by all my teachers and friends, particularly my batch-mates Litty and Dann are also remembered.

I also acknowledge UGC for financial assistance and CELOS for providing experimental facilities. Thanks to all staff of ISP and CELOS and to Murali, Gopi and Joshi of Instrumentation department.

Finally, I express my happiness to my parents and relatives for their support throughout my research. Thanks to my cousin Anju for proof reading. Last, but most important of all, I thank ***Almighty God***

Lyjo K Joseph

General remarks regarding the thesis:

The author has taken reasonable care in the preparation of the thesis. All the available information regarding the references is given including doi and URL. However, certain publishers do not have these options and hence the reader may find some references without doi and URL. Some publishers are providing articles without page numbers. In such cases the article number and the number of pages are specified. A list of abbreviations is also given at the beginning of the thesis for better readability. The division of the chapters is based on the materials used for the studies.

Lyjo K Joseph
(Author)

Preface

The photoacoustic (PA) effect was first reported by Alexander Graham Bell in 1880. Up to 1970s the applications of PA were limited and after the development of the Rosencwaig-Gersho theory, numerous inventions and detection schemes were evolved in this field. This has led to consider PA spectroscopy as one of the great rediscoveries of modern science. It is one of the classes of the photothermal phenomena in which the photothermal heating effect is detected by an indirect acoustic method. Photothermal science encompasses a wide range of non-destructive techniques and phenomena based on the conversion of absorbed optical energy into heat. It is an effective research and analytical tool for the characterization of matter in different states. The characteristics of the thermal waves generated in the sample are simply controlled by the frequency of the light source modulator. In PA, the temperature changes in the samples are monitored using a PA cell which uses a sensitive microphone. The net photothermal effect depends on both the optical and the thermal properties of the materials under investigation. As the photothermal methods monitor the non-radiative path, several material properties which are difficult to measure using the conventional spectroscopic methods can be investigated. Laser induced non-destructive PA and photothermal deflection (PTD) techniques are two common methods used for the evaluation of material parameters because of its simplicity and versatility. These methods are intrinsically non-contact in nature. The PTD approach allows point by point scanning of the sample surface and the characterization of anisotropy in thermo-physical properties of the specimens under investigation. In the thesis, the non-destructive and versatile nature of the photothermal experiments have been exploited for the characterization of the materials.

The development of more complex materials necessitates a finer characterization of their physical properties and a better knowledge of the physical phenomena that determine their behaviour at the macroscopic level. Nano-composite materials, which contain organic dyes incorporated in a solid matrix, are used in various applications, such as optical sensors, devices for photo-induced switching, solid state lasers and in memory media. Clay minerals are very attractive matrices for the intercalation of dye molecules. Aqueous dispersions of swelling clay minerals are known for their colloidal and rheological properties and have several industrial applications. The increasing interest in dye/ inorganic nano-composites is focused on changes in optical and thermal properties during adsorption and / or intercalation of the dye in an inorganic matrix. Various dye-clay systems offer an interesting area of research, and

spectroscopic techniques have been successfully used to study such systems. Montmorillonites are used as a very convenient host structure for the intercalation of organic dyes. In this thesis, non-destructive PA and optical spectroscopic techniques have been effectively utilised to characterise the dye intercalated montmorillonites.

The rare-earth doped laser crystals, glasses and ceramics, which possess trivalent rare-earth ions, are popular solid state gain media. Rare-earth based phosphors play a critical and indispensable role as luminescent materials in the display industry. Synthesis of high quality rare earth based phosphor materials is thus important. Rare earth titanates ($R_2Ti_2O_7$) (RET) have interesting dielectric, piezoelectric and ferroelectric properties. Pyrochlore RETs and zirconates find numerous applications such as hosts for fluorescence centres, high temperature pigments, catalysts, thermal barrier coatings, ionic/ electronic conductors, host phase in nuclear waste control etc.

The advent of high optical quality transparent nano-structured glasses, the so-called transparent glass ceramics or vitroceraamics disclosed the possibility of producing nano-sized photonic devices based on rare-earth doped up-converters. Transparent glass ceramics have been investigated as hosts for lanthanide ions envisioning the production of materials that are easy to shape and with high performance for photonic applications. Rare earth doped glasses have been extensively studied due to their potential applications in optical devices such as solid state lasers and optical fibers. Various photothermal and optical techniques have been successfully applied for the thermal and optical characterization of these rare earth doped materials.

In the present thesis, the effective thermal parameters like thermal diffusivity and thermal effusivity of complex materials for various applications have been investigated using photothermal methods along with their optical characterization utilising the common optical absorption as well as fluorescence spectroscopic techniques. These sensitive optical procedures are also essential for exploiting these materials for further photonic applications.

Chapter 1 gives an overview of the materials, methods and measurement techniques used in the present study. This chapter of introductory nature is divided into three sections. The first section includes the fundamental details of different materials used in the present research work. The details of the clay minerals, especially montmorillonites and dye aggregation in clay mineral dispersions are given. The

fundamentals of rare-earths and the rare-earth doped materials are also given in this section.

Second section discusses the various methods used for the characterization and preparation of these materials. The basics of the photothermal phenomena, particularly PA and PTD are presented with a detailed description of the Rosencwaig Gersho theory. The salient features of the combustion synthesis and sol-gel techniques are also given in this section.

The last section explains the basic details of the light sources and measuring instruments used for characterising the samples. Moreover, the important features of the PA cell used for the present investigation are also given in this section.

Chapter 2 deals with the thermal and optical characterization of dye intercalated montmorillonites. The first section of the chapter presents thermal diffusivity measurement on dye intercalated commercial K-10 and KSF montmorillonites carried out by PA technique. Methylene blue adsorbed K-10 samples show distinct thermal diffusivity changes when compared to the ordered KSF samples. PA method is carried out to determine thermal diffusivity of some industrially important dyes as well; such as auramine O, malachite green and rhodamine B adsorbed by K-10 montmorillonites. The repeatedly adsorbed methylene blue and auramine O samples show a lesser thermal diffusivity than the single adsorbed samples. The sintered methylene blue adsorbed samples show a higher thermal diffusivity though they exhibit a similar trend as un-sintered pellets.

The optical absorption and fluorescence studies on rhodamine B and malachite green intercalated acid activated K-10 montmorillonite dispersions prepared from the dried dye intercalated montmorillonite are presented in the second section. The absorption and fluorescence peaks of rhodamine B dispersions show a bathochromic shift with respect to the dye concentrations due to the formation of J-aggregates. The samples have a fluorescence emission at 421 nm which is having an intensity variation depending on the concentration of the dyes. The behaviour of rhodamine B samples of same concentration prepared by two different routes is also presented. Similar studies conducted on pure K-10 and KSF dispersions are also described.

Chapter 3 includes the photoluminescence and photothermal studies on RETs prepared by self propagating high temperature synthesis or combustion synthesis

method. The laser induced luminescence studies of the RETs ($R_2Ti_2O_7$, $R=La, Pr, Nd, Sm, Gd, Dy$ and Y) using 355 nm radiation from an Nd: YAG laser are presented. Some of these samples with submicron or nanometre size are prepared by the combustion synthesis method and there is no known fluorescence shown by these rare earths in the visible region. Hence, the luminescence transitions shown by the $La_2Ti_2O_7$ near 610 nm are interesting to notice. Though La^{3+} ions with no 4f electrons have no electronic energy levels that can induce excitation and luminescence processes in the visible region, the presence of the Ti^{3+} ions leads to luminescence. The PA spectra of these samples are also given. Frequency up-conversion study on $La_2Ti_2O_7$ is also conducted using femto second Ti: sapphire laser output at 810 nm.

In the second section, the approximate thermal diffusivity values of these RETs are obtained using PTD studies and an attempt is made to describe the possible fractal nature of the samples. Thermal effusivity values of these samples are also obtained using the PA method.

Chapter 4 is based on the characterization of rare earth doped sol-gel glasses. Rare earth (Y, La, Dy, Nd, Tb, Er and Yb) doped silica glasses are prepared by sol gel technique with various weight percentage of the rare earth in the silica matrix. The glasses are sintered at three different temperatures (500, 600 and 700 °C) and their optical absorption and fluorescence spectra are obtained. These glasses also show a luminescent behaviour near 421 nm similar to that of the dye intercalated montmorillonites. PA method is used for the thermal characterization of these glasses.

The summary and conclusions based on the present work are given in the **Chapter 5**. A brief report on the future prospects and possibility of the continuation of the present work are also included in this chapter.

List of publications:

(a) In international journals:

1. "Photoluminescence studies on rare earth titanates prepared by self propagating high temperature synthesis method" *Lyjo K Joseph*, K R Dayas, Soniya Damodar, Bindu Krishnan, K Krishnankutty, V P N Nampoori and P Radhakrishnan; *Spectrochimica Acta Part A: Molecular and Biomolecular Spectroscopy*. **71 (4)**, 1281-1285 (2008). doi:10.1016/j.saa.2008.03.030
2. "Thermal characterization of methylene blue intercalated montmorillonites by photoacoustic technique" *Lyjo K Joseph*, H Suja, G Sanjay, S Sugunan, V P N Nampoori and P Radhakrishnan; *Applied Clay Science*. **42 (3-4)**, 483-487 (2009). doi:10.1016/j.clay.2008.06.006
3. "Thermal characterization of dye intercalated K-10 montmorillonite ceramics using photoacoustic technique" *Lyjo K Joseph*, Sanjay G, Suja H, Sugunan S, Nampoori V P N and Radhakrishnan P; *Philosophical Magazine*. **89 (10)**, 895-905 (2009). doi: 10.1080/14786430902806652
URL: <http://www.informaworld.com/10.1080/14786430902806652>
4. "Photoacoustic Study on the Photostability of Polymethyl methacrylate (PMMA) films doped with Rhodamine 6G-Rhodamine B dye mixture system" Annieta Philip K, *Lyjo K Joseph*, Litty Mathew Irimpan, P Radhakrishnan and V P N Nampoori; *J. Phys. D: Appl. Phys.* **38 (6)**, 2904-2909 (2005). doi:10.1088/0022-3727/38/16/024
5. "Thermal Characterization of Ceramic Tapes using Photoacoustic Effect" Annieta Philip K, *Lyjo K Joseph*, Litty M Irimpan, Bindu Krishnan, P Radhakrishnan, V P N Nampoori and Raghu Natarajan ; *Phys. Stat. Sol. (A)* **204 (3)**, 737-744 (2007). doi: 10.1002/pssa.200622287 URL: <http://dx.doi.org/10.1002/pssa.200622287>
6. "Thermal Diffusivity Measurements of Dental Resin using Photoacoustic Effect" N Smijesh, *Lyjo K Joseph*, Achamma Kurian and V P N Nampoori; *IEEE Preceedings of International Conference on Intelligent & Advanced Systems 2007 (ICIAS 2007)* 25 - 28 November 2007 Kuala Lumpur, Malaysia. P 311-314. doi: 10.1109/ICIAS.2007.4658397

(b) International seminar/ conference presentations

1. "Excitation wavelength dependent fluorescence behaviour of CdS nanoparticles" Mathew S, Litty Mathew Irimpan, John Thomas, **Lyjo K Joseph**, M N Muralidharan, V P N Nampoori and C P G Vallabhan. *Ninth International Conference on Optoelectronics, Fiber Optics and Photonics, Photonics 2008*, New Delhi, 13-17 December 2008 .
2. "Thermal Diffusivity Measurements of Dental Resin using Photoacoustic Effect" N Smijesh, **Lyjo K Joseph**, Achamma Kurian and V P N Nampoori. *International Conference on Intelligent & Advanced Systems 2007 (ICIAS 2007)* 25 - 28 November 2007 Kuala Lumpur, Malaysia. P 311-314.
doi: 10.1109/ICIAS.2007.4658397
3. "Nonlinear Optical properties of Nd Doped Silica Glasses using Z-scan Technique" **Lyjo K Joseph**, Ritty J Nedumpara, K J Thomas, V P N Nampoori and P Radhakrishnan. *Proceedings of Eighth International Conference on Optoelectronics, Fiber Optics and Photonics, Photonics 2006*, Hyderabad, 13-16 December, NLO 15
4. "Thermal Diffusivity Measurements of Dental Resin Using Photoacoustic Effect" N Smijesh, **Lyjo K Joseph**, Achamma Kurian and V P N Nampoori. *Proceedings of Eighth International Conference on Optoelectronics, Fiber Optics and Photonics, Photonics 2006*, Hyderabad, 13-16 December, PMD 49.
5. "Photothermal Deflection and Photoacoustic Studies of Rare earth Titanates" **Lyjo K Joseph**, K R Dayas, Soniya Damodar, Bindu Krishnan, Ritty J Nedumpara, K Krishnankutty, P Radhakrishnan and V P N Nampoori. *Proceedings of International Conference on Optics & Optoelectronics ICOL-2005*. 12-15 December 2005, Dehradun PP-OMSD-23
6. "Testing the Purity of Gold using Photoacoustic Technique" P P Saratchandran, **Lyjo K Joseph** and P Radhakrishnan; *Proceedings of International Conference on Optics & Optoelectronics ICOL-2005*. 12-15 December 2005, Dehradun PP-OMSD-24
7. "Photosensitivity of Laser Dye Mixtures in Polymer Matrix. A Photoacoustic Study" Annieta Philip K, **Lyjo K. Joseph**, Litty Irimpan, P Radhakrishnan and V P N Nampoori. *Photonics 2004 (Seventh International conference on Optoelectronics, Fiber optics and Photonics)*, Kochi, India, December 9-11, (2004).

(c) National seminar/ conference presentations

1. "Thermal characterization of $Ba_3DyTa_3O_{12}$ ceramic by photoacoustic technique" S P Sithara, **Lyjo K Joseph**, J Linesh, B Nithyaja, P Radhakrishnan and V P N Nampoore. Eighth DAE-BRNS National Laser Symposium (NLS-08), New Delhi, 7-10 January 2009. P11-016.
2. "Study of colour change in *Hibiscus mutabilis*" Jemy James, **Lyjo K Joseph**, C M Sreekanth and V P N Nampoore. Contemporary optics and optoelectronics (Ed. P P Sahu and P Deb) *Proceedings of the XXXIII Optical Society of India (OSI) Symposium 2007*. 18-20 December 2007, Tezpur (Tata McGraw-Hill, New Delhi, 2008) 82-4.
3. "Thermal characterization of dye doped clay based ceramics using photoacoustic effect" **Lyjo K Joseph**, Suja H, Sanjay G, Asha P, Sugunan S, V P N Nampoore and P Radhakrishnan. *Seventh DAE-BRNS National Laser Symposium (NLS-2007)* 17-20 December 2007, Vadodara 143-4.
4. "Studies on the time dependence on nonlinear optical properties of deoxyribonucleic acid (DNA) using z-scan technique" B Nithyaja, V K Jayasree, **Lyjo K Joseph** and V P N Nampoore. *Seventh DAE-BRNS National Laser Symposium (NLS-2007)* 17-20 December 2007, Vadodara 437-8.
5. "Thermal characterization of methylene blue doped clay based ceramics using photoacoustic effect" **Lyjo K Joseph**, Suja H, Sanjay G, Asha P, Sugunan S, V P N Nampoore and P Radhakrishnan. *National conference on New Horizons in Theoretical and Experimental Physics (NHTEP-2007)* October 8-10, 2007, Kochi OP.9 20-22
6. "Thermal Diffusivity Measurements of Dental Resin using Photoacoustic Effect" N Smijesh, **Lyjo K Joseph**, Achamma Kurian and V P N Nampoore. *Proceedings of National Conference on Current Trends in Materials Science (CTMS 07)*. 25-27 March 2007, Chengannur, Kerala. H1 217-9
7. "Photoacoustic Study of Rare Earth Double Titanates" K R Dayas, Bindu Krishnan, N P Prasanth, **Lyjo K Joseph** and K Krishnankutty. *Progress on tunable lasers for ultrafast processes and applications (PTLUPA6)* December 21-22, 2006, Chennai
8. "Non-destructively Testing the Purity of Gold using Photoacoustic Technique" P P Saratchandran, **Lyjo K Joseph** and P Radhakrishnan. *Proceedings of National Seminar on Nondestructive Testing and Evaluation (NDE-2005)*. Kolkata, 2-4 December 2005.
9. "Photoacoustic Studies of Dysprosium Titanate Prepared by SHS Method" **Lyjo K Joseph**, K R Dayas, Soniya Damodar, Bindu Krishnan, K Krishnankutty, P

Publications

Radhakrishnan and V P N Nampoorei. *Proceedings of DAE- BRNS NLS-5*. 358-9(2005) Vellore, 7-10 December 2005.

10. “Fluorescence Study of Lanthanum Titanate” **Lyjo K Joseph**, Litty Mathew Irimpan, Dann V J, Radhakrishnan P and V P N Nampoorei. *Proceedings of DAE- BRNS NLS-5*. 181-2(2005) Vellore, 7-10 December 2005.

11. “Concentration Dependent Photostability of Dye Doped Polymer Films – A PA Study” Annieta Philip K, **Lyjo K Joseph**, Litty M Irimpan, P Radhakrishnan and V P N Nampoorei. *National Laser Symposium (NLS-2005)*, BARC, Mumbai, January 10-13 (2005).

12. “Measurement of Thermal Diffusivity of Thin film Brass Sample using Photothermal Deflection” **Lyjo K Joseph**, T P Shiji, P Radhakrishnan and V P N Nampoorei. *National Laser Symposium (NLS-2005)*, BARC, Mumbai, January 10-13 (2005).

13. “Thermal Characterization of Zirconia and Alumina-Zirconia Ceramic Tapes Using Photoacoustic Technique” Annieta Philip K, **Lyjo K Joseph**, Litty M Irimpan, Bindu Krishnan, P Radhakrishnan, V P N Nampoorei and Raghu Natarajan. *National Laser Symposium (NLS-2005)*, BARC, Mumbai, January 10-13 (2005).

14. “Thermal diffusivity measurement using photothermal technique- Fractal approach” **Lyjo K Joseph**, K R Dayas, J Linesh, V P N Nampoorei and P Radhakrishnan. *National Laser Symposium (NLS-09)*, BARC, Mumbai, January 13-16 (2010). (Communicated)

15. “Frequency up-conversion studies on lanthanum titanate” **Lyjo K Joseph**, K J Thomas, K R Dayas, V P N Nampoorei and P Radhakrishnan. *National Laser Symposium (NLS-09)*, BARC, Mumbai, January 13-16 (2010). (Communicated)

16. “Thermal characterization of rare earth doped sol gel glasses using photoacoustic method” **Lyjo K Joseph**, K Sudeesh, M N Muralidharan, J Linesh, V P N Nampoorei and P Radhakrishnan. *National Laser Symposium (NLS-09)*, BARC, Mumbai, January 13-16 (2010). (Communicated)

List of abbreviations:

AO-	auramine O	PL-	photoluminescence
BET-	Brunauer Emmett Teller	PT-	photothermal
BJH-	Barrett Joyner Halenda	PTD-	photothermal deflection
CCD-	charge coupled device	PV-	pore volume
CEC-	cation exchange capacity	RB-	rhodamine B
DCCA-	drying control chemical additive	RE-	rare earth
DOI-	digital object identifier	RET-	rare earth titanate
DPSS-	diode pumped solid state	RG-	Rosencwaig and Gersho
ICDD-	International Centre for Diffraction Data	SEM-	scanning electron microscope
IR-	infrared	SHS	Self propagated High temperature Synthesis
JCPDS-	Joint Committee on Powder Diffraction Standards.	SI-	le Système international d'unités
KD*P-	potassium dideuterium phosphate	SSA-	specific surface area
LIF	laser induced fluorescence	TC-	thermal conductivity
Ln-	lanthanide	TD-	thermal diffusivity
MB-	methylene blue	TE-	thermal effusivity
MG-	malachite green	TEOS-	tetraethoxy silane
NIR-	near infrared	TGA-	thermo-gravimetric analysis
NMR-	nuclear magnetic resonance	TMOS -	tetramethoxy silane
OPC-	open photoacoustic cell	TPM-	triphenylmethane
PA-	photoacoustic	URL-	uniform resource locator
PAC-	photoacoustic cell	UV-	ultraviolet
PAS-	photoacoustic spectroscopy	VHC-	volumetric heat capacity
		XRD-	X-ray diffraction

Chapter 1

Materials, Methods and Measurements- An Overview

Abstract

This chapter is of introductory nature and is divided into three sections. The first section includes the details of different materials used in the present research work. This consists of the basic features of the clay minerals, dyes and rare earth doped materials such as rare earth titanates and glasses. Second section discusses the various methods used for the preparation and characterization of these materials. The subdivisions of this section contain the fundamentals of self propagated high temperature synthesis, sol gel techniques, and photothermal and fluorescence studies. The last section explains the basic details of the instruments used for characterising the samples. This section gives the particulars of light sources, fluorescence spectrophotometer, spectrophotometer, photoacoustic cell and other measuring instruments. Finally, the scope of the work presented in this thesis is also given.

1.1. Section I –Materials	3
1.1.1. Part A: Clay minerals	3
1.1.2. Part B: Dyes	12
1.1.3. Part C: Dye adsorbed clay minerals	15
1.1.4. Part D: Rare earth doped materials	18
1) Rare earth titanates	24
2) Rare earth doped glasses	25
1.2. Section II- Methods	26
1.2.1. Part A: Self propagated high temperature synthesis	26
1.2.2. Part B: Sol gels	31
1.2.3. Part C: Photothermal phenomena	42
1) Photoacoustic	45
2) Rosencwaig Gersho theory	54
3) Photothermal deflection	61
4) Thermal property determination	62
1.2.4. Part D: Fluorescence and absorption	65
1.3. Section III- Measurements	67
1.3.1. Part A: Light sources	67
1.3.2. Part B: Photoacoustic cell	68
1.3.3. Part C: Measuring instruments	71
1.4. Scope of the thesis	73
1.5. References	74

1.1. Section I –Materials:

1.1.1. Part A: Clay minerals:

A1. Introduction:

Clay has become indispensable to modern living. It is the material of many kinds of ceramics, such as porcelain, bricks and tiles as well as an essential constituent of plastics, paints, paper, rubber, and cosmetics. Clay is non-polluting and can be used as a depolluting agent. Of great importance for the near future is the potential of some clays to be dispersed as nanometre-size unit particles in a polymer phase, forming novel nano-composite materials with superior thermo-mechanical properties.^[1]

Clay is a widely distributed, abundant mineral resource of major industrial importance for an enormous variety of uses.^[2] The term 'clay' is ambiguous and has multiple meanings: a group of fine grained minerals- i.e., the clay minerals; and a type of rock- i.e., a sedimentary deposit of fine grained material usually composed largely of clay minerals.^[3, 4] Clay also includes fine grained deposits of non-alumino-silicates such as shale and some argillaceous soils.^[5]

Clay minerals are a common constituent of hydrothermal deposits and occur abundantly in all types of sediments and sedimentary rocks, perhaps comprise as much as 40% of the minerals. The fine grained clay minerals are built up of tetrahedrally (T) (Si, Al, Fe³⁺) and octahedrally (M) (Al, Fe³⁺, Fe²⁺, Mg) coordinated cations organised to form either sheets or chains. Naturally occurring inexpensive clay materials may be found in all countries and have innumerable uses and applications in our daily life which demand their characterization.^[6]

A2. Clay mineral properties:

All clay minerals are hydrous.^[7] The clay mineral properties are very complex and are dependent on environmental conditions. The complexity arises from the occurrence of different species and properties as well as various modifications of natural clays. Clay minerals are characterised by certain properties,^[11] including

1. A layer structure with one dimension in the nanometre range; the thickness of the 1:1 (TM) layer is about 0.7 nm, and that of the 2:1 (TMT) layer is about 1 nm,
2. The anisotropy of the layers or particles,
3. The existence of several types of surfaces: external basal (planar) and edge surfaces as well as internal (interlayer) surfaces,^[8]

4. The ease with which the external, and often also the internal, surface can be modified (by adsorption, ion exchange, or grafting),
 5. Plasticity, and
 6. Hardening on drying or firing; this applies to most (but not all) of the clay minerals.
- Table 1.1 gives the major differences between the clay and clay minerals.

Table 1.1: Distinction between clay and clay mineral.^[1]

Clay	Clay mineral
Natural	Natural and synthetic
Fine grained (<2 μm or <4 μm)	No size criterion
Phyllosilicates as principal constituents	May include non-phyllosilicates
Plastic ^a	Plastic
Hardens on drying or firing	Hardens on drying or firing

^aWith some exceptions like flint clays.

Clay minerals belong to the phyllosilicates.^[9]The basic structural units in layer silicates are two-dimensional arrays of silicon-oxygen tetrahedra and two-dimensional arrays of aluminium- or magnesium-oxygen-hydroxyl octahedra. The former unit is called the *tetrahedral sheet*^[7](T) or the *silica sheet*.^[9]The *brucite* or *gibbsite* sheets consist of two planes of hydroxyl ions between which lies a plane of magnesium or aluminium ions which is octahedrally coordinated by the hydroxyls. This latter unit is known as the *octahedral sheet* (M). These sheets are combined so that the oxygens at the tips of the tetrahedra project into a plane of hydroxyls in the octahedral sheet and replace two-thirds of the hydroxyls. This combination of sheets forms a layer.^[7]In most clay minerals, such sheets of tetrahedra and of octahedra are superimposed in different fashions.^[9]

The structures of phyllosilicates are all based on a T and a M sheet that may condense in either a 1:1 or 2:1 proportion to form an anisotropic TM or TMT layer. The layers or sheets may be negatively charged (as for the majority of clay minerals), positively charged, or essentially uncharged (as in talc). The layer charge density and the nature of the compensating or charge-balancing cation determine many important surface and colloidal properties. An assembly of layers is a 'particle', and an assembly of particles is an 'aggregate' (Figure 1.1).^[1]All phyllosilicates are therefore porous, containing pores of varied size and shape.^[1]

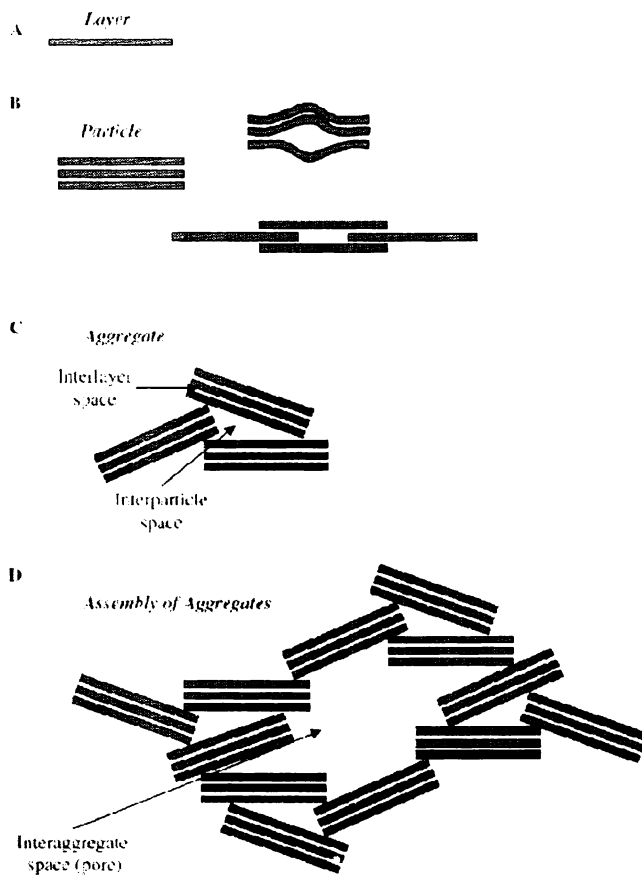


Figure 1.1: Diagram showing (A) a clay mineral layer; (B) a particle, made up of stacked layers; layer translation and deformation can give rise to a lenticular pore; (C) an aggregate, showing an interlayer space and an inter-particle space; and (D) an assembly of aggregates, enclosing an inter-aggregate space (pore).

A3. Structures and mineralogy of clay minerals:^[10]

A3.1. Tetrahedral sheet:

In the *tetrahedral sheet* or the *silica sheet*, the silicon atoms are coordinated with four oxygen atoms. The oxygen atoms are located at the four corners of a regular tetrahedron with the silicon atom in the center. In the sheet, three of the four atoms of each tetrahedron are shared by three neighbouring tetrahedra. The fourth oxygen atom of each tetrahedron is pointed downward. The SiO_4^{2-} tetrahedra connected at three

corners in the same plane form a hexagonal network. All the tips of the tetrahedra point in the same direction.

Each tetrahedron consists of a cation, coordinated to four oxygen atoms, and linked to adjacent tetrahedra by sharing three corners (the basal oxygen atoms, O_b) to form an infinite two-dimensional 'hexagonal' mesh pattern along the a, b crystallographic directions (Figure 1.2).¹¹⁰¹

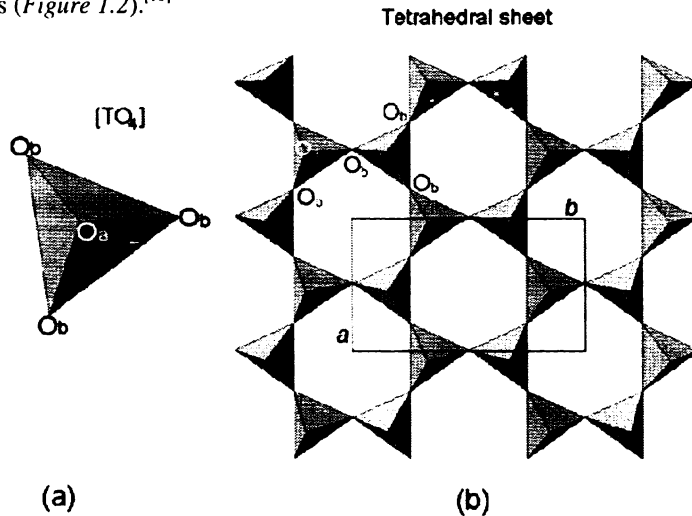


Figure 1.2: (a) Tetrahedron $[TO_4]$; (b) tetrahedral sheet. O_a and O_b refer to apical and basal oxygen atoms, respectively. a and b refer to unit-cell parameters.

A3.2. Octahedral sheet:

In the Al-, Mg-O-OH sheets, the Al or Mg atoms are coordinated with six oxygen atoms or OH groups which are located around the Al or Mg atom with their centers on the six corners of a regular octahedron. The sharing of oxygen atoms by neighbouring octahedrons results in a sheet. The oxygen atoms and hydroxyl groups lie in two parallel planes with Al or Mg atoms between these planes. The oxygen and hydroxyl groups form a hexagonal close packing. This sheet is called the *octahedral sheet*. This is subdivided into *alumina* or *magnesia sheet*, which is also called *gibbsite sheet* or *brucite sheet*, respectively.

In the octahedral sheet, connections between each octahedron to neighbouring octahedra are made by sharing edges. The edge-shared octahedra form sheets of hexagonal or pseudo-hexagonal symmetry (Figure 1.3). Common tetrahedral cations

are Si^{4+} , Al^{3+} , and Fe^{3+} . Octahedral cations are usually Al^{3+} , Fe^{3+} , Mg^{2+} and Fe^{2+} , but other cations, such as Li^+ , Mn^{2+} , Co^{2+} , Ni^{2+} , Cu^{2+} , Zn^{2+} , V^{3+} , Cr^{3+} and Ti^{4+} are also identified. Octahedra show two different topologies related to OH position, i.e., the cis- and the trans-orientation (*Figure 1.3*).^[10]

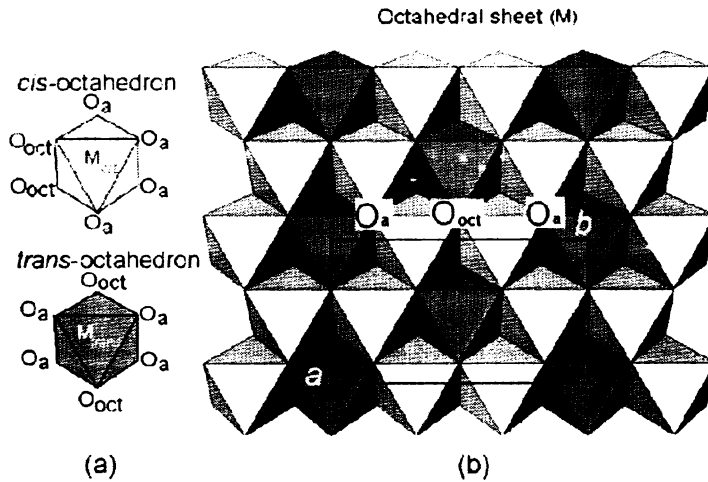


Figure 1.3: (a) O_{oct} (OH, F, Cl) orientation in cis-octahedron and trans-octahedron; (b) location of cis- and trans-sites in the octahedral sheet. O_a and O_b refer to apical and basal oxygen atoms, respectively. a and b refer to unit cell parameters.

A3.3. Subdivision of layer lattice silicates:

The major subdivision of the layer lattice silicates (*Figure 1.4*)^[5] is based on the type of combinations of the tetrahedral and octahedral sheets. Additional subdivision is based on:^[7]

- * whether the octahedral sheet contains two cations per half unit cell (dioctahedral) as in gibbsite or three cations per half unit cell (trioctahedral) as in brucite;
- * the manner of stacking of the tetrahedral-octahedral units upon each other;
- * the amount and type of isomorphous replacement of the cations.

The analogous symmetry and the almost identical dimensions in the tetrahedral and the octahedral sheets allow the sharing of oxygen atoms between these sheets. The fourth oxygen atom protruding from the tetrahedral sheet is shared by the octahedral sheet. This sharing of atoms may occur between one silica and one alumina sheet, as in the so-called 1: 1 *layer minerals*. In the 2: 1 *layer minerals*, one alumina or magnesia sheet shares oxygen atoms with two silica sheets, one on each side. This combination of an octahedral sheet and one or two tetrahedral sheets is called a *layer*.

Most clay minerals consist of such layers, which are stacked parallel to each other.^[9] The cohesive force between the layers is primarily electrostatic, augmented by van der Waals attraction.^[11]

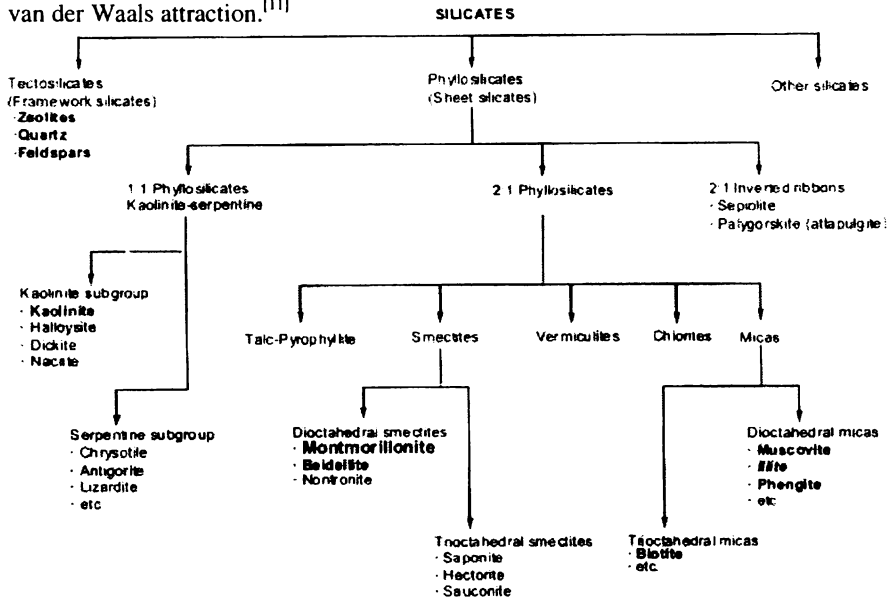


Figure 1.4: Major subdivisions of layered silicates.

The neutral 2: 1 layer structure represents the structure of the mineral *pyrophyllite*. Since in this material two of the three possible octahedral positions are occupied by trivalent Al, this structure is called *dioctahedral*. If the three octahedral positions are filled by three divalent Mg atoms, the electro-neutral structure of the mineral *talc* is represented. This arrangement is called *trioctahedral*.^[9]

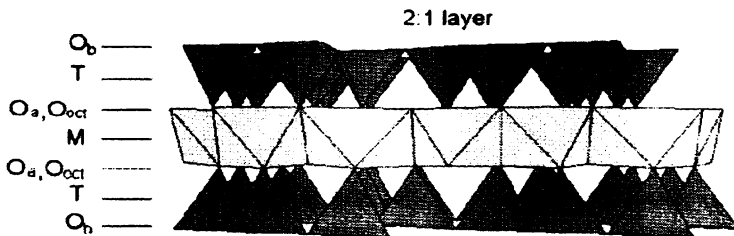


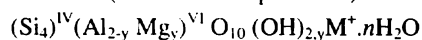
Figure 1.5: Model of a 2:1 layer structure. O_a, O_b, and O_{oct} refer to tetrahedral basal, tetrahedral apical, and octahedral anionic position, respectively. M and T indicate the octahedral and tetrahedral cation, respectively.

The three-sheet or 2: 1 layer lattice silicates (*Figure 1.5*)^[10] consist of an octahedral sheet in between two silica tetrahedral sheets. These three sheets form a layer approximately 10 Å thick. The oxygens, at the tips of the tetrahedral, point towards the center octahedral sheet and substitute for two-thirds of the octahedrally coordinated hydroxyls. The 2: 1 clay minerals include the mica and smectite groups which are by far the most abundant of the clay minerals.

Clay minerals are traditionally classified under 'silicates' but since their chemical compositions have more oxygen than Si, Al, or Mg, these minerals may arguably be considered as (hydr)oxides of silicon, aluminium, or magnesium. Thus clay minerals and related layer materials may be referred to as porous layered (hydr)oxides. Clay minerals may also be considered as salts of rigid polyanions with infinite radius and their compensating cations or as inorganic polymers where the continuous octahedral sheet is based on a repetition of an octahedron monomer. The other basic monomer is the silica tetrahedron, which is bound on one or both sides to the octahedral sheet.^[11]

A4. Montmorillonite:

Montmorillonites belong to the group of layer silicates. The low layer charge (0.3-0.6) dioctahedral minerals which have most of their charge originating in the octahedral sheet are called dioctahedral smectites or montmorillonites. The isomorphous substitution in montmorillonite occurs in the octahedral sheet rather than in the tetrahedral sheet. Most of the montmorillonites were formed by the alteration of volcanic material and basic igneous rocks and have a relatively small amount of Al substituting for Si in the tetrahedral sheet. Montmorillonite species belongs to dioctahedral type smectite group with a layer charge ~0.2-0.6 (Charge per formula unit) and has hydrated exchangeable cations as interlayer material.^[11] The idealised formulae (chemical compositions) of montmorillonite^[11] is



Many people associate clay minerals with smectites, which have the following properties:^[11]

- ✍ particles of colloidal size,
- ✍ high degree of layer stacking disorder,
- ✍ high specific surface area (SSA),
- ✍ moderate layer charge,
- ✍ large cation exchange capacity (CEC) that is little dependent on ambient pH.
- ✍ small pH-dependent anion exchange capacity.

- ✍ variable interlayer separation, depending on ambient humidity,
- ✍ propensity for intercalating^{*} extraneous substances, including organic compounds and macromolecules, and
- ✍ ability of some members to show extensive interlayer swelling in water; under optimum conditions, the layers can completely dissociate.

Montmorillonite is an acid leached clay which is used as an adsorbent for decolourization and deodorization of vegetable and animal oils. Leaching of the clay increases its SSA and the pore volume (PV) to improve its adsorption capacity for metallic impurities, phosphatides, oxidation products and pigmentary substance in oils.^[12-14]The acidity of the montmorillonite clay arises from H^+ in the surface exchange sites.^[15]Acid leaching increases the relative SiO_2 content and as a result the depletion of cations from the interlayers and octahedral sheets of the montmorillonite.^[16]Dissolution of the montmorillonite usually starts by leaching of the octahedral layer from the edge of the particles and the hexagonal cavities.^[17]

Montmorillonites swell in water, and the extent of the swelling is influenced by the hydration of the interlayer cations. The large internal surface area of montmorillonite provides most of the adsorption surface. In addition, the external surface area of montmorillonite is generally greater than that of other clay minerals, due to its small particle size. The most important chemical properties of montmorillonites include high values of CEC, ion selectivity and molecular sorption. The main physical properties of montmorillonites are expansion and collapse, retention of large quantities of water, high cohesion and adhesion, small particle size and an extremely large SSA.^[18]Montmorillonites, activated in acids, yield products with a highly amorphous SiO_2 ^[16] content and a new microstructure with pores that have greater adsorption properties.^[19]Their reactivity is mainly controlled by their large internal SSA, the mean specific charge, and the nature of the interlayer-exchangeable cations.^[20-24]

Clays are used as catalysts and catalyst-supports in many organic syntheses. Montmorillonite is the most important clay mineral for these uses.^[25]Montmorillonites are one of the most commonly used clay mineral in industrial applications.^[1]Montmorillonite remains the most difficult mineral to crystallise in high purity. This may be due, at least in part, to its low magnesium content.^[26]

* 'Intercalation' denotes both interlayer adsorption and interlayer ion exchange reactions.

Montmorillonite are good adsorbents, and may be recommended for the treatment of pesticide poisoning.^{127, 281}

A5. Clay-water interactions:

The chemical and physical properties of clay minerals are integrally linked to some aspect of how water interacts with the clay surface. Many of the interesting features of clay-water interactions are observable at the macroscopic level, including such properties as shrink-swell phenomena, water sorption, plasticity and catalysis.¹²⁹¹

Grandjean and Laszlo¹³⁰¹ deduced from deuterium NMR studies of montmorillonite-water dispersions that the water molecules are strongly polarised and are simultaneously bound to a negative centre by a hydrogen bridge and to an interlayer cation by electrostatic forces. As a consequence, the acidity of interlayer water molecules is increased. An outstanding property of dispersed montmorillonite particles is delamination into individual silicate layers.¹³¹¹

Smectites can sorb up to half of their mass with water and that the water sorption behaviour is strongly dependent on the nature of the exchangeable cation.¹³²¹ Smectites are nano-materials. The elementary platelets are a few tenths to a few hundreds of nanometres wide and long and 0.96-1.50 nm thick, the exact thickness depending on the number of adsorbed water layers. The elementary platelets carry a negative charge, due to isomorphous substitution. The typical negative charge per $O_{10}(OH)_2$ unit is 0.25 - 0.60 e ($e = 1.6 \times 10^{-19}$ C). The corresponding charge-neutralising and exchangeable cations together with one or two water layers are located in the inter-lamellar space between the elementary platelets. A group of elementary platelets forms a clay particle. If such a particle is immersed in water, water molecules are attracted into the inter-lamellar spaces and the clay particle swells. Ultimately, the aqueous clay suspension consists of randomly-oriented, more or less freely moving, elementary clay platelets. The degree of swelling depends on the charge density of the clay mineral, size and shape of the elementary platelets and particles, the type and charge of the exchangeable cation and the chemical and thermal history of the clay mineral sample.¹³³¹

Thus, one can transform a clay particle, consisting of a number of more or less well-oriented elementary platelets, into an aqueous suspension with randomly moving, elementary clay platelets. In this state the charge compensating cations are exchangeable with almost any type of cation, be it inorganic, organic or organo-

metallic.^[34, 35] This property is the basis for the idea that the elementary platelets of smectites can be converted into nano-particles with preset properties. One needs (1) an exchangeable cation with the desired property such as light absorption, light emission, redox, acid or base; (2) a specific organisation of the exchangeable cation at the surface of the elementary clay platelets; (3) the organisation of the elementary platelets into monolayers and multi-layers. This means that a double organisation is necessary: (i) organisation of the molecules at the surface, and (ii) organisation of the elementary platelets, carrying the desired molecules.^[33]

Besides ion exchange, other mechanisms of functionalization of clay mineral particles can be envisaged, such as embedding of the clay mineral particles in a polymer matrix. All these methods can be brought together in the notion of intercalation or intercalation chemistry.^[33, 36, 37]

1.1.2. Part B: Dyes:

B1. Introduction:

Dyes are synthetic aromatic water-soluble dispersible organic colorants, having potential application in various industries. The dyestuff usage has increased day by day due to the tremendous growth of industrialisation and man's urge for colour.^[38] Colour removal from dye bearing waste-water is a complex problem because of the difficulty in treating such waste-waters by conventional treatment methods.^[39, 40]

In this thesis, some of the thermal and optical properties of certain industrially important dye adsorbed montmorillonites are presented which are evaluated using simple non-destructive techniques. The present investigations are carried out using four industrially important dyes; the basic details of which are given below.

B2. Methylene blue:

Methylene blue (MB) is heterocyclic aromatic chemical compound which is used as a stain in bacteriology and as an oxidation-reduction (redox) indicator. It is an antidote to cyanide and an antiseptic in veterinary. It is also known as tetramethylthionine chloride or Swiss blue and the molecular structure of MB is given^[41] in *Figure 1.6*.

B3. Malachite green:

Malachite green (MG) is a toxic chemical, primarily used as a dye. It is a common basic synthetic dyestuff of triphenylmethane or triarylmethane dye^[42] series, which is most widely used for dyeing^[43] silk and wool directly and cotton mordanted with

tannin. MG is inexpensive, effective and readily available for many uses. MG is widely used in aquaculture as a parasiticide and in food, health, textile and other industries for one or the other purposes.^[42] When diluted, it can be used as a topical antiseptic or to treat parasites, fungal infections, and bacterial infections in fish and fish eggs. It is also used as a bacteriological stain. MG is also called aniline green, benzaldehyde green, china green, diamond green B, or victoria green B. The molecular structure of MG is given in *Figure 1.7*.

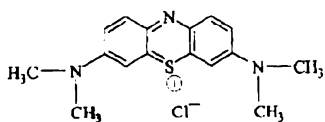


Figure 1.6: Molecular structure of methylene blue.

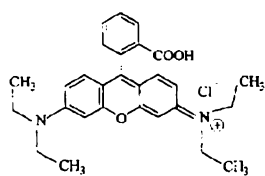


Figure 1.8: Molecular structure of rhodamine B.

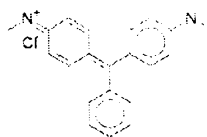


Figure 1.7: Molecular structure of malachite green.

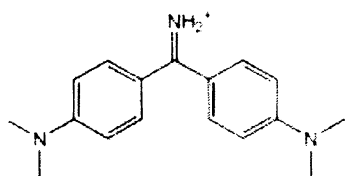


Figure 1.9: Molecular structure of auramine O.

B4. Rhodamine B:

Rhodamine B (RB) is a fluorescent tracer dye which is also widely used in many industries. RB is used as a dye laser gain medium. It is a biological stain and a suspected carcinogen. RB is also known as FD and C Red No. 19; Rhodamine O;^[44] Tetraethylrhodamine; Rheonine B; Brilliant Pink B; Basic Rose Red;^[45] Geranium lake N; Symulex Pink F; Rhodamine 610;^[46] Pigment Violet 1 etc.^[44-46] The properties of RB are given^[47] in *Table 1.2*. *Figure 1.8* shows the molecular structure of RB.

B5. Auramine O:

Auramine O (AO) is a yellow fluorescent dye used to stain acid-fast bacteria in sputum or in paraffin sections of infected tissue and as an antiseptic agent. It can also be used as a fluorescent version of Schiff reagent.^[48] AO fluorescence can be used as a probe for the survey of the physical parameters of chromatophore membranes.^[49] AO is also called Pyocatanium aureum; aizen auramine; Pyoktanin Yellow; Canary Yellow;

Auramine hydrochloride; Benzophenoncidum etc.^[48, 50] Molecular structure of AO is given in *Figure 1.9*.

B6. Concluding remarks:

All the dyes used for the present study are basic dyes. Basic dyes are salts of the coloured organic bases containing amino and imino groups. Basic dyes are cationic which has positive electrical charge and are used for anionic fabrics which are negative-charge-bearing, such as wool, silk, nylon, and acrylics where bright dyeing is the prime consideration. The main characteristics of the dyes used in the present investigation are given in *Table 1.2*.

Table 1.2: Characteristics of the selected dyes for the adsorption study.

Dye →	MB ^[51]	MG	RB ^[51]	AO
Properties				
λ_{ab}^{max} (nm)	662	616 ^[52]	554	431 ^[53]
C. I. [*] Number	52015	42000	45170	41000
C. I. [*] Name	Basic blue 9	Basic green 4	Basic violet 10	Basic yellow 2
Class	Thiazin	triarylmethane	Rhodamine (xanthene)	diarylmethane
Colour	Blue	Green	Red	Yellow
Molecular Weight	319.8	364.9	479.0	303.8
IUPAC [#] Name	3,7-bis(Dimethyl amino)-phenothiazin-5-ium chloride	4-[(4-dimethylaminophenyl)-phenyl-methyl]-N,N-dimethyl-aniline	[9-(2-carboxyphenyl)-6-diethylamino-3-xanthenylidene]-diethylammonium chloride	bis[4-(dimethylamino)phenyl]methaniminium chloride
Molecular formula	C ₁₆ H ₁₈ ClN ₃ S	C ₂₃ H ₂₅ ClN ₂	C ₂₈ H ₃₁ ClN ₂ O ₃	C ₁₇ H ₂₂ ClN ₃

* C. I. Colour Index; [#]IUPAC- International Union of Pure and Applied Chemistry

1.1.3. Part C: Dye intercalated clay minerals:

C1. Introduction:

Clay minerals are natural layered silicates composed of sub-microscopic particles.¹³⁵¹ One of the most important groups of clay minerals is represented by expandable minerals, smectites. Due to isomorphous substitutions within the structure, smectite layers bear a negative charge. Some interesting physical and chemical properties, such as the tendency to form colloids and their inherent ion-exchange properties, relate to the layered structure and the presence of the net negative charge present in these minerals.¹⁹¹ These properties have a great influence on many chemical and physical parameters of these materials and are important for some processes taking place in nature or utilised by industry.

Research on clay mineral- dye complexes has been stimulated by the possibility of developing

1. photo-functional materials for application in, e.g., photonic devices¹⁵⁴¹ and
2. photoactive materials for the protection of pesticides from breakdown in the soil.^{155, 561}

C2. Organisation of molecules at clay mineral surfaces:¹³³¹

Adsorption always involves a kind of organisation of molecules at surfaces. Surfaces usually contain a number of sites, different in strength of interaction. Adsorbing molecules will first fill the sites with the strongest interactions, followed by the weaker ones. In the hypothetical case, that all sites are equal, molecules may occupy surface sites randomly. However, if the molecule-surface interaction is strong, the adsorbing molecules do not distinguish between sites of different strength. They occupy the first site they encounter and fill up the other sites progressively. Thus, depending on the type of sites and the strength of interaction, several models of site filling or organisation of molecules at surfaces are possible. There are also other types of interaction which must be considered besides the molecule-surface interaction. The first one is the molecule-molecule interaction, which is usually described by a Lennard-Jones type of potential: molecules will be organised so as to maximise the intermolecular interaction energy. If adsorption is performed from liquid solution, e.g. aqueous ion exchange, solvent-surface interactions and solvent-molecule interactions come into play. The final organisation of the molecules at the clay mineral surface will be determined by the subtle balance between all possible interactions. Many examples of adsorption and organisation of molecules at clay mineral surfaces can be found in the literature.¹³⁴¹

C3. Dye aggregation in clay dispersions:

The interaction of organic dyes with clay minerals has been studied extensively for decades and reviewed.^[54, 57, 58] Dye molecular aggregation in clay mineral colloids was reported for the first time by Bergman and O'Konski.^[59] The aggregation behaviour is sensitive to the kind and amount of metallic ions present in the lattice of the clays, the amount of adsorbed water as well as the structure of the organic guests to be intercalated.^[57] According to exciton theory[‡], the band's position and shape depend on the number and relative arrangement of interacting molecules and their transition moments in the molecular aggregate. Therefore, energies of the observed transitions are variable and may deviate.^[60]

In the vicinity of clay particles, dye aggregation takes place^[61] due to an enhanced polarity of water molecules induced by present inorganic ions in electric double layer. The presence of water as a polar solvent is essential for the aggregation of dye cations.^[62] Increasing the polarity of the environment increases the degree of aggregation. Enhanced aggregation is observed in aqueous solutions of inorganic salts and is found to be related to the polarising effects of ions.^[63] A re-arrangement of the dye cations occurs in extant aggregates, which is directed by the charge distribution so that each cation balances one negatively-charged site, thus mapping an intrinsic distribution of the negative charge on the clay surface.^[61, 64]

The dye/ silicate dispersions are dynamic systems, where complex re-organisation and re-distribution of the dye assemblies take place. The layer charge of the silicate substrate controls the formation of the dye's molecular assemblies, such as dimers and aggregates. The dye species (monomers, aggregates) are characterised by distinctly different optical properties using UV/ visible and fluorescence spectroscopies. New bands in the spectra of the dye/ clay dispersions are due to the formation of dye cation dimers and/ or higher aggregates.^[64] The aggregation of dye cations on a clay surface may significantly vary depending on the clay specimen.^[65] The formation of rhodamine aggregates in clay dispersions is interpreted in terms of clay colloid properties. The dye-clay suspension's spectra depend on parameters like dye loading, clay type, exchangeable cation, clay concentration and age of the suspension.^[66]

Clay minerals adsorb cationic dyes from aqueous or organic solutions by a cation exchange process. Many investigators have studied the adsorption of organic cations

[‡] The details are given in chapter 2.

by clay minerals from the point of view of 'long range' electrostatic interaction, i.e., the exchange of inorganic metallic cations by organic cations. However, 'short range' forces begin to operate when the organic cations penetrate the interlayer space. This includes H bonds between proton donor groups on the organic cations and interlayer water or the O-plane of the silicate layer. In these H bonds, oxygen atoms of interlayer water molecules or of the O-plane act as proton acceptors. An additional type of H bond between water molecules and aromatic cations can be obtained with a geometry in which one of the hydrogen in water molecules is oriented toward the center of the aromatic ring. For this H bond all of the π electrons of the aromatic ring contribute to the bonding interaction.¹⁵⁸ With greater adsorption, the clay flocculates and dimers and higher dye aggregates are formed in the inter-particle space, leading to metachromasy. Metachromasy then increases with the length of the chain.

When smectites are suspended in aqueous solutions, the expansion of the clay mineral structure occurs.¹⁶⁷ The swelling process relates to the expansion of interlayer spaces and is important for adsorption (intercalation) of various organic species. Numerous works have reported on the significant influence of clay minerals on optical properties of organic dyes.^{161, 68} Cationic chromophores are frequently adsorbed via an ion exchange reaction in the form of molecular assemblies¹⁶¹ which are formed by the hydrophobic interactions between dye molecules in water. This process is followed by significant changes of the electronic properties arising due to coupling between transition moments of the chromophores, which is observable using absorption spectroscopy in the visible region.¹⁶⁹ Several works have studied the factors affecting spectral properties of cationic dyes adsorbed on clay mineral surfaces.^{161, 68, 70, 71} Molecular aggregation and electronic properties of chromophores are strongly influenced by various parameters, including dye concentration and structure, pH and ionic strength, temperature and presence of organic co-solvents, etc.^{161, 68, 70, 71} It is also reported that the dye initially gets adsorbed extremely fast on the surface followed by a re-distribution over the total available surface and the thermodynamic instability of clay mineral suspensions, giving rise to continuous aggregation-deaggregation phenomena of individual clay mineral platelets.¹⁷²⁻⁷⁴

The changes of dye optical properties in clay mineral dispersions depend much on clay specimen used. Even minerals of the same type and structure may induce significantly different aggregation of dye molecules.^{175, 76} Although, dye adsorption by smectites results in metachromasy, different types of bonding in clays are observed.¹⁷⁷ Metachromasy¹⁷⁸ is a deviation from Beer's law, occurring in planar dye molecules

which tend to adhere to each other. Metachromic absorption bands are shifted from the monomer band and reflect different modes of aggregation of the dye molecules.¹⁷⁹⁾In montmorillonite, metachromasy results from π interactions¹⁷⁹⁾ between the adsorbed aromatic dye and the oxygen plane of the alumino-silicate.¹⁷⁷⁾

Metachromic dyes had been called 'finger-print probes' of surface properties of clays.¹⁸⁰⁾ However, for decades, the effect of clay mineral had not been clearly identified. Later, negative charge of clay mineral layers was identified as a chief parameter, which controls molecular aggregation of cationic dyes.^{165, 76)} The mineral layers consist of alumino-silicate leaflets of 0.95 nm thick. Each leaflet is made up of a layer of alumina sandwiched between two layers of silica. On the face surfaces (the oxygen planes) there is an array of hexagonal pits of oxygen atoms. At the edges, where the leaflet had been broken, one finds mainly oxygen with broken bonds, some of which are protonated, depending on pH. The face surface is negatively charged, because some alumina had been isomorphously substituted by magnesia and Fe^{2+} (octahedral substitution) and some silica was substituted by alumina and Fe^{3+} (tetrahedral substitution). In aqueous suspensions, the exchangeable cations and water form a diffuse double layer around the charged alumino-silicate leaflets. When diluted in water to < 0.01%, monovalent cations (Na or Li) allow the delamination of the clay particles into separate leaflets. Most of the other exchangeable cations would link 3-10 leaflets face to face, producing tactoids. With increasing clay concentration or in the presence of electrolytes, the clay flocculates. Exchangeable cations facilitate the dissociation of interlayer water, producing local acidity. Organic compounds are adsorbed into the interlayer space of montmorillonite either as cations, by electrostatic attraction, or by van der Waals forces.¹⁷⁹⁾

1.1.4. Part D: Rare earth doped materials:

D1. Rare earth elements:

The rare earth (RE) elements include the lanthanides ($Z=58-71$) but sometimes taken to contain ^{57}La , and even ^{21}Sc and ^{39}Y .¹⁸¹⁾ Some authors have classified the REs into two groups of 14 elements each- the lanthanides and actinides. Although these elements share many electronic properties, lanthanides are of greater importance in lasers and amplifiers. Many actinides have no isotopes stable enough to be useful for such devices.¹⁸²⁾

The term REs was coined to these elements because of their extraction from certain (**rare**) oxide (**earth**) minerals.^[83, 84] In fact; they are more abundant in the earth's crust than gold, silver, mercury, tungsten, etc. RE elements are never found as the free metals in the earth's crust. Pure minerals of individual REs do not exist in nature; all their minerals contain mixtures of the RE elements.^[85]

D2. Optical properties of rare earth ions:

The optical and magnetic applications of RE ions in luminescent devices using single crystals, powders and glasses are important. The following characteristics distinguish the REs from other optically active ions^[82]

1. They emit and absorb over narrow wavelength ranges.
2. The wavelengths of emission and absorption transitions are relatively insensitive to host material.
3. The intensities of these transitions are weak.
4. The lifetimes of metastable states are long.
5. The quantum efficiencies tend to be high, except in aqueous solutions.

All these properties result from the nature of states involved in these processes and lead to excellent performance of RE ions in many optical applications.

Sc^{3+} , Y^{3+} , La^{3+} and Lu^{3+} have no electronic energy levels that can induce excitation and luminescence processes in the visible region or near to it. In contrast, the ions Ce^{3+} to Yb^{3+} , which have partially filled 4f orbitals, have energy levels characteristic of each ion and show a variety of luminescence properties around the visible region.^[86]

D3. General properties of lanthanides:

The lanthanides (Lns) are all very reactive and electropositive. Their chemistry is dominated by the +3 oxidation state. Despite the high charge, the large size of the Ln(IV) ions results in low charge densities and their compounds are predominately ionic in character.^[81] The REs are strongly paramagnetic, in some cases ferromagnetic or anti-ferromagnetic at low temperatures. Their trivalent salts have absorption spectra and in some cases fluorescence spectra with sharp lines in the visible or neighbouring spectral regions.^[87]

D3.1. Lanthanide contraction:

The ionic radii of lanthanide decrease smoothly across the series. This decrease in size is the famous *lanthanide contraction*.^[88] which is due to the imperfect screening by the 4f electrons, which leads to an increase in effective nuclear charge as the atomic

number increases in the lanthanide series. As a result, the 4f electrons become increasingly more tightly bound with increasing Z .^[89] This is seen in every period as a shell is filled. It is particularly important for the lanthanides, however, because of the:

- ⊕ length of a f-series. (There are 2 elements in a s-block, 6 in a p-block, 10 in a d-block but 14 in a f-block)
- ⊕ directional characteristics of f-orbitals. The f-orbitals are 'angularly diffuse'; the electrons can occupy different volumes of space (lobes) and so avoid each other.
- ⊕ relativistic contraction consequences for the elements with high Z .

The lanthanide contraction makes the Lns to have a regular variation in chemical properties. The salts become less ionic.^[81]

D3.2. Radiative transitions in rare earth ions:

The REs, particularly the Lns are characterised by a partially filled 4f shell that is shielded from external fields by $5s^2 5p^6$ electrons. Hence, the free-ion energy levels are only weakly perturbed by the surrounding environment and the 4f intra-configurational transitions retain their atomic-like characteristics, e.g. spectral sharpness of the order of 10 cm^{-1} in good crystalline hosts and long lifetime of the order of 1 ms. Such narrow lines provide sensitive probes of weak perturbations. Technologically, the phosphors emitting spectrally narrow lines are favourable in display devices, where they can provide very pure primary colours. The most intriguing property of trivalent RE ions is that the spectral position of the emission lines is almost independent of the host lattice.^[82]

When incorporated in crystalline or amorphous hosts, the REs exist as 3^+ , or occasionally 2^+ , ions. The trivalent level of ionisation is the most stable for Ln ions and most optical devices use trivalent ions. All the 3^+ ions exhibit intense narrow-band intra-4f luminescence in a wide variety of hosts, and the shielding provided by the $5s^2$ and $5p^6$ electrons means that RE radiative transitions in solid hosts resemble those of the free ions and electron-phonon coupling is weak. The trivalent species are the more interesting, though some of the divalent species are luminescent. The positions of RE electronic levels are more influenced by spin orbit interactions than the applied crystal field. The intra- 4f transitions are partly forbidden and are made partially allowed by crystal field interactions, mixing opposite parity wave functions. Luminescence lifetimes are therefore long, and line widths are narrow. By careful selection of appropriate ion; intense narrow band emission can be obtained across much of the visible region and into the near IR. Radiative transitions between 4fⁿ

electronic states of RE ions in crystals are characterised by very sharp optical transitions- a consequence of

- (i) the weak coupling between the 4f electrons and the ionic lattice environment of the RE ion, and
- (ii) the fact that the RE ions generally enter identical sites in the crystal.^[90]

The RE ions in glass find a range of site types available to them which leads to relatively large inhomogeneous broadening.^[91]

The consequences for the static interactions are energy levels that are relatively insensitive to host, have small host-induced splittings, and are only weakly mixed with higher energy states. The dynamic consequences are little or no vibronic structure (phonon- assisted transitions) and weak non-radiative relaxation of excited states, which occurs through phonon emission. The net results are optical transitions between 4f states that manifest themselves as narrow, weak bands or sharp lines, and emission that can be highly efficient. Because the 4f electrons interact only weakly with electrons on other ions, the Hamiltonian for an individual RE ion can be written as^[82]

$$H = H_{\text{free ion}} + V_{\text{ion-static lattice}} + V_{\text{ion-dynamic lattice}} + V_{\text{EM}} + V_{\text{ion-ion}} \quad (1.1)$$

Here $H_{\text{free ion}}$ is the Hamiltonian of the ion in complete isolation,

$V_{\text{ion-static lattice}}$ and $V_{\text{ion-dynamic lattice}}$ contain the static and dynamic interactions of ion with the host,

V_{EM} treats the interaction of the ion with the electromagnetic field, and

$V_{\text{ion-ion}}$ describes the interaction between RE ions.

The static interactions produce the observed electronic structure and dynamic perturbations induce transitions between the electronic states.

Because of the shielding effect, the valence electrons of the trivalent RE ions are weakly affected by the ligand^[92] ions in the crystals; a situation that corresponds to the case of a weak crystalline field. Consequently, the spin-orbit interaction of the free ion Hamiltonian is dominant over the crystalline field Hamiltonian term. This causes the $^{2S+1}L_J$ states of the $(RE)^{3+}$ ions to be slightly perturbed when these ions are incorporated in crystals. The effect of the crystal field is to produce a slight shift in the energy of these states and to additional level splitting. However, the amount of this shift and the splitting energy are much smaller than the spin-orbit splitting, and thus, the optical spectra of $(RE)^{3+}$ ions are fairly similar to those expected for free ions. This implies that the main features of a $(RE)^{3+}$ ion spectrum are similar from one crystal to

Appendages not including another metal or metalloid atom.

another. The interpretation of the absorption and luminescence spectra of lanthanide (RE)³⁺ ions in crystals is based on systematic spectral measurements made in a particular host, lanthanum chloride, given by the Dieke diagram.^[87, 93]

Russell- Saunders coupling (LS coupling) is most often used for the states of lanthanides and actinides.^[82] Electrons in closed shells impart a constant energy shift to all terms, and thus only the interaction between the 4f electrons need be considered. The LS mixing is more significant for the high-Z REs (Ho, Er, Tm). The host has the least influence on the electronic structure and changes the positions of these levels only slightly. The static effects of the host on the RE dopant customarily are treated by replacing the host with an effective crystal field potential at the ion site.^[82]

For luminescent devices, the electromagnetic field interaction term V_{EM} is the most important since it gives rise to the emission and absorption of photons. This involves both the interaction between the electron charge and the electric field, and the interaction between the electron spin and the magnetic field.^[82]

For RE ions, the optical transitions from the IR to the UV are between states composed of 4f wave functions. Because the initial and final states have the same parity, electric-dipole processes are forbidden and transitions for free ions can occur only by the much weaker magnetic-dipole and electric-quadrupole processes. Radiative lifetimes for fully allowed electric-dipole transitions are roughly 10^{-8} s.^[82]

In terms of their spatial extend, the 4f wave-functions for La lie outside the xenon shell, but by Nd they have contracted so much that the maximum lies within the $5s^2 5p^6$ closed shells of the Xe structure.^[89]

Optical spectroscopy provides information about the interaction between the metallic central ion and its environment through the so-called '*nephelauxetic effect*' that determines the relative spatial extension of the f-orbitals and subsequently the overlapping with the ligand valence orbitals. But in lanthanide ions, the f-electrons belong to inner orbitals and therefore when engaged in compounds, they are more or less protected from the ligand interactions by closed more external s and p orbitals. The 4f electrons are well localised and they can be considered as quasi-core electrons with a small influence upon the bonding that explains the dominant +3 oxidation state across the lanthanide series.^[82]

The RE ion-host systems generally fluoresce with radiative lifetimes in the microseconds and milliseconds range. This property makes them ideal for high resolution studies in both the frequency and the time domains.¹⁹⁴ Also, due to their high quantum conversion efficiencies and due to the existence of fast relaxing states above the ground level, these ion-host systems have found application as active laser materials.¹⁹⁵ Spectral holes burnt in the purely electronic transitions observed in the RE doped crystalline or glassy hosts at the cryogenic temperatures may turn out to be the most efficient optical devices for the storage and fast retrieval of information.¹⁹⁶

The use of RE based phosphor, based on 'line type' f-f transitions, can narrow the emissions to the visible range, resulting in high efficiency and a high lumen equivalence.¹⁹⁷ The position of the 4f-5d levels is greatly influenced by the crystal field interaction. This effect is known as the *crystal field depression* of the 5d level, and consequently, the host crystal depresses 4f-5d energy levels for all Lns.^{197, 98}

D3.3. Magnetism of lanthanides:

The magnetism of lanthanides arises from almost no overlap between f and ligand orbitals and then, magnetic properties are directly related to the degree of localisation. The latter increases with the ability of the ligand to form an ionic bonding. The intra-configuration transitions within the f-configuration are called f-f transitions and are predominantly electric dipole or magnetic-dipole in nature.¹⁹¹

D3.4. Non-radiative transitions in rare earth ions:

In addition to changing their electronic state through interaction with the electromagnetic field (emission and absorption of photons), RE ions in solids can undergo transitions as a result of their interaction with vibrations of the host material. In crystals, this corresponds to the emission and absorption of phonons. The absence of translational invariance in glasses means that vibrational modes will not have a well-defined wave vector. Reisfeld¹⁹⁹ carried out the first quantitative studies on the non-radiative processes on RE ions in glasses.¹⁹¹ If the electronic states are spaced closely enough that they can be bridged by one or two photons and the transitions will occur rapidly. The ion makes a non-radiative transition to a lower electronic state through the emission of multiple phonons to conserve energy.^{100, 101} If the non-radiative relaxation rate of a level is comparable with its radiative transition rate, the efficiency of luminescent processes originating on that level is degraded. As the transitions occur across gaps many times the energy of the largest phonon, the analysis requires high-order perturbation theory. Although high order electromagnetic

processes (i.e., multi-photon) are extremely weak, multi-phonon processes can be significant because the electron- phonon interaction is stronger and phonons have a density of states that typically are 11 orders of magnitude larger than that of photons.^[100] The large variation in vibrational spectra among materials makes the non-radiative relaxation rate extremely host dependent. For a given host, all levels with the same energy gap below them will have roughly the same non-radiative rate. This rate is relatively independent of the nature of the electronic states involved, or even the identity of the RE ion, unless a strong selection rule is involved.^[102]

D4. Applications of rare earth elements:

The RE elements play very important role in industrial manufacturing, technology development and biological processes.^[103] The RE industry is vital in the economy because of their special photogenic, magnetic, mechanical and nuclear properties. Chemists are increasingly paying attention to studies of the environmental, medical and biological applications of RE elements to develop a RE industry. Therefore, the methods for their rapid, sensitive and accurate determination and separation are of great importance. However, it is extremely difficult to determine them individually without a pre-separation due to the similarity of their chemical properties.^[104]

REs and their compounds find applications in metallurgy,^[105] petroleum cracking catalysis,^[105] ceramic and glass industries,^[84] electronics,^[84] optoelectronics,^[105] superconductivity,^[105] computers,^[83] permanent magnets,^[83] alloys, hydrogen storage and transport, rechargeable hydride batteries, space applications,^[105] agriculture and natural science, etc. Ce and Er are used in high performance alloys,^[83] Nd, Ho and Dy are employed for laser crystals, Sm for high performance strong permanent magnets,^[83] Yb and Tb are applied in magnetic bubble and magneto-optic devices to store computer data^[83, 105] and Eu functions as red phosphor in colour television screens.^[83] The trichromatic fluorescent lamps made from rare earths such as Eu, Tb as activators and Y, La, Gd as hosts, consume less power than conventional types.^[105] Gd is used for detection of tumors, cancer by mammography.^[105]

D5. Rare earth titanates:

RE titanates ($\text{RE}_2\text{Ti}_2\text{O}_7$ - RETs) have been used as photocatalysts. The photocatalytic activity strongly depends on the crystal structure. RETs possess a cubic pyrochlore structure with small RE^{3+} ions (Yb^{3+} - Sm^{3+}), while RET with their larger RE^{3+} (Nd^{3+} - La^{3+}) exhibit a monoclinic perovskite structure.^[106] Synthesis and characterization of RETs were first reported in the 1950s. Generally pyrochlore structures are analogous

to modified cubic fluorite structure,^[107-109] with unit cell containing eight molecules and four crystallographically non-equivalent sites.^[110, 111] In RET, the different RE ions on a pyrochlore lattice exhibit specific magnetic properties. The RETs have low dielectric constant values which remain almost constant with temperature changes. This peculiar property makes the RETs and their doped compositions to be attractive candidates for microwave applications as resonators,^[112-118] ceramic capacitor formulations,^[119-125] etc. The high permittivity of titanates and other ferroelectric materials offer the advantage of obtaining high capacitance values for small volume of material. Also, ceramic titanates generally have low loss factor.

The pyrochlore structure of $Y_2Ti_2O_7$ possesses a larger unit cell than the other RET pyrochlore, which accommodates large vacancy concentrations without affecting stability of the compound and offers large ionic conductivity for the material.^[126, 127] $Y_2Ti_2O_7$ pyrochlore is one of the interesting candidate materials for reinforcement of titanium-based matrices.^[128] $Gd_2Ti_2O_7$ is an attractive candidate for solid-state ionic devices like fuel cells, chemical sensors^[129] and electrochemical devices.^[126, 127, 129-131] $La_2Ti_2O_7$ conducts photocurrent in the UV region due to the charge transfer between oxygen ions and titanium or lanthanum ions.^[132, 133] Some applications of pyrochlore are as fluorescence centers, catalysts, host phase in nuclear waste control, as electrolyte and as conducting electrodes in solid oxide fuel cells.^[109, 134-139] Optical wave guiding properties were demonstrated for thin films of $La_2Ti_2O_7$ that were deposited by laser ablation on substrates like silica-coated silicon and fused silica.^[133, 135, 140] $La_2Ti_2O_7$ exhibits piezoelectric properties at very high temperature^[135, 140] and sustain very high applied fields without dielectric breakdown. $Nd_2Ti_2O_7$ addition increases fracture toughness of zirconia.^[141] The static optical permittivity values increase with decreasing temperature in $Dy_2Ti_2O_7$.^[142] Single crystals of $Dy_2Ti_2O_7$ exhibit optical properties when the far IR rays fall on it at different temperatures.^[142]

D6. Rare earth doped glasses:

The absorption and fluorescence spectra of Ln^{3+} ions embedded in a crystalline or a glassy matrix consist of groups of relatively sharp spectral lines well separated from each other. Each such group corresponds to the Stark (crystal field) structure of a 'free ion' level. The mean energies of these groups do not change significantly from host to host and in that sense may represent the energy states of the corresponding free ion.

The covalent bonding between the RE ion and its ligands partially screens the 4f electrons and reduces the effective nuclear charge. This manifests itself as a rescaling

of the entire energy level diagram, which is known as the *nephelauxetic effect*.^[143] For glasses this translates into host- to- host shifts of up to a few percent in the separations between the energy levels. Covalent silicate glasses emit and absorb at longer wavelengths while ionic fluoride glasses emit and absorb at shorter wavelengths.^[144]

Lasers and amplifiers are devices that provide gain and so they must have low scattering losses. Hence, one is restricted to use single-crystal or glass hosts. In many applications, crystalline materials are preferred for reasons that include higher peak cross sections and better thermal conductivities, the versatility of glasses and the broader emission and absorption spectra they provide have led to the use of RE doped glasses in many applications.

1.2. Section II –Methods:

1.2.1. Part A: Self propagated high temperature synthesis (SHS):

E1. Introduction:

The processing techniques such as alkoxide method,^[145, 146] sol gel techniques,^[147] self propagated high temperature synthesis (SHS), etc. are some of the low temperature methods to produce functional ceramic powders. Among these, the SHS is a very simple and cost effective technique^[148] to synthesise phase pure nano-sized ceramic products which are attracting worldwide attention in high-tech ceramics. SHS^[149, 150] is also described by the terminologies like auto-combustion, combustion synthesis and a lot of other names,^[148, 151] depending on the nature of the reactants and the exothermicity.^[148] This technique, an offshoot of pyro-techniques, was evolved by the studies conducted by Merzhanov et al.^[152] The term 'Self propagated High temperature Synthesis' (SHS) was coined by Merzhanov et al. in 1972, for the process of combustion synthesis of refractory inorganic compounds.^[153-161] To date, the range of SHS products, besides refractory compounds, includes intermetallics, complex oxides, hydrides, chalcogenides, phosphides, etc.^[162]

E2. Advanced ceramics:

Conventional ceramics including refractories are generally made by crushing, grinding, sieving and physical mixing of the raw materials, whereas for producing 'advanced ceramics'^[163-169] or 'high performance ceramics', chemically homogenous submicron particles of highly reactive ceramic powders are essential to ensure products having minimum porosity, high density, and controlled microstructure. Modern developments in ceramic products are mainly based on non-silicate and much

more sophisticated materials such as binary oxides, carbides, perovskites and also certain completely synthetic materials. Such materials are referred as *advanced ceramics* or *high performance ceramics*. There are several advantages for these materials over traditional ceramics. They are further classified on the basis of their chemical composition and specific functional applications.^[167-171] Different methods reported for the production of advanced ceramic powders are mentioned in *Table 1.3*.

Table 1.3: Different methods for the production of advanced ceramic powders.^[85]

Solid state technique	Solution technique	Vapour-phase technique
a) Solid decomposition	a) <i>Precipitation-Filtration</i>	a) <i>Vapourization-condensation</i>
b) Solid state reaction at high temperatures	(i) Co-precipitation (ii) Forced hydrolysis (iii) Alkoxide hydrolysis (iv) Hydrothermal precipitation	b) <i>Vapour decomposition</i> c) <i>Vapour-vapour reaction</i> (i) Conventionally heated (ii) Plasma heated (iii) Laser heated
c) SHS method	b) <i>Solvent vapourization</i>	d) <i>Vapour-liquid reaction</i> e) <i>Vapour- solid reaction</i>
d) Pechini method	(i) Simple evaporation (ii) Spray drying (iii) Spray roasting (iv) Freeze drying (v) Emulsion drying c) <i>Liquid drying</i> d) <i>Sol-gel</i>	

SHS has emerged as a facile and economically viable technique for the synthesis and processing of advanced ceramics, nanomaterials etc.^[148, 172] Recent innovations in the combustion and processing parameters have resulted in a better understanding of combustion phenomena and control of microstructure and property of the products.

E3. Basics of reactions:

The SHS reaction is similar to the well known Thermite process developed by Goldschmidt in 1895, for the reduction of metallic compounds,^[173, 174] at specified sites. Vladimir Hlavacek suggested that Goldschmidt deserves the credit for the discovery of self propagating reactions of solid-solid non-catalytic systems.^[85, 174]

SHS is a science-intensive process. Its comprehension requires erudition in thermodynamics, chemical kinetics, general and structural macrokinetics, materials science, and other allied fields of knowledge.^[175]

SHS method uses the energy produced by the exothermic decomposition of a redox mixture of metal salt, usually metal nitrates, with an organic compound like urea glycine, alanine etc. as activator. In the combustion mixture, the nitrates and the activator behave like conventional 'oxidants' and 'fuels'. The reaction is usually carried out by dissolving metal nitrates and fuels in a minimum amount of water in a pyrex beaker and heating the mixture to evaporate off the water. The resulting viscous liquid foams, ignites, and undergoes self-sustained combustion, producing ashes containing the oxide product.^[148, 176, 177] During the combustion, exothermic redox reactions associated with nitrate decomposition and fuel oxidation take place. Gases such as N₂, steam and CO₂ evolve favouring the formation of fine particle ashes within a few minutes. The properties of the final product, such as particle size, surface area and porosity, depend on the method of combustion. The liberation of gases favours the de-segregation of the products that increases the porosity, and heat dissipation which inhibits the sintering of the products. Exothermicity of combustion is controlled by the nature of the fuel and the oxidiser to fuel ratio.^[85] The reaction paths for synthesis have been described in the literature.^[148, 173, 178-185]

The combustion reaction occurs spontaneously by utilising the energy released during the exothermic fuel oxidation reaction. Due to the profuse liberation of gases, instant flame is formed which can have temperatures of more than 2000 °C, a stage at which self propagated high temperature is attained.^[173, 183-187] During the SHS reaction, the reactants undergo dehydration, the fuel melts, disperses and decomposes with evolution of gases so that the product froths and swells to a foam-like structure and readily starts glowing with instant flame to form the ceramic powders.

The combustion reaction initiates at the sample surface when a heated wire, electric spark, laser beam, etc. induces a heat flux, and the reaction proceeds spontaneously and rapidly.^[148, 178-181, 188, 189] The rate of SHS process depends on the exothermic nature of the reaction as well as on the mode of heat supplied/received by the system, state of aggregation of reactants, kinetics of phase/structure transformations^[183-187, 190, 191] etc.

The products formed in SHS reactions may be ordinary loose powders, particle agglomerates, foams, cakes, ingots, films, whiskers, fibres and crystals.^[179-181] Products

formed under optimum conditions are of green composition and contain only traces of unreacted reactants or contaminants.^[176, 183] The grain size depends on the rate of cooling and kinetics of crystallisation. The products can have porosities in the range of zero for compact materials and 90-95% for foam materials. A range of products like refractory compounds, inorganic composites, organic compounds and polymers by frontal polymerisation have been made by SHS method.^[173]

E4. Advantages:

Perhaps the most important and interesting aspect of SHS reaction is the conversion of a simple metallic compound into a highly useful ceramic material of desired properties. Common organic compounds are used as activators or fuels through this cost effective method to prepare numerous metal oxide ceramics.

SHS based on exothermic oxidising reduction reactions has many advantages.^[192]

- Utilisation of reaction heat generated during the reaction instead of external power,^[193] i.e., self generation of energy.^[151, 194]
- Low energy capacity of equipment due to the absence of extrinsic heating sources.
- High productivity^[151] due to high reaction or burning velocity.^[193, 194]
- Simple reagents with fewer operation stages and high combustion temperature.^[193]
- The feasibility of remote-handling the processes.
- The lack of considerable amounts of facility-decommission wastes.^[192]
- Low boiling point impurities evaporate at the combustion temperature to yield to form high purity^[148, 194] and quality^[193] products under optimal conditions.^[162]
- Stabilisation of metastable phases.^[148]
- Formation of virtually any size and shape products.^[148]
- A highly cost effective method for the manufacture of ceramics.^[193]
- Simple^[148] and inexpensive technological equipment is enough.^[194]
- Scaling up of the process is not encountered.
- Reactions approach complete conversion with larger quantities, resulting in better yields of products^[151, 194] with limited powder agglomeration.
- Process yields hitherto unknown products with unique properties.^[194]

In general, SHS is a material and energy saving process^[195] and can be used for the production of finished machine parts. SHS technology is free of the so called scale effect typical of other chemical processes – on going from the laboratory scale to industrial-scale production; the quality of SHS products tends to increase.

E5. Features:^[192]

The three main stages of the SHS process are ignition, front propagation, and product cooling.^[162] SHS processes are characterised by high temperatures, fast heating rates and short reaction times.^[148] The basic features of the SHS technology are:^[192]

- Duration of initiation - 0.05-5.0 s;
- Temperature in a combustion wave is dependent upon the ratio of precursor[§] components and is within 1500-3000 °C.
- The velocity of moving up the combustion wave is 0.5-150 mm/s.

The main feature of SHS is a very short time required for attaining high combustion temperatures due to heat released during exothermic reactions. This feature explains other specific characteristics, such as the high degree of conversion, partial self-purification from impurities, and the feasibility for the direct synthesis of items with a desired structure and even shape, size, and service parameters. The most attractive features of SHS as a method for the preparation of materials and compounds are:^[162]

- ◆ SHS can be carried out by using relatively simple facilities or even in open air;
- ◆ Sometimes (but rarely), a good practical result can be obtained without having any detailed information about the process;
- ◆ The process parameters can be roughly estimated by performing thermodynamic calculations;
- ◆ The parameters of SHS can be determined by measuring the values of the velocity of the front propagation, the maximum combustion temperature, the extent of conversion, the chemical/ phase composition, the amount of impurities, and some structural data as a function of reagents' particle size, charge density, sample size, initial temperature, ambient gas pressure, etc.;
- ◆ The quality control requires a profound knowledge of the structural macrokinetics, which considers the positive and negative nonlinear feedback between the rates of chemical reactions, structural transformations, and heat/mass transfer processes;
- ◆ In most cases, controlling the parameters of the end product is a major task objective of these studies.

These features make SHS an attractive method for the manufacture of technologically useful materials at lower costs compared to conventional ceramic processes.^[148]

[§] Starting compounds

E6. Drawback:

The porous nature of the products necessitates a densification step for any practical application.^[196]

E7. Applications:

SHS products find their extensive application in mechanical engineering, metallurgy, chemical industry, electrical and electronic engineering, aerospace industry, building industry, etc. SHS products are also used in medicine.^[175]

An important task in the synthetic chemistry of SHS is the direct synthesis of materials with a desired structure, thus avoiding preliminary preparation of powders. The greatest advance here was achieved in the synthesis of multi-component ceramics and hard alloys. SHS can be used to prepare crystalline, agglomerate (polycrystalline), and composite powders.^[197] The SHS method has the advantages on the control of reaction rate, temperature and the microstructure of resultant product.^[156, 157, 180-182, 184] SHS retains a strong position in the manufacturing of ceramic powders. To date, almost any compound can be prepared by SHS upon proper variation of the charge composition and process conditions, such that the expediency of using SHS in solving this or another task is defined only by the economic factors. The world-wide importance of SHS research is evident from various publications.^[149, 150, 152, 161, 178, 190, 198-200]

1.2.2. Part B: Sol gel:^[192, 201- 203]

F1. Introduction:

Sol gel process is a colloidal route used to synthesise ceramics with an intermediated stage including a sol and/ or a gel state.^[203] Sol gel processing has been known for a long time; the first silica gels were made in 1845 by M Ebelmen. Sol gel processing methods were first used historically for decorative and constructional materials. Today sol gel methods are reaching their full potential, enabling the preparation of new generations of advanced materials not easily accessible by other methods, yet using mild, low energy conditions.

Sol gel materials encompass a wide range of organic/ inorganic composite materials which share a common preparation strategy. The sol gel processing involving the generation of colloidal suspensions called 'sols' which are subsequently converted to viscous gels and thence to solid materials.^[192]

F2. Sol and gel:

A sol is a dispersion of colloidal particles^[204] suspended in Brownian motion within a fluid matrix. Colloids are suspensions of particles of linear dimensions between 1nm and 1µm. The stability of colloidal particles is determined by their resistance to aggregation, and can be remarkably high. When the particles in the sol form long polymeric chains that span the entire sol, a *gel* is formed.

F3. The silicon alkoxide sol gel process:

The silica produced by the sol gel route starting with hydrolysis of silicon alkoxides occur slowly enough to allow detailed study by a variety of methods. For other alkoxides, such as metal alkoxides which are much more reactive, some reactions occur so rapidly that they are not amenable to either study or control, though they follow the same series of steps. The steps are:

1. hydrolysis
2. condensation
3. gelation – formation of a ‘spanning cluster’ across the vessel, giving a network which entraps the remaining solution, with high viscosity.
4. ageing- formation of further cross-links, associated shrinkage of the gel as covalent links replace non-bonded contacts with changes in pore sizes and pore wall strengths.
5. drying- loss of volatile components, first syneresis (expulsion of the liquid as the gel shrinks), then evaporation of the liquid from within the pore structure with associated development of capillary stress which frequently leads to cracking.
6. densification- thermal treatment leading to collapse of the open structure and formation of a dense ceramic.

F4. Advantages of sol gel synthesis:

1. The temperature required for all stages apart from densification are low (~ room temperature). Thus thermal degradation of both the material itself and any entrapped species is minimised and high purity and stoichiometry can be achieved.
2. Precursors are volatile and easily purified to very high levels.
3. Since organo-metallic precursors involving different metals are frequently miscible, homogeneous controlled doping is easy to achieve.
4. Mild and convenient chemical processing conditions.
5. Highly porous materials and nano-crystalline materials may be prepared with controlled pore size distribution, both by the chemical composition of the starting material. as well as by the processing conditions.

6. By appropriate chemical modification of the precursors, control may be achieved over the rates of hydrolysis and condensation, and over colloid particle size and the pore size, porosity and pore wall chemistry of the final material.
7. Using functionalised precursors, covalent attachment of organic and biological species to porous silicate glass structures is possible.
8. By controlling the ageing and drying conditions, further pore size and mechanical strength control may be achieved.
9. Organo-metallic precursors containing polymerisable organic ligands may be used to produce materials containing both inorganic and organic polymer networks.
10. Entrapped organic species may serve as templates for creation of pores with controlled size and shape. Subsequent removal of these species leaves 'molecular footprints' with potential as catalytic sites.
11. Since liquid precursors are used ceramic materials, thin films or fibers as well as monoliths of complex shapes can be cast without machining or melting.
12. The optical quality of the materials is often good.
13. The low temperature of sol gel method allows the production of unusual amorphous materials^[203] as it is below the crystallisation temperature for oxides.
14. It not only allows for materials to have any oxide composition, but it also permits the production of new hybrid organic-inorganic materials which do not exist naturally.
15. The association of the solid colloidal state with the liquid medium avoids any pollution by the eventual dispersion of dust.
16. The kinetics of the various chemical reactions can be easily controlled by the narrow processing temperatures and by the often dilute conditions.
17. The sol gel method begins by dissolving the materials in a sol. This process allows for a more homogenous distribution of dopant in the final product.

F5. Limitations of sol gel synthesis:

The precursors are often expensive and sensitive to moisture, limiting large scale production plants to specialised applications such as optical coatings. The process is also time-consuming, particularly where careful ageing and drying are required. Finally the problems of dimensional change on densification, and of shrinkage and stress cracking on drying, although not insuperable, do require careful attention. Thus it is necessary to optimise sol gel materials to exploit their advantages to the maximum in applications.^[201]

F6. Silica sol gels- Reaction mechanisms and chemical control of reactions:

The properties of the sol gel materials e.g., transparency, porosity, pore size distribution, surface functionality, strongly depend on the preparation method. By controlling the conditions during the stages of the process: hydrolysis, condensation, ageing, drying, one can fine-tune the characteristics of the resulting material.

F6.1. Hydrolysis- Acid and base catalysis:

The first step of the hydrolysis of a silicon alkoxide can occur by acid catalysed or base-catalysed processes.

a) The role of the precursor molecule:

Hydrolysis of the silicon alkoxide precursor is very sensitive to steric hindrance. Larger alkoxy groups lead to more steric hindrance and over-crowding of the transition state, and thus lead to slower reaction. Thus, tetramethoxy silane (TMOS) hydrolysis is faster than tetraethoxy silane (TEOS). Chain elongation and in particular chain branching in the alkoxide ligands lead to a dramatic decrease of the reaction rate.^[205] A higher alcohol (e.g., n-propanol) as a co-solvent leads to replacement of ethoxide ligands during the first hydrolysis step of TEOS. Stable modifying ligands reduce the hydrolysis and condensation rate so that less-condensed gels are obtained.^[206] Due to hindrance this precursor exhibits a low reactivity towards hydrolysis and, therefore, the structure of the gels only depends on pH and reaction temperature, rather than on the amount of water present in the reaction mixture. The gel structure can be modified through the modification of the reactivity of precursors in the replacement of the alkoxy groups by other ligands such as acetate.

Because of the hydrophobic nature of the ethoxy groups, TEOS and water are immiscible and it is necessary to add a co-solvent to achieve miscibility to facilitate hydrolysis. Many different co-solvents have been used, including different alcohols, formamide, dimethylformamide, etc. The choice of added co-solvent is important, since use of a different alcohol from that generated by hydrolysis of the alkoxide can lead to trans-esterification and affect the whole hydrolysis and condensation reaction sequence. The co-solvent may also influence the drying process. Such a co-solvent is referred to as a drying control chemical additive (DCCA).

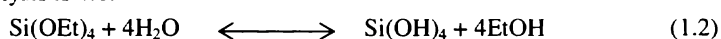
b) The role of the catalyst:

The hydrolysis of silicon alkoxides is dramatically promoted by the use of a catalyst. Under acid catalysis the initial step of the hydrolysis i.e., the conversion of the

precursor molecules into the trialkoxy silanol $(RO)_3Si-OH$, proceeds rapidly. Since one of the electron donating alkoxy groups has been removed, protonation of this silanol species will be less favourable and hence the second hydrolysis step will be slower. Base catalysis proceeds faster when electron donating $-OR$ groups are removed. The consequent generation of completely hydrolysed monomers leads to cross-linking already at early stages in the process where un-hydrolysed monomer is still present. Due to the high condensation rate and the interlinking of the highly cross-linked polymers a porous network is formed and gelation occurs fast.

c) The role of water:

The ratio of water: alkoxide (R) determines the amount of co-solvent required, but this ratio also influences the reaction rate. The stoichiometric ratio of water: alkoxide for complete hydrolysis is 4:1.



When silicon alkoxides are reacted with low concentrations of water ($H_2O/Si < 2$) initially, partially hydrolysed monomers are formed which condense to form almost completely esterified- either linear or branched- polymeric species. Increasing the water content to 4-10 H_2O/Si leads to almost completely hydroxylated polymeric strands in acid catalysed systems. In base catalysed gels this leads to the generation of a fully hydrolysed polymer in the presence of still unhydrolysed monomer which induces phase separation. Consequently aqueous regions solvating the hydrophilic polymer and solvent-rich regions with unreacted hydrophobic monomer are formed.¹²⁰⁷ Increased water concentration (25-50 H_2O/Si) leads to separation of the individual polymeric strands and hinders the intermolecular condensation reactions. This leads to the formation of isolated cyclic structures and consequently to the formation of more dense spherical particles.¹²⁰⁸ The presence of surface silanol groups promotes gelation by increasing the condensation rate.¹²⁰⁹

Addition of solvents such as alcohols affects the structure of water by breaking the hydrogen bonds. This increases the solvation of H^+ and OH^- ions and thereby decreases, respectively, the acidity or basicity of the solution and consequently hydrolysis. Increasing the water concentration increases the activity of the catalyst and hydrolysis is promoted.¹²¹⁰

F6.2. Condensation:

Condensation reactions can be either water condensation or alcohol condensation.

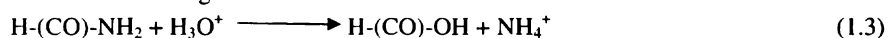
F6.3. Gelation:

Gelation is a process according to which a sol, or a solution, transforms to a gel. Gelation occurs when links form between silica sol particles, produced by hydrolysis and condensation, to such an extent that a giant spanning cluster reaches across the containing vessel. This initial gel has a high viscosity but low elasticity. There is no exotherm or endotherm, nor any discrete chemical change, at the gel point; only the sudden increase in viscosity. Following gelation, further cross-linking and chemical inclusion of isolated sol particles into the spanning cluster continues, leading to an increase in the elasticity of the sample.

At neutral pH the polymerisation reaction proceeds through nucleophilic attack of the Si-O⁻ group. The nucleophilicity of this group can be fine-tuned through the addition of solvents. Polar protic solvents such as formamide and alcohols lower the reactivity through the formation of hydrogen bonds. This decreases the efficiency of the condensation process leading to more highly branched structures and consequently to reduced gel times. The replacement of an alcoholic solvent by dioxane leads to activation of the Si-O⁻ group. Due to the efficiency of the condensation process, dense gels are obtained. Increasing the amount of formamide leads to a coarsening of the gel structure and to an increase of the pore size.

By acting as a hydrogen bond acceptor formamide and dimethylformamide decrease the acidity of the reaction mixture and thereby the hydrolysis rate in acid catalysed reactions. For the same reasons the nucleophilicity of the silanol groups is enhanced, leading to faster condensation.^[211, 212]

In an acid catalysed system formamide is hydrolysed to yield formic acid and ammonia according to:



This leads to an increase in pH^[213] and gives the process initially the character of an acid catalysed process and later of a base catalysed process, leading to high interconnectivity of small oligomers.^{**} and hence to a decrease of the gelation time.^[214]

F6.4. Ageing:

The ageing rate of the samples depends on pH, temperature and gel composition. As a final result the samples get stiffened and shrunken. Shrinkage occurs because new

^{**} a polymer molecule consisting of a small number of monomers.

bonds are formed where there were formerly only weak interactions between surface hydroxy and alkoxy groups. This shrinkage leads to expulsion of liquid from the pores of the gel, so that gel samples in sealed containers gradually change in appearance from homogeneous gel to transparent shrunken solid monoliths immersed in liquid. This process is known as *syneresis*.

Coarsening or ripening occurs associated with ageing, in which the material dissolves from the surface of large particles and deposits on the initially narrow 'necks' which join particles to each other.

Phase transformations can also occur where gelation has occurred very rapidly or where several precursors of different miscibility with water have been used; there is a possibility that the porous gel contains isolated regions of unreacted precursor. On prolonged soaking in water; this material may react either completely or partially, giving inclusions of material of different structure and composition. If the refractive index of such regions is sufficiently different from that of the host matrix, the whole sample may have a white opaque appearance characteristic of a phase-separated material. This undesirable situation may be avoided by modifying the reaction rate and use of more effective co-solvents in the initial mixture.

During the ageing process the gel hardens by the formation of cross-links. However, the number of new Si-O-Si bonds responsible for this rigidification was found to be remarkably low. The pore structure of sol gel silicates can be modified by ageing them in solvents^[215] or solutions other than the mother liquor. The rate of ageing is directly related to solubility: higher temperatures, hydroxide and fluoride ions increase the rate of ageing and thereby the development of the pore size and the pore size distribution.^[216] By dissolution and re-precipitation, neck formation occurs between particles, which lead to strengthening of the pore wall preventing collapse of the pores during the drying process.

F6.4.1. Significance of ageing:

Ageing effects are often cited as a significant disadvantage in the use of sol gel materials in technological applications, particularly where the sol gel method is proposed as a low-temperature, mild-conditions method for entrapment of organic or biological species.

- i) Ageing usually improves the properties of the material
- ii) The ageing process can be controlled by varying the pH, temperature, pressure, ageing liquid medium and initial precursor mixture composition, and may thus be optimised.
- iii) Where regular production is envisaged, ageing need not lead to production delay once an initial aged stock has been generated, provided production requirements can be anticipated.

F6.5. Drying:

There are four main stages in the drying of the gelled sample, the details of which are available in literature.^[92, 201-203]

F6.5.1. Consequences of drying:

- i) As a flat monolith sample dries with its lower face in contact with the container, evaporation is greater from the upper surface. The lower region of the sample therefore has filled pores while an increasingly large region of the upper surface has empty pores. The region of empty pores is able to distribute the residual capillary stress, and thus expands slightly relative to the lower region. Hence these samples tend to develop lower concave surfaces, even on flat- bottomed containers.
- ii) Soluble materials from the bulk of the material may be transported along the thin film of liquid on pore walls and deposited as a white efflorescence at or near the surface of the sample. This may be avoided by washing out the material before drying.
- iii) As surface layers dry before the bulk of the sample, a slight surface cloudiness may sometimes be observed in partially-dried samples, depending on pore sizes.

F6.5.2. Avoiding cracks:

The cracks formation can be avoided by

- 1) Supercritical drying.
- 2) Freeze drying
- 3) Drying control chemical additives (DCCAs) addition
- 4) Ageing
- 5) Gels with large pores

F6.6. Densification:

Heat treatment produces dense glasses and ceramics from gels. By control of the hydrolysis, condensation, ageing and drying stages, materials with a wide range of pore sizes, pore wall characteristics and general microstructure can be prepared. The

detailed effects of the heat treatment therefore depend on the particular characteristics of the material at the end of the low-temperature drying process.

- 1) At low temperatures (<200 °C) weight loss occurs as pore surface water or alcohol is desorbed, but little further shrinkage takes place, and in some cases a net expansion is observed. In this range, the skeletal structure of the silica gel behaves as a molecular solid rather than as bulk silica.
- 2) At intermediate temperatures (150-200 °C to 500-700 °C), samples generally show both weight loss and shrinkage. Three processes occur in this range:
 - ✓ loss of organics (leading to weight loss but little shrinkage),
 - ✓ further condensation (producing both weight loss and shrinkage) and
 - ✓ structural relaxation (giving shrinkage with no associated weight loss).
- 3) At higher temperatures (>700 °C) a sharp increase in shrinkage rate is observed with little or no further weight loss. The transition temperature is close to the glass transition temperature for the material, above which viscous flow occurs leading to rapid densification as thermal energy permits extended structural reorganisation.

F7. Additives for structuring and processing:

F7.1. Drying and control additives:

Fracture and crack formation during the drying of gels is a serious problem which is caused by stress due to changes in pore size during the process and the capillary forces arising from evaporation of the solvent. The methods adopted to overcome these are:

1. Slow rate evaporation method: Here the removal of the solvent is slow and carefully controlled. It requires very long processing times.^[217, 218]
2. Supercritical drying: The solvent is removed under controlled pressure. It is the fastest and most reliable process. Since this is a discontinuous process which limits its industrial application.^[219]
3. Use of drying control chemical additives (DCCAs): e.g. formamide,^[211] dimethylformamide (DMF),^[220, 221] and acetonitrile.^[222] These agents allow drying at elevated temperatures and ambient pressures without crack formation. The DCCAs change the structure of the sol gel materials. They cause the generation of large pores with narrow size distribution. The capillary forces will be weaker and hence the stress exerted on the gel during drying will be smaller. Since the vapour pressure is higher in larger pores, the increased pore size promotes the evaporation of the solvent.^[223] The DCCA binds to the silica surface through hydrogen bonds. This will facilitate the removal of water molecules by preventing their interaction with the silanol groups on the pore walls and the remaining fluid as a lower surface tension.

4. Addition of surfactants: By adhering to the particle surface the surfactant influences the pore formation, but more importantly it modifies the inner pore surface with alkyl chains. These hydrophobic groups decrease the interaction of the water with the pore wall and thereby reduce drying stress.

F8. Entrapment of functional materials- Efficiency of entrapment:

The sol gel route is a low temperature method that allows doping of inorganic materials with organic compounds, thereby adding functionality to the resulting glass. The entrapment efficiency depends on^[20,31]

- * pore size distribution and porosity of the gel,
- * the size of the dopant and
- * the development and stability of the matrix network.

F9. The characterization of sol gel materials:

The analysis of sol gel derived materials is a far from trivial task for two main reasons:

- a) The starting materials are very different from the final products both chemically and physically.
- b) Due to the enormous versatility of the sol gel method, the resulting materials and their precursors can cover a vast range of both physical and chemical properties.

F10. Application of sol gel silicates:

Sol gel technology provides an alternative route to the production of ceramics and glasses. Compared to conventional techniques the sol gel route offers a number of advantages that make the method interesting for the production of materials tailored to specific applications. The special features of the sol gel materials, i.e. they are porous and generally transparent, have opened up the way for many possible applications.

⊗ **Optical materials:**

⊗ *Undoped glasses:* The sol gel method has been extensively explored as a low temperature route to optical components^[224, 225] in modern communication and information technologies

⊗ *Doped glasses:* The inclusion of organic compounds in the final glass by sol gel technology allows for a great variety of functions including laser action,^[226] photoluminescence (PL), photochemical hole burning,^[227] photochromism,^[228] non linear optical behaviour^[229] and contrast enhancement.

⊗ *Contact lenses:* Materials for hard contact lenses with good mechanical, biomedical and optical properties can be prepared by sol gel process.

⊗ **Chemical sensors:**

⊗ *Optical chemical sensing:* The immobilisation of complexation reagents on optical fibers can be achieved by sol gel process.^[230]

⊗ *Biosensors:* The highly selective and extremely efficient reactions of enzymes make them desirable reagents for sensing purposes. Sol gel materials immobilise the enzymes without losing their function.

⊗ **Catalysts:**

Due to its porous nature silica has been extensively explored as a catalytic material. For this purpose advantage has been taken of two of its principal properties:

- ◇ Silica contains a large number of surface hydroxyl groups that can act as acid catalysts, and
- ◇ the surface of the silica can be easily loaded with catalytically active sites through impregnation with various metals.

The key parameters which can be controlled through sol gel processing of the catalysts are:

- ⊗ High SSA.
- ⊗ Controlled pore size distribution.
- ⊗ Stable pore structure under preparation and reaction conditions
- ⊗ Active material distributed on pore surfaces, not in the bulk.
- ⊗ Active material homogeneously and effectively distributed over surface.
- ⊗ High purity of active material.
- ⊗ Easy control of composition for multi-component catalytic species.
- ⊗ Effective control of crystalline or amorphous structure as desired.
- ⊗ Mechanical properties adapted to desired operating environment.
- ⊗ Catalyst resistant to chemical or physical blocking of active sites

⊗ **Coatings and membranes:**

The sol gel approach offers the possibility to coat large, curved substrates using simple deposition techniques and the ability to obtain homogeneous coatings, as well as coatings with tailored inhomogeneity. Sol gel methods can be conveniently used to produce multilayer coatings and organic-inorganic hybrid materials. Sol gel layers have been used to achieve conductive-, porous-, optical-control-, antireflection-, biocompatible- coatings etc.^[231, 232]

However, a number of problems occur, notably the difficulty of obtaining thicker films for micro-machined components, the prevention of substrate structure adversely

affect the nucleation of the desired solid phase from the sol gel film, and the possibility that the reaction and/ or inter-diffusion may occur on heat treatment to nucleate the desired phase despite the lower temperatures generally required for alternative processes. The sol gel process is being increasingly used for the preparation of homogeneous and fine ceramic powders suitable for various nuclear,^[170] machinable ceramics, and superconductor applications.^[233, 234]

1.2.3. Part C: Photothermal phenomena:

G1. Introduction:

Photothermal (PT) science encompasses a wide range of techniques and phenomena based on the conversion of absorbed electromagnetic energy into heat.^[235] Optical energy is absorbed and eventually converted into thermal energy by an enormous number of materials. Although the initial absorption processes in many materials are very selective, it is common for excited electronic states in atoms or molecules to lose their excitation energy by a series of non-radiative transitions that result in a general heating of the material.^[236] PT phenomena in solid materials are generated by a combination of thermal expansion, thermal diffusion and thermo-elastic bending effects.^[237-240] One of these mechanisms may predominate depending on the particular material and/ or on the experimental conditions.^[241]

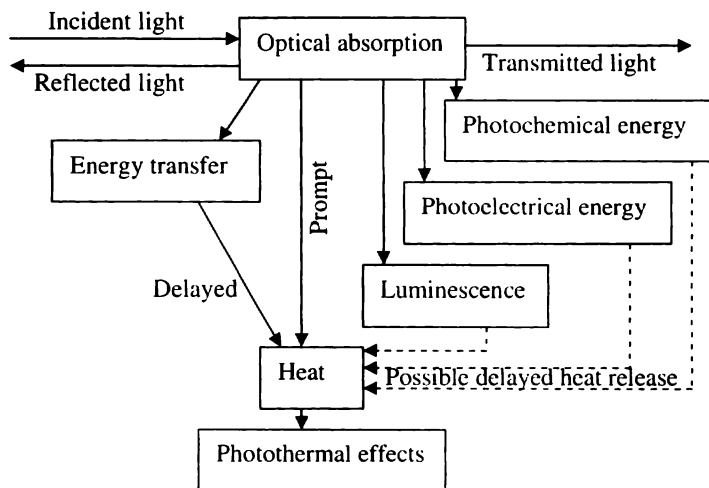


Figure 1. 10: Block diagram showing the possible consequences of electromagnetic radiation absorption, leading to 'prompt' or 'delayed' heat production in competition with other de-excitation channels.

PT generation has three types of applications^[235]

- a) PT material probing - no sample modification.
- b) PT material processing- the sample changes to another useful form.
- c) PT material destruction- applications render the sample useless.

PT material probing is based on the ideas shown in *Figure 1. 10*. The optical excitation of the sample produces several forms of energy: heat, luminescence, chemical energy, or electrical energy. The heat can be produced promptly, or at various time delays due to energy-transfer mechanisms. All these resulting energy forms must add up to equal the absorbed optical energy; in other words, the various de-excitation branches shown in *Figure 1. 10* are 'complementary'.^[235]

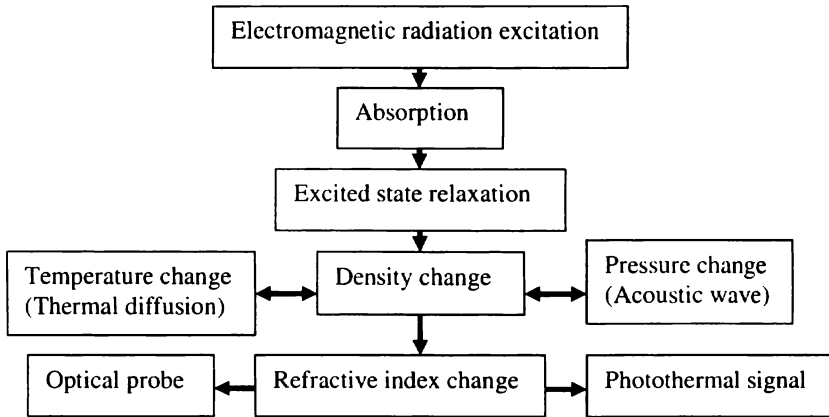


Figure 1.11: Basic processes responsible for photothermal (PT) signal generation.

PT material probing or characterization techniques generally rely on the use of high-sensitivity detection methods to monitor the effects caused by PT heating of the sample. Many of these PT effects occur simultaneously (*Figure 1.11*); e.g., PT heating of a sample in air will produce temperature rise, photoacoustic (PA) waves, and refractive index changes in the sample and in the adjacent air, IR thermal radiation changes, etc., at the same time. Thus, the choice of a suitable PT effect for detection will depend on the nature of the sample and its environment, the light source used, and the purpose of the measurement.^[235]

The PT method relies on a fraction of the optical energy being absorbed by the sample and being converted rapidly to heat. PT effect:^[236]

- 1) is intrinsically non-invasive / non-contact

- 2) provides the means of producing a precisely defined region of modulated heating.
- 3) can be used to obtain spectroscopic information about some materials through their selective absorption of parts of the electromagnetic spectrum.
- 4) as a whole will depend on the optical properties of the material under investigation as well as its thermal properties for all applications.

G2. Photothermal detection and applications:

PT measurements have been proved to be very useful in various fields such as spectroscopy, thermal characterization, and non-destructive evaluation. When a sample is irradiated by a periodic or a pulsed light source, a temperature rise is induced in the sample. It can be measured by probing the variation of some physical parameters either of the sample itself or of the surrounding medium; this latter dependence distinguishes PT from other spectroscopic experiments.^[242]The former case is the 'direct PT detection' and the latter is the 'indirect PT detection'. All the PT detection schemes require a modulation in the excitation light or at least a step change in the form of short intense pulses separated by long dark periods (pulsed PT detection) or continuous train of pulses at nearly 50% duty cycle (continuous-modulated PT detection). The former detection scheme is in the 'time domain' where the PT signal magnitude and shape are recorded after the pulse excitation, whereas the latter detection scheme is typically in the 'frequency domain' where the PT signal magnitude and phase are measured by 'lock-in detection' with respect to the excitation.^[235]Detection methods for various PT effects are summarised in *Table 1.4*.

PT experiments can lead to quantitative results for various applications such as:^[242]

- ❖ Spectroscopy (absorption coefficients);
- ❖ Thermal measurements (diffusivity, effusivity, etc.);
- ❖ Transport properties (carrier diffusivity, spectral dimension, etc.);
- ❖ Geometrical parameters (thickness, fractal dimension, etc.).

PT measuring techniques exploit the time dependent heat flow that takes place when a time varying heat source is applied to the sample. This can be appropriately realised either by periodical laser heating or pulsed illumination. Both excitation techniques initiate propagating temperature oscillations, so-called thermal waves. PT measuring techniques are employed to detect subsurface structures inside opaque solids.^[243-245]

Table 1.4: Various photothermal (PT) effects and the corresponding detection techniques.^[235]

Photothermal effects	Detection methods (D/I)*
Temperature rise	Laser calorimetry (D/I)
Pressure change	Photoacoustic (PA) detection (D/I)
Refractive index change (thermal or acoustic)	Probe- beam refraction (D/I) Probe- beam diffraction (D/I) Thermal lens (D/I) Photothermal deflection-PTD (D/I) Other optical probes (D/I)
Surface deformation (thermal or acoustic)	Probe- beam deflection (D) Optical interference (D)
Thermal emission change	Photothermal radiometry (D)
Reflectivity/ absorptivity change	Transient thermal reflectance (D) Transient piezo-reflectance (D) Optical transmission monitoring (D/I)

*Note: D- direct PT detection, I- indirect PT detection.

H. Photoacoustics:

H1. Introduction:

Pressure variation or modulation resulting from the absorption of modulated light by a sample is usually referred to as PA or 'optoacoustic' generation. The name PA is preferred to optoacoustic to reduce confusion with the acousto-optic effect in which light interacts with acoustic or elastic waves in a crystal.^[246] PA generation mechanisms include electrostriction, thermo-elastic expansion, volume changes due to photochemistry, gas evolution, boiling or ablation, and dielectric breakdown.^[235] PA technique is a part of a class of PT effects, in which an impinging light beam is absorbed and alters the thermal state of the sample. This 'thermal state' can manifest itself as a change in temperature, density, or other measurable property of the sample. One method of detection is to measure the temperature or density of the absorbing material. This is referred to as '*thermometric detection*',^[247]

The absorbing sample warms and cools in a cycle if the incoming light is modulated. If the cycle is so fast that the sample does not have time to expand and contract in response to the modulated light, a change in pressure develops. This pressure 'wave' can lead to the production of a sound wave. These sound waves can be detected by a sensitive microphone, piezoelectric devices, or optical methods. These techniques are more properly called PA techniques.^[246]

Since PA measures the internal heating of the sample, it is clearly a form of calorimetry and a form of optical spectroscopy. Although a more appropriate name for the technique is photo-calorimetry, the term PA is used for this methodology whether it employs microphones or piezoelectric detectors. PA is, however, much more than spectroscopy. It is, after all, a photo-calorimetric method that measures how much of the electromagnetic radiation absorbed by the sample is actually converted to heat.^[246]

The magnitude of the acoustic signal depends on such properties of the sample as^[248]

- ☞ the absorption coefficient,
- ☞ the duration of the processes of conversion of absorbed radiation to heat,
- ☞ the thermo-physical properties, and
- ☞ the geometry.

The acoustic oscillations also acquire a certain phase shift relative to the incident modulated radiation, mainly because of a considerable time lag of heat transfer processes in comparison with the propagation of radiation.^[248]

H2. Photothermal spectroscopy:

PT spectroscopy is a group of highly sensitive spectroscopic techniques used to measure optical absorption and thermal characteristics of a sample based on the change in thermal state of the sample resulting from the absorption of radiation. This absorption leads to the heating of the sample. The heat raises temperature thereby influencing the sample thermodynamic properties. Measurements of the temperature, pressure, and/ or density changes that occur due to optical absorption are ultimately the basis for the PT spectroscopic measurements.

There are several methods and techniques used in PT spectroscopy. Each of these has a name indicating the specific physical effect measured.^[249]

- Photoacoustic spectroscopy (PAS) is an indirect method for measuring optical absorption. Indirect methods do not measure light transmission or emission but rather measure an effect of sample absorption. The term 'indirect' applies to the optical measurement, not the optical absorbance.
- PT lens spectroscopy measures the thermal blooming that occurs when a beam of light heats a transparent sample. It is typically applied for measuring minute quantities of substances in homogeneous gas and liquid solutions.
- Photothermal deflection (PTD) spectroscopy or the mirage effect measures the bending of light due to optical absorption. This technique is particularly useful for measuring surface absorption and for profiling thermal properties of layered materials.

- PT diffraction, a type of four wave mixing, monitors the effect of transient diffraction gratings 'written' into the sample with coherent lasers. It is a form of real-time holography.
- PT emission measures an increase in sample IR radiance resulting from absorption. Sample emission follows Stefan's law of thermal emission. These methods are used to measure the thermal properties of solids and layered materials.

The basic principle of PT spectroscopies is the detection of the heat produced in the sample due to non-radiative de-excitation processes resulting from the absorption of intensity-modulated light by the sample. All PT methods exploit the light-induced thermal wave signal which is proportional to the light-to-heat conversion efficiency, and thus they are complementary to other photo-induced energy conversion processes (e.g. photovoltaic and photo-galvanic).^[250] The fraction of incident chopped radiation, when absorbed by the sample, raises the molecules of the sample from the ground electronic state to the excited electronic state and the excited molecules relax to the ground state through non-radiative de-excitation, i.e. periodic heat emission.

H2.1. Photoacoustic spectroscopy:

PAS is the oldest form of PT spectroscopy.^[250,251] To get a quantitative spectrum of a sample, the wavelength of excitation is scanned and the corresponding magnitude of the acoustic signal normalised by the excitation pulse energy is measured to provide an 'excitation spectrum' called a PA spectrum.^[235] The PA spectrum complements the fluorescence excitation spectrum in that it responds to that part of the absorbed energy which is not radiated. The phase of the PA signal with respect to the phase of the input modulation can give information both on the lifetime of the excited state and on the heat energy transfer between the gas and walls of the chamber.^[252]

H2.2. Principle of photoacoustic spectroscopy:

When light of appropriate energy falls on a sample, absorption of the light can occur leading to excitation of molecules to higher energy states. The excited species have several options to return to the ground state:

- a) Emission of light and thus return to the initial state by luminescent decay.
- b) Utilisation of the energy for excited state photo-processes such as photochemical events or energy transfer.
- c) Dissipation of the extra energy through non-radiative means of relaxation and return to the ground state by the thermal de-excitation mode.

Of the three processes, the most common mode of de-excitation is the thermal one. The amount of heat released by the sample to its surroundings will be correspondingly less if either or both of the competing processes a) and b) were to occur.^[253]

In PAS^[241, 254-257] the irradiation of the sample contained in a closed gas cell produces temperature and pressure fluctuations in the gas synchronous with the modulated source signal. A microphone placed in the gas cell picks up these fluctuations. An associated amplifying system produces an electrical signal. The signal's amplitude and phase monitored over a range of wavelengths contain information about a wide range of optical phenomena.^[250] A recording of the pressure variations versus wavelength of illumination reflects the absorption spectra of the material.^[241] In PT spectroscopy, one records the variation in thermal emission from the object induced by irradiation.

The physics of PAS involves concepts in^[250]

- thermodynamics (internal energy, volume, temperature),
- optics (interference, absorption, Beer's law),
- heat (diffusion, conduction),
- acoustics (pressure wave propagation), and
- mechanics (viscosity and elasticity).

The experimental parameters obtainable are the magnitude, the phase angle, the in-phase and the quadrature components of the PA signal, while the variable parameters are scanning wavelength, modulation frequency, spectral bandwidth, and phase (of the phase sensitive detector in the PA channel).^[250]

The light from the source is intensity modulated, with angular modulation frequency $\omega = 2\pi f$, usually with a rotating blade chopper at frequency f , before entering the closed cell containing the sample so that $I = I_0 \sin \omega t$ (1.4)

$$I_t = I e^{-\beta t} \quad (1.5)$$

$$\begin{aligned} I_a &= I(1 - e^{-\beta t}) \\ &\approx I\beta c t \\ &= I_0 \beta c t \sin \omega t \end{aligned} \quad (1.6)$$

If the sample absorbs some of this light, a part of the absorbed energy will be degraded to random translational motion of the molecules: that is, heat, thus leading to a temperature rise in the cell. This temperature rise in a constant volume enclosure, has associated with it an increase in pressure, through the ideal gas equation $PV = nRT$

for n moles of gas. Thus, if the gas responds rapidly enough, the pressure in the cell changes in sympathy with the intensity modulations of the incident beam, thus producing a sound wave so as to produce PA signal $Q = Q_0 \sin \omega t$ (1.7)

and $Q_0 \propto I_0 \beta c l$. Rigorous theoretical treatment is outlined in 'I'. A microphone within the cell detects this sound and is usually followed by amplifiers and other processing electronics.^[252]

H3. Historical perspective:

The PA effect in both non-gaseous and gaseous matter was first reported by Alexander Graham Bell in 1880.^[258, 259] He demonstrated that the PA effect in solids was dependent on the absorption of light and that the strength of the acoustic signal was in turn dependent on how strongly the incident light was absorbed by the material in the cell. Bell called his device the 'photophone' since he discovered the effect whilst working on ideas for new telephones and experimenting with a voice modulated beam incident on a selenium detector. Later the phenomenon was termed as the PA effect and, when combined with a wavelength dispersed light beam, the 'photophone' has become the 'spectrophone' or PA detector. The earlier works on PA were done by Tyndall,^[260] Röntgen,^[261] Rayleigh,^[262] Preece^[263] et al. After the initial flurry of interest generated by Bell's original work, experimentation with PA effect apparently ceased.

The PA effect was completely dormant for nearly 50 years, until the advent of the microphone. Gorelik first proposed that measurement of the phase of the PA signal could be used to investigate the rate of energy transfer between the vibrational and translational degrees of freedom of gas molecules.^[264] This was experimentally proved by Slobodskaya and the use of PA effect to study the vibrational lifetimes of gaseous molecules quickly became an established technique.^[265] It was not until the early 1970s that the PA effect in nongaseous matter was 're-discovered' by Allen Rosencwaig and his co-workers at Bell Labs and provided a theoretical basis. The Rosencwaig- Gersho (RG) theory of the PA effect for a sample in PA cell (PAC) provided a comprehensive theoretical framework which led to the rapid development and application of the effect. This led to the invention of numerous other detection schemes and to the current widespread interest in PT science.^[246, 266]

After the official debut of PAS in 1973, the PAS has been developed to study those materials that are unsuitable for the conventional transmission or reflection methodologies.^[257, 267-269] PAS is different from the conventional techniques chiefly in

that even though the incident energy is in the form of optical photons, the interaction of these photons with the material under investigation is studied not through subsequent detection and analysis of some of the photons, but rather through the direct measurement of the energy absorbed by the material as a result of its interaction with the photon beam.^[236]

H4. Instrumentation aspects of photoacoustics:

The basic requirements of the PA detection technique are the following:^[236, 270]

- ◆ light source + focussing instruments (if needed)
- ◆ means of modulating light
- ◆ appropriate photoacoustic cell
- ◆ microphone and processing electronics

H4.1. The light source:

The modulated optical source is a common feature of all PT techniques and phenomena. The heating produced in all cases is non-stationary. There are two major classes of light sources that have been used for PA studies. These sources are arc lamps/ glow sources and lasers.

- 1) arc lamps/ glow sources have –
 - (a) broad wavelength output from UV to far IR
 - (b) fast modulation incapability
 - (c) made it necessary to use external spectral selection elements like monochromators to get tuneable wavelength
 - (d) low intensity
- 2) lasers have-
 - (a) high intensity
 - (b) narrow spectral line width
 - (c) modulation capability
 - (d) no need of focussing

The source beam is focused in many PT systems to provide high spatial resolution and/ or optical density.^[236]

H4.2. Modulation techniques:

Several methods have been employed to impose a temporal variation on the optical energy applied to a sample. The type of modulation can be:^[236]

1. periodic (sinusoidal or square wave);
2. transient (short, long or finite pulse);

3. frequency multiplexed (pseudo-random or frequency modulated);
4. spatially modulated (scanned or periodic).

The first three options impose a temporal variation on the optical beam at a stationary spot on a sample. The last option produces a modulation at the sample surface by moving the heated spot.^[236]

The simplest form of modulating the light is using a rotating slotted wheel placed in the path of the light beam. It offers 100% modulation depths for frequencies from a few Hz to 5-8 kHz. At higher frequencies, the mechanical vibrations and sound associated with the fast rotating blade of the chopper assembly has to be isolated acoustically from the PAC.

Electrical modulation is generally employed in gas discharge tubes. The electro-optic modulation involves the changing of the plane of polarisation of the incoming polarised laser beam in a non-linear crystal with the application of electric field on it. Acousto-optic modulation involves the spatial modulation of the laser by acoustic diffraction of the light in a crystal.

H4.3. Detection schemes:

PA signal detection techniques employ either a gas condenser microphone for the detection of the pressure variations in air or a piezoelectric transducer for the detection of thermo-elastic waves in solid media.^[236] The PAC will generally incorporate a suitable microphone with its preamplifier.^[271] The details of the PAC will be given later in 1.3.2.

H4.4. Signal processing:

For periodic modulation, phase-sensitive detection (lock-in-amplifier) can be utilised to process the detected signal. The technique is extremely efficient for extracting very weak signals contaminated along with noise.

H5. Advantages of photoacoustics: ^[247, 272]

- 1) It can be performed on all phases of matter.
- 2) Light that is transmitted, reflected or elastically scattered by the sample is not detected^[250, 251] as the absorption of the electromagnetic radiation is required for the PA signal production. Hence, these signals do not interfere with the inherently absorptive PA measurements. This is of crucial importance when one is working with essentially transparent media, such as pollutant-containing gases, that have few absorbing centers^[246] of the order of parts per trillion.^[273]

- 3) The insensitivity to scattered radiation also permits to obtain optical absorption data on highly light scattering materials.^[246]
- 4) It is non-destructive to the sample; the sample does not have to be dissolved in some solvent or embedded in a solid-state matrix. Samples can be used 'as is'.^[274]
- 5) Depth profiles of analytes can be performed in optically transparent media.
- 6) The PA effect results from a radiationless energy conversion process and is therefore a complimentary to radiative and photochemical processes.^[246]
- 7) PAS itself is a sensitive, though indirect method for studying the phenomena of fluorescence and photosensitivity in matter.^[246]
- 8) The basic simplicity of the experimental set up.
- 9) Optical absorption spectra of completely opaque materials can be obtained as PA does not depend on the detection of photons.^[246]
- 10) Non-destructive depth-profile analysis^[270] of absorption as a function of depth into a material can be performed, which is a unique advantage of the PAS.^[246]
- 11) Since the sample itself constitutes the electromagnetic radiation detector, no photoelectric device is necessary.^[246]
- 12) Studies over a wide range of optical and electromagnetic wavelengths are possible without the need to change the detector systems.^[246]
- 13) The feasibility of direct measurement of non-radiative lifetimes.
- 14) The ability to gather information from sub-surface layers.
- 15) The scope to obtain information on thermal parameters of the sample.^[270]
- 16) PA can be applied to samples which are difficult to examine by conventional spectroscopic methods.^[251]
- 17) Determination of absolute quantum yields by employing calorimetric techniques which are free from the geometrical correction problems of optical methods.^[251]
- 18) Measurement and detection of absorption coefficient of weakly absorbing or opaque and diffuse materials – cases in which straight photoelectric measurement is not possible.^[250]
- 19) PA spectrum complements the fluorescence excitation spectrum.
- 20) An increase in S/N ratio with increase in input power.^[236]
- 21) Requires minimal sample preparation.^[236]
- 22) Operation in hostile environmental conditions.^[236]
- 23) Non-contact and the potential for remote sensing.^[236]
- 24) Can be used to determine a very wide range of absorption coefficient magnitudes- 10^{-3} to 10^5 m^{-1} .^[236]
- 25) Investigation of non-radiative relaxation processes.^[270]

H6. Limitations of photoacoustics:

1. The source should be sufficiently energetic (at least $10 \mu\text{W cm}^{-2}$).^[246]
2. The windows of PAC should be reasonably transparent to the radiation.^[246]

There are a number of limitations to high sensitivity of PA systems.^[270]

- 1) The background signal arises due to:
 - (a) misalignment of the light beam into the cavity and subsequent interaction of the radiation with the walls
 - (b) diffraction and scattering at the input elements like diaphragm, edge of the chopper blades etc.
 - (c) acoustic noise that can arise from ambient acoustic noise, building vibration and the vibrations of the mechanical chopper.
- 2) Brownian motion or thermal fluctuation of the gas in the PAC produces noise.
- 3) The electronic noise is mainly due to the microphone, its related electronics and the pick-up due to the cables.
- 4) External noises like source and chopper fluctuations can affect the sensitivity of the PAC.

H7. Applications of photoacoustics:^[275]

With its various spectroscopic and non-spectroscopic attributes, PA has already found many important applications in the research and characterization of all type of materials, inorganic, organic, biological, and on all three states of matter^[247] PA is particularly useful for samples that are powdered (like catalysts), amorphous, or otherwise not conducive to reflective or transmission forms of optical spectroscopy.

Some of the applications of the PA are listed below.

◇ The measurement of optical absorption spectra.

1. Quantitative evaluation of the optical quality of different materials.^[276]
2. Band shapes of PA spectra of transparent solids doped with localised absorbing centres.^[277]

◇ The characterization of non-radiative relaxation processes in solids.

Since the PA signal is sensitive only to the heat deposited in the sample, any absorbed energy which is re-radiated as fluorescence does not contribute to the signal. Therefore PA provides information concerning the balance between radiative and non-radiative relaxation processes in solids.

1. Use of PA to qualitatively infer the existence of levels with strong non-radiative decay channels.^[276, 278]

2. The measurement of absolute quantum efficiencies in solids^[253] by
 - A.) concentration quenching^[279]– absolute quantum efficiencies of some localised centres in solids^[279-281] and
 - B.) chopping frequency dependence of the PAS^[282]
3. The PA response of a multilevel luminescent system, both in frequency^[283] and time^[284] domains.
 - ◇ Optical absorption coefficient measurement.^[246, 266, 267]
 - ◇ Geophysics, solid state electronics, optics and material science.^[250]
 - ◇ Optical characterization of thin films,^[285] thick films, crystalline, and amorphous semiconductors.^[250]
 - ◇ Determination of thermal diffusivity (TD) of solids.^[250]
 - ◇ Investigations of phase transitions.^[250]
 - ◇ Study of metals and ceramic materials.^[250]
 - ◇ Analysis of particulate matter for their applications to in-stream measurements of powder characteristics.^[286]
 - ◇ Application to biological materials,^[253, 287-289] gases,^[252, 290] biology and medicine,^[291] imaging or PA microscopy.^[292]
 - ◇ Spectroscopic measurements^[246]
 - 1) Measurement of absorption or excitation spectrum.^[246]
 - 2) Excited state lifetime measurements.^[246]
 - 3) The energy yield of radiative processes.^[246]
 - ◇ Applications arising from the calorimetric or acoustic aspect^[246]
 - 1) Measurement of thermal and elastic properties of materials^[246]
 - 2) Study of chemical reactions
 - 3) Thickness measurement of layers and thin films
 - 4) Performance of a variety of other non-spectroscopic investigations.

I. Rosencwaig- Gersho (RG) theory:^[266]

11. Introduction:

The theory of the gas-microphone PA detector was developed in stages. The importance of heat flow from the solid to the gas was identified by Parker.^[293] Rosencwaig and Gersho^[266] proposed a one-dimensional model that attributed signal generation to the action of the heated layer of the gas at the surface of the sample. This 'thermal piston' model successfully describes the dependence of the PA signal on acoustic frequency, the optical and thermal properties of the sample, and the thermal

properties of the gas.^[294] Effects of thermal expansion of the solid- 'mechanical piston' effects- can be important for thick samples of weak absorbers.^[295]

In PA effect- essentially an energy-conversion process- the radiant energy absorbed by the sample is converted into kinetic energy of the gas molecules within the solid which is transferred as heat through the solid-gas boundary, eventually resulting in the PA signal.^[250] The gas present in the cell behaves as a passive coupling agent between light and the solid and it does not contribute to the final acoustic signal. Nor does the adsorbed gas lying just over the surface of the solid- the solid-gas interfacial layer- seem to give rise to the PA signal.^[250, 268]

The PA effect is a non-equilibrium transport process.^[296] The PA effect in solids may be modelled by a 'reservoir 1- system- reservoir 2' configuration in which the sample is the first reservoir, and the system is the sample-gas interface (really extending up to the microphone), while the microphone could be regarded as the second reservoir. Energy transport takes place via particle transport (which is via gas molecules), the driving forces for the two intimately connected processes being the temperature and the chemical gradients (the former is also time dependent). Thus, all the three important thermal properties: thermal conductivity, thermal diffusivity, and viscosity seem to control the PA effect in a complicated manner.^[250, 296]

The RG theory shows that the PA signal depends both on the generation of an acoustic pressure disturbance at the sample- gas interface and the transport of this disturbance through the gas to the microphone. The generation of the surface pressure disturbance depends in turn on the periodic temperature at the sample- gas interface. The RG theory derived exact expressions for this temperature, while it treated the transport of the disturbance in the gas in an approximate heuristic manner, which is, however, valid for most experimental conditions.^[250]

12. The thermal diffusion equations:

Light absorbed by a solid is converted, in part, or in whole into heat by non-radiative de-excitation processes within the solid. Consider that the PAC (*Figure 1.12*) has a diameter D and length L . The sample is considered to have a diameter D and thickness l_s and is mounted such that its back surface is against a poor thermal conductor of thickness l_b . The length l_g of the gas column in the cell is $l_g = L - l_s - l_b$ (1.8)

The following assumptions are made in framing the thermal diffusion equations:

- L is small compared to the wavelength of the acoustic signal.
- The microphone detects the average pressure produced in the cell.
- The gas and the backing materials are not light absorbing.
- A sinusoidally chopped monochromatic light with wavelength λ is incident on the sample.
- The dimensions of the cell are small enough to ignore convective heat flow in the gas at steady-state conditions.
- The temperature relative to ambient is zero at the ends of the cell.

The parameters defined in the development of RG theory are:

κ_j -thermal conductivity of the material j ($\text{Wm}^{-1}\text{K}^{-1}$)

ρ_j -density of the material j (kg m^{-3})

$\alpha_j = \kappa_j / \rho_j C_j$ -thermal diffusivity (TD) of the material j (m^2s^{-1})

$a_j = (\omega / 2\alpha_j)^{1/2}$ -thermal diffusion coefficient of the material j (m^{-1})

$\mu_j = 1 / a_j$ -thermal diffusion length of the material j (m)

where j can be s , g and b for the solid, gas and backing material respectively.

$\omega = 2\pi f$ the angular chopping frequency of the incident light beam (radians per s) and f is the chopping frequency (Hz).

I_0 - the incident monochromatic light flux (Wm^{-2}).

β - optical absorption coefficient of the sample for the wavelength λ (m^{-1})

The intensity of the light incident on the sample $I = \frac{1}{2} I_0 (1 + \cos \omega t)$ (1.9)

The heat density produced at any point x , due to light absorbed at this point in the

solid is $\frac{1}{2} \beta I_0 e^{-\beta x} (1 + \cos \omega t)$

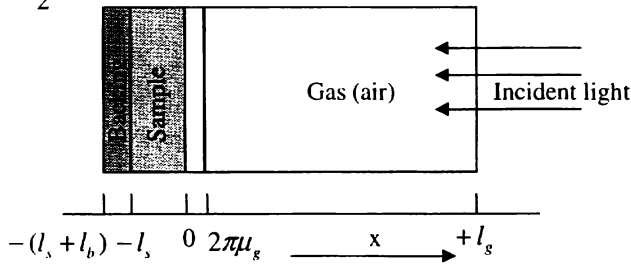


Figure 1.12: cross sectional view of a simple cylindrical photoacoustic cell (PAC).

The thermal diffusion equations are

$$\frac{\partial^2 \theta}{\partial x^2} = \frac{1}{\alpha_s} \frac{\partial \theta}{\partial t} - A e^{\beta x} (1 + e^{i\alpha}) \quad \text{for } -l_s \leq x \leq 0 \quad (\text{sample}) \quad (1.10)$$

$$\frac{\partial^2 \theta}{\partial x^2} = \frac{1}{\alpha_b} \frac{\partial \theta}{\partial t} \quad -l_b - l_s \leq x \leq -l_s \quad (\text{backing}) \quad (1.11)$$

$$\frac{\partial^2 \theta}{\partial x^2} = \frac{1}{\alpha_g} \frac{\partial \theta}{\partial t} \quad 0 \leq x \leq -l_g \quad (\text{gas}) \quad (1.12)$$

where, θ is the temperature, $A = \frac{\beta I_0 \eta}{2\kappa_s}$ (1.13)

and η - efficiency at which the absorbed light at wavelength λ is converted to heat by the non-radiative de-excitation processes. For most solids at room temperature $\eta=1$.

The real value of the complex valued solution $\theta(x,t)$ represents the temperature in the cell relative to the ambient temperature as a function of position and time. The actual temperature field in the cell is $T(x,t) = \text{Re} \theta(x,t) + T_0$ (1.14)

where T_0 -the ambient temperature and Re denotes the 'real part'.

13. Temperature distribution in the cell:

The general solution for $\theta(x,t)$ in the cell neglecting the transients

$$\theta(x,t) = \begin{cases} \frac{1}{l_b} (x + l_s + l_b) W_0 + W e^{\sigma_b(x+l_s)} e^{i\alpha t}, & -l_b - l_s \leq x \leq -l_s, \\ b_1 + b_2 x + b_3 e^{\beta x} + (U e^{\sigma_s x} + V e^{-\sigma_s x} - E e^{\beta x}) e^{i\alpha t}, & -l_s \leq x \leq 0 \\ \left(1 - \frac{x}{l_g}\right) F + \theta_0 e^{-\sigma_g x} e^{i\alpha t}, & 0 \leq x \leq -l_g \end{cases} \quad \dots(1.15)$$

where W , U , V , E and θ_0 are complex-valued constants, b_1 , b_2 , b_3 , W_0 and F are real-valued constants, and $\sigma_j = (1+i)\alpha_j$. θ_0 and W represent the complex amplitudes of the periodic temperatures at the sample-gas boundary ($x=0$) and the sample-backing boundary ($x=-l_s$). The quantities W_0 and F denote the dc component of the temperature (relative to ambient) at the sample surfaces $x=-l_s$ and $x=0$, respectively.

The complex amplitude of the periodic temperature at the solid-gas boundary ($x = 0$) is given by

$$\theta_0 = \frac{\beta I_0}{2\kappa_s(\beta^2 - \sigma_s^2)} \left\{ \frac{(r-1)(b+1)e^{\sigma_s l} - (r+1)(b-1)e^{-\sigma_s l} + 2(b-r)e^{-\beta l}}{(g+1)(b+1)e^{\sigma_s l} - (g-1)(b-1)e^{-\sigma_s l}} \right\} \quad (1.16)$$

where,

$$b = \frac{\kappa_b a_b}{\kappa_s a_s} \quad (1.17)$$

$$g = \frac{\kappa_g a_g}{\kappa_s a_s} \quad (1.18)$$

$$r = \frac{(1-i)\beta}{2a_s} \quad (1.19)$$

The actual temperature at $x = 0$ is given by

$$T(0, t) = T_0 + F_0 + \theta_1 \cos \omega t - \theta_2 \sin \omega t \quad (1.20)$$

where F_0 is the increase in temperature owing to the steady-state component of the absorbed heat. θ_1 and θ_2 are the real and imaginary parts of the complex number θ_0 which determine the in-phase and quadrature components of the periodic temperature variation at the surface $x = 0$ of the sample.

14. Production of the acoustic signal:

The periodic diffusion process produces a periodic temperature variation in the gas as given by the sinusoidal (ac) component of the solution θ

$$\theta_{ac}(x, t) = \theta_0 \exp(-\sigma_g x + i \omega t) \quad (1.21)$$

Taking the real part, the actual physical temperature variation in the gas is

$$T_{ac}(x, t) = e^{-a_g x} \{ \theta_1 \cos(\omega t - a_g x) - \theta_2 \sin(\omega t - a_g x) \} \quad (1.22)$$

The time dependent component of the temperature in the gas attenuates rapidly to zero with increasing distance from the surface of the solid. At a distance of only $2\pi\mu_g$, the periodic temperature variation in the gas is effectively fully damped out. This thickness of gas is capable of responding thermally to the periodic temperature at the surface of the sample.

The periodic heating of the boundary layer expands and contracts it periodically; making to act as an acoustic piston on the rest of the gas column. This produces an acoustic pressure signal that travels through the entire gas column. If this response is adiabatic, the acoustic pressure in the cell is derived from the adiabatic gas law

$$PV^\gamma = \text{constant.} \quad (1.23)$$

where P is the pressure, V is the gas volume in the cell and γ is the ratio of the specific heats.

The complex envelope of the sinusoidal pressure variation is given by

$$Q = \frac{\beta I_0 \mathcal{P}_0}{2\sqrt{2}\kappa_g l_g a_g T_0 (\beta^2 - \sigma_g^2)} \left\{ \frac{(r-1)(b+1)e^{\sigma_g l} - (r+1)(b-1)e^{-\sigma_g l} + 2(b-r)e^{-\beta l}}{(g+1)(b+1)e^{\sigma_g l} - (g-1)(b-1)e^{-\sigma_g l}} \right\} \quad (1.24)$$

where P_0 , T_0 is the ambient pressure. This equation is evaluated for the magnitude and phase of the acoustic pressure wave produced in the cell by the PA effect.

15. Special cases:

The earliest theory of the PA effect- RG theory¹²⁶⁶¹- developed an analytical expression for the PA signal in terms of (i) the variations of the gas pressure $\Delta P(t)$ as a function of time, as the ultimate consequence of the interrupted illumination of the sample which results in the propagation of a temperature wave from the sample surface, and (ii) characteristic parameters of the different media, the solid, the material backing it, and the gas which couples the solid to the detector.

$$\Delta P(t) = \frac{\mathcal{P}_0 \theta \mu_g}{\sqrt{2} l_g T_0} \exp \left[i \left(\omega t - \frac{\pi}{4} \right) \right] \quad (1.25)$$

One defines optical transparency or opacity from a comparison of the optical absorption length and the sample thickness. Likewise, a sample is defined as thermally thin or thick depending on the relative values of the thermal diffusion length and the sample thickness. The reciprocal of the absorption coefficient and represents the distance into the sample to which the photon penetrates before its intensity is reduced to 1/e of its initial value. The thermal diffusion length of the sample is related to its thermal properties and is a measure of the distance that the released heat diffuses from the point of its generation before it is attenuated to 1/e of its initial value.¹²⁵³¹

In the one-dimensional heat conduction model of the RG theory the acoustic signal is supposed to arise primarily from the periodic heat flow from the solid to the surrounding gas as the solid is cyclically heated by the chopped light. This heat is generated by light absorbed by the sample and subsequent, predominantly non-radiative, de-excitation processes within the sample. The three important physically measurable 'lengths' in the PA effect are sample thickness l_s , optical absorption

length $l_\beta = 1/\beta$, and thermal diffusion length μ_s on the relative magnitudes of which arise the various cases of practical interest:

A. Optically transparent solids ($l_\beta > l_s$) in which light is absorbed throughout the sample length and some light is transmitted: (Figure 1.13a)

- (i) thermally thin ($\mu_s \gg l_s$ and $\mu_s > l_\beta$), the acoustic signal is proportional to ω^{-1} , or
- (ii) thermally thin but with $\mu_s > l_s$ and $\mu_s < l_\beta$; even now the signal varies as ω^{-1} . However, when $\mu_s \gg l_s$, the thermal properties of the backing material come into play;
- (iii) thermally thick ($\mu_s < l_s$ and $\mu_s \ll l_\beta$); the signal is proportional to $\beta\mu_s$, and, although light absorbed within the first thermal diffusion length μ_s contributes to the signal; when $\mu_s < l_s$, thermal properties of the backing material are unimportant.

The signal is proportional to $\omega^{-3/2}$.

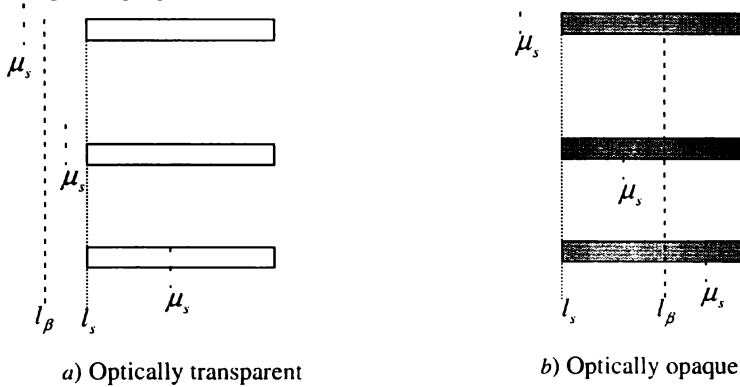


Figure 1.13: Schematic representation of special cases for the photoacoustic (PA) effect in optically a) transparent solids, b) opaque solids.

B. Optical opaque solids ($l_\beta \ll l_s$) wherein practically no light is transmitted. (Figure 1.13b)

- (i) thermally thin samples ($\mu_s \gg l_s, \mu_s \gg l_\beta$) with both optical and photoacoustic opaqueness, where the signal is independent of β . A strong signal depending upon the thermal properties of backing material and varying as ω^{-1} results.

(ii) thermally thick solids ($\mu_s < l_s, \mu_s > l_\beta$); thermal properties are those of the solid but the signal is still independent of α and varies as ω^{-1} ;

(iii) thermally thick solids but with $\mu_s \ll l_s, \mu_s < l_\beta$; optically very opaque but photoacoustically not opaque (since $\mu_s < l_\beta$); the signal depends on thermal properties of the solid and varies as $\omega^{-3/2}$.

I6. Importance of RG theory:¹²⁴⁶¹

The RG theory predicts that the PAS is always linearly proportional to the power of the incident photon beam, and that this dependence holds for any sample or cell geometry and this is experimentally verified.

When the thermal diffusion length in the sample is greater than the optical absorption path length, the PAS is independent of optical absorption coefficient of the sample. Since the thermal diffusion length μ_s can be changed by changing the chopping frequency ω , it is possible to obtain the optical absorption spectra on all but most highly opaque solids. This capability of the PAS technique, together with its insensitivity to scattered light, makes its use as a spectroscopic tool for the investigation of solid and semisolid materials. These features give PA a unique potential for non-invasive in vivo studies of tissues, a potential that have important implications in biological and medical research and in medical diagnostics.

If one has a full knowledge of the thermal and geometrical parameters of the sample, one can obtain absolute values for the optical absorption coefficient by measuring the dependence of the PAS on modulation frequency.

J. Photothermal deflection (PTD):

J1. Introduction:

In 1979, Boccara et al. proposed and demonstrated¹²⁹⁷¹ that PT beam deflection (PTD) or *mirage effect* can be advantageously used for monitoring the temperature gradient field close to a sample surface or within the bulk of a sample.¹²⁴²¹ This technique was found to be sensitive and very simple to set up. It is based on the measurement of the time dependent beam deflection, which can be computed for various kinds of probe beams. The mirage effect is sensitive to the gradient of temperature averaged along a line parallel to the probe beam.¹²⁹⁸¹ The calculation of the mirage effect is more complicated for three reasons:¹²⁹⁸¹

- (1). The method is essentially three dimensional.
- (2). The detection destroys the axial symmetry of the pump beam generally used.
- (3). The calculation needs the derivatives of the temperature with respect to the spatial coordinates.

J2. Limitations:

The difficulty with PTD localisation is precisely the difficulty of obtaining a probe beam that is small compared with the scale of imaging detail desired. As the probe must pass over the entire sample, it cannot be highly convergent without interference with the sample surface. One is then limited to the probe diameters of the order 50-100 μ m at the pump position even though one possibly desires to detect defects much smaller in size.^[245] Moreover, the sample surface must be reasonably flat, so that the probe can skim the surface.^[299]

J3. Advantages:

- o Vertical cracks may be detected using PTD,^[300,301]but not with PA.^[245]
- o Direct TD measurement can be performed with high degree of accuracy.^[299]
- o It requires neither contact with the sample nor thermometry.^[299]
- o Only one surface of the sample needs to be accessible.^[299]
- o The measurement is inherently local so that measurement of non-uniform or small samples can be made.^[299]
- o The diffusivity can be measured in different orientations on anisotropic materials simply by rotating the probe-beam direction.^[299]
- o It provides a simple, non-destructive and in situ measurement of TD.^[302]

For materials that have a layered structure, the frequency dependence of the mirage signal can be exploited to provide more detailed information other than TD, such as the thickness of a thin film or the relative thermal effusivity (TE) at the interface.^[302]

K. Thermal property determination by photothermal techniques:

K1. Introduction:

There is an undiminishing demand for reliable measurements of the basic thermal properties of the vast range of materials in use today. The determination of the thermal properties has become an attractive, important and well established application of PT science because the PT techniques combine the non-contact application of well defined amounts of thermal energy with methods for the determination of the resulting temperature changes. The temperature changes employed in a property determination

can be very small because of the very high sensitivity detection techniques that have been developed in the PT sciences. A material's PT response depends on the two parameters: TD and TE. Consequently, these are the thermal properties that can be obtained by PT methods rather than the primary quantities such as thermal conductivity and specific heat.^[302]

K2. Thermal diffusivity (TD): (α)

TD is a physical parameter, the measurement of which provides both direct and indirect information on materials of industrial interest.^[303] This thermo-physical property is defined as

$$\alpha = k / \rho C . \quad (1.26)$$

TD is the ratio of thermal conductivity k and volumetric heat capacity (VHC) or thermal capacitance ρC where the latter is the product of density ρ and specific heat capacity C . TD indicates the rate at which heat is distributed in a material. This rate depends not only on the thermal conductivity but also on the rate at which energy can be stored. This thermal transport parameter determines the rate of heat diffusion in the medium. Thus, TD is an indication of the speed with which an unstable temperature distribution has become stable.^[270] TD is a pertinent parameter of a PT experiment.^[304]

VHC describes the ability of a given volume of a substance to store internal energy while undergoing a given temperature change, but without undergoing a phase change. It is different from specific heat capacity in that the VHC depends on the volume of the material, while the specific heat is based on the mass of the material. If given a specific heat value of a substance, one can convert it to the VHC by multiplying the specific heat by the density of the substance.^[305]

Both frequency and time domain PT techniques can be used for TD evaluation. The measurement is based on the detection of a phase or time delay in PT response with respect to the applied thermal excitation. These non-stationary heat flow techniques have gained acceptance because they are less affected by heat losses, which are difficult to quantify, than a stationary heat flow technique.

The TD is a dynamic thermal property which characterises heat conduction inside a material under non-stationary conditions. This characteristic makes this thermal property essential for the study and modelling of thermal processes.^[306, 307] TD is a parameter that governs heat flow. If a material is subjected to heat input that varies

over time. TD describes how the heat 'spreads out' in between the changes in heat input. The rate of the heat flow, and hence how deep the changes in the temperature at the surface penetrate, depends on TD.¹³⁰⁸¹

The thermal characteristics of a solid have a predominant influence on its PA signal. TD determines the rate of transient (or unsteady) state heat flow through a solid and thus is useful in the calculation of thermal conductivity.¹²⁵⁰¹ This parameter governs the ease of glass formation by rapid quenching of metallic alloys. Microscopically, TD represents the dynamical aspect of the heat conductivity of carriers, and in the kinetic theoretical framework, is proportional to the mean free path of carriers. Thus, from TD and its temperature dependence one can deduce the mechanism of carrier scattering. The higher the TD of a solid, the higher is the rate of temperature propagation.¹²⁵⁰¹

K3. Thermal effusivity (TE): (e)

Thermal inertia or TE of a material is the square root of the product of the material's bulk thermal conductivity and VHC. Thermal inertia is a measure of the thermal mass and the velocity of the thermal wave which controls the surface temperature of a material. In heat transfer, a higher value of the VHC means a longer time for the system to reach equilibrium. Thermal inertia is a term commonly used by scientists and engineers modelling heat transfers¹³⁰⁹¹ and is a bulk material property related to thermal conductivity and VHC. SI units of thermal inertia are $\text{Jm}^{-2}\text{K}^{-1}\text{s}^{-1/2}$ and also occasionally referred to as Kieffers,¹³¹⁰¹ or more rarely, tiu.¹³¹¹¹ As the name implies, thermal inertia represents the ability of a material to conduct and store heat.

TE measures the thermal impedance of the material. It is the ability of the sample to exchange heat with the environment and hence it is an important parameter for surface heating and cooling processes. TE is a surface property¹³¹²¹ which is defined as

$$e = \frac{k}{\sqrt{\alpha}} = \sqrt{k\rho C} \quad (1.27)$$

Powders would have different effusivity readings depending on their ability to transfer heat through and between their particles. This is also a function of the particle size, shape, density, and moisture of the material. Therefore, one can expect that any change in one of these parameters should result in change of the TE value.¹³¹³¹

The ability of a material to exchange its thermal energy with surroundings is essentially determined by its TE. Its importance lies not only on the thermal exchange

characteristics, but also on its utility in making complete thermo-physical property of materials.^[314] Knowing the value of the TE is useful in calculating the heat accumulation capacity of materials in a transient state.^[315, 316] Both the thermal conductivity and the TE of composite materials depend upon various parameters, such as the thermal properties of the constituent phases, and micro-structural parameters including the volumic fraction of each phase, the shape of the particles, the size, the size distribution of the particles and so on.

TE characterises the thermal contact of two samples.^[304] TE is a heat transfer property that determines the interfacial temperature when two semi-infinite objects at different temperatures touch. The effusivity of materials varies due to their differing ability to transfer heat. This is due to differences in heat transfer through and between particles. Powders have effusivities that are strongly correlated with their moisture content. In conclusion, TE characterises the transient thermal behaviour that occurs when two materials are brought into contact with each other.^[317]

1.2.4. Part D: Fluorescence and absorption:

L1. Introduction:

Optical spectroscopy is a powerful tool to study the non-occupied electronic states of optically active ions containing unpaired electrons when they are embedded in condensed phase media.^[318] In the case of RE ions, it provides information about the interaction between the metallic central ion and its environment through 'nephelauxetic effect' that determines the relative spatial extension of the f-orbitals and subsequently the overlapping with the ligand valence orbitals.

L2. Absorption spectroscopy:

The electronic excitations between two energy levels cause absorption.^[319] In absorption spectroscopy, the attenuation of the transmitted light is monitored to determine the absorption coefficient or the number density of absorbing species. For small absorptions this means the measurement of a small difference of two large quantities, which limits, the signal to noise ratio.^[273]

L3. Fluorescence:

Light produced by illuminating a compound with UV radiation is known as '*photoluminescence*' (PL). Fluorescence is distinguished from other types of PL by the fact that the excited molecule returns to the ground state immediately after excitation,

the time spent in the excited state being typically of the order of 10^{-8} s. Fluorescence is the spin allowed transition. The luminescent mineral consists of a host lattice and a luminescent center, called an 'activator'.^[320]

Although the 0, 0 transition gives rise to a band in both the fluorescence excitation and emission spectra, its wavelength may not in fact be identical in both spectra. A small displacement to longer wavelength is usually observed in the emission spectrum due to stoke's shift arising out of the interaction between the fluorescent solute molecules and molecules of the solvent. In a solution the solvent molecules distribute themselves around the solute molecules in a way which leads to the greatest stability for the system. The greatest stability corresponds to the minimum energy.^[320]

L4. Fluorescence excitation spectroscopy:

The excitation spectrum directly reflects the absorption spectrum with respect to the line positions.^[273] It is still useful to measure the absorption lines with extremely high sensitivity, although their relative intensities may not be recorded accurately. Excitation spectroscopy has its highest sensitivity in the visible, UV and NIR regions at low molecular densities.^[273]

L5. Laser induced fluorescence (LIF):

LIF is spontaneous emission from atoms or molecules that have been excited by laser radiation. Two radiative transitions are involved in the LIF process. First, absorption takes place, followed by a photon-emission step.

LIF has a large range of applications in spectroscopy.^[273]

- LIF is a dominant laser spectroscopic technique in the probing of unimolecular and bimolecular chemical reactions.
- LIF serves as a sensitive monitor for the absorption of laser photons in fluorescence excitation spectroscopy.
- It is well suited to gain information on molecular states if the fluorescence spectrum excited by a laser on a selected absorption transition is dispersed by a monochromator.
- The spectroscopic study of collision processes.
- Application to the determination of the internal state distribution in molecular reaction products of chemical reactions.

The emission and absorption spectra bear a 'mirror image' relationship to each other. The emission spectrum is obtained by irradiating the sample at the wavelength of maximum absorption and observing the emitted fluorescence with a scanning monochromator which gives a plot of intensity versus wavelength.

1.3. Section III –Measurements:

1.3.1. Part A: Light sources:

M1. Argon ion laser:

LiCONiX® 5300 series water cooled argon ion laser with TEM₀₀ transverse mode and beam diameter 1.3 mm was used as the excitation source in the TD measurement using PT studies. 488 nm output from model 5302A laser has power stability of $\pm 0.5\%$ under light regulation and $\pm 3.0\%$ under current regulation. Forced air cooled 5000PS power supply was used to provide the power to the laser system. The laser system can be operated with an ambient air temperature of 10 to 35 °C and the optimum air temperature is 22 ± 2 °C. LiCONiX® 60HE heat exchanger is used in the water cooling system.^[321]

M2. Pulsed Nd: YAG laser:

355 nm output from model LAB 170, Spectra-Physics Quanta-Ray GCR-170 pulsed Nd: YAG laser is used for the PL studies of RETs. The GCR-170 model has a repetition frequency of 10Hz with maximum output energy of 240 mJ. The harmonic generator of the laser is a KD*P crystal.^[322]

M3. Xenon arc lamp:

1000W ozone free Newport model 6271 xenon lamp was used for the PAS studies. The lamp has the ORIEL model 8540 arc lamp power supply and model 66021 ORIEL universal arc lamp housing. The model 8540 is compact, light weight, constant wattage and regulated power supply with a drive circuit for external ignitors and lamp housings with internal ignitors.^[323]

M4. Mode-locked Ti: sapphire laser:

Model 3941 mode-locked *Tsunami*® laser uses Ti: sapphire laser medium. The laser head contains the Ti: sapphire rod and the optics that form the resonator cavity. Broadband femto second performance is obtained from a *Tsunami*® laser when pumped by a 532 nm Millennia Pro-5sJ laser to give an average power output of 700mW near 790 nm. The pulse width is <100 fs with a peak power >85 kW.^[324]

M5. Diode pumped solid state (DPSS) laser:

Micro DPSS laser model BWT-50 (B&W) at 532 nm was also used in PA studies. BWT series are miniature diode-pumped Nd: YVO₄ lasers with integrated internal thermoelectric cooler. They can be operated over a temperature range of -10 to 50 °C. It has TEM₀₀ mode with a spectral line width <0.1 nm and a beam size of 1 mm.^[325]

M6. He- Ne laser:

JDS Uniphase He- Ne gas laser emitting at 633 nm with 4 mW power was used as the probe beam in PTD studies.

1.3.2. Part B: Photoacoustic cell (PAC):^[236]

N1. Introduction:

The PAC monitors the temperature changes in the sample, produced by its absorption of optical energy. The cell is a small gas- tight enclosure with a sensitive acoustic microphone built into one wall. Sample temperature changes cause pressure variations in the enclosed gas that are converted to an electrical signal by the microphone. The light incident on the sample is modulated by a mechanical light chopper. The resulting sample heating is periodic and causes a periodic pressure change in the enclosed gas which is converted by the microphone into an ac electrical signal that may be processed using low noise narrow bandwidth techniques. The PAC has proved to be a very sensitive, though indirect, means of detecting the sample temperature changes caused by the PT effect. Many geometric and optical arrangements for the sample chamber, optical source and microphone can be conceived.^[290]

N2. Standard photoacoustic cell:

The standard PAC configuration has a solid sample in a small, gas filled cell, a window above the sample through which a modulated beam is incident, and a microphone in the main gas chamber. Parker^[293] and Rosencwaig and Gersho^[266] showed that periodic heat flow between the sample and gas is the basic mechanism causing a pressure variation in the gas.^[245]

N3. Designing aspects of photoacoustic cell:

While designing a PAC the following aspects are to be considered:^[270]

1) Proper acoustic shielding from the ambient atmosphere. - This can be done with good acoustic sealing, rather thick walls and acoustic isolation of the cells from vibrations in the laboratory.

For the study of solid samples, a simple and sensitive open PAC (OPC), indigenously designed, was used. In conventional OPC the sample is placed directly on top of the microphone, by leaving a small volume of gas in between the two.^[328-330] Such OPCs can be employed only in the heat transmission configuration. However, the design of the OPC fabricated for the present studies allows one to illuminate the sample from both sides, i.e. it can be used either as an OPC or as a conventional PAC. In order to achieve this goal the microphone is kept in a side chamber and is acoustically coupled to the main chamber through a small cylindrical cavity. The cross-sectional view of the cell is shown in *Figure 1.14*. When the sample is irradiated through the glass window, it is known as the reflection configuration. In the transmission configuration, irradiation has to be made at the rear surface of the sample.^[331]

The major building block of the cell is an acrylic (perspex) disc of thickness 1 cm and diameter 5.5 cm. The acoustic chamber was made by drilling a bore of diameter 3 mm across the thickness at the centre of the disc. One end of this cylindrical hole was closed with an optical quality glass slide of thickness 1.4 mm and the other end was left open. Another fine bore of diameter 1.5 mm pierced at the middle of the main chamber and perpendicular to it served as the acoustic coupler between the main chamber and the microphone. At a distance of 8 mm from the main chamber the microphone was firmly glued to the orifice of the side tube. Shielded wires were used to take the electrical connections directly from the microphone. Plate-like solid samples having uniform surface quality can be easily stuck at the open end of the sample chamber by using vacuum grease.

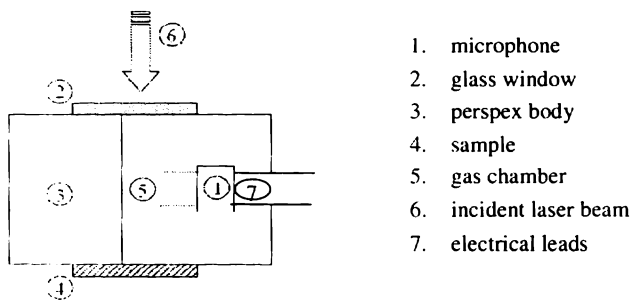


Figure 1.14: Cross sectional view of the open photoacoustic cell (OPC).

- 2) Minimisation of unwanted signals due to interaction of the excitation light with cell walls, windows and microphone. - The material of the cell elements both walls and windows should be able to produce a maximum signal and to suppress background signals. Windows should be chosen with minimum absorption and large enough so that the scattered radiation can be reflected back from the cell. To reduce the background signals from the walls it is necessary to choose highly reflecting or highly transparent materials. Besides, all the inner surfaces must be clean to eliminate the possibility of background signals from surface impurity.
- 3) Proper configuration and placement of microphone and sample. - To eliminate the influence of scattered radiation on the microphone, it should be located next to the cell chamber and connected by an acoustic channel. To overcome undesirable loss of sensitivity, the volume near the microphone and the volume connecting the acoustic channel should be minimised.
- 4) Means for maximising the signal from the PAC. - The maximum output signal is obtained when the gas column length in the cell is around the thermal diffusion length of the used gas. The acoustic signal can be enhanced by the use of gases with a lower thermal conductivity, high gas pressures and lower gas temperatures.
- 5) If needed, heating and cooling facilities for temperature variation of the cell.
- 6) The cell must be designed and operated to minimise the interaction between detector surfaces and the sample.^[326]

The PA signal is an average measurement of the local modulated temperature rise resulting from optical heating. The design of PAC needs to be optimised with regard to signal detection and noise minimisation. The principal noise components arise from environmental noises and secondary PA signal generation due to light absorption by the cell walls and windows. Other factors that may need consideration are: the acoustic response (resonances) of the cell; the type of material to be studied (solid, liquid or gas); the temperature range required and the modulation frequency range. The cell and the detection scheme can be designed to reduce the coherent noise sources. PA noise signals resulting from absorption in cell windows can be reduced by the use of acoustic baffles placed close to the cell windows. PA noise caused by optical absorption at the cell walls can be reduced by highly polishing them.^[236]

N4. Photoacoustic cell design:

Design and fabrication of PACs having high signal to noise ratio becomes very important in experiments.^[327] Many designs of PACs have been described in literature aiming at signal amplitude enhancement, noise reduction and ease of use.^[307]

1.3.3. Part C: Measuring instruments:

O1. Spectrophotometer:

JASCO V-570 UV/VIS/NIR Spectrophotometer was used for the absorption and reflectance measurements of the samples.

O1.1. Specifications:

Optical system: single monochromator. UV/ VIS region 1200 lines/ mm plane grating.

NIR region: 300 lines/ nm plane grating. Czerny –Turner mount double beam type

Resolution: 0.1 nm (UV/ VIS region) 0.5 nm (NIR region).

Light source: 30 W deuterium discharge tube in 190 to 350 nm region.

20 W tungsten iodine lamp in 330 to 2500 nm region.

Wavelength range 190 to 2500 nm.^[332]

The beam from the light source is converged and enters the monochromator. It is dispersed by the grating in the monochromator and the light passes out through the exit slit. This light is split into two light paths by a sector mirror, one incident on the sample to be measured and the other on the reference sample such as solvent. The light that has passed through the sample or reference sample is incident on the photomultiplier tube and PbS photoconductive cell which are the detectors.^[332]

O1.2. Reflectance measurement:

The Model SLM-468 single reflection attachment is designed to measure the relative reflectance of sample using the forward reflected light from the aluminium-deposited plane mirror as reference. It permits the measurement of the reflectance of metal-deposited film, metal plating etc. The wavelength range is 220 to 2200 nm with a beam port diameter of 7 mm and angle of incidence approximately 5°.^[333]

O2. Fluorescence spectrophotometer:

The fluorescence excitation and emission spectrum of the samples were taken using Cary Eclipse Fluorescence spectrophotometer of VARIAN. It has a single cell holder for liquid sample analysis and a solid sample holder accessory to perform fluorescence measurements on solid samples. The solid sample holder accessory provides both rotational and translational adjustment of the sample. The angle of incidence of the excitation may be varied from 20°- 35°. This is the angle between the exciting light and a line perpendicular to the surface of the sample mounting slide. The source of excitation is xenon lamp.^[334]

O3. Monochromator:

ORIEL compact 77250 1/8 meter monochromator with model 77298 grating was used for the wavelength selection for PAS studies. The monochromator has a high throughput or effective aperture $f/3.7$. The 30×30 mm replicated ruled type grating has a blaze wavelength of 500 nm. The grating has a groove spacing of 1200 lines/mm and reciprocal dispersion of 6.4 nm/ mm. The primary wavelength region is 330-750nm and the usable range is 300- 1000 nm.^[335]

O4. Monochromator CCD assembly:

Princeton Instruments NTE/CCD air cooled detectors have three distinct sections. The front vacuum enclosure contains the CCD array seated on a cold finger. This finger is in turn seated on a four-stage Peltier thermoelectric cooler. The back enclosure contains the heat exchanger. An internal fan cools the heat exchanger and the heat exits the unit through openings in the housing. The CCD array used is Roper Scientific NTE/CCD-1340/100-EM.

The electronics enclosure contains the preamplifier and array driver board. This keeps all signal leads to the preamplifier as short as possible, and also provides RF shielding.^[336] SPEC-10 controller of Princeton Instruments controls the CCD.

SpectraPro-500i is a 500 mm focal length monochromator/spectrograph. It features an astigmatism-corrected optical system, triple indexable gratings and triple grating turret. The SpectraPro-500i includes a direct digital grating scan mechanism with full wavelength scanning capabilities, plus built-in RS232 and IEEE488 computer interfaces. The 1200 grooves/mm grating has an aperture ratio $f/6.5$. The scan range is 0 to 1400 nm (mechanical range) and an operating range of 185 nm to the far IR and a resolution of 0.05 nm at 435.8 nm.^[337]

WinSpec, the spectroscopic software, of Princeton Instruments is used for collecting, storing and processing data from the Roper Scientific system.^[338]

O5. Chopper:

The light beam modulation was carried out using mechanical choppers. HMS/ITHACO model 230 light beam chopper with a set of three interchangeable blades of slots 2, 10 or 30 provides three frequency ranges. The frequency ranges from 4 to 200 Hz, 20 to 1 kHz and 60 to 3 kHz for 2, 10 and 30 slotted blades

respectively.^[339] Model SR 540 optical chopper of Stanford Research Systems has options of 6 and 30 slot blades with 4 to 400 Hz and 400 to 3.7 kHz respectively.^[340]

O6. Lock- in amplifier:

Model SR830 DSP Lock-In Amplifier of Stanford Research Systems^[341] has IEEE-488 and RS 232 interfaces. The lock in amplifier is interfaced to computer using LabVIEW™ 7 Express of National Instruments.^[342]

O7. Preamplifier:

Model SR 560 low-noise preamplifier (Stanford Research Systems) provides DC-coupled low noise amplification of single-ended and true differential input signals at gains of 1 to 50,000.^[343]

O8. Micrometer:

Mitutoyo digital outside micrometer, series 193 with a resolution ± 0.001 mm was used for measuring the thickness of the samples.

1.4. Scope of the thesis:

The present thesis deals with the non-destructive characterization of three different types of materials which can be utilised for photonic applications. The simple and cost effective techniques like PA, PTD and absorption and fluorescence spectroscopy are mainly used for the optical and thermal characterization of these materials. Montmorillonites are efficient absorbers of dyes in waste-water. After the dye adsorption, this clay mineral itself is a waste material. Hence, further characterization is necessary for the efficient usage of the dye intercalated clay minerals. RE doped materials have significant roles in the photonics industry due to their atomic line shaped spectra which are almost host independent. Novel advanced ceramic materials can be manufactured by the SHS method. RETs prepared by SHS methods are not much studied using non-destructive photonic techniques. In the present investigations, optical and thermal characterizations of these samples have been carried out. Sol gel process helps one to make low temperature glasses doped with materials of industrial importance in the photonics field. RE doped sol gel silica glasses are also characterised using PA and spectroscopic techniques for further applications in the field of photonics.

1.5. References:

- [1] F. Bergaya and G. Lagaly (2006). 'General introduction: Clays, clay minerals, and clay science': in: "Handbook of clay science" F. Bergaya, B. K. G. Theng and G. Lagaly (Eds.). Developments in Clay Science, Vol. 1. Chapter 1. Elsevier Science, Amsterdam. doi: 10.1016/S1572-4352(05)01001-9
- [2] Ampian S. G (1985). 'Clays'; in: "Minerals facts and problems". A. W. Knoerr (Ed.). Washington, DC, US Bureau of mines, p 1-13 (Bulletin 675).
- [3] Patterson S. H. and Murray H. H. (1983). 'Clays'; in: "Industrial minerals and rocks", Lefond S. I. (Ed). 5th edition. American Institute of Mining, Metallurgical and Petroleum Engineers, New York, p 585-651.
- [4] Bates R. E. and Jackson J. A. (Eds.) (1987). 'Glossary of geology', 3rd ed. Alexandria, Virginia. American Geological Institute, p 65, 123, 262, 432.
- [5] Zoltán Adamis and Richard B Williams (2005). 'Environmental health criteria 231. Bentonite, Kaolin, and Selected Clay Minerals'. World Health Organization. Geneva. 175pp.
- [6] R. W. Berry, F. Bergaya and G. Lagaly (2006). 'Teaching clay science: A great perspective': in: "Handbook of clay science". F. Bergaya, B. K. G. Theng and G. Lagaly (Eds.). Vol. 1. Chapter 16. Elsevier Science, Amsterdam. doi:10.1016/S1572-4352(05)01044-5
- [7] Charles Edward Weaver and Lin Davis Pollard (1975). 'The chemistry of clay minerals'. Elsevier Scientific Publishing Company, Amsterdam. 213pp.
- [8] F Annabi-Bergaya, M I Cruz, L Gatineau and J J Fripiat (1979). 'Adsorption of alcohols by smectites. I. Distinction between internal and external surfaces'. *Clay Minerals*: **14** (4), p 249–258. URL: http://www.minersoc.org/pages/Archive-CM/Volume_14/14-4-249.pdf
- [9] H van Olphen (1977). 'An Introduction to Clay Colloid Chemistry: For Clay Technologists, Geologists and Soil Scientists' 2nd Edition. Wiley Interscience Publication, John-Wiley & Sons. Toronto. 318pp.
- [10] M. F. Brigatti, E. Galan and B. K. G. Theng (2006). 'Structures and mineralogy of clay minerals': in: "Handbook of clay science". F. Bergaya, B. K. G. Theng and G. Lagaly (Eds.). Developments in Clay Science, Vol. 1. Chapter 2. Elsevier Science, Amsterdam. doi: 10.1016/S1572-4352(05)01002-0
- [11] R F Giese Jr. (1975). 'Interlayer bonding in talc and pyrophyllite'. *Clays Clay Minerals*; **23** (2), p 165-166.
- [12] G. E. Christidis, P. W. Scott and A. C. Dunham (1997). 'Acid activation and bleaching capacity of bentonites from the islands of Milos and Chios, Aegean, Greece'. *Applied Clay Science*.: **12** (4), p 329-347. doi:10.1016/S0169-1317(97)00017-3
- [13] Francisco R. Valenzuela Díaz and Pérsio de Souza Santos (2001). 'Studies on the acid activation of brazilian smectitic clays'. *Quim. Nova*; **24** (3), p 345-353. doi: 10.1590/S0100-40422001000300011
- [14] W. P. Gates, J. S. Anderson, M. D. Raven and G. J. Churchman (2002). 'Mineralogy of a bentonite from Miles, Queensland, Australia and characterisation of its acid activation products'. *Applied Clay Science*; **20** (4-5), p 189-197. doi:10.1016/S0169-1317(01)00072-2
- [15] Prakash Kumar, Raksh V. Jasra and Thirumaleshwara S. G. Bhat (1995). 'Evolution of Porosity and Surface Acidity in Montmorillonite Clay on Acid Activation'. *Ind. Eng. Chem. Res.*; **34** (4), p 1440–1448 doi: 10.1021/ie00043a053.
- [16] Jadambaa Temuujin, Mamoru Senna, Tsedev Jadambaa, Dashdendev Burmaa, Shaarii Erdenechimeg and Kenneth JD MacKenzie (2006). 'Characterization and bleaching properties of acid-leached montmorillonite'. *J Chem Technol Biotechnol.*; **81** (4), p 688 – 693. doi: 10.1002/jctb.1469
- [17] P. Komadel (2003). 'Chemically modified smectites'. *Clay Minerals*: **38** (1), p 127-138; doi: 10.1180/0009855033810083

- [36] M. S. Whittingham and A. J. Jacobson (Eds.) (1982). 'Intercalation Chemistry'. Academic Press, London. 595pp.
- [37] Ramamurthy V. (Ed.) (1991). 'Photochemistry in Organized and Constrained Media'. VCH Publishers, New York. 875pp.
- [38] S. Venkata Mohan, N. Chandrasekhar Rao, K. Krishna Prasad and J. Karthikeyan (2002). 'Treatment of simulated reactive yellow 22 (Azo) dye effluents using *Spirogyra* species'. *Waste Manage.*; **22** (6), p 575–582. doi:10.1016/S0956-053X(02)00030-2
- [39] S. Salman Ashraf, Muhammad A. Rauf and Scham Alhadrami (2006). 'Degradation of Methyl Red using Fenton's reagent and the effect of various salts'. *Dyes and Pigments*; **69** (1-2), p 74-78. doi:10.1016/j.dyepig.2005.02.009
- [40] K. Vasanth Kumar, V. Ramamurthi and S. Sivanesan (2006). 'Biosorption of malachite green, a cationic dye onto *Pithophora* sp., a fresh water algae'. *Dyes and Pigments*; **69** (1-2), p 102-107. doi:10.1016/j.dyepig.2005.02.005
- [41] Scott Prah. 'Optical absorption of methylene blue'. [http://www.chem.mblindex.html](#)

- [18] Barrer R. M. (1978). 'Zeolites and Clay Minerals as Sorbents and Molecular Sieves'. Academic Press, New York. p 406-486.
- [19] Komkrich Pimpukdee, Bundit Tengjaroenkul, Prapansak Chaveerach and Benjamas Mhosatanun (2004). 'The characterization of clays and cetylpyridinium-exchanged clays for their ability to adsorb zearalenone'. *Thai J. Vet. Med.*: **34** (4), p 23-31.
URL: http://www.vet.chula.ac.th/~tjvm/full_text/v34/v344/02-344.pdf
- [20] Zielke R. C, Pinnavaia T. J and Mortland M. M (1989). 'Adsorption and reactions of selected organic molecules on clay mineral surfaces': in: "Reactions and movement of organic chemicals in soils". *SSSA Special Publication* . B L Sawhney and K Brown (Eds.). Soil Science Society of America. Madison, WI. p 81-98.
- [21] Soma Y and Soma M (1989). 'Chemical reactions of organic compounds on clay surfaces'. *Environ. Health Perspect.*: **83**, p 205-214.
- [22] Cleve A. I. Goring and John W. Hamaker (Eds.) (1972). 'Organic chemicals in the soil environment'. Marcel Dekker, Inc. New York. 544pp.
- [23] Garrison Sposito (1984). 'The chemistry of soils'. Oxford University Press: New York, USA. 304pp.
- [24] M. Ilic, E. Koglin, A. Pohlmeier, H. D. Narres, and M. J. Schwuger (2000). 'Adsorption and Polymerization of Aniline on Cu(II)-Montmorillonite: Vibrational Spectroscopy and ab Initio Calculation'. *Langmuir*; **16** (23), p 8946-8951. doi: 10.1021/la000534d
- [25] C. C. Harvey and G. Lagaly (2006). 'Conventional applications'; in: "Handbook of clay science". F. Bergaya, B. K. G. Theng and G. Lagaly (Eds.). Developments in Clay Science, Vol. 1. Chapter 10. 1. Elsevier Science, Amsterdam. doi: 10.1016/S1572-4352(05)01016-0
- [26] K. A. Carrado, A. Decarreau, S. Petit, F. Bergaya and G. Lagaly (2006). 'Synthetic clay minerals and purification of natural clays'; *ibid.* Ch. 4. doi: 10.1016/S1572-4352(05)01004-4
- [27] T. J. Meredith and J. A. Vale (1987). 'Treatment of paraquat poisoning in man: Methods to prevent absorption'. *Hum. Exp. Toxicol.*: **6** (1), p 49-55. doi: 10.1177/096032718700600108
- [28] M.T. Droy-Lefaix and F. Tateo (2006). 'Clays and clay minerals as drugs'; in: "Handbook of clay science". F. Bergaya, B. K. G. Theng and G. Lagaly (Eds.). Developments in Clay Science, Vol.1. Ch 11.6. Elsevier Science, Amsterdam. doi: 10.1016/S1572-4352(05)01025-1
- [29] R. A. Schoonheydt and C. T. Johnston (2006). 'Surface and interface chemistry of clay minerals'; *ibid.* Chapter 3. doi: 10.1016/S1572-4352(05)01003-2
- [30] Jean Grandjean and Pierre Laszlo (1989). 'Deuterium nuclear magnetic resonance studies of water molecules restrained by their proximity to a clay surface'. *Clays and Clay Minerals*; **37** (5), p 403-408.
- [31] G. Lagaly (2006). 'Colloid clay science'; in: "Handbook of clay science". F. Bergaya, B. K. G. Theng and G. Lagaly (Eds.). Developments in Clay Science, Vol.1. Chapter 5. Elsevier Science, Amsterdam. doi: 10.1016/S1572-4352(05)01005-6
- [32a] R. W. Mooney, A. G. Keenan and L. A. Wood (1952). 'Adsorption of water vapor by montmorillonite. I. Heat of desorption and application of BET theory'. *J. Am. Chem. Soc.*: **74** (6), p 1367-1371. doi: 10.1021/ja01126a001
- [32b] R. W. Mooney, A. G. Keenan and L. A. Wood (1952). 'Adsorption of water vapor by montmorillonite. II. Effect of exchangeable ions and lattice swelling as measured by X-ray diffraction'. *J. Am. Chem. Soc.*: **74** (6), p 1371- 1374. doi: 10.1021/ja01126a002
- [33] Robert A. Schoonheydt (2002). 'Smectite-type clay minerals as nanomaterials'. *Clays and Clay Minerals*: **50** (4), p 411-420
- [34] B. K. G. Theng (1974). 'The Chemistry of Clay-Organic Reactions'. Adam Hilger, London. 343pp.
- [35] A. C. D. Newman (Ed.) (1987). 'Chemistry of Clays and Clay Minerals'. Longman Scientific and Technical, Harlow, Essex, UK. 480pp. Mineralogical Society (Monograph No. 6, New York).

- [36] M. S. Whittingham and A. J. Jacobson (Eds.) (1982). 'Intercalation Chemistry'. Academic Press, London. 595pp.
- [37] Ramamurthy V. (Ed.) (1991). 'Photochemistry in Organized and Constrained Media'. VCH Publishers, New York. 875pp.
- [38] S. Venkata Mohan, N. Chandrasekhar Rao, K. Krishna Prasad and J. Karthikeyan (2002). 'Treatment of simulated reactive yellow 22 (Azo) dye effluents using *Spirogyra* species'. *Waste Manage.*; **22** (6), p 575–582. doi:10.1016/S0956-053X(02)00030-2
- [39] S. Salman Ashraf, Muhammad A. Rauf and Seham Alhadrami (2006). 'Degradation of Methyl Red using Fenton's reagent and the effect of various salts'. *Dyes and Pigments*; **69** (1-2), p 74-78. doi:10.1016/j.dyepig.2005.02.009
- [40] K. Vasanth Kumar, V. Ramamurthi and S. Sivanesan (2006). 'Biosorption of malachite green, a cationic dye onto *Pithophora* sp., a fresh water algae'. *Dyes and Pigments*; **69** (1-2), p 102-107. doi:10.1016/j.dyepig.2005.02.005
- [41] Scott Prahl. 'Optical absorption of methylene blue'.
URL: <http://omlc.ogi.edu/spectra/mb/index.html>
- [42] Shivaji Srivastava, Ranjana Sinha and D. Roy (2004). 'Toxicological effects of malachite green'. *Aquatic Toxicology*; **66** (3), p 319-329. doi:10.1016/j.aquatox.2003.09.008
- [43] V. K. Gupta, Alok Mittal, Lisha Krishnan and Vibha Gajbe (2004). 'Adsorption kinetics and column operations for the removal and recovery of malachite green from wastewater using bottom ash'. *Sep. Purif. Technol.*; **40** (1), p 87–96. doi:10.1016/j.seppur.2004.01.008
- [44] URL:<http://www.jtbaker.com/msds/englishhtml/r5400.htm>
- [45] URL: [http://environmentalchemistry.com/yogi/chemicals/cn/Ammonium,%A0\(9-\(o-carboxyphenyl\)-6-\(diethylamino\)-3H-xanthen-3-ylidene\)diethyl-,%A0chloride.html](http://environmentalchemistry.com/yogi/chemicals/cn/Ammonium,%A0(9-(o-carboxyphenyl)-6-(diethylamino)-3H-xanthen-3-ylidene)diethyl-,%A0chloride.html)
- [46] URL:<http://www.exciton.com/pdfs/R610.pdf>
- [47] A. Edwin Vasu (2008). 'Studies on the Removal of Rhodamine B and Malachite Green from Aqueous Solutions by Activated Carbon'. *E-Journal of Chemistry*; **5** (4), p 844-852.
URL: <http://www.e-journals.in/PDF/V5N4/844-852.pdf>
- [48] URL: http://www.absoluteastronomy.com/topics/Auramine_O
- [49] Yoshichika KOBAYASHI and Mitsuo NISHIMURA (1972). 'Fluorescence Change of Auramine O Bound to Chromatophores of *Rhodospirillum rubrum* - Analysis in Connection to Ionic Environment and Ion Transport'. *J. Biochem.*; **71** (2), p 275-284.
- [50] URL:<http://www.jtbaker.com/msds/englishhtml/a7750.htm>
- [51] V. P. Vinod and T. S. Anirudhan (2003). 'Adsorption behaviour of basic dyes on the humic acid immobilized pillared clay'. *Water, Air, and Soil Pollution.*; **150** (1-4), p 193–217. doi: 10.1023/A:1026145631713
- [52] F. J. Green (1990). *The Sigma-Aldrich Handbook of Stains, Dyes and Indicators*, Aldrich Chem. Comp.
- [53] Werner MÜLLER and Fritz GAUTIER (1975). 'Interactions of heteroaromatic compounds with nucleic acids. A.T-specific non-intercalating DNA ligands'. *Eur. J. Biochem.*; **54** (2), p 385-394. doi: 10.1111/j.1432-1033.1975.00385.pp.x
- [54] Makoto Ogawa and Kazuyuki Kuroda (1995). 'Photofunctions of intercalation compounds'. *Chem. Rev.*; **95** (2), p 399–438. doi: 10.1021/cr00034a005
- [55] Leon Margulies, Theodor Stern, Baruch Rubin and Luis O. Ruzo (1992). 'Photostabilization of trifluralin adsorbed on a clay matrix'. *J. Agric. Food Chem.*; **40** (1), p 152–155. doi: 10.1021/jf00013a030
- [56] Leon Margulies, Theodor Stern and Baruch Rubin (1994). 'Slow Release of S-Ethyl Dipropylcarbamothioate from Clay Surfaces'. *J. Agric. Food Chem.*; **42** (5), p 1223–1227. doi: 10.1021/jf00041a033
- [57] Tetsuya Shichi and Katsuhiko Takagi (2000). 'Clay minerals as photochemical reaction fields'. *J. Photochem. Photobiol. C: Photochem. Rev.*; **1** (2), p 113–130.

doi:10.1016/S1389-5567(00)00008-3

- [58] Shmuel Yariv (2002). 'Staining of clay minerals and visible absorption spectroscopy of dye-clay complexes': in: "Organo-Clay Complexes and Interactions". Shmuel Yariv and Harold Cross (Eds.), p. 463. Marcel Dekker, Inc., New York. 688pp.
- [59] K. Bergmann and C. T. O'Konski (1963). 'A spectroscopic study of methylene blue monomer, dimer, and complexes with montmorillonite'. *J. Phys. Chem.*: **67** (10), p 2169-2177. doi: 10.1021/j100804a048
- [60] Juraj Bujdák (2006). 'Effect of the layer charge of clay minerals on optical properties of organic dyes. A review'. *Appl. Clay Sci.*: **34** (1-4), p 58-73. doi:10.1016/j.clay.2006.02.011
- [61] J. Bujdák, N. Iyi and T. Fujita (2002). 'The aggregation of methylene blue in montmorillonite dispersions'. *Clay Minerals.*: **37** (1), p 121-133. doi: 10.1180/0009855023710022
- [62] Ching-Hsing Yu, Susan Q. Newton, Mya A. Norman, David M. Miller, Lothar Schäfer and Brian J. Teppen (2000). 'Molecular dynamics simulations of the adsorption of methylene blue at clay mineral surfaces'. *Clays and Clay Minerals*: **48** (6), p 665-681.
- [63] Bose H (1987). 'Environmental effects on dye aggregation/ effect of electrolytes on metachromasy of thiazine dyes'. *Indian Journal of Chemistry, Section A*: **26**, p 652-655.
- [64] Juraj Bujdák and Nobuo Iyi (2002). 'Visible spectroscopy of cationic dyes in dispersions with reduced-charge montmorillonites'. *Clays and Clay Minerals*: **50** (4), p 446-454.
- [65] Juraj Bujdák, Marián Janek, Jana Madejová and Peter Komadel (1998). 'Influence of the layer charge density of smectites on the interaction with methylene blue'. *J. Chem. Soc., Faraday Trans.*: **94** (23), p 3487-3492. doi: 10.1039/a805341c
- [66] Katrien Y. Jacobs and Robert A. Schoonheydt (1999). 'Spectroscopy of methylene blue-smectite suspensions'. *J. Colloid Interface Sci.* **220** (1), p 103-111. doi:10.1006/jcis.1999.6513
- [67] A. R. Mermut (1994). 'Layer Charge Characteristics of 2:1 Silicate Clay Minerals'. CMS Workshop Lectures Vol. 6 (The Clay Minerals Society, Boulder, Colorado) 134pp.
- [68] J. Cenens and R. A. Schoonheydt (1988). Visible spectroscopy of methylene blue on hectorite, laponite B, and barasym in aqueous suspension'. *Clays Clay Miner.* **36**(3), p214-224.
- [69] L. Antonov, G. Gergov, V. Petrov, M. Kubista and J. Nygren (1999). 'UV-Vis spectroscopic and chemometric study on the aggregation of ionic dyes in water'. *Talanta*: **49** (1), p 99-106. doi:10.1016/S0039-9140(98)00348-8
- [70] Adriana Czímerová, Ľuboš Jankovič and Juraj Bujdák (2004). 'Effect of the exchangeable cations on the spectral properties of methylene blue in clay dispersions'. *J. Colloid Interface Sci.*: **274** (1), p 126-132. doi:10.1016/j.jcis.2003.10.025
- [71] Adriana Czímerová, Alexander Čeklovský and Juraj Bujdák (2009). 'Interaction of montmorillonite with phenothiazine dyes and pyronin in aqueous dispersions: A visible spectroscopy study'. *Cent. Eur. J. Chem.*: **7** (3), p 343-353. doi: 10.2478/s11532-009-0035-x
- [72] Fergus Gessner, Carla C. Schmitt, Miguel G. Neumann (1994). 'Time-Dependent Spectrophotometric Study of the Interaction of Basic Dyes with Clays. I. Methylene Blue and Neutral Red on Montmorillonite and Hectorite'. *Langmuir*: **10** (10), p 3749-3753. doi: 10.1021/la00022a059
- [73] Miguel G. Neumann, Carla C. Schmitt and Fergus Gessner (1996). 'Time-Dependent Spectrophotometric Study of the Interaction of Basic Dyes with Clays II: Thionine on Natural and Synthetic Montmorillonites and Hectorites'. *J. Colloid Interface Sci.*: **177** (2), p 495-501. doi:10.1006/jcis.1996.0063
- [74] Ana P. P. Cione, Miguel G. Neumann and Fergus Gessner (1998). Time-Dependent Spectrophotometric Study of the Interaction of Basic Dyes with Clays: III. Mixed Dye Aggregates on SWy-1 and Laponite'. *J. Colloid Interface Sci.*: **198** (1), p 106-112. doi:10.1006/jcis.1997.5268
- [75] F. López Arbeloa, M. J. Tapia Estévez, T. López Arbeloa and I. López Arbeloa (1995).

- 'Adsorption of Rhodamine 6G on saponite. A comparative study with other Rhodamine 6G-Smectite aqueous suspensions'. *Langmuir*; **11** (8), p 3211–3217. doi: 10.1021/la00008a054
- [76] Juraj Bujdák and Peter Komadel (1997). 'Interaction of methylene blue with reduced charge montmorillonite'. *J. Phys. Chem. B*; **101** (44), p 9065–9068. doi: 10.1021/jp9718515
- [77] C. Dobrogowska, L. G. Hepler, D. K Ghosh and Sh. Yariv (1991). 'Metachromasy in clay mineral systems'. *J. Therm. Anal. Calorim.*; **37** (6), p 1347-1356. doi: 10.1007/BF01913866
- [78] H. Zollinger (1987). 'Color Chemistry: Syntheses, Properties and Applications of Organic'. VCH-Verlag: Weinheim. p 60-65.
- [79] Z. Chernia, D. Gill and S. Yariv (1994). 'Electric Dichroism. The Effect of Dialysis on the Color of Crystal Violet Adsorbed to Montmorillonite'. *Langmuir*; **10** (11), p 3988–3993. doi: 10.1021/la00023a015 and the references therein.
- [80] Juraj Bujdák and Nobuo Iyi (2009). 'Optical properties of molecular aggregates of oxazine dyes in dispersions of clay minerals'. *Colloid Polym Sci.*; **287** (2), p 157-165. doi: 10.1007/s00396-008-1959-y
- [81] S. J. Archibald. 'Lanthanides and actinides'.
URL: <http://chemistry.hull.ac.uk/lectures/sja/lanthanide%20notes%2006541%20SJA.pdf>
- [82] William J Miniscalco (2001). 'Optical and electronic properties of rare earth ions in glasses'; in: "Rare earth doped fiber lasers and amplifiers". Michel J F Digonnet (Ed). 2nd ed. Marcel Dekker, Inc. NewYork, USA. Chapter 2.
- [83] Gunter K. Muecke and Peter Muller (1988). 'The not-so-rare-earths'. *Scientific American*; **258** (1), p 72-77.
- [84] B. R. Lipin and G. A. McKay (Eds.) (1989). 'Geochemistry and Mineralogy of Rare Earth Elements'. Reviews in mineralogy. Vol. **21**. 348pp.
- [85] K. R. Dayas (2006). 'Self propagated high temperature synthesis of electroceramic rare earth titanates and its characterization'. Ph.D. Thesis, Calicut University, Calicut, India.
- [86] William M. Yen, Shigeo Shionoya and Hajime Yamamoto (Eds.) (2006). 'Fundamentals of Phosphors'. CRC Press Inc, Ltd. Boca Raton, FL. 335pp.
- [87] Gerhard Heinrich Dieke (1968). 'Spectra and energy levels of rare earth ions in crystals'. H M Crosswhite and Hannah Crosswhite (Eds.). Interscience Publishers, John Wiley & Sons New York, USA. 401pp.
- [88] M. Goepfert Mayer (1941). 'Rare-earth and transuranic elements'. *Phys. Rev.*; **60** (3), p 184 -187 doi: 10.1103/PhysRev.60.184 URL: <http://link.aps.org/doi/10.1103/PhysRev.60.184>
- [89] Brian G. Wybourne (1965), 'Spectroscopic properties of rare earths'. Wiley-Interscience Publishers, New York. 236pp.
- [90] Imbush G F (1991). in 'Advances in non-radiative processes in solids' Baldassare Di Bartolo (Ed.), Plenum Publishing Corporaton, London. p 261.
- [91] Vinoy Thomas (2002). 'Spectroscopic Studies of Certain doped Melt and Sol-gel Glasses'. Ph. D. Thesis, M G University, Kottayam.
- [92] C. Jeffrey Brinker and George W. Scherer (1990). 'Sol-gel science: The physics and chemistry of sol-gel processing'. Academic Press: London, UK. 908pp.
- [93] Jose Garcia Sole, Luisa E Lopez Bausa and Daniel Jaque Garcia (2005). 'An introduction to the optical spectroscopy of inorganic solids'. John Wiley & Sons Ltd. England. 283pp.
- [94] W M Yen and P M Selzer (Eds.) (1981). 'Laser spectroscopy of solids' Springer Verlag, Berlin. 310pp.
- [95] M. J. Weber (1979). 'Methods of experimental physics: Quantum Optics'. vol. **15**. part4 , Quantum Electronics ; C. L. Tang (Ed.). Academic, New York. p 167.
- [96] W E Moerner, W Lenth and G C Bjorklund (1988). 'Persistent spectral hole burning: science and applications' W E Moerner (Ed.): Springer Berlin, p 251.
- [97] Yu-Chun Li, Yen-Hwei Chang, Yee-Shin Chang, Yi-Jing Lin and Chih-Hao Laing (2007). 'Luminescence and Energy Transfer Properties of Gd³⁺ and Tb³⁺ in LaAlGe₂O₇'. *J.Phys.*

- Chem. C.*: **111** (28), p 10682–10688. doi: 10.1021/jp0719107
- [98] P. Dorenbos (2000). 'The $4f^n \leftrightarrow 4f^{n-1}5d$ transitions of the trivalent lanthanides in halogenides and chalcogenides'. *J. Lumin.*: **91** (1-2), p 91-106. doi:10.1016/S0022-2313(00)00197-6
- [99] Renata Reisfeld (1975). 'Radiative and non-radiative transitions of rare-earth ions in glasses' *Structure & Bonding.*: **22**, p 123-175. doi: 10.1007/BFb0116557
- [100] Kiel A (1964). 'Multi-phonon spontaneous emission in paramagnetic crystals'; in: 'Third international conference on quantum electronics'. vol **1**. P. Grivet and N. Bloembergen (Eds.) Columbia University Press, New York. p 765-772
- [101] L. A. Riseberg and H. W. Moos (1968). 'Multi-phonon orbit-lattice relaxation of excited states of rare earth ions in crystals'. *Phys. Rev.*: **174** (2), p 429-438. doi: 10.1103/PhysRev.174.429 URL: <http://link.aps.org/doi/10.1103/PhysRev.174.429>
- [102] L. A. Riseberg and M. J. Weber (1976). 'Relaxation phenomena in rare earth luminescence'; in: "Progress in Optics". Vol **14**. Emil Wolf (Ed.). North- Holland, Amsterdam. p 90-159.
- [103] Sheng Gu, Hai Ying, Zhigang Zhang, Zhixia Zhuang, Pengyuan Yang, Xiaoru Wang, Benli Huang and Bing Li (1997). 'High-resolution spectra of selected rare earth elements and spectral interferences studied by inductively coupled plasma-atomic emission spectroscopy (ICP-AES)' *Spectrochimica Acta Part B: Atomic Spectroscopy*: **52** (11), p 1567-1574. doi: 10.1016/S0584-8547(97)00065-7
- [104] Yongnian Ni and Yingliang Wu (1999). 'Spectrophotometric determination of europium, terbium and yttrium in a perchloric acid solution by the Kalman filter approach'. *Analytical Sciences*: **15** (11), p 1123-7. URL: http://www.jstage.jst.go.jp/article/analsci/15/11/1123/_pdf
- [105] R. K. Garg (1995). 'Rare Earths-Conventional applications and Emerging Technologies'. Proceedings of 'Recent Dev. in the S&T of Rare Earths, Cochin, Kerala.
- [106] Ryu Abe, Masanobu Higashi, Kazuhiro Sayama, Yoshimoto Abe and Hideki Sugihara (2006). 'Photocatalytic Activity of R_3MO_7 and $R_2Ti_2O_7$ ($R= Y, Gd, La; M= Nb, Ta$) for Water Splitting into H_2 and O_2 '. *J. Phys. Chem. B.*: **110** (5), p 2219-2226. doi: 10.1021/jp0552933
- [107] François Brisse and Osvald Knop (1967). 'Pyrochlores. II. An investigation of $La_2Ce_2O_7$ by neutron diffraction'. *Can. J. Chem.* **45** (6), p 609–614. doi:10.1139/v67-101
- [108] Osvald Knop, François Brisse and Lotte Castelliz (1969). 'Pyrochlores. V. Thermoanalytic, X-ray, neutron, infrared, and dielectric studies of $A_2Ti_2O_7$ titanates'. *Can. J. Chem.*: **47** (6), p 971–990 doi:10.1139/v69-155
- [109] Srečo D. Škapin, Drago Kolar and Danilo Suvorov (2000). 'Phase stability and equilibria in the La_2O_3 - TiO_2 system'. *J. European. Ceram. Soc.*: **20** (8), p 1179 -1185. doi:10.1016/S0955-2219(99)00270-8
- [110] Michael Kestigian and Roland Ward (1955). 'The Lanthanum-Titanium-Oxygen System'. *J. Am. Chem. Soc.*: **77** (23), p 6199–6200. doi: 10.1021/ja01628a035
- [111] S. T. Bramwell and M. J. Harris (1998). 'Frustration in Ising-type spin models on the pyrochlore lattice'. *J. Phys.: Condens. Matter*: **10** (14), p L215-L220. doi: 10.1088/0953-8984/10/14/002
- [112] Sanghun Jeon and Hyunsang Hwang (2002). 'Electrical and physical characteristics of $PrTi_2O_7$ for metal-oxide-semiconductor gate dielectric applications'. *Appl. Phys. Lett.*: **81** (25), p 4856- 4858. doi:10.1063/1.1528731 URL: <http://link.aip.org/link/?APPLAB/81/4856/1>
- [113] Hyung J. Jung, Hyun J. Kim, Kyong Y. Kim, Seok J. Yoon, Sang O. Yoon, Tetsuro Nakamura, Mitsuru Itoh and Yoshiyouki Inaguma (1996). 'Compositions of High Frequency Dielectrics'. US Patent 5569632.
- [114] C. W. A. Paschoal, R. L. Moreira, C. Fantini, M. A. Pimenta, K. P. Surendran and M. T. Sebastian (2003). 'Raman scattering study of $RETiTaO_6$ dielectric ceramics'. *Journal of the European Ceramic Society.*: **23** (14), p 2661-2666. doi:10.1016/S0955-2219(03)00141-9

- [115] P. Laffez, G. Desgardin and B. Raveau (1992). 'Influence of calcination, sintering and composition upon microwave properties of the $Ba_{6-x}Sm_{8+2x/3}Ti_{18}O_{54}$ -type oxide'. *J. Mater. Sci.*: **27** (19), p 5229- 5238. doi: 10.1007/BF02403821
- [116] Mailadil T. Sebastian, Sam Solomon, Ravindran Ratheesh, Jacob George and Pezhholil Mohanan (2001). 'Preparation, Characterization, and Microwave Properties of $RETiNbO_6$ (RE = Ce, Pr, Nd, Sm, Eu, Gd, Tb, Dy, Y, and Yb) Dielectric Ceramics'. *J. Am. Cer. Soc.*: **84** (7), p 1487 -1489. doi: 10.1111/j.1151-2916.2001.tb00865.x
URL: <http://dx.doi.org/10.1111/j.1151-2916.2001.tb00865.x>
- [117] X Qi, T P J Han, H G Gallagher, B Henderson, R Illingworth and I S Ruddock (1996). 'Optical spectroscopy of $PrTiNbO_6$, $NdTiNbO_6$ and $ErTiNbO_6$ single crystals'. *J. Phys.: Condens. Mater.*: **8** (26), p 4837 – 4845. doi: 10.1088/0953-8984/8/26/015
- [118] G. L. Roberts, R. J. Cava, W. F. Peck Jr. and J. J. Krajewski (1997), *J. Mater. Res.*: **12** (2), p 526-530. doi: 10.1557/JMR.1997.0075
- [119] R. L. Withers, J. G. Thompson and A. D. Rae (1991). 'The crystal chemistry underlying ferroelectricity in $Bi_4Ti_3O_{12}$, Bi_3TiNbO_9 , and Bi_2WO_6 '. *J. Solid State Chem.*: **94** (2), p 404 - 417. doi:10.1016/0022-4596(91)90207-X
- [120] J. Xu, A. S. Shaikh and R. W. Vest (1989). 'High $KBaTiO_3$ films from metalloorganic precursors'. *IEEE Trans. Ultrason, Ferroelectr., Freq. Control*: **36** (3), p 307-312. doi: 10.1109/58.19168
- [121] Octavio Alvarez-Fregoso (1997). 'Structural and dielectric characterization of $Sm_2Bi_2Ti_3O_{12}$ ferroelectric ceramics'. *J. Appl. Phys.*: **81** (3), p 1387-1391 doi:10.1063/1.364176 URL: <http://link.aip.org/link/?JAPIAU/81/1387/1>
- [122] Robert J. Cava, James J. Krajewski and William F. Peck (1996). 'Compensation of the temperature coefficient of the dielectric constant of barium strontium titanate'. US Patent 5552355
- [123] R. J. Cava, W. F. Peck Jr., J. J. Krajewski and D. A. Fleming (1995). 'Compensation of the temperature coefficient of the dielectric constant of barium strontium titanate'. *Appl. Phys. Lett.* **67**(25), p3813-5 doi:10.1063/1.115392 URL: <http://link.aip.org/link/?APPLAB/67/3813/1>
- [124] Yung Park and Yoon H. Kim (1996). 'Dielectric Ceramic composition for high frequency and method for preparation of the same'. US Patent 5538928
- [125] Hiroaki Yanagida, Kunihito Kawamoto and Masaru Miyayama (1996). 'Chemistry of Ceramics', John Wiley & Sons, USA. 280pp.
- [126] Dan Goldschmidt and Harry L. Tuller (1986). 'Small-polaron conduction in $Y_2Ti_2O_7$ '. *Phys. Rev. B.*: **34** (8), p 5558 - 5561 doi: 10.1103/PhysRevB.34.5558
URL: <http://link.aps.org/doi/10.1103/PhysRevB.34.5558>
- [127] S. Kramer, M. Spears and H. L. Tuller (1994). 'Conduction in titanate pyrochlores: role of dopants'. *Solid State Ionics*; **72** (2), p 59- 66 doi:10.1016/0167-2738(94)90125-2
- [128] J. H. Sheehan, R. J. Prince, G. H. Reynolds, J. S. Haggerty and J. Sigalovski (1996). 'Preparation and Evaluation of Single-Crystal Yttrium Titanate-Based Monofilaments'. Air force office of scientific research, MSNW, Inc., San Marcos, CA. DC. pp 43.
- [129] O. Porat, C. Heremans and H. L. Tuller (1997). 'Stability and mixed ionic electronic conduction in $Gd_2(Ti_{1-x}Mo_x)_2O_7$ under anodic conditions'. *Solid State Ionics*: **94** (1-4), p 75- 83. doi:10.1016/S0167-2738(96)00586-3
- [130] Ofer Porat, Catherine Heremans and Harry L. Tuller (1997). 'Phase Stability and Electrical Conductivity in $Gd_2Ti_2O_7$ - $Gd_2Mo_2O_7$ Solid Solutions'. *J. Am. Cer. Soc.*: **80** (9), p 2278- 2284. doi: 10.1111/j.1151-2916.1997.tb03118.x
URL: <http://dx.doi.org/10.1111/j.1151-2916.1997.tb03118.x>
- [131] J.K. Park, C.H. Kim, K.J. Choi, H.D. Park and S.Y. Choi (2001). 'Photoluminescence behavior of Al^{3+} , Pr^{3+} doped perovskite $La_{2/3}TiO_3$ and pyrochlore $La_2Ti_2O_7$ '. *J. Mat. Res.*: **16** (9), p 2568-2571. doi: 10.1557/JMR.2001.0352

- [132] Masakazu Kimura, Satoshi Nanamatsu, Kikuo Doi, Shigeo Matsushita and Masao Takahashi (1972). 'Electrooptic and Piezoelectric Properties of $\text{La}_2\text{Ti}_2\text{O}_7$ Single Crystal'. *Jpn. J. Appl. Phys.*: **11** (6), p 904.
doi: 10.1143/JJAP.11.904 URL: <http://jjap.ipap.jp/link?JJAP/11/904/>
- [133] S. B. Xiong, W. P. Ding, Z. G. Liu, X. Y. Chen, X. L. Guo, T. Yu, Y. Y. Zhu, and W. S. Hu (1996). 'Layered defective lanthanum titanate thin films prepared by pulsed laser ablation of potassium lanthanum titanate ceramics'. *Appl. Phys. Lett.*: **69** (2), p 191- 193.
doi:10.1063/1.117368 URL: <http://link.aip.org/link/?APPLAB/69/191/1>
- [134] A. V. Shlyakhtina, O. K. Karyagina and L. G. Shcherbakova (2004). 'Order-Disorder Transformations in $\text{Ln}_2\text{Ti}_2\text{O}_7$ (Ln = Lu, Yb, Tm, Gd)'. *Inorg. Mater.*: **40** (1), p 59-65.
doi: 10.1023/B:INMA.0000012180.80891.72
- [135] Hiroaki Takeda, Hideki Sako, Hiroyuki Shimizu, Kacru Kodama, Masahiro Nishida, Hiroshi Nakao, Takashi Nishida, Soichiro Okamura, Takashi Shikida and Tadashi Shiosaki (2003). 'Growth and Characterization of Lanthanum Calcium Oxoborate $\text{LaCa}_2\text{O}(\text{BO}_3)_3$ Single Crystals'. *Jpn. J. Appl. Phys.*: **42** (9B), p 6081-6085. doi: 10.1143/JJAP.42.6081
URL: <http://jjap.ipap.jp/link?JJAP/42/6081/>
- [136] A. Srinivas, Dong-Wan Kim, Kug Sun Hong, and S. V. Suryanarayana (2003). 'Observation of ferroelectromagnetic nature in rare-earth-substituted bismuth iron titanate'. *Appl. Phys. Lett.*: **83** (11), p 2217- 2219. doi:10.1063/1.1610255
URL: <http://link.aip.org/link/?APPLAB/83/2217/1>
- [137] J. Moon, T. Li, C. A. Randall and J. H. Adair (1997). 'Low temperature synthesis of lead titanate by a hydrothermal method'. *J. Mater. Res.*: **12** (1), p 189-197.
doi: 10.1557/JMR.1997.0025
- [138] Jooho Moon, Jeffrey A. Kerchner, Henrik Krarup and James H. Adair (1999). 'Hydrothermal synthesis of ferroelectric perovskites from chemically modified titanium isopropoxide and acetate salts'. *J. Mater. Res.*: **14** (2), p 425 – 435.
doi: 10.1557/JMR.1999.0061
- [139] P. A. M. Berdowski and G. Blasse (1986). 'Luminescence and energy transfer in a highly symmetrical system: $\text{Eu}_2\text{Ti}_2\text{O}_7$ '. *J. Solid State Chem.*: **62** (3), p 317-327.
doi:10.1016/0022-4596(86)90246-X
- [140] S. Nanamatsu , M. Kimura , K. Doi , S. Matsushita and N. Yamada(1974). 'A new ferroelectric: $\text{La}_2\text{Ti}_2\text{O}_7$ '. *Ferroelectrics*; **8** (1), p 511-513. doi: 10.1080/00150197408234143
- [141] Xiao Qiang Liu and Xiang Ming Chen (2005). 'Toughening of 8Y-FSZ Ceramics by Neodymium Titanate Secondary Phase' *J. Am. Ceram. Soc.*: **88** (2), p 456- 458.
doi: 10.1111/j.1551-2916.2005.00065.x URL: <http://dx.doi.org/10.1111/j.1551-2916.2005.00065.x>
- [142] C. Z. Bi, J. Y. Ma, B. R. Zhao, Z. Tang, D. Yin, C. Z. Li, D. Z. Yao, J. Shi and X. G. Qiu (2005). 'Far infrared optical properties of the pyrochlore spin ice compound $\text{Dy}_2\text{Ti}_2\text{O}_7$ '. *J. Phys.: Condens. Matter*: **17** (34), p 5225-5233 doi: 10.1088/0953-8984/17/34/007
- [143] Jørgensen C K (1962). 'Orbitals in atoms and molecules'. Academic Press, NY. 162pp.
- [144] Masayuki Yamane and Yoshiyuki Asahara (2000). 'Glasses for photonics'. Cambridge University Press, Cambridge, UK. 271pp.
- [145] Frédéric Chaput, Jean-Pierre Boilot and Alain Beauger (1990). 'Alkoxide-Hydroxide Route to Synthetize BaTiO_3 -Based Powders'. *J. Am. Ceram. Soc.*: **73** (4), p 942-948.
doi: 10.1111/j.1151-2916.1990.tb05141.x
URL: <http://dx.doi.org/10.1111/j.1151-2916.1990.tb05141.x>
- [146] Shingo Katayama, Ikuko Yoshinaga, Noriko Yamada and Toru Nagai (1996). 'Low-Temperature Synthesis of $\text{Ba}(\text{Mg}_{1/3}\text{Ta}_{2/3})\text{O}_3$ Ceramics from Ba-Mg-Ta Alkoxide Precursor'. *J. Am. Ceram. Soc.*: **79** (8), p 2059- 2064. doi: 10.1111/j.1151-2916.1996.tb08937.x
URL: <http://dx.doi.org/10.1111/j.1151-2916.1996.tb08937.x>
- [147] James S. Reed (1989). 'Introduction to the principles of ceramic processing'.

John Wiley, New York. 506pp.

- [148] Kashinath C. Patil, S. T. Aruna and Tanu Mimani (2002). 'Combustion synthesis: an update'. *Curr. Op. Solid State. Mater. Sci.*; **6** (6), p 507-512.
doi:10.1016/S1359-0286(02)00123-7
- [149] Zuhair A. Munir and Umberto Anselmi-Tamburini (1989). 'Self-propagating exothermic reactions: The synthesis of high-temperature materials by combustion'. *Materials Science Reports*; **3** (7-8), p 277-365. doi:10.1016/0920-2307(89)90001-7
- [150] H. C. Yi and J. J. Moore (1990). 'Self-propagating high-temperature (combustion) synthesis (SHS) of powder-compacted materials'. *J. Mater. Sci.*; **25** (2), p 1159- 1168.
doi: 10.1007/BF00585421
- [151] J. Subrahmanyam and M. Vijayakumar (1992). 'Self-propagating high-temperature synthesis'. *J. Mater. Sci.*; **27** (23), p 6249-6273. doi: 10.1007/BF00576271
- [152a] A. G. Merzhanov, V. M. Shkiro and I. P. Borovinskaya (1985). 'Gasless combustion synthesis of refractory inorganic compounds'. Noyes, New Jersey, USA. 152pp.
- [152b] *Idem.* (1972). French Patent 2088 668.
- [152c] *Idem.* (1973). US Patent 3726643.
- [152d] *Idem.* (1974). UK Patent 1321084.
- [152e] *Idem.* (1982). Japan Patent 1098 839.
- [153] Vladimir Hlavacek and Jan A. Puszynski (1996). 'Chemical Engineering Aspects of Advanced Ceramic Materials'. *Ind. Eng. Chem. Res.*; **35** (2), p 349-377.
doi: 10.1021/ie9501034
- [154] A. G. Merzhanov (1996). 'Combustion processes that synthesize materials'. *J. Mater. Process. Technol.*; **56** (1-4), p 222- 241. doi:10.1016/0924-0136(95)01837-9
- [155] A. G. Merzhanov(1992). 'Combustion: new manifestations of an ancient process'; in: 'Chemistry of Advanced Materials'. C. N. R. Rao (Ed.), (An IUPAC 21st Century Monograph). Blackwell Scientific Publications, Oxford. 388pp.
- [156] A. G. Merzhanov (1995). 'Ten research directions in the future of SHS'. *Int. J. of SHS*; **4** (4), p 323-350.
- [157] A. G. Merzhanov (1993). 'Theory and practice of SHS: worldwide state of the art and the newest results'. *Int. J. of SHS*; **2** (2), p113-158.
- [158] A. G. Merzhanov (1997). 'Worldwide evolution and present status of SHS as a branch of modern R&D (to the 30th Anniversary of SHS)'. *Int. J. of SHS*; **6** (2), p119-163.
- [159] A. G. Merzhanov (1990). 'Self-propagating high-temperature synthesis of ceramic (oxide) superconductors'; in: 'Ceramic Transactions. Superconductivity and Ceramic Superconductors'. K.N. Nair, E.I. Dupont de Nemours and E.A. Giess. (Eds.). Westerville, Ohio: Amer. Ceram. Soc. Publ., v.13, p.519-549.
- [160] A. G. Merzhanov (1995). 'Fluid Dynamics Phenomena in the Processes of Self-Propagating High-Temperature Synthesis'. *Combustion Science and Technology*; **105** (4 – 6), p 295 - 325 . doi: 10.1080/00102209508907756
- [161] William L. Frankhouser, Keith W. Brendley, Michael C. Kieszek and Stephen T. Sullivan (1985). 'Gasless combustion synthesis of refractory compounds'. Noyes Publications, New Jersey, USA. 152pp.
- [162] Alexander G. Merzhanov (2004). 'The chemistry of self-propagating high-temperature synthesis'. *J. Mater. Chem.*; **14** (12), p 1779 – 1786. doi: 10.1039/b401358c
- [163] A. J. Moulson and J. M. Herbert (1992). 'Electroceramics: Materials Properties Applications'. Chapman & Hall. London, UK. 464pp.
- [164] F. H. Norton (1970). 'Fine Ceramics Technology and Applications'. McGraw Hill, New York. 507pp.
- [165] David Segal (1991). 'Chemical Synthesis of Advanced Ceramic Materials'. Chemistry of Solid State Materials- I. Cambridge University Press, Cambridge, UK. 200pp.

- [166] W. David Kingery, Harvey Kent Bowen and Donald Robert Uhlmann (1976). 'Introduction to Ceramics'. John Wiley, New York, second edition. 1032pp.
- [167] Charles River Associates (1985). 'Advanced ceramic materials: technological and economic assessment'. Noyes Publications, Park Ridge, N.J., U.S.A. 651pp.
- [168] Relva C Buchanan (2004). 'Ceramic Materials for Electronics'. Third edition. Marcel Dekker Inc., New York. 676pp.
- [169] Shinroku Saito (1985). 'Fine Ceramics'. Elsevier Publishers, New York. 352pp.
- [170] V. N. Vaidya, S. K. Mukherjee, J. K. Joshi, R. V. Kamat and D. D. Sood (1987). 'A study of chemical parameters of the internal gelation based sol-gel process for uranium dioxide'. *J. Nucl. Mat.*; **148** (3), p 324-331. doi:10.1016/0022-3115(87)90026-2
- [171] S. K. Mukerjee, J. V. Dehadraya, V. N. Vaidya and D. D. Sood (1991). 'Kinetics of the carbothermic synthesis of uranium mononitride microspheres'. *J. Nucl. Mater.*; **185** (1), p 39-49. doi:10.1016/0022-3115(91)90363-C
- [172] Kashinath C Patil, Singanahally T Aruna and Sambandan Ekambaram (1997). 'Combustion synthesis'. *Curr. Opin. Solid State Mater. Sci.*; **2** (2), p 158-165 doi:10.1016/S1359-0286(97)80060-5
- [173] I. P. Borovinskaya (1992). 'Chemical classes of the SHS processes and materials'. *Pure Appl. Chem.*; **64** (7), p 919-940. doi:10.1351/pac199264070919
- [174] V. Hlavacek (1991). *Acers. Bull.*; **70** (2), p 240.
- [175] URL: http://www.ism.ac.ru/handbook/_shs.htm
- [176] D. Bahadur, S. Rajakumar and Ankit Kumar (2006). 'Influence of fuel ratios on auto combustion synthesis of barium ferrite nano particles'. *J. Chem. Sci.*; **118** (1), p 15- 21. URL: <http://www.ias.ac.in/chemsci/index.html>
- [177] Arvind Varma and Jean-Pascal Lebrat (1992). 'Combustion synthesis of advanced materials'. *Chem. Eng. Sci.*; **47** (9-11), p 2179-2194. doi:10.1016/0009-2509(92)87034-N
- [178] James W. McCauley (1990). 'An Historical and Technical Perspective on SHS'. 14th Annual Conference on Composites and Advanced Ceramic Materials, Part 2 of 2: *Ceramic Engineering and Science Proceedings*; vol. **11** (9/10). John B. Wachtman Jr. (Ed.). The American Ceramic Society, Inc. p 1137-1181. doi: 10.1002/9780470313053.ch1 URL: <http://dx.doi.org/10.1002/9780470313053.ch1>
- [179] Holt J. B. (1984). 'Combustion Synthesis: a New Area of Research in Materials Science'. Energy & Technology Review LLNL. p 11-15.
- [180] Grigoryan E.H.(1997). 'SHS Catalysts and Supports'. *Intern. J. of SHS*; **6** (3), p 307-325.
- [181] Grigor'ev Yu.M and Merzhanov A.G(1992). 'SHS coatings'. *Int J. of SHS*; **1**(4), p600-639.
- [182] V. V. Barzykin (1992). 'Initiation of SHS processes'. *Pure Appl. Chem.*; **64** (7), p 909-918. doi:10.1351/pac199264070909
- [183] J. J. Moore, A. O. Kunrath, R. Torres, I. Reimanis, G. Mustoe, K. Upadhyya and E.A. Levashov (1997). 'Self-propagating high-temperature synthesis of dense ceramic composite'. *Int. J. of SHS*; **6** (3), p 277-294.
- [184] J. S. Haggerty, Y. -M. Chiang (1990). 'Reaction-Based Processing Methods for Ceramics and Composites'. A Collection of Papers Presented at the 14th Annual Conference on Composites and Advanced Ceramic Materials, Part 1 of 2: *Ceramic Engineering and Science Proceedings*; Vol. **11** (7/8). John B. Wachtman Jr. (Ed.) The American Ceramic Society, Inc. p 757-781. doi: 10.1002/9780470313008.ch19 URL: <http://dx.doi.org/10.1002/9780470313008.ch19>
- [185] Feng H. J, Hunter K. R and Moore J. J (1994). 'Combustion synthesis of ceramic and metal-matrix composites'. *J. Mater. Synth. Process*; **2**, p 71-86.
- [186] John J. Moore and H. J. Feng (1995). 'Combustion synthesis of advanced materials: Part I. Reaction parameters'. *Progr. Mater. Sci.*; **39** (4-5), p 243-273. doi:10.1016/0079-6425(94)00011-5

- [187] John J. Moore and H. J. Feng (1995). 'Combustion synthesis of advanced materials: Part II. Classification, applications and modelling'. *Progr. Mater. Sci.*: **39** (4-5), p 275-316. doi:10.1016/0079-6425(94)00012-3
- [188] Kaibyshev O. A. and Zaripov N. G. (1997). 'Self-propagating high-temperature synthesis and superconductivity'. *Int. J. of SHS*: **6** (2), p 203.
- [189] Matkowsky B. J., Aldushin A. P., Shkadinsky K. G. and Shkadinskaya G. V. (1997). 'Gravitational effects in SHS'. *Int. J. of SHS*: **6** (3), p 243.
- [190] Munir Z. A. (1997). 'Electrical simulated SHS'. *Int. J. of SHS*: **6** (2), p 165.
- [191] Shiryayev A. (1995). 'Thermodynamics of SHS processes: An advanced approach'. *Int. J. of SHS*: **4** (4), p 351-362.
- [192] E. M. Glagovsky, A. V. Kouprine, L. F. Pelevine, S. V. Yudinsev, V. I. Velichkin, E. E. Konovalov and B. F. Myasoedov (2003). 'Study of matrices synthesised by a self-propagating high-temperature synthesis'. *Czech J. Phys.*: **53** (1), Suppl. A. A657- A663. doi: 10.1007/s10582-003-0084-x
- [193] K Krishnankutty and K R Dayas (2008). 'Synthesis and characterization of monoclinic rare earth titanates, RE₂Ti₂O₇ (RE = La, Pr, Nd), by a modified SHS method using inorganic activator'. *Bulletin of Materials Science.*: **31** (6), p 907-918. doi: 10.1007/s12034-008-0145-7
- [194] J. Subrahmanyam, K. Somaraju and M. P. Srivastava (1995). 'Preparation of TiB₂ powders by self propagating high temperature synthesis (SHS)' in "Ceramic powders for high-tech applications" BVS Subba Rao (Ed.). Universities Press, Hyderabad, India. p124.
- [195] Chyi-Ching Hwang, Tsung-Yung Wu, Jun Wan and Jih-Sheng Tsai (2004). 'Development of a novel combustion synthesis method for synthesizing of ceramic oxide powders'. *Mater. Sci. & Engg. B.*: **111** (1), p 49-56. doi:10.1016/j.mseb.2004.03.023
- [196] C. Divakar, S. K. Bhaumik, L. Rangaraj, Jayaprakash and A. K. Singh (2000). 'Self-propagating synthesis and sintering of dense ceramic materials at high pressures and temperatures'; in: "Proceedings of the AIRAPT-17", p 674-677. URL: http://nal-ir.nal.res.in/4835/01/32self_propagating.PDF
- [197] A. G. Merzhanov (1992). 'Self-propagating high-temperature synthesis and powder metallurgy: unity of goals and competition of principles'; in: "Particulate Materials and Processes: Advances in Powder Metallurgy, Metal Powder Industries". Proc. of the 1992 Powder Metall. World. Congr., San Francisco, CA, USA, 21-26 June 1992. V.9. Princeton: Metal Powder Ind. Federation Publishers, Princeton, NJ, p 341-368.
- [198] Joey F. Crider (1982). 'Self-Propagating High Temperature Synthesis--A Soviet Method for Producing Ceramic Materials' Ceramic Engineering and Science Proceedings Proceedings of the 6th Annual Conference on Composites and Advanced Ceramic Materials: *Ceramic Engineering and Science Proceedings*; Vol. **3** (9/10), William J. Smothers (Ed.), p 519-528 doi: 10.1002/9780470318782.ch8 URL: <http://dx.doi.org/10.1002/9780470318782.ch8>
- [199] Merzhanov A.G (1990). 'Self-propagating high-temperature synthesis: Twenty years of search and findings'; in: "Combustion and Plasma Synthesis of High-Temperature Materials". Z.A. Munir and J. B. Holt (Eds.) VCH, New York, p.1-53.
- [200] J.B. Holt (1987). 'The Use of Exothermic Reactions in the Synthesis and Densification of Ceramic Materials'. *MRS Bull.*: **12** (7), p 60-65.
- [201] John Dalton Wright and Nico A J M Sommerdijk (2001). 'Sol-Gel Materials Chemistry and applications'. Gordon and Breach Science Publishers, The Netherlands 125pp.
- [202] Lisa C Klein (1994). 'Sol gel optics: Processing and applications'. Springer. 605pp.
- [203] Alain C Pierre (1998). 'Introduction to sol-gel processing'. Kluwer Academic Publishers, USA. 394pp.
- [204] Duncan J. Shaw (1992). 'Introduction to colloid and surface chemistry'. Butterworth-Heinemann, Oxford, UK. 4th Ed. 320pp.

- [205] R Aelion, A Loebel and F Eirich (1950). 'Hydrolysis of Ethyl Silicate'. *J. Am. Chem. Soc.*: **72** (12), p 5705-5712. doi: 10.1021/ja01168a090
- [206] J. Livage, M. Henry and C. Sanchez (1988). 'Sol-gel chemistry of transition metal oxides'. *Progress in Solid State Chemistry*: **18** (4), p 259-341. doi:10.1016/0079-6786(88)90005-2
- [207] C.J. Brinker, K.D. Keefer, D.W. Schaefer, R.A. Assink, B.D. Kay and C.S. Ashley (1984). 'Sol-gel transition in simple silicates II'. *J. Non-Cryst. Solids.*: **63** (1-2), p 45-59. doi:10.1016/0022-3093(84)90385-5
- [208] I Strawbridge, A. F Craievich and P. F James (1985). 'The effect of the H₂O/TEOS ratio on the structure of gels derived by the acid catalysed hydrolysis of tetraethoxysilane'. *J. Non-Cryst. Solids.*: **72** (1), p 139- 157. doi:10.1016/0022-3093(85)90170-X
- [209] A. H. Boonstra and T. N. M. Bernards (1989). 'Hydrolysis-condensation reactions in the acid step of a two-step silica sol-gel process, investigated with ²⁹Si NMR at -75°C'. *J. Non-Cryst. Solids.*: **108** (3), p 249-259. doi:10.1016/0022-3093(89)90295-0
- [210] R P J Corriu, D LeCleck, A Vioux, M Pauthe and J Phalippou (1986). 'Ultrastructure processing of advanced ceramics' John D. Mackenzie and Donald R. Ulrich (Eds.), p 113-26, Wiley- Interscience, New York. 1048pp.
- [211] Gérard Orcel and Larry Hench (1986). 'Effect of formamide additive on the chemistry of silica sol-gels: Part I: NMR of silica hydrolysis'. *J. Non-Cryst. Solids.*: **79** (1-2), p 177-194. doi:10.1016/0022-3093(86)90045-1
- [212] Gérard Orcel, Jean Phalippou and Larry Hench (1988). 'Structural evolution at low temperature of formamide modified silica xerogels'. *J. Non-Cryst. Solids.*: **104** (2-3), p 170-180. doi:10.1016/0022-3093(88)90385-7
- [213] Hironori Kaji, Kazuki Nakanishi and Naohiro Soga (1995). 'Formation of porous gel morphology by phase separation in gelling alkoxy-derived silica. Affinity between silica polymers and solvent'. *J. Non-Cryst. Solids.*: **181** (1-2), p 16- 26. doi:10.1016/0022-3093(94)00417-L
- [214] Nathalie Viart and Jean Luc Rehspringer (1996). 'Study of the action of formamide on the evolution of a sol by pH measurements and Fourier transformed infra-red spectroscopy'. *J. Non-Cryst. Solids.*: **195** (3), p 223-231. doi:10.1016/0022-3093(95)00540-4
- [215] Pamela J. Davis, C. Jeffrey Brinker, Douglas M. Smith and Roger A. Assink (1992). 'Pore structure evolution in silica gel during aging/drying II. Effect of pore fluids'. *J. Non-Cryst. Solids.*: **142**, p 197-207. doi:10.1016/S0022-3093(05)80026-2
- [216] R Y Sheinfain, I E Neiwmark (1973). 'Absorption and Absorbents' D N Strazhesko (Ed.), No 1, Wiley NY. p 87-95.
- [217] B. S. Shukla and G. P. Johari (1988). 'Effect of ethanol on the density and morphology of monolithic SiO₂ glass prepared by the sol-gel method'. *J. Non-Cryst. Solids.*: **101** (2-3), p 263- 270. doi:10.1016/0022-3093(88)90162-7
- [218] D. M. Krol and J. G. van Lierop (1984). 'The densification of monolithic gels'. *J. Non-Cryst. Solids.*: **63** (1-2), p 131-144. doi:10.1016/0022-3093(84)90392-2
- [219] J. Zarzycki, M. Prassas and J. Phalippou (1982). 'Synthesis of glasses from gels: the problem of monolithic gels'. *J. Mater. Sci.*: **17** (11), p 3371-3379. doi: 10.1007/BF01203507
- [220] Tatsuhiko Adachi and Sumio Sakka (1988). 'The role of N,N-dimethylformamide, a DCCA, in the formation of silica gel monoliths by sol-gel method'. *J. Non-Cryst. Solids.*: **99** (1), p 118-128. doi:10.1016/0022-3093(88)90464-4
- [221] T. Adachi and S. Sakka (1988). 'Sintering of silica gel derived from the alkoxy silane solution containing N,N-dimethylformamide'. *J. Non-Cryst. Solids.*: **100** (1-3), p 250-253. doi:10.1016/0022-3093(88)90027-0

- [222] I. Artaki, T. W. Zerda and J. Jonas (1986). 'Solvent effects on the condensation stage of the sol-gel process'. *J. Non-Cryst. Solids.*; **81** (3), p 381-395.
doi:10.1016/0022-3093(86)90504-1
- [223] Peter W. Atkins and Julio de Paula (2002). *Physical Chemistry*. 7th edition. Oxford University Press. 1149pp.
- [224] David Levy and Luis Esquivias (1995). 'Sol-gel processing of optical and electrooptical materials'. *Adv. Mater.*; **7** (2), p 120-129. doi: 10.1002/adma.19950070204
URL: <http://dx.doi.org/10.1002/adma.19950070204>
- [225] Sumio Sakka (1994). 'The current state of sol-gel technology' *J. Sol-Gel Sci. Technol.*; **3** (2), p 69-81. doi: 10.1007/BF00486713
- [226] David Levy and David Avnir (1991). 'Room temperature phosphorescence and delayed fluorescence of organic molecules trapped in silica sol-gel glasses'. *J. Photochem. Photobiol. A.: Chem.*; **57** (1-3), p 41-63. doi:10.1016/1010-6030(91)85006-3
- [227] Toshiro Tani, Hiroshi Namikawa, Kazuo Arai and Akio Makishima (1985). 'Photochemical hole-burning study of 1,4-dihydroxyanthraquinone doped in amorphous silica prepared by alcoholate method' *J. Appl. Phys.*; **58** (9), p 3559-3565. doi:10.1063/1.335731
URL: <http://link.aip.org/link/?JAPIAU/58/3559/1>
- [228] David Levy, Shlomo Einhorn and David Avnir (1989). 'Applications of the sol-gel process for the preparation of photochromic information-recording materials: synthesis, properties, mechanisms'. *J. Non-Cryst. Solids.*; **113** (2-3), p 137-145.
doi:10.1016/0022-3093(89)90004-5
- [229] Donald R. Ulrich (1990). 'Prospects for sol-gel processes'. *J. Non-Cryst. Solids.*; **121** (1-3), p 465-479. doi:10.1016/0022-3093(90)90177-N
- [230] K. T. V. Grattan, G. E. Badini, A. W. Palmer and A. C. C. Tseung (1991). 'Use of sol-gel techniques for fibre-optic sensor applications'. *Sensors and Actuators A: Physical*; **26** (1-3), p 483-487. doi:10.1016/0924-4247(91)87037-4
- [231] D. R. Uhlmann, T. Suratwala, K. Davidson, J. M. Boulton and G. Teowee (1997). 'Sol-gel derived coatings on glass'. *J. Non-Cryst. Solids.*; **218**, p 113-122.
doi:10.1016/S0022-3093(97)00162-2
- [232] Donald R. Uhlmann, J. M. Boulton, Gimtong T. Teowee, Lori Weisenbach and Brian J. Zelinski (1990). 'Sol-gel synthesis of optical thin films and coatings'; in: "Sol-Gel Optics". John D. Mackenzie and Donald R. Ulrich (Eds.). *SPIE Proc.*; **1328**, p 270-295. 494pp.
doi: 10.1117/12.22567
- [233] D D Sood (1995). 'Sol gel process for ceramics'; in: "Ceramic powders for high-tech applications". BVS Subba Rao (Ed.). Universities Press, Hyderabad, India. P124.
- [234] Larry L. Hench and Jon K. West (1990). 'The sol-gel process'. *Chem. Rev.*; **90** (1), p 33-72. doi: 10.1021/cr00099a003
- [235] A C Tam (1989). 'Overview of photothermal spectroscopy'; in: "Photothermal Investigations of Solids and Fluids" Jeffrey A Sell (Ed.). p 1-34. Academic Press, Inc. San Diego, CA. 346 pp
- [236] Darryl P Almond and Pravin M Patel (1996). 'Photothermal Science and Techniques'. Chapman & Hall, London. 241pp.
- [237] M. J. Adams and G. F. Kirkbright (1977). 'Analytical optoacoustic spectrometry. Part III. The optoacoustic effect and thermal diffusivity'. *Analyst*; **102** (1213), p 281 - 292.
doi: 10.1039/AN9770200281
- [238] Warren Jackson and Nabil M. Amer(1980). 'Piezoelectric photoacoustic detection: Theory and experiment'. *J. Appl. Phys.*; **51** (6), p 3343-3353. doi:10.1063/1.328045
URL: <http://link.aip.org/link/?JAPIAU/51/3343/1>
- [239] G. Rousset, F. Lepoutre and L. Bertrand (1983). 'Influence of thermoelastic bending on photoacoustic experiments related to measurements of thermal diffusivity of metals'. *J. Appl.*

- Phys.*: **54** (5), p 2383-2391 doi:10.1063/1.332352
 URL: <http://link.aip.org/link/?JAPIAU/54/2383/1>
- [240] P. Charpentier, F. Lepoutre and L. Bertrand (1982). 'Photoacoustic measurements of thermal diffusivity description of the drum effect' *J. Appl. Phys.*: **53** (1), p 608-614. doi:10.1063/1.329966 URL: <http://link.aip.org/link/?JAPIAU/53/608/1>
- [241] W L Barros Melo and R M Faria (1995). 'Photoacoustic procedure for measuring thermal parameters of transparent solids'. *Appl. Phys. Lett.*: **67** (26), p 3892-3894. doi:10.1063/1.115308 URL: <http://link.aip.org/link/?APPLAB/67/3892/1>
- [242] D Fournier and A C Boccara 'Photothermal investigation of solids: basic physical principles'; in: "Photothermal Investigations of Solids and Fluids" Jeffrey A Sell (Ed.). p 35-79. Academic Press, Inc. San Diego, CA. 346 pp.
- [243] Y H Wong, R L Thomas and G F Hawkins (1978). 'Surface and subsurface structure of solids by laser photoacoustic spectroscopy'. *Appl. Phys. Lett.*: **32** (9), p 538-539. doi:10.1063/1.90120 URL: <http://link.aip.org/link/?APPLAB/32/538/1>
- [244] Andreas Mandelis (1989). 'Theory of photothermal wave diffraction and interference in condensed media'. *J. Opt. Soc. Am. A. (JOSA A)*; **6** (2), p 298-308. doi:10.1364/JOSAA.6.000298
 URL: <http://www.opticsinfobase.org/josaa/abstract.cfm?URI=josaa-6-2-298>
- [245] F. Alan McDonald (1986). 'Photoacoustic, photothermal and related techniques: a review'. *Can. J. Phys.*: **64** (9), p 1023-1029. doi:10.1139/p86-174
- [246] A. Rosencwaig (1980). 'Photoacoustics and Photoacoustic Spectroscopy' John Wiley, New York. 309pp.
- [247] David W Ball (2006). 'Photoacoustic Spectroscopy'. *Spectroscopy*; **21** (9), p 14-16. URL: <http://spectroscopyonline.findanalyticchem.com/spectroscopy/data/articlestandard/spectroscopy/382006/373853/article.pdf>
- [248] S A Vinokurov (1983). 'Optoacoustic effect and the thermal diffusivity of solids' translated from *Inzhenero-Fizicheskii Zhurnal*; **44**(1), p 60-66. *Journal of Engineering Physics and Thermophysics*; **44** (1), p 50-55. doi:10.1007/BF00826703
- [249] Andreas Mandelis. 'A Century of Photothermal and Photoacoustic Spectroscopies and Microscopies'. URL: <http://flux.aps.org/meetings/YR99/CENT99/abs/S4250.html#SLC17.004>
- [250] C S Sunandana (1988). 'Physical applications of photoacoustic spectroscopy'. *Phys.Stat. Sol. (A)*; **105** (1), p 11-43. doi: 10.1002/pssa.2211050102
 URL: <http://dx.doi.org/10.1002/pssa.2211050102>
- [251] George H. Brilmeyer, Akira Fujishima, K. S. V. Santhanam and Allen J. Bard (1977). 'Photothermal spectroscopy'. *Anal. Chem.*: **49** (13), p 2057-2062. doi: 10.1021/ac50021a042
- [252] M J Colles, N R Geddes and E Mehdizadeh (1979). 'The optoacoustic effect'. *Contemp. Phys.*: **20** (1), p11-36. doi: 10.1080/00107517908227800
- [253] D Balasubramanian (1983). 'Photoacoustic spectroscopy and its use in biology'. *Bioscience Reports*: **3** (11), p 981-995. doi:10.1007/BF01121025
- [254] Arthur V Houghton and Russell U Acton (1964). 'Optical-acoustic effects in solid film'. *American Institute of Aeronautics and Astronautics Journal (AIAA J)*; **2** (1), p 120-121. URL: <http://pdf.aiaa.org/jaPreview/AIAAJ/1964/PVJAPRE2234.pdf>
- [255] William R. Harshbarger and Melvin B. Robin (1973). 'Opto-acoustic effect. Revival of an old technique for molecular spectroscopy' *Acc. Chem. Res.*: **6** (10), p 329-334 doi: 10.1021/ar50070a001
- [256] A A King and G F Kirkbright (1976). 'Optoacoustic spectrometry for the examination of solid and solid samples'. *Lab. Pract.*: **25**, p 377- 383.
- [257] A. Rosencwaig (1973). 'Photoacoustic spectroscopy of solids'. *Opt. Commun.*: **7** (4), p 305 -308. doi:10.1016/0030-4018(73)90039-4

- [258] A G Bell (1880). 'On the production and reproduction of sound by light'. *Am. J. Sci. (American Journal of Science)*; **20**, p 305- 314.
- [259] Alexander Graham Bell (1881). 'Upon the production of sound by radiant energy'. *Philosophical Magazine Series 5*; **11 (71)**, p 510-528. doi: 10.1080/14786448108627053 URL: <http://www.informaworld.com/10.1080/14786448108627053>
- [260] John Tyndall (1880). 'Action of an intermittent beam of radiant light upon gaseous matter'. *Proc. R. Soc. Lond. (Proceedings of Royal Society of London)*; **31 (206-211)**, p 307-317. doi:10.1098/rspl.1880.0037
- [261] Wilhelm C Röntgen (1881). 'On tones produced by the intermittent irradiation of a gas'. *Philosophical Magazine Series 5*; **11 (68)**, p 308- 311. doi: 10.1080/14786448108627021 URL: <http://www.informaworld.com/10.1080/14786448108627021>
- [262] Rayleigh (1881). 'The Photophone'. *Nature*; **23 (586)**, p 274-275. doi:10.1038/023274a0
- [263] William Henry Preece (1881). 'On the Conversion of Radiant Energy into Sonorous Vibrations'. *Proc. R. Soc. Lond. (Proceedings of the Royal Society of London)*; **31 (206-211)**, p 506- 520 doi:10.1098/rspl.1880.0071
- [264] G Gorelik (1946). *Dokl. Akad. Nauk SSSR*; **54**, p 779.
- [265] P V Slobodskaya (1948). *Izv. Akad. Nauk SSSR, Ser. Fiz.*; **12**, p 656.
- [266] Allan Rosencwaig and Allen Gersho (1976). 'Theory of the photoacoustic effect with solids'. *J. Appl. Phys.*; **47 (1)**, p 64-69. URL: <http://link.aip.org/link/?JAPIAU/47/64/1> doi:10.1063/1.322296
- [267] Rosencwaig A (1975). 'Photoacoustic spectroscopy. New tool for investigation of solids'. *Anal. Chem.*; **47 (6)**, p. 592A-604a doi: 10.1021/ac60356a015
- [268] Allan Rosencwaig (1978). 'Photoacoustic Spectroscopy'. *Advances in Electronics and Electron Physics*; **46**, p 207-311. doi:10.1016/S0065-2539(08)60413-8
- [269] Allan Rosencwaig and Stan S. Hall (1975). 'Thin-layer chromatography and photoacoustic spectrometry' *Anal. Chem.*; **47 (3)**, p 548-549. doi: 10.1021/ac60353a056
- [270] Frank Koppens (1999). 'Feasibility of photo-acoustic spectroscopy on semiconductor quantum wells'. Project report, CUSAT, Kochi.
- [271] Allan Rosencwaig (1977). 'Solid state photoacoustic spectroscopy'; in: "Optoacoustic spectroscopy and detection". 244pp. Yoh Han Pao (Ed.), Academic press, Inc. New York USA, p 193-239.
- [272] Thomas Schmid (2006). 'Photoacoustic Spectroscopy for Process Analysis'. *Analytical and Bioanalytical Chemistry*; **384 (5)**, p 1071-1086. doi:10.1007/s00216-005-3281-6
- [273] Wolfgang Demtröder (2004). 'Laser spectroscopy: Basic concepts and instrumentation'. (3rd edition) Springer, New Delhi, India. 990pp.
- [274] Sohan S. Chitlange. 'Photoacoustic Spectroscopy for Depth Profiling'. URL: <http://www.pharmainfo.net/reviews/photoacoustic-spectroscopy-depth-profiling>
- [275] R S Quimby and W M Yen (1980). 'Photoacoustic theory including energy migration'. *J. Appl. Phys.*; **51 (9)**, p 4985-4989. doi:10.1063/1.328377 URL: <http://link.aip.org/link/?JAPIAU/51/4985/1>
- [276] Larry D. Merkle and Richard C. Powell (1977). 'Photoacoustic spectroscopy investigation of radiationless transitions in Eu²⁺ ions in KCl crystals'. *Chem. Phys. Lett.*; **46 (2)**, p 303-306. doi:10.1016/0009-2614(77)85266-4
- [277] Jesús Etxebarria and Joaquín Fernández (1983). 'Photoacoustic spectra of transparent solids doped with localised absorbing centres'. *J. Phys. C: Solid State Phys.*; **16 (19)**, p 3803-3811. doi: 10.1088/0022-3719/16/19/020
- [278] Robert G. Peterson and Richard C. Powell (1978). 'Photoacoustic spectroscopy investigation of radiationless relaxation processes of Cr³ in crystals'. *Chem. Phys. Lett.*; **53 (2)**, p 366- 368. doi:10.1016/0009-2614(78)85417-7
- [279] R. S. Quimby and W. M. Yen (1978). 'Photoacoustic measurement of absolute quantum

- efficiencies in solids'. *Opt. Lett.*; **3** (5), p181-183. doi:10.1364/OL.3.000181
 URL: <http://www.opticsinfobase.org/ol/abstract.cfm?URI=ol-3-5-181>
- [280] Richard C. Powell, Dean P. Neikirk, and Dhiraj Sardar (1980). 'Radiationless decay processes of Nd³⁺ ions in solids'. *J. Opt. Soc. Am.*; **70** (5), p 486-490. doi:10.1364/JOSA.70.000486
 URL: <http://www.opticsinfobase.org/josa/abstract.cfm?URI=josa-70-5-486>
- [281] Allan Rosencwaig and Edward A. Hildum (1981). 'Nd³⁺ fluorescence quantum-efficiency measurements with photoacoustics'. *Phys. Rev. B*; **23** (7), p 3301 - 3307. doi: 10.1103/PhysRevB.23.3301 URL: <http://link.aps.org/doi/10.1103/PhysRevB.23.3301>
- [282] R. S. Quimby and W. M. Yen (1980). 'Photoacoustic measurement of the ruby quantum efficiency'. *J. Appl. Phys.*; **51** (3), p1780- 1782. doi:10.1063/1.327739
 URL: <http://link.aip.org/link/?JAPIAU/51/1780/1>
- [283] J. C. Murphy and L. C. Aamodt (1977). 'Photoacoustic spectroscopy of luminescent solids: Ruby'. *J. Appl. Phys.*; **48** (8), p 3502-3509. doi:10.1063/1.324199
 URL: <http://link.aip.org/link/?JAPIAU/48/3502/1>
- [284] L. C. Aamodt and J. C. Murphy (1978). 'Size considerations in the design of cells for photoacoustic spectroscopy. II. Pulsed excitation response'. *J. Appl. Phys.*; **49** (6), p 3036-3045. doi:10.1063/1.325318 URL:<http://link.aip.org/link/?JAPIAU/49/3036/1>
- [285] Seema Kandpal and R P S Kushwaha (2007). "Photoacoustic spectroscopy of thin films of As₂S₃, As₂Se₃ and GeSe₂." *Pramana- Journal of Physics*; **69** (3), p481-484. doi: 10.1007/s12043-007-0150-1
- [286] Svein Otto Kanstad and Per-Erik Nordal (1978). 'Photoacoustic and photothermal spectroscopy- Novel tools for the analysis of particulate matter'. *Powder Technol.*; **22** (1), p 133-137. doi:10.1016/0032-5910(79)85016-0
- [287] David Cahen, Gerard Bults, Haim Garty and Shmuel Malkin (1980). 'Photo acoustic in life sciences'. *J. Biochem. Biophys. Methods*; **3** (5), p 293-310. doi:10.1016/0165-022X(80)90010-X
- [288] D. Balasubramanian (1981). 'Photoacoustic spectroscopy of biological systems'. *Photochem. Photobiol.*; **34** (6), p 749-752. doi: 10.1111/j.1751-1097.1981.tb09435.x
 URL: <http://dx.doi.org/10.1111/j.1751-1097.1981.tb09435.x>
- [289] D. Balasubramanian and Ch. Mohan Rao (1982). 'Biological application of photoacoustic spectroscopy' *Current Science*; **51** (3), p 111-117. URL: http://www.ias.ac.in/j_archive/cursci/51/3/111-117/viewpage.html
- [290] Y H Pao (Ed.) (1977). 'Optoacoustic spectroscopy and detection'. Academic press, Inc. New York USA, 244pp.
- [291] Rosencwaig A (1980). 'Photoacoustic Spectroscopy'. *Ann. Rev. Biophys. Bioeng.*; **9**, p 31-54. doi:10.1146/annurev.bb.09.060180.000335
- [292] Eric A Ash (Ed.)(1980). 'Scanned Image Microscopy'. Academic Press NY. 461pp.
- [293] J. G. Parker (1973). 'Optical Absorption in Glass: Investigation Using an Acoustic Technique'. *Appl. Opt.*; **12** (12), p 2974-2977. doi:10.1364/AO.12.002974
 URL: <http://www.opticsinfobase.org/ao/abstract.cfm?URI=ao-12-12-2974>
- [294] John B Kinney and Ralph H Staley (1982). 'Applications of photoacoustic spectroscopy' *Annu. Rev. Mater. Sci.* **12**, p 295-321. doi:10.1146/annurev.ms.12.080182.001455
- [295] F. Alan McDonald (1979). 'Photoacoustic determination of small optical absorption coefficients: extended theory'. *Appl. Opt.*; **18** (9), 1363-1367. doi:10.1364/AO.18.001363
 URL:<http://www.opticsinfobase.org/ao/abstract.cfm?URI=ao-18-9-1363>
- [296] Charles Kittel (1969). 'Thermal Physics'. Ch 13. Wiley. New York. 432 pp.
- [297] A C Boccara, D Fournier and J Badoz (1979). 'Thermo-optical spectroscopy: Detection by the "mirage effect"'. *Appl. Phys. Lett.*; **36** (2), p 130-132. doi:10.1063/1.91395
 URL: <http://link.aip.org/link/?APPLAB/36/130/1>

- [298] F Lepoutre, B K Bein and L J Inglehart (1986). 'Three dimensional calculation of the mirage effect with a personal computer'. *Can. J. Phys.*; **64** (9), p1037- 1041. doi:10.1139/p86-176
- [299] P. K. Kuo, M. J. Lin, C. B. Reyes, L. D. Favro, R. L. Thomas, D. S. Kim, Shu-Yi Zhang, L. J. Inglehart, D. Fournier, A. C. Boccara, and N. Yacoubi (1986). 'Mirage-effect measurement of thermal diffusivity. Part I: experiment'. *Can. J. Phys.*; **64** (9), p 1165–1167. doi:10.1139/p86-202
- [300] F A McDonald, G C Wetsel Jr. and G E Jamieson (1986). 'Photothermal beam deflection imaging of vertical interfaces in solids'. *Can. J. Phys.*; **64** (9), p 1265- 1268. doi:10.1139/p86-218
- [301] K R Grice, L J Inglehart, L D Favro, P K Kuo and R L Thomas (1984). 'Thermal wave imaging of closed cracks in opaque solids'. *J. Appl. Phys.*; **54** (11), p 6245 -6255. doi:10.1063/1.331942 URL: <http://link.aip.org/link/?JAP/AU/54/6245/1>
- [302] P. K. Kuo, E. D. Sandler, L. D. Favro, and R. L. Thomas (1986). 'Mirage-effect measurement of thermal diffusivity. Part II: theory'. *Can. J. Phys.*; **64** (9), p 1168–1171. doi:10.1139/p86-203
- [303] P Cielo, L A Utracki and M Lamontagne (1986). 'Thermal diffusivity measurements by the converging thermal wave technique'. *Can. J. Phys.*; **64** (9), p1172-1177 and the references therein. doi:10.1139/p86-204
- [304] Subhash L. Shindé, Jitendra Singh Goela (2006). 'High thermal conductivity materials'. Springer Verlag, 271pp.
- [305] Nathaniel E. Putzig. (2006). 'Thermal inertia and surface heterogeneity on Mars'. Ph D thesis. University of Colorado.
URL:<http://nathaniel.putzig.com/research/dissertation/dissertation.pdf>
- [306] J. A. Balderas-López (2006). 'Photoacoustic signal normalization method and its application to the measurement of the thermal diffusivity for optically opaque materials'. *Rev. Sci. Instrum.*; **77** (6), Article 064902, 4pp. doi:10.1063/1.2209951 URL: <http://link.aip.org/link/?RSINAK/77/064902/1>
- [307] Andrew C. Tam (1986). 'Applications of photoacoustic sensing techniques'. *Rev. Mod. Phys.*; **58** (2), p 381 – 431. doi: 10.1103/RevModPhys.58.381 URL: <http://link.aps.org/doi/10.1103/RevModPhys.58.381>
- [308] Clare Smith (2001). 'Environmental Physics'. Routledge, London. 320pp.
- [309] Mohamed K. Ghorab, Ramarao Chatlapalli, Shamim Hasan and Arwinder Nagi (2007). 'Application of thermal effusivity as a process analytical technology tool for monitoring and control of the roller compaction process'. *AAPS PharmSciTech*; 8 (1), Article 23, p E155-E161. doi: 10.1208/pt0801023
- [310] URL: <http://scienceworld.wolfram.com/physics/ThermalInertia.html>
- [311] URL: http://nathaniel.putzig.com/research/ti_primer.html
- [312] Annieta Philip K, Lyjo K. Joseph, Litty M. Irimpan, Bindu Krishnan, P. Radhakrishnan, V. P. N. Nampoori and Raghu Natarajan (2007). 'Thermal characterization of ceramic tapes using photoacoustic effect'. *phys. stat. sol. (a)*; **204** (3), p 737–744. doi: 10.1002/pssa.200622287 URL: <http://dx.doi.org/10.1002/pssa.200622287>
- [313] A. Sikorska, B. B. J. Linde and W. Żwirbla (2005). 'Study of thermal effusivity variations in water solutions of polyethylene glycol 200 using photoacoustic method'. *Chem. Phys.*; **320** (1), p 31-36. doi:10.1016/j.chemphys.2005.06.024
- [314] Firas Kamel Mohamad Al-asfoor, W. Mahmood Mat Yunus, Azmi Zakaria, Mohd Maarof Moksni, Noor Jawad Ridha and L.Y.C. Josephine (2008). 'Thermal Effusivity Measurement of Virgin Coconut Oil-Methanol Mixtures using Photoacoustic Technique'. *American J. of Engineering and Applied Sciences*; **1** (3), p 200-203. URL: <http://www.scipub.org/fulltext/ajecas/ajecas13200-203.pdf>

- [315] Shrotriya A K, Verma L S, Singh R and Chaudhary D R (1991). 'Prediction of the heat storage coefficient of a two-phase system' *J. Phys. D: Appl. Phys.*; **24** (6), p 849-853. doi: 10.1088/0022-3727/24/6/008
- [316] A Bouguerra, A Ledhem, J P Laurent, M B Diop and M Queneudec(1998) . 'Thermal effusivity of two-phase wood cement-based composites' *J. Phys. D: Appl. Phys.*; **31** (17), p 2184-2190. doi: 10.1088/0022-3727/31/17/017
- [317] URL: <http://www.evitherm.org/default.asp?ID=277>
- [318] B. N. Jagatap and A. Venugopalan (Eds.) (2006). 'Recent developments in spectroscopy of lanthanides and actinides'. R V Enterprises, Mumbai. 235pp.
- [319] Joseph H Simmons and Kelly S Potter (2000). 'Optical materials'. Academic Press. San Diego. USA. 391pp.
- [320] Helmut H. Telle, Ángel González Ureña and Robert J. Donovan (2007). 'Laser chemistry: spectroscopy, dynamics and applications. JohnWiley & Sons Ltd, England. 502pp.
- [321] LiCONiX® 5300 series water cooled ion laser operations manual, USA (1993).
- [322] Quanta-Ray, Pulsed Nd:YAG lasers User's manual GCR-100 series, Spectra-Physics, USA (1997).
- [323a] ORIEL 1000 watt universal xenon arc lamp power supplies models 8540 and 8541D operating instructions. ORIEL corporation USA, (1986).
- [323b] ORIEL universal arc lamp housings models 66020 thru 66023 instruction manual. ORIEL corporation USA, (1985).
- [324] Tsunami. Mode-locked Ti: sapphire laser. User's manual. Spectraphysics USA. (2002).
- [325] Instruction manual. Diode pumped solid state lasers. BWH/ BWT-xx series.
- [326] G L Loper, J A Gelbwachs and S M Beck (1986). 'CO₂ laser photoacoustic spectroscopy applied to low level toxic vapor monitoring'. *Can. J. Phys.*; **64** (9), p 1124- 1131. doi:10.1139/p86-194
- [327] O. Raghu and J. Philip. 'A dual channel photoacoustic cell for imaging experiments on solid samples'. *J. Instrum. Soc. India*; **33** (3), p 155-158.
URL: [http://www.isoi.in/Journal/BackIssues/33\(3\).pdf](http://www.isoi.in/Journal/BackIssues/33(3).pdf)
- [328] M. V. Marquezini, N. Cella, A. M. Mansanares, H. Vargas and L. C. M. Miranda (1991). 'Open photoacoustic cell spectroscopy'. *Meas. Sci. Technol.*; **2** (4), p 396 -401
doi: 10.1088/0957-0233/2/4/020
- [329] C García-Segundo, M Villagrán-Muniz and S Muhl (1998). 'Determination of thin film optical properties by the photoacoustic OPC technique'. *J. Phys. D: Appl. Phys.*; **31** (2), p 165-171. doi: 10.1088/0022-3727/31/2/002
- [330] A. M. Mansanares, H. Vargas, F. Galembeck, J. Buijs and D. Bicanic (1991). 'Photoacoustic characterization of a two-layer system'. *J. Appl. Phys.*; **70** (11), p 7046- 7050. doi:10.1063/1.349782 URL:<http://link.aip.org/link/?JAPIAU/70/7046/1>
- [331a] Sajan D George (2003). ' Laser induced photothermal investigations on thermal and transport properties of certain selected photonic materials'. Ph. D. Thesis. CUSAT. Kochi.172p
- [331b] Nibu A George (2001). 'Photoacoustic and photothermal deflection studies on certain selected photonic materials'. Ph. D. Thesis. CUSAT. Kochi. 152pp
URL: http://www.photonics.cusat.edu/_private/Nibu_Thesis.pdf
- [332] Model V-550/560/570 Spectrophotometer Hardware/Function manual (data station type). JASCO Corporation, Tokyo, Japan. (1996).
- [333] Model SLM-468 single reflection attachment instruction manual. JASCO Corporation, Tokyo, Japan. (1994).
- [334] Cary Eclipse Hardware operation manual. VARIAN. Australia 2000.
- [335] ORIEL compact 1/8 meter monochromator and1/8 monochromator gratings and slits brochure. ORIEL corporation USA.
- [336] Princeton Instruments NTE/CCD, Manual, Roper Scientific, Inc. USA (2001).

Materials- Methods-Measurements

- [337] Operating instructions, Acton Research. SpectraPro-500i , 0.500m focal length triple grating imaging monochromator/spectrograph, Acton Research corporation USA, (2001).
- [338] WinSpec, spectroscopic software of Princeton Instruments, Roper Scientific, USA 2001
- [339] HMS light beam chopper instruction manual Ithaco model 230. New York (1985).
- [340] Model SR540 optical chopper instruction manual, Stanford Research Systems, USA. (1997).
- [341] Model SR830 DSP Lock-In Amplifier operating manual and programming reference, Stanford Research Systems. USA, (2002).
- [342] LabVIEW™ 7 Express, User manual, Measurements manual, Getting started with LabVIEW, National Instruments Corporation, USA. (2003).
- [343] Model SR 560 low-noise preamplifier, Stanford Research Systems, USA, (1999).

Chapter 2

Thermal and optical characterization of dye intercalated montmorillonites

Abstract

The first section of the chapter presents thermal diffusivity (TD) measurement on dye intercalated commercial K-10 and KSF montmorillonites carried out by photoacoustic (PA) technique. Methylene blue (MB) adsorbed K-10 samples showed distinct TD changes due to a regular decrease in specific surface area and pore volume as a result of pore filling by dye molecules when compared to the ordered KSF samples which do not have a regular change in specific surface area and pore volume. PA method was carried out to determine TD of some other industrially important dyes -auramine O (AO), malachite green (MG) and rhodamine B (RB) - adsorbed K-10. The repeatedly adsorbed MB and AO samples showed a lesser TD than the samples which have adsorbed once. The sintered MB samples showed a higher TD though they exhibited a similar trend as un-sintered pellets. The optical absorption and fluorescence studies on RB and MG intercalated acid activated K-10 montmorillonite dispersions prepared from the dried dye intercalated montmorillonite are presented in the second section. The absorption and fluorescence peaks of RB dispersions showed a bathochromic shift with respect to the dye concentrations. The samples exhibited a fluorescence emission at 421 nm which is attributed to silica and is having an intensity variation depending on the concentration of the dyes.

2.1. Prologue	95
2.2. Sample details	96
2.3. Dye molecular aggregates- Molecular exciton coupling theory	96
2.4. Section I - Thermal characterization of dye intercalated montmorillonites using photoacoustics	101
Part A: Thermal diffusivity dependence on host montmorillonite	104
Part B: Thermal diffusivity dependence on sintering temperature	111
Part C: Thermal diffusivity dependence on dye	114
2.5. Section II - Spectroscopic studies on dye intercalated K-10 montmorillonite aqueous dispersions	122
Part A: Rhodamine B intercalated K-10	123
Part B: Malachite green intercalated K-10	131
Part C: Dispersions of KSF and K-10	134
2.6. Summary	136
2.7. References	137



L. K. Joseph, G. Sanjay, H. Suja, S. Sugunan, V. P. N. Nampoori, P. Radhakrishnan; "Thermal characterisation of dye-intercalated K-10 montmorillonite ceramics using photoacoustic technique" *Philosophical Magazine* **89** (10), 2009, pp 895-905
[doi: 10.1080/14786430902806652](https://doi.org/10.1080/14786430902806652)



Lyjo K. Joseph, H. Suja, G. Sanjay, S. Sugunan, V. P. N. Nampoori, P. Radhakrishnan; "Thermal characterization of methylene blue intercalated montmorillonites by photoacoustic technique" *Applied Clay Science* **42** (3-4), 2009, pp 483-487
[doi:10.1016/j.clay.2008.06.006](https://doi.org/10.1016/j.clay.2008.06.006)

2.1. Prologue:

The developments of complex materials necessitate a finer characterization of their physical properties and a better knowledge of the physical phenomena that determine their behaviour at the macroscopic level. Synthetic dyestuffs are used extensively in textile, paper, printing industries and dye-houses. The dyestuff usage has been increasing day by day because of the tremendous increase of industrialisation and man's urge for colour.¹¹ Dye stuff pollution through the waste-water generated in the industry causes adverse aesthetic effects on organisms.¹²⁻⁵¹ Although various industries are responsible for contributing hazardous organic wastes into our water supplies, the textile industry is of particular concern. Anywhere from 1% -20% of the world's production of dyes are lost during dyeing processes and is released as textile effluents. These effluents are generally quite toxic. Of all the dyes available, approximately 50% to 70% are aromatic azo compounds, which are known carcinogens. Waste-waters from dyeing and textile industries easily produce toxic trihalomethanes when chlorinated.¹⁶¹ Removal of colour from dye bearing waste-water is a complex problem because of the difficulty in treating such waste-waters by conventional treatment methods.¹⁷¹ Several physico-chemical processes^{11, 8-171} like electro and chemical coagulation,¹¹⁷⁻²⁵¹ ozonization,^{126, 271} membrane filtration,¹²⁸⁻³⁵¹ electrolysis,^{120, 361} oxidation,^{120-22, 37-421} biodegradation,^{110, 42-571} flocculation,^{119, 271} precipitation,¹⁵⁸⁻⁶¹¹ crystallisation,¹⁵⁸¹ froth flotation, anaerobic decolourisation,¹⁶²¹ reverse osmosis,^{117, 63, 641} ion exchange,^{21-23, 61, 65-701} reduction,¹⁴³¹ biological stabilisation¹⁷¹⁻⁷³¹ and adsorption^{174, 751} by activated charcoal¹⁵¹ or carbon¹⁷⁶¹ have been developed for the dye exclusion during the waste-water treatment.¹⁷⁷¹ Some of these methods are selective,¹⁷⁸¹ expensive, less efficient,^{140, 791} of limited applicability, may need special infrastructure and even produce wastes, which are difficult to dispose of. Among all these treatment processes adsorption is found to be highly effective and non-destructive in nature.¹⁵¹ A variety of physical, chemical and biological methods have been used for the dye exclusion during the waste-water treatment¹⁸⁰⁻⁹²¹ and diverse clays can be employed for dye adsorption.¹⁹³⁻⁹⁹¹

Nano-composite materials, which contain organic dyes incorporated in a solid matrix, are used in various applications, such as optical sensors, devices for photo-induced switching, solid lasers and in memory media.¹¹⁰⁰¹ The optical properties of the dyes crucially depend on the properties of the hosts which are extremely vital in the applied research of materials.¹¹⁰¹¹

2.2. Sample details:

2.2.1. Commercial clay samples: KSF and K-10:

The commercially available montmorillonites K-10 and KSF were purchased from Fluka, Sigma- Aldrich Chemicals Pvt. Ltd. KSF and K-10 are two differently modified acid-activated montmorillonites;^[102] the extent of leaching is lower for KSF than for K-10. K-10 clay mineral has a layered structure. Each layer is composed of one octahedral alumina sheet sandwiched between two tetrahedral silica sheets. The sheets are connected via Si-O-Al linkages. In the silica sheet, isomorphous substitution of Si by Al occurs whereas in the Al sheet, isomorphous substitution by Mg and Fe occurs. This leads to a net negative charge on the layers which are compensated by exchangeable cations Na^+ , K^+ , Mg^{2+} and Ca^{2+} . Many such layers are stacked together with an inter-layer spacing of ~ 1 nm. Acid leaching leads to the removal of some Al and Fe from the framework and also results in the replacement of the exchangeable cations with H^+ which imparts acidity to the system. As a result of acid treatment, de-lamination takes place and a disordered structure result.^[102,103] Acid activated clays in nature can be used as efficient decolourising agents^[98] due to their enhanced bleaching power^[104] arising from increased specific surface area (SSA), meso/ micro- pore volume (PV) and surface acidity of clay samples.^[105]

2.2.2. Sample preparation- Dye adsorption from solution:

1g of clay was treated with 100 ml dye solution (10^{-5} , 10^{-4} and 10^{-3} M concentration respectively) and stirred magnetically for 24 hours. It was then filtered, Soxhlet extracted with deionised water and dried at 120 °C for 12 hours. To measure the maximum adsorption capacity, the same process was repeated with 10^{-3} M solution for three times. These powdered samples were used for the experiments.^[106,107]

2.3. Dye molecular aggregates - Molecular exciton coupling theory:

Organic dyes may change their colour and other optical and chemical properties in relation to their chemical environment.^[108, 109] Therefore, dyes have often been used as probes or sensors in various scientific fields.^[110-114] The idea of using dyes to help identification of clay minerals or to probe their properties first appeared several decades ago.^[115] The molecular aggregation is due to hydrophobic interactions, which is a general tendency of non-polar molecules to associate physically in aqueous solutions. The presence of non-polar molecules in water disrupts the hydrogen bond network of water molecules, resulting in a loss of translational and rotational degrees

of freedom of the solvent within the hydrophobic hydration shell. Such a mechanism is generally referred to as a loss of entropy of the system.^[116]

2.3.1. The exciton model:

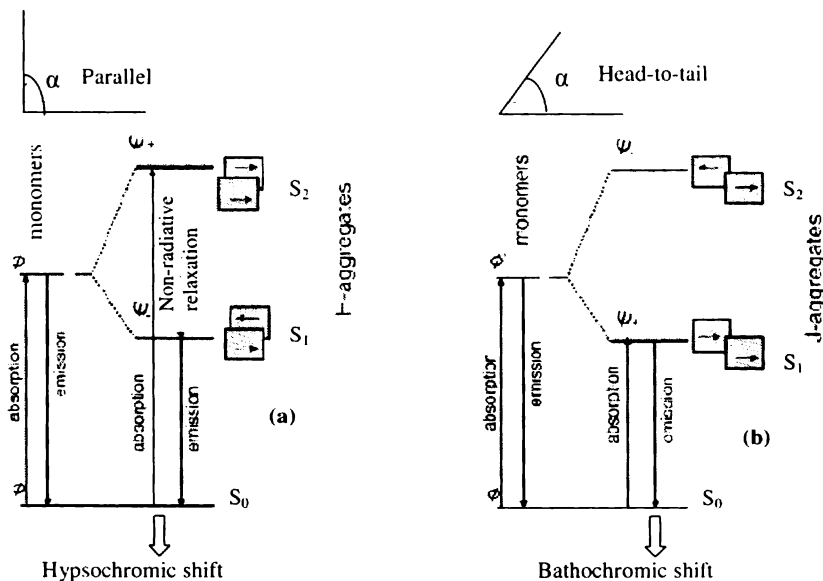


Figure 2.1: Schematic representation of the energy graphs for the dye dimers of (a) H- and (b) J-type types according to molecular exciton theory. Ψ_+ -directions of the transition moments are parallel, and the transition is non-zero. Ψ_- directions of the transition moments are anti-parallel, and the transition is zero. α is the slip angle between the long axis and any one of the parallel molecule.

Absorption spectra of dye molecular aggregates usually show large differences when compared to the individual molecules. Optical properties of the dye molecular aggregates are explained by the molecular exciton* model^[117](Figure. 2.1). The model considers electrostatic interactions between transition moments of individual dye molecules, called an exciton coupling. Exciton coupling leads to the splitting of the excited electronic state of the molecule, the magnitude of which depends on distances between interacting transition dipoles and their arrangement in space. Two excited energy levels are the result of electrostatic attraction and repulsion between the transition moments.^[118] According to exciton theory, the dye molecule is regarded as a point dipole and the excitonic state of the dye aggregate splits into two levels through

* Exciton is an electrically neutral excited state, often regarded as a bound state of an electron and a hole.

the interaction of transition dipoles. A transition to the upper state in parallel aggregates having parallel transition moments and to a lower state in a head-to-tail arrangement with perpendicular transition moments leads to hypsochromic[‡] (blue) and bathochromic[§] (red) shifts, respectively (Figure 2.1).

2.3.2. Angle of slippage (α):

The angle between the long axis (line passing through the center of the aggregates or parallel to it) and one of the parallel molecule is called the '*angle of slippage*' or the '*slip angle*' or the '*slippage angle*'. Large molecular slippage ($\alpha < 32^\circ$) results in a bathochromic shift (J - aggregate), and small slippage ($\alpha > 32^\circ$) results in a hypsochromic shift (H - aggregate). Most importantly, the exciton theory is valid only when the interaction between orbitals of constituent molecules is negligible.^[116]

2.3.3. H and J aggregates:

There are two main types of dye molecular aggregates, formally and originally assigned according to their optical properties, but closely related to their structure and the type of intermolecular association. Certain molecular aggregates consisting of organic dyes are remarkable in exhibiting an intense and very narrow absorption peak, known as a J-band[§] or Scheibe-Peak, which is red-shifted away from the region of monomer absorption. Apart from those dyes showing the J-band on aggregation, there are also dyes for which the absorption maximum is shifted to higher energies forming H-band^{**}. The width of the resulting absorption band is comparable to that of the monomeric dyes and shows a complicated vibrational structure.^[119] Scheibe^[120] found that for some dyes, the aggregate absorption band is red-shifted with respect to that of the monomer. These are the J-aggregates showing a very narrow band whose position is well-predicted by a theory ignoring intra-molecular vibrations. By contrast, other dyes showed a shift towards the blue (i.e. higher absorption energies) and were termed H-aggregates (hypsochromic shift). Unlike the J-band, the line-shape of the H-band

[‡] Hypsochromic shifts are often referred to as blue shifts in photochemistry in which the frequency of an electromagnetic wave emitted by a source moving towards the observer is shifted towards the blue side of the electromagnetic spectrum (i.e., its wavelength is decreased, or its energy is increased).

[§] Bathochromic shift is a change of spectral band position in the absorption, reflectance, transmittance, or emission spectrum of a molecule to a longer wavelength (lower frequency). This can occur because of a change in environmental conditions. Bathochromic shifts are often referred to as red shifts. It has no relation to Doppler shift or other wavelength - independent meanings of redshift.

[§] J for Jelley, one of the first workers who investigated these shifts.

^{**} H for hypsochromic

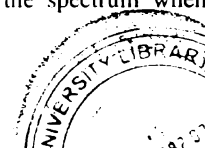
generally shows a rich vibrational structure and has a width of the order of that of the monomer band. Some substances exhibit both a J-band and a H-band on aggregation. As a result of this complicated vibrational structure, although there exists a considerable literature on the simpler case of the J-band, there have been only a few theoretical articles which address the line-shape of H-aggregates.^[119, 121-124]

Extensive studies on J- and H- aggregates have resulted in the proposal that these aggregates exist as a one-dimensional assembly in solution that could be in (a) ladder type, (b) staircase type, or (c) brickwork type of arrangement (*Figure 2.2*).



Figure 2.2: Schematic representation of the different arrangement of dyes in the solid surface and in solution. (a) ladder type, (b) staircase type and (c) brickwork type.

H-aggregates are based on a sandwich-type intermolecular association^[125] (*Figure 2.1a*). Less frequent J-aggregates (*Figure 2.1b*) are formed by head-to-tail intermolecular interactions.^[126] In the H-aggregates, coupled transition moments could be oriented in either the parallel or anti-parallel fashion. The anti-parallel orientation (Ψ_-) of an H-dimer has a lower energy state, due to the electrostatic attraction between the transition moments. In the J-aggregates, anti-parallel moments (Ψ_-) result in a higher energy due to electric repulsion. Resulting dipole for the anti-parallel arrangements of the transition moments is always zero; and therefore, the transitions to such states are symmetry forbidden. Only the transitions to the states with parallel orientations (Ψ_+) are allowed, which is to the lower energy state for the J-aggregates and to the higher energy state for the H-aggregates. The perfect H- and J-aggregates are just two ideal states of all possible forms and variations of molecular assemblies. Many dyes may form such assemblies, which include the structural features of both the H- and J-aggregates. In such cases, the molecular aggregates absorb light with energies corresponding to both the higher and lower energy states. The assignments of the bands absorbing at the low- and high-energy transitions indicate the structural features of the dye supramolecular assemblies. Unfortunately, there are serious problems to identify structures of molecular assemblies from the spectrum when several types of assemblies are present in a mixture.^[116]



H- and J-aggregates have their optical properties according to their structural packing. Actually the difference in structure is due to the different slip angles of the stacked molecules. It is generally agreed that both H- and J-aggregates are composed of parallel dye molecules stacked plane-to-plane and end-to-end and form two-dimensional dye crystal molecule, according to exciton theory, and is regarded as a point dipole. When molecules or chromophores are aligned parallel, two new excitonic bands are generated according to a simple exciton theory: one with higher energy and the other with lower than the monomer energy level as mentioned earlier.

H-dimers or larger H-aggregates would require very short distances between neighbouring negatively charged sites. The clay surface would need to be almost fully covered with the dye in order to form homogeneous two-dimensional coverage of only H-aggregates.^[101] In H-aggregates, the lower state is much stabilised. So the transition from the excited state to the ground state is very fast and happens mostly between the excitonic bands with vanishing dipole moments as a result of which most of the energy losses are non-radiative like thermal losses.^[126-128] Due to this reason the H aggregates have very low fluorescence which is difficult to measure by regular techniques. The H-aggregates have large stoke's shift with low fluorescence yield. The transition energy of such aggregates is explained by the differences in the geometry of the molecular packing within the aggregates,^[126, 127] and thus, these aggregates are structurally distinguished by the different slip angles between the molecular transition moment and the long axis of the aggregates - small slip angle for the J-aggregates and a large slip angle for the H-aggregates.

In J-aggregates, transitions are allowed only to low energy states and as a consequence, J-aggregates are characterised by small stoke's shift fluorescence with a high quantum yield.^[129] J-aggregation is due to only partial, head-to-tail association between the dye cations.^[118, 130] The formation of large two-dimensional J-aggregates does not require full coverage on the clay surface. The distance between two neighbouring negative charge sites is larger for the formation of stable J-dimer than that required for the formation of H-dimer. With decreasing layer-charge density the distances between neighbouring dye cations increase. Consequently, the sandwich type association with H-aggregates association breaks down in favour of J-aggregates with a 'head-to-tail' type association of transition dipoles and less dense packing of the dye cations.^[101, 118] Ordered J-aggregates usually exhibit sharp bands in the spectra.^[126, 127] Absence of any sharp bands of studied dyes indicates the formation of less-ordered J-aggregates.

In the systems with clay minerals, the dye aggregation is also sensitive to the surface properties of clay mineral templates and depends on the type of exchangeable cations.^[131, 132] It has been proven that the main parameter which controls dye molecular aggregation on clay mineral surfaces is the layer charge.^[116] Lower charge densities induce longer distances between adsorbed dye cations. Consequently, the monomeric form of isolated dye cations is preferentially adsorbed in such cases. If the layer charge density of clay minerals is sufficiently high, the distances between neighbouring adsorbed dye cations are smaller and H-aggregates are preferentially formed. Less densely packed J-aggregates resulting from a head-to-tail coupling^[127] occur less frequently under specific conditions on the surfaces of clay minerals of medium to low charge densities.^[116, 127, 131-134]

2.4. Section I - Thermal characterization of dye intercalated montmorillonites using photoacoustics:

2.4.1. Preamble:

The thermal diffusivity (TD), a thermo-physical parameter, determines the diffusion of the heat through the sample. In ceramics, the thermal energy is basically carried away by phonons.^[135] The composition, structure and arrangements of phases determine the thermal properties of the ceramics. Morphological features like pores, grain boundaries, line defects etc. influence the propagation of phonons through the ceramic body.^[136, 137]

The photothermal techniques, based on the absorption of pulsed or modulated optical radiation and subsequent release of the absorbed energy through non-radiative de-excitation, are widely used, well established, non-contact, simple and highly sensitive for the determination of the thermal and optical properties of a variety of materials.^[106,107,135-143] This non-radiative relaxation produces temperature fluctuations in the sample. These temperature fluctuations facilitate an indirect measurement of the thermal and optical properties of the sample.^[106, 107, 136, 144-147] The laser induced photoacoustic (PA) method has gained more popularity due to its simple, elegant experimental technique as well as the versatility in employing different configurations to measure the required thermo-physical parameters with great accuracy. In PA, a periodic heat flow from the solid to the surrounding gas produces pressure variations within the cell. This is the primary source of the acoustic signal and is detected by a sensitive microphone.^[148] Thermal characterization contributes to the development and optimisation of new materials.

The surfaces of clay minerals exhibit strong affinity to dye i.e., montmorillonites show an interesting capacity in separating dyes from water.^{197, 125, 149} They are found to be an efficient adsorbent for the uptake of the dyes^{102, 150} and their utilisation for further applications like 'wall plastering' demands their thermal characterization. The curing time required for these materials may be less if their TD is higher. Moreover, if the stability of the dye in montmorillonite host material is higher, the colour fading of the walls will also be lesser.

2.4.2. Thermal diffusivity measurement - photoacoustic theory:

The Rosencwaig and Gersho (RG) theory of the PA effect¹⁴⁷ confirmed by more complete calculations^{151, 152} shows that pressure variations at the front surface of an optically thick sample depend on the TD of the sample.¹⁵³ As the RG theory indicates, the PA effect is primarily dependent on the relationship between three 'length' parameters of the sample: the sample thickness l , the optical absorption length l_b and the thermal diffusion length $\mu = (2\alpha / \omega)^{1/2}$. While dealing with an optically very opaque solid, as long as the solid is not photoacoustically opaque ($\mu < l_b$), only the light absorbed within the first thermal diffusion length contributes to the acoustic signal. The RG theory also predicts that for an opaque material ($l_b < l$), the PA signal will vary as ω^{-1} when $\mu > l_b$ and as $\omega^{-3/2}$ when $\mu < l_b$ by varying the chopping frequency.^{146, 147} Charpentier¹⁵³ et al. (1982) demonstrated that the pressure variations at the front surface of an optically thick sample can be written as the product of two terms. One depends on the modulation frequency f of excitation and the other independent of f . When $f > f_c$ the variations of the frequency dependent term is independent of the diffusivity and when $f < f_c$ the variations in pressure depends on the sample diffusivity. Here the characteristic frequency f_c is given by the relation: $\alpha = l^2 f_c$. As thermal diffusion length is a function of chopping frequency, PA amplitude spectrum has a slope change from -1 to -1.5 at this particular frequency f_c depending on sample thickness. Thus by knowing the sample thickness l and the transition frequency f_c , the TD of the sample can be evaluated using the expression $\alpha = l^2 f_c$. A slope variation occurs at f_c in the log (amplitude) versus log (frequency) plot and knowing the sample thickness l , one can find the TD.^{106, 107, 136, 137, 153, 154}

2.4.3. Experimental setup:

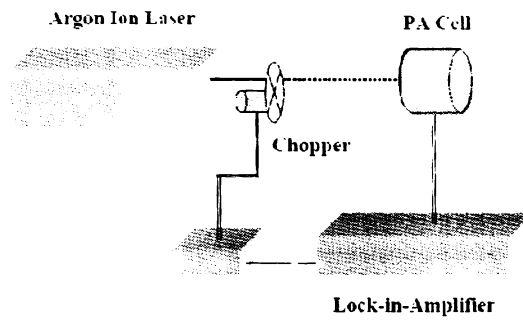


Figure 2.3: Schematic representation of photoacoustic experimental setup.

The schematic representation of the experimental set up is given in *Figure 2.3*. Optical radiation from an Argon ion laser at 488 nm, 25 mW (cw, Liconix 5300) with a stability of $\pm 0.5\%$ was used as the source of excitation. It was intensity modulated using a mechanical chopper (HMS Light Beam Chopper 230) before it reached the sample. Detection of the PA signal was made using a sensitive electret microphone (Knowles BT 1754). The amplitude of the PA signal was measured by means of a dual phase lock-in-amplifier (Stanford Research Systems SR 830). The reflection mode geometry (*Figure 2.4*) of the open cell PA technique was used in this experiment.

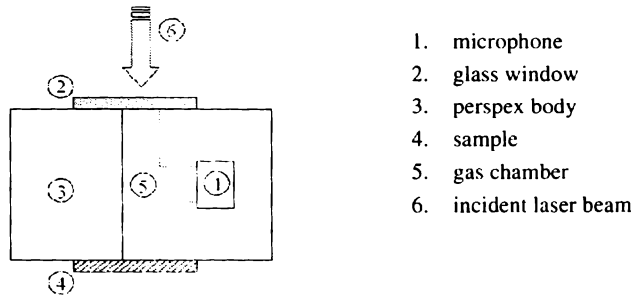


Figure 2.4: Reflection mode geometry of photoacoustic setup.

2.4.4. Sample details:

Pelletised samples were used for PA studies. The pellets were prepared using a hydraulic pellet press at a pressure of 10^6 kgm^{-2} . The sample thickness was measured using Mitutoyo micrometer, which can measure thickness with an accuracy of $\pm 1 \mu\text{m}$.

2.4.5. Part A: Thermal diffusivity dependence on host montmorillonite:

A1. Introduction:

The variation in TD of the dye intercalated montmorillonites was investigated and the results are presented. The effect of dye loading on TD in two types of montmorillonites- KSF and K-10- was studied using the PA technique. The effect of repeated adsorption on the TD of the clay samples was also studied. The TD dependence of selective dye adsorption and porosity of two types of montmorillonites are presented here. An attempt is made to understand the change in TD of methylene blue (MB) adsorbed montmorillonites and to make suitable materials with tuneable thermal properties because TD is a thermo-physical quantity which can be obtained directly from the PA studies.^[155]

MB is a toxic, halogenated, aromatic hydrocarbon that is seen in the textile factory effluent streams. Clay mineral surfaces have strong affinity to MB ions.^[125, 156, 157] 'Montmorillonites' exhibit a remarkable capacity in separating MB from water^[149] and are found to be a competent adsorbent for the uptake of the dyes.^[102] The thermal characterization of the dye-montmorillonite complexes is necessary to find out further applications.^[158]

A2. Materials and methods:

A2.1. Sample details:

MB was purchased from Sd fine Chem. The MB adsorbed samples were prepared as described in 2.2.2. The MB intercalated K-10 samples were designated as MB-Z where -Z denoted the concentration. The repeated adsorbed K-10 sample was denoted as MB-X. Similarly MB adsorbed KSF samples were named as KSFMB-Z. The repeated adsorbed KSF sample was designated as KSFMB-X.

A2.2. Reflectance spectra measurement:

The MB intercalated K-10 and KSF samples taken in pellet form were employed for the PA studies. The Model SLM-468 single reflection attachment of a JASCO V-570 UV/VIS/NIR spectrophotometer was used to measure the relative reflectance of these samples using the forward reflected light from the aluminium-deposited plane mirror as reference at an angle of incidence ~ 5°.

A2.3. Specific surface area and porosity measurement:

The Specific surface area (SSA) and porosity measurements were made in a Micromeritics Tristar 3000 surface area & porosity analyser. SSA was calculated using the BET (Brunauer Emmett Teller) interpretation of the nitrogen adsorption isotherm at $p/p_0 < 0.3$. Pore size distribution was calculated from t-plot measurements using the Barrett Joyner Halenda (BJH) method. Prior to the analysis, the samples were degassed in nitrogen at 120 °C for 12 hours.

A2.4. TG/DTA measurement:

Perkin Elmer, Pyris Diamond TG/DTA^{††} instrument was used for the TGA^{‡‡} measurement at a rate of 20°C/min under nitrogen atmosphere conditions.

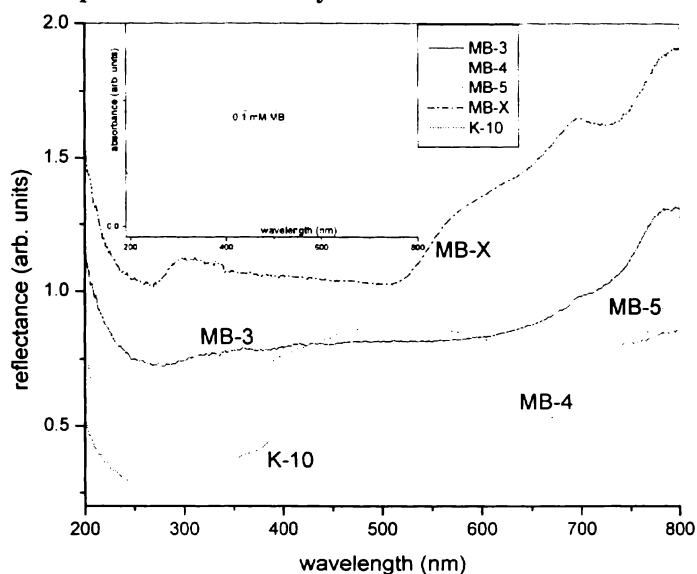
A3. Results and discussions:**A3.1. Optical reflectance study:**

Figure 2.5: Reflectance spectra of methylene blue (MB) intercalated K-10 pellets. Inset: Absorption spectrum of 0.1 mM methylene blue aqueous solution.

^{††} DTA- differential thermal analysis.

^{‡‡} The thermo-gravimetric analysis (TGA) is a commonly used method to determine the degradation temperature of the organic and inorganic components in the materials.

All samples under investigation were visibly well opaque and hence a transmission spectrum of the specimen was impossible at 488nm. Lindberg and Snyder^[159](1972) from their diffuse reflectance spectral studies of clay minerals observed that montmorillonite minerals had a higher absorption coefficient in the near UV and blue regions of the visible spectrum. The qualitative character of the absorption spectra of the material could be obtained from the reflectance spectrum. The reflectance spectra of the MB intercalated K-10 and KSF samples are given in *Figure 2.5* and *Figure 2.6* respectively.

The bandwidth and the location of the monomer band are affected by the increasing loading. An increase of loading also induces the formation of dimers and higher aggregates.^[160]

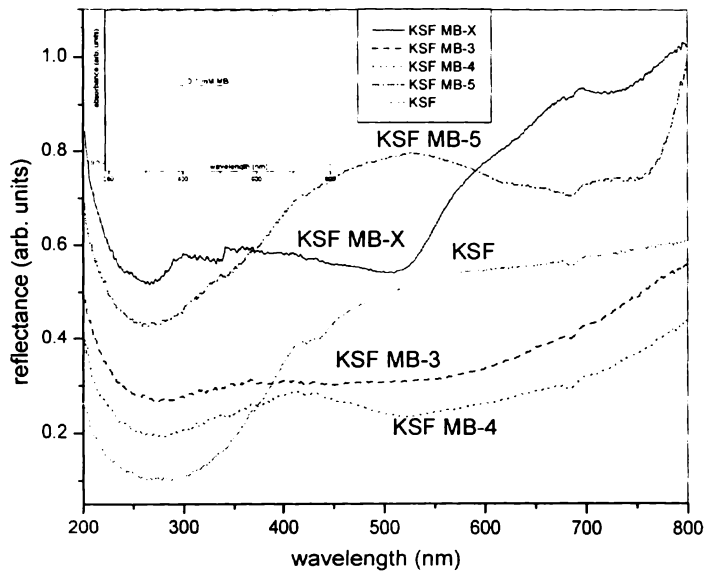


Figure 2.6: Reflectance spectra of methylene blue (MB) intercalated KSF pellets
Inset: Absorption spectrum of 0.1mM methylene blue aqueous solution.

A3.2. Photoacoustic study:

A typical variation of the PA amplitude spectrum for MB-5, characterised by the slope change is given in *Figure 2.7*. All other samples showed similar behaviour, in accordance with the RG theory.^[147] The measured TD values of the MB intercalated K-10 samples are given in *Table 2.1* and those of KSF samples are given in *Table 2.2*. Clay samples and soils possess TD of the order of 10^{-7} to $10^{-4} \text{ m}^2\text{s}^{-1}$.^[106, 107, 144, 161-165]

However, TD is a transient thermo-physical parameter which measures how effectively phonons carry heat through the sample. In the case of pelletised samples, particles are compressed together. Hence, the average inter-particle distance is less^[166] and allows easy propagation of thermal waves through the sample. Thereby, they yield relatively high TD values. The preparation conditions and procedure affect the thermal parameters of these kinds of ceramic materials.^[137]As shown in *Figure 2.8*, MB decomposed at > 200 °C while the dye intercalated clay mineral was stable up to 400°C.

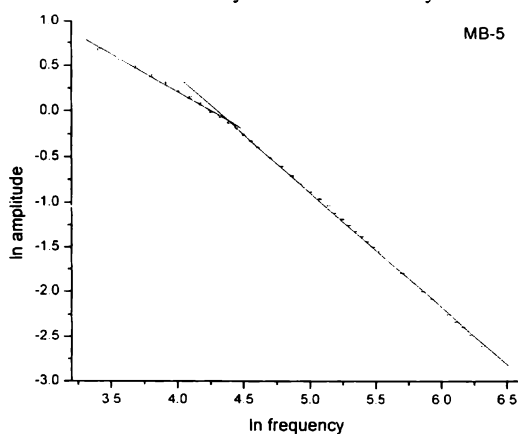


Figure 2.7: Photoacoustic (PA) amplitude plot of the MB-5 pellet.

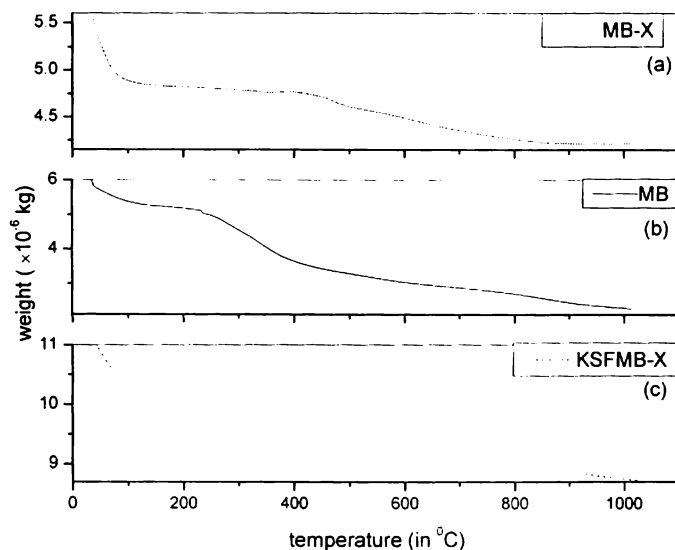


Figure 2.8: TGA of (a) MB-X, (b) pure methylene blue and (c) KSFMB-X.

Table 2.1: Thermal diffusivity (TD) values of methylene blue (MB) adsorbed K-10 samples obtained at room temperature.

Dye loading (mg/g clay)	K-10 samples	Sample thickness $\times 10^{-3}$ m	TD $\times 10^{-4}$ m ² s ⁻¹
32.0	MB-3	1.072 \pm 0.001	0.945 \pm 0.002
3.2	MB-4	0.833 \pm 0.001	0.778 \pm 0.002
0.32	MB-5	0.974 \pm 0.001	0.753 \pm 0.002
96.0	MB-X	0.775 \pm 0.001	0.461 \pm 0.002
0.0	K-10	0.934 \pm 0.001	0.676 \pm 0.002

A3.3. Effect of pore volume on thermal diffusivity:

The porosity of a pellet is an important property to ascertain its quality.^[167] In general, it affects the compressive strength, thermal conductivity and also plays an important role in controlling its swelling during its reduction.^[168] Nishioka^[169] reported that, not only porosity but pore size and their distribution also have an effect on thermal conductivity. It was explained that pellet with lower average pore size has more solid/pore interface area for same porosity which adds resistance to heat transfer. This effect of solid/pore interface area will be more predominant in small pore size ranges, where increase in specific surface area of pore is more for a similar decrease in pore sizes.^[169, 170] The porosity of a pellet controls thermal conductivity by two ways:^[170]

1. Decrease in porosity increases solid/solid contact area and increases solid state conduction.
2. At the same porosity level, decrease in average pore size increases the pore/solid surface area, which in turn increases resistance to heat conduction.

The net change in thermal conductivity with porosity will depend on the contribution by the above two factors. At high porosity level and with larger pores, decrease in porosity or PV will increase particle to particle contact area and decrease the pore/solid interfacial area. However, after certain pore volume/size the increase in contact area is likely to be less predominant than change in particle pore surface area. The decrease in pore size, at constant porosity, will increase pore/particle interface area with almost no change in contact area. This adds resistance to heat flow and decreases thermal conductivity.^[170] The decrease in porosity reduces the free zones of particle contact leading to a considerable increase in the material density. In porous materials this parameter may affect deeply the permeability and as a consequence, the TD and the thermal conductivity.^[171]

Effective thermal conductivity and TD of the pellet decreases gradually with increase in porosity. The decrease in TD and thermal conductivity must hence be attributed to the increase in SSA of pores and added resistance to heat conduction.^[170]

Table 2.2: Thermal diffusivity (TD) values of the KSF samples obtained at room temperature.

Dye loading (mg/g clay)	KSF samples	Sample thickness $\times 10^{-3}$ m	TD $\times 10^{-4}$ m ² s ⁻¹
32.0	KSFMB-3	0.982 \pm 0.001	0.931 \pm 0.002
3.2	KSFMB-4	0.971 \pm 0.001	0.898 \pm 0.002
0.32	KSFMB-5	0.980 \pm 0.001	0.893 \pm 0.002
96.0	KSFMB-X	0.931 \pm 0.001	0.864 \pm 0.002
0.0	KSF	1.029 \pm 0.001	0.625 \pm 0.002

The TD increased with increasing dye concentration. The dye adsorption changes the TD value and by controlled adsorption, samples with desired TD can be prepared. The presence of air in the porous network of K-10 contributed to a low TD value of 0.676×10^{-4} m²s⁻¹. When a small amount of MB enters the matrix, it displaces some of the air which reduces the PV as seen in MB-5 and increases TD to 0.753×10^{-4} m²s⁻¹. When larger amounts of MB was adsorbed, more of air was displaced resulting in decrease of porosity and subsequent increase in TD.^[136] The PV of the K-10 was decreased with increase in concentration of the dye molecules (Table 2.3). The pores in the structure act as scattering centres for phonons and hence affect the phonon mean free path and consequently the TD value.^[136]

Table 2.3: Specific surface area (SSA) and pore volume (PV) obtained from N₂ adsorption measurements for the methylene blue (MB) intercalated K-10 samples.

Sample	SSA ($\times 10^3$ m ² kg ⁻¹)	PV ($\times 10^{-3}$ m ³ kg ⁻¹)
MB-3	166 \pm 5	0.307 \pm 0.001
MB-4	177 \pm 5	0.318 \pm 0.001
MB-5	181 \pm 5	0.336 \pm 0.001
MB-X	117 \pm 5	0.276 \pm 0.001
K-10	202 \pm 5	0.369 \pm 0.001

A3.4. Effect of repeated adsorption on K-10:

Repeated adsorption (sample MB-X) decreased the TD value (0.461×10^{-4} m²s⁻¹) showing that the thermal properties of the samples could be changed by repeated

adsorption. On repeated adsorption of the dye the effective TD was reduced because of the low TD values of the dye. Dyes exhibit typical diffusivities of the order of $10^{-2} \text{ cm}^2 \text{ s}^{-1}$.^[140, 141] MB-X had a well defined reflectance spectrum compared to MB-3 due to the larger amount of MB adsorbed (*Figure 2.5*). In MB-X, the thermal wave generation or/ and propagation was less due to the presence of strongly interlinked dye molecules and these samples showed less TD. At maximum loading (MB-X), there was a drastic decrease in SSA and porosity as evidenced from N_2 adsorption measurements (*Table 2.3*). The lower TD may be due to the clustering and dense packing of MB molecules.^[106, 107]

A3.5. Pore volume effect on the thermal diffusivity of dye adsorbed KSF:

The dye intercalated KSF samples had higher TD than the pure KSF. But, TD of MB adsorbed samples did not show appreciable variation. Initially, SSA and PV increase due to the inter-layer expansion as a result of dye intercalation (*Table 2.4*). Dye molecules prevent access of nitrogen molecules into the pores at higher loadings resulting in lowering SSA and PV. The TD values of KSFMB-4 ($0.898 \times 10^{-4} \text{ m}^2 \text{ s}^{-1}$) and KSFMB-5 ($0.893 \times 10^{-4} \text{ m}^2 \text{ s}^{-1}$) were similar (*Table 2.2*). This may be attributed to the greater SSA and PV of KSFMB-4 than that of KSFMB-5. The interlayer expansion may increase SSA and PV of the KSFMB-5 and KSFMB-4. As the dye concentration is increased, the enrichment of dye molecules decreases SSA and PV of the samples, as seen in case of KSFMB-3 and KSFMB-X (*Table 2.4*).

Table 2.4: Specific surface area (SSA) and pore volume (PV) obtained from N_2 adsorption measurements for the methylene blue (MB) intercalated KSF samples.

Sample	SSA ($\times 10^3 \text{ m}^2 \text{ kg}^{-1}$)	PV ($\times 10^{-3} \text{ m}^3 \text{ kg}^{-1}$)
KSFMB-3	76 \pm 5	0.171 \pm 0.001
KSFMB-4	98 \pm 5	0.186 \pm 0.001
KSFMB-5	57 \pm 5	0.160 \pm 0.001
KSFMB-X	39 \pm 5	0.110 \pm 0.001
KSF	14 \pm 5	0.075 \pm 0.001

A3.6. Effect of repeated adsorption on KSF:

The multiple adsorbed KSFMB-X had a lesser TD ($0.864 \times 10^{-4} \text{ m}^2 \text{ s}^{-1}$) than the single adsorbed KSFMB-3 ($0.931 \times 10^{-4} \text{ m}^2 \text{ s}^{-1}$). This is due to the presence of heavily loaded dye in the host material, which is evident from the distinct reflectance spectra of KSFMB-X when compared to that of KSFMB-3 (*Figure 2.6*). A steep decrease in PV

and SSA was also seen in the case of KSFMB-X (*Table 2.4*). Thus, the clustering and dense packing of the dye molecules contributed to the lower TD of the KSFMB-X.¹¹⁰⁶¹

A3.7. Thermal diffusivity of methylene blue adsorbed K-10 and KSF –

A comparison:

The dye intercalated K-10 samples showed considerable changes in the TD values compared to the dye intercalated KSF samples. Though PV and SSA of KSF were small compared to K-10, it had a smaller TD ($0.625 \times 10^{-4} \text{ m}^2\text{s}^{-1}$) than K-10 ($0.676 \times 10^{-4} \text{ m}^2\text{s}^{-1}$). This may be due to their more highly ordered structure with respect to K-10. SSA and PV of KSF were much lower than that of K-10. As the amount of the loaded dye increased, the PV and SSA of dye intercalated K-10 samples gradually decreased while that of KSF samples initially increased and then decreased. The initial increase in PV and SSA was due to the interlayer expansion and pore filling reduced PV and SSA. Thus, a substantial change in TD was not observed in the dye intercalated KSF samples.¹¹⁰⁶¹

A4. Conclusions:

The selective adsorption of dye by montmorillonite can be used for obtaining samples with desired TD. The contribution of MB towards TD becomes more significant as the amount of dye increases. Repeatedly adsorbed samples have a lower porosity and TD due to the clustering and dense packing of the MB molecules in the clay mineral network. The decomposition temperature of the intercalated dye was higher than that of the pure dye. The dye intercalated K-10 showed significant changes of TD with the amount of MB adsorbed compared to KSF. Hence, K-10 is more suitable for obtaining samples with desired TD values by MB adsorption.

2.4.6. Part B: Thermal diffusivity dependence on sintering temperature:

B1. Introduction:

Sintering is broadly defined as a consolidation of a loose mass to a dense mass through heating. Generally, it causes a decrease in both the SSA and the porosity, but an increase in the density of the samples.¹¹⁷²¹Sintering expels organic material, volatile impurities and moisture content in the sample. The sample becomes more uniform on sintering. Thus the phonon scattering due to various scattering mechanisms is reduced. During the process of sintering, there is the diffusion of different elements that compose the material. This provides mass transport and gives rise to better homogeneity in terms of pore distribution.¹¹⁷³¹Thus lattice connectivity is enhanced.

the scattering centres are reduced and the mean free path is increased. This increase in mean free path of heat carrier results in an increased value for TD of the sintered samples.^[137, 142] With the increase of sintering temperature, the sintering driving force increases and the self-diffusion and inter-diffusion of atoms enhance as well, which accelerates the densification of materials. On the other hand, due to components of low fusing point in the matrix, some liquid phase will appear at higher temperature, which can fill some pores and then strengthen the densification of the composites to a certain extent.^[174]

The thermal characterization of MB intercalated montmorillonites - K-10 and KSF - revealed that K-10 samples have well defined changes compared to KSF samples.^[106] Hence, the variation in TD of the MB intercalated K-10 montmorillonites at various sintering temperatures and the effect of dye loading on TD were studied using the PA technique.

B2. Experimental details:

The reflectance spectra of the pelletised samples were obtained with the help of a JASCO V-570 UV/VIS/NIR spectrophotometer. The same samples were employed for the PA studies. The details of the PA measurement are given in section 2.4.3.

B3. Sample details:

The samples, prepared by the methods described earlier in 2.2.2. and 2.4.4, were sintered at 300 °C and 500 °C for overnight. The dye (MB) adsorbed K-10 samples are employed here for the TD measurements.

B4. Results and discussion:

B4.1. Samples sintered at 300 °C:

Figure 2.9 shows the reflectance spectra of the sintered pellets used for the PA study. Still, the dye intercalated samples have noticeable changes in the reflectance compared to the K-10 pellet.

Table 2.5 shows the TD values of the MB intercalated K-10 samples sintered at 300°C. It is known that the TD values of the ceramic samples can be modulated by varying the sintering temperature.^[136] All the sintered samples have a higher TD value compared to un-sintered samples.^[106]

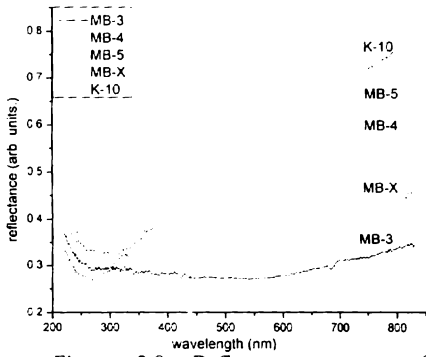


Figure 2.9: Reflectance spectra of methylene blue intercalated K-10 pellets sintered at 500 °C.

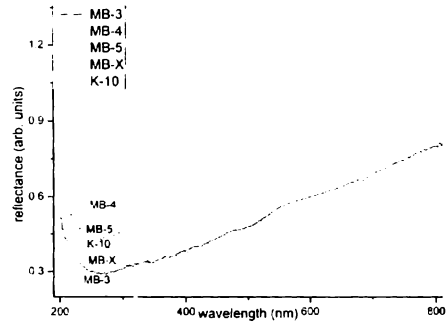


Figure 2.10: Reflectance spectra of methylene blue adsorbed K-10 pellets sintered at 500 °C.

Table 2.5: Thermal diffusivity (TD) values of methylene blue (MB) intercalated K-10 montmorillonites sintered at 300 °C.

Sample	Thickness $\times 10^{-3}$ m	TD($\times 10^{-4}$ m ² s ⁻¹)
MB-3	0.959 \pm 0.001	0.972 \pm 0.002
MB-4	0.924 \pm 0.001	0.870 \pm 0.002
MB-5	0.849 \pm 0.001	0.830 \pm 0.002
MB-X	0.930 \pm 0.001	0.889 \pm 0.002
K-10	1.003 \pm 0.001	1.006 \pm 0.002

MB intercalated sintered samples (at 300 °C, Table 2.5) also show the same trend as the un-sintered ones.^[106] But, it is observed that the TD of MB-5 is less than that of K-10. The higher TD of K-10 can be due to the enhanced lattice connectivity.^[137,142,173] Here also, the repeatedly adsorbed sample, MB-X, has a lesser TD than the single adsorbed sample, MB-3, which may be due to the densely packed dye molecules as in the case of the un-sintered samples.^[106]

B4.2. TGA analysis of methylene blue intercalated K-10:

The TGA of pure MB and MB-X (Figure 2.8) shows that MB decomposes after 200°C while the dye intercalated K-10 is stable even near 400°C. Hence, the decomposition temperature of the dye within the clay is higher than that of the pure dye.^[106]

B4.3. Samples sintered at 500 °C:

Studies were also carried out on the pellets sintered at 500 °C. The reflection spectra of the samples are given in Figure 2.10. All the samples showed the same nature in the

visible range. They are found to be bleached and the TD measurements on K-10 and MB-X samples with thickness $(0.985 \pm 0.001) \times 10^{-3} \text{m}$ and $(0.910 \pm 0.001) \times 10^{-3} \text{m}$ respectively, which are the two extremes of the present study, show a value of $(1.017 \pm 0.002) \times 10^{-4} \text{m}^2 \text{s}^{-1}$ and $(0.961 \pm 0.002) \times 10^{-4} \text{m}^2 \text{s}^{-1}$ respectively. The reduced TD of MB-X at 500 °C can be attributed to the presence of only a few MB molecules, which are still present in the clay network. However, it is obvious that the dye doped samples are slowly approaching the TD value of the pure K-10 as the sintering temperature increases.^[107]

B5. Conclusions:

The sintered samples exhibit higher TD values. When the sintering temperature increases, the dye starts decomposing and the TD values of the MB intercalated samples gradually approach to that of the pure montmorillonite. Thus a variation in the sintering temperature and dye concentration can be used for changing the effective TD values of the ceramic samples.

2.4.7. Part C: Thermal diffusivity dependence on dye:

C1. Introduction:

From the studies described in the earlier parts of this section, K-10 is found to be showing noticeable changes in TD values on dye intercalation. This part of the studies deals with the TD dependence of fluorescent and non-fluorescent dye adsorbed K-10.

C2. Experimental setup:

The absorption spectra of the samples taken in a thin-film form were obtained with the help of a JASCO V-570 UV/VIS/NIR spectrophotometer. The same samples taken in a pellet form were employed for the PA studies. The PA measurement details are given in section 2.4.3. The pore volume (PV) and specific surface area (SSA) measurements were carried out as described in A2.3.

C3. Sample details:

The samples were prepared as described in 2.2.2. The samples were designated as D-Z where -Z denoted the dye concentration and D represented the corresponding dye (AO, MG and MB). The repeatedly adsorbed sample was denoted as D-X. The dye AO was purchased from Loba Chemie and the oxalate salt of MG from Sigma.

C4. Results and discussions:

C4.1. Absorption studies on dye intercalated samples:

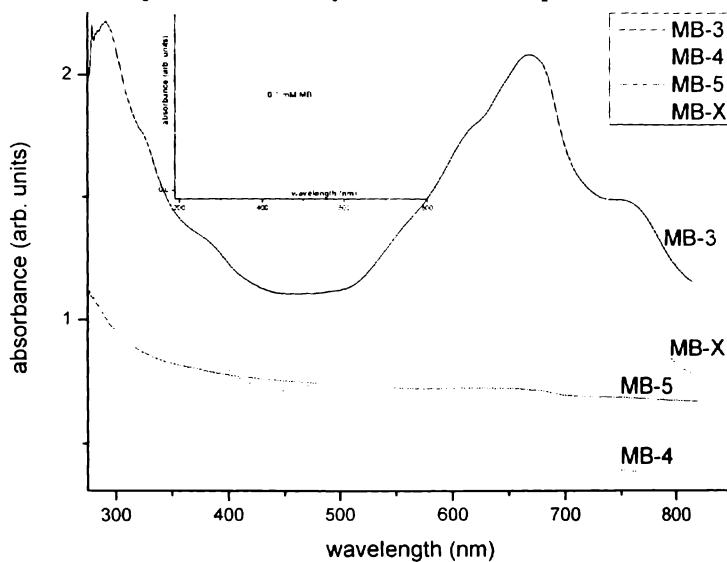


Figure 2.11: Absorption spectra of methylene blue intercalated K-10 montmorillonites. Inset: Absorption spectrum of 0.1 mM aqueous solution of methylene blue (MB).

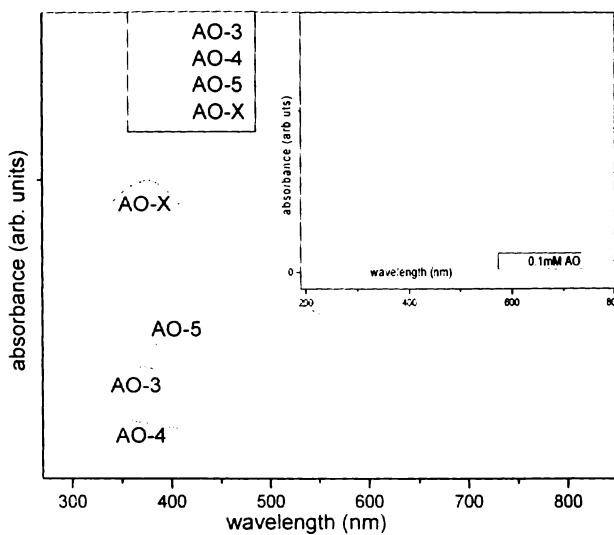


Figure 2.12: Absorption spectra of auramine O intercalated K-10 montmorillonites. Inset: Absorption spectrum of 0.1 mM aqueous solution of auramine O (AO).

The absorption spectra of the MB intercalated samples (*Figure 2.11*), taken as a film, showed a broadened nature with respect to the pure dye at 10^{-4} molar concentration. The absorption spectra of AO and MG intercalated samples, taken as films, are given in *Figure 2.12* and *Figure 2.13* respectively.

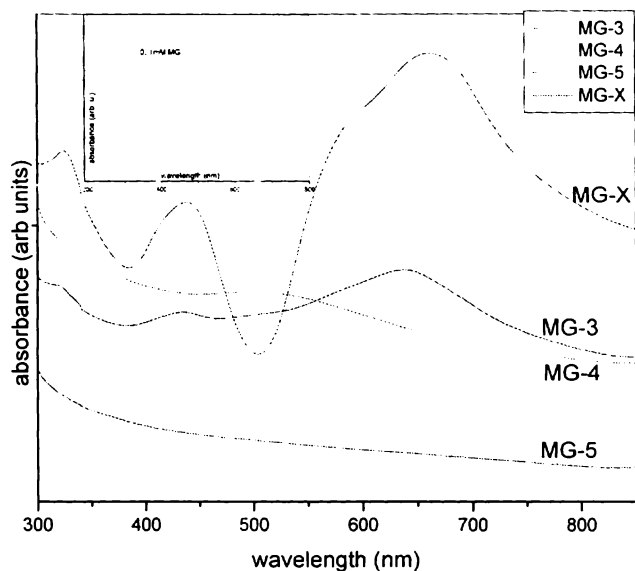


Figure 2.13: Absorption spectra of malachite green intercalated K-10 montmorillonites. Inset: Absorption spectrum of 0.1 mM aqueous solution of malachite green (MG).

The observed broadening and shifts in the absorption spectra are due to the formation of clusters. The excitonic interactions between the chromophores in a very dense packed structure result in a red shift in the spectra.^[175] Moreover, the phonon scattering of excitons results in a strong reduction of the peak height of each constituent absorption band and the broadened band overlap each other.^[176] The superposition of lattice phonon spectra on the absorption spectrum of the dye makes the spectrum broad as observed in the present case.^[177] It should also be noted that the dye gets immobilised in a solid matrix. The shape of the absorption peak and the position of its maximum depend much on the matrix quality. In solution, the maximum wavelength of the cationic dyes depends on the relative permeability of the solvent. In a solid matrix, the absorption peak becomes broader and the maximum wavelength is shifted towards higher values. Due to the van der Waals intermolecular interactions, deviations from planarity may decrease in solid matrix, so that it can be reasonably expected that the maximum absorption wavelength of the dyes will be much higher in a solid matrix than in a solution. It is very likely that the distribution of the strength of

the solid matrix-dye interactions is much broader than that of the solvent dye interaction. Consequently, the solid matrix-dye interaction also brings about the broadening of the absorption bands.^[178]

C4.2. Photoacoustic study:

The PA amplitude spectrum of the pellets, characterised by the slope change, is similar^[106] to that given in the previous section A3.2. The measured TD values of the samples under investigation are given in *Table 2.1*, *Table 2.6* and *Table 2.7*.

Table 2.6: Thermal diffusivity (TD) values of auramine O (AO) intercalated K-10 montmorillonites obtained at room temperature.

Sample	Thickness $\times 10^{-3}$ m	TD ($\times 10^{-4}$ m ² s ⁻¹)
AO-5	0.965 \pm 0.001	0.987 \pm 0.002
AO-4	0.982 \pm 0.001	0.990 \pm 0.002
AO-3	0.939 \pm 0.001	1.029 \pm 0.002
AO-X	0.928 \pm 0.001	0.927 \pm 0.002

Table 2.7: Thermal diffusivity (TD) values of malachite green (MG) intercalated K-10 montmorillonites obtained at room temperature.

Sample	Thickness $\times 10^{-3}$ m	TD ($\times 10^{-4}$ m ² s ⁻¹)
MG-5	0.811 \pm 0.001	0.481 \pm 0.002
MG-4	0.835 \pm 0.001	0.687 \pm 0.002
MG-3	0.888 \pm 0.001	0.695 \pm 0.002
MG-X	0.878 \pm 0.001	0.805 \pm 0.002

The TD of the dye intercalated samples increases with increase in dye concentration. When a small amount of dye (10^{-5} M) enters the matrix, it displaces some of the air and cations in K-10 which leads to a reduction in porosity and hence the TD is increased.^[136] The PV of the samples decreases with the increase in concentration of the dye molecules within the clay network^[106] (*Figure 2.14*, *Table 2.3*, *Table 2.8* and *Table 2.9*). As more of dye gets adsorbed, more of air gets displaced, and an increase in TD is expected due to the decrease in porosity.^[136] For samples under the present investigation, not only PV but the dye concentration is also changing. This suggests that the dye also contributes to the TD and this contribution becomes more significant as the amount of dye increases.

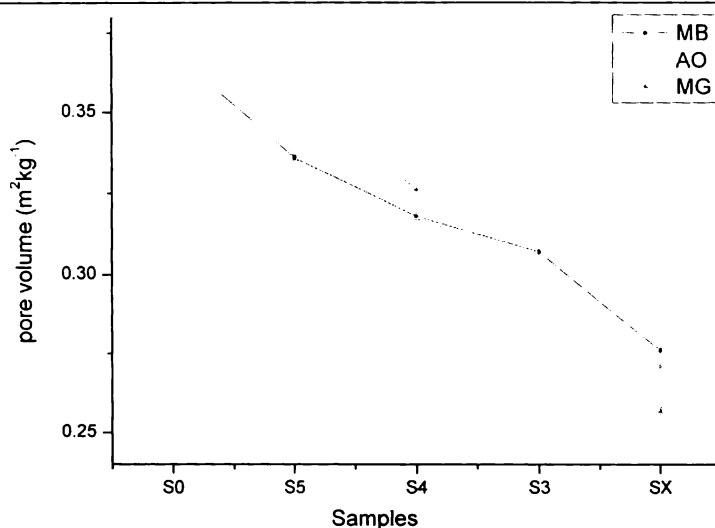


Figure 2.14: Pore volume (PV) of different dye intercalated K-10 montmorillonites. Here S=MB- methylene blue, AO- auramine O and MG- malachite green. S0=K-10. Details of the samples are given in Table 2.3, Table 2.8 and Table 2.9.

Table 2.8: The specific surface area (SSA) and pore volume (PV) obtained from N₂ adsorption measurements for the auramine O (AO) intercalated K-10 samples.

Sample	SSA (m ² kg ⁻¹) × 10 ³	PV(m ³ kg ⁻¹) × 10 ⁻³
AO-5	191±5	0.365±0.001
AO-4	182±5	0.337±0.001
AO-3	166±5	0.293±0.001
AO-X	116±5	0.271±0.001

Table 2.9: The specific surface area (SSA) and pore volume (PV) obtained from N₂ adsorption measurements for the malachite green (MG) intercalated K-10 samples.

Sample	SSA (m ² kg ⁻¹) × 10 ³	PV(m ³ kg ⁻¹) × 10 ⁻³
MG-5	190±5	0.359±0.001
MG-4	180±5	0.326±0.001
MG-3	145±5	0.270±0.001
MG-X	103±5	0.257±0.001

As the concentration of the dye increases, the porosity gets reduced by the filling of dye molecules in the pores thereby increasing the TD. Repeated adsorption of the dye reduces the effective TD of the system because of the low TD values of the dye.^[140]

This confirms that the dye also contributes to the TD. Thus the controlled adsorption can be used to obtain samples with the desired TD.

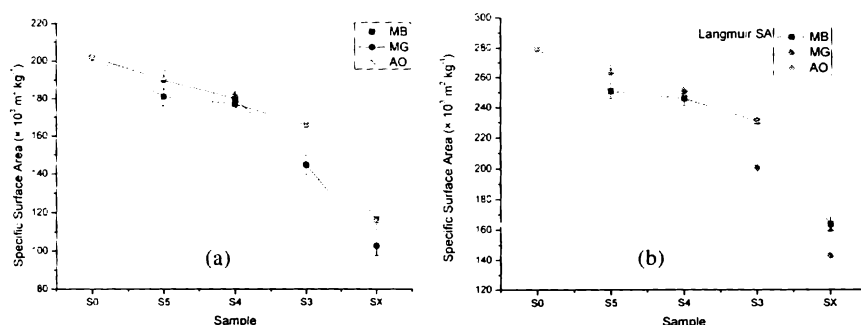


Figure 2.15: Specific surface area (SSA) of different dye intercalated K-10 montmorillonites measured by (a) BET (Brunauer Emmett Teller) and (b) Langmuir methods. Here S=MB-methylene blue, AO- auramine O and MG- malachite green. S0=K-10. Details of the samples are given in Table 2.3, Table 2.8 and Table 2.9.

Figure 2.15 shows the SSA obtained for the dye intercalated K-10 montmorillonites using BET and Langmuir methods. At maximum loading, there is a drastic decrease in SSA and PV (Figure 2.14) as evidenced from N₂ adsorption measurements.

MB-X, AO-X and MG-X have a more broadened spectrum compared to MB-3, AO-3 and MG-3 respectively (Figure 2.11, Figure 2.12 and Figure 2.13). Pore volume and specific surface area show a steep decrease in the case of repeatedly adsorbed samples (Figure 2.14 and Figure 2.15 & Table 2.3, Table 2.8 and Table 2.9) and a higher TD can be expected due to the decrease in porosity.^[136] However, a lesser TD was observed in this case; except for MG-X. The lower TD may be due to the clustering and dense packing of dye molecules.^[106, 107] These dye molecules usually exhibit low TDs of the order of 10⁻⁶ m²s⁻¹.^[140] In this case, the contribution of the dyes towards TD is more and so the effective TD is less.

C4.3. Anomalous behaviour of repeatedly adsorbed MG-X sample:

The repeated adsorption decreases the TD value in the case of MB-X^[106] and AO-X. But, MG-X does not show this property which may be due to the very small absorbance of MG at 488 nm (Figure 2.13). Since the absorption of MG at 488 nm is low, there is limited non-radiative relaxation of MG in the case of MG-X. The only contribution towards PA signal arises from the clay mineral. Moreover, the pore volume is again decreased due to the filling of dye molecules.^[107] Hence, as stated

earlier, the TD increases due to the decrease in porosity.^[136] Thus, the thermal properties of the clay samples can be changed by the selective dye adsorption. The dye adsorption changes the TD value and samples with the desired TD can be obtained with a change in adsorption.

C4.4. Thermal diffusivity of rhodamine B intercalated K-10 samples:

A similar experiment with rhodamine B (RB) intercalated K-10 pellets was also conducted and the result was similar to that of AO intercalated K-10. The reflectance spectra of the samples are as shown in *Figure 2.16*. The TD values of the samples obtained using PA technique is given in *Table 2.10*. In this case also the repeatedly adsorbed RB-M showed a low TD compared to the single adsorbed RB-3.

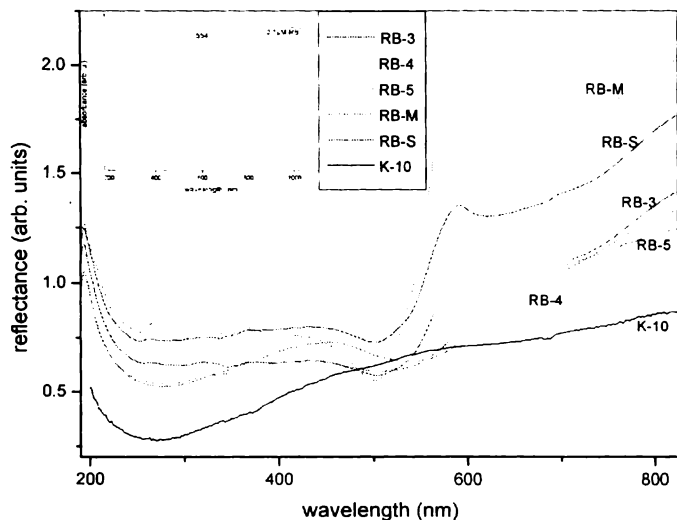


Figure 2.16: Reflectance spectra of rhodamine B intercalated K-10 montmorillonites. Inset: Absorption spectrum of 0.1 μM aqueous solution of rhodamine B (RB).

C4.5. Ultrasonicated dye adsorbed sample:

Many researchers have studied the effects of ultrasound on adsorption processes because ultrasonic waves accelerate mass transport phenomena and thus enhance and improve the sorption rate.^[179]

C4.5.1. Sample preparation:

About 100 ml of the dye solution (10^{-3} M) was mixed with 1 g clay and was subjected to ultrasonic treatment in a *Sartorius Labsonic® M* ultrasonicator (maximum amplitude 125 mm, maximum sound rating density 130 W/cm²) fitted with a 10mm Ti

probe at an operating frequency of 30kHz at room temperature for a period of 3 hours. A continuous time cycle was provided with 60% amplitude. After the required time, the solution was allowed to settle overnight, centrifuged, washed and air dried. It was subjected to Soxhlet extraction with distilled water to remove any weakly adsorbed dye and further dried at 120 °C for 12 hours. The sample was designated as RB-S.

C4.5.2. Thermal diffusivity of the sample:

Both RB-S and RB-3 pellets were of same concentration and showed almost similar reflectance spectra. But the ultra-sonication helped the dye to distribute more uniformly into the clay network and its contribution to TD was more prominent. The sonication produces significant de-lamination and lateral size reduction while the crystalline structure is retained. This improves the surface characteristics and enhances the dye uptake capacity.^[180] The increased adsorption of dye on ultra-sonication, makes a contribution to the TD analogous to the repeatedly adsorbed sample, RB-M. Hence RB-S has a TD lesser than that of RB-3 and it is very close to that of RB-M.

Table 2.10: Thermal diffusivity (TD) values of rhodamine B (RB) intercalated K-10 montmorillonites obtained at room temperature.

Sample	Thickness $\times 10^{-3}$ m	TD ($\times 10^{-4}$ m ² s ⁻¹)
RB-5	0.870 \pm 0.001	0.648 \pm 0.002
RB-4	0.947 \pm 0.001	0.845 \pm 0.002
RB-3	0.970 \pm 0.001	0.997 \pm 0.002
RB-M	0.942 \pm 0.001	0.778 \pm 0.002
RB-S	0.963 \pm 0.001	0.796 \pm 0.002

C5. Conclusions:

The PA based TD studies on dye intercalated K-10 montmorillonites showed that the intercalation of dye in the clay network remarkably affect the TD values of the samples. The adsorption of more concentrated dye resulted in increasing the TD while the repeatedly adsorbed sample showed a low TD than the single adsorbed one, except in MG-X. The case of MG-X is explained as a result of the relatively low absorption of MG near 488 nm. The ultrasonicated dye adsorbed sample showed a low TD compared to the sample prepared by the direct dye adsorption from solution which is attributed to the presence of more adsorbed and uniformly distributed dye in the clay network without the chances of forming aggregates.

2.5. Section II - Spectroscopic studies of dye intercalated K-10 montmorillonite aqueous dispersions:

2.5.1. Preamble:

Clay minerals are very attractive matrices for the intercalation of dye molecules. Clay particles are structurally lamellar and often highly colloidal in nature which makes them suitable substrates for studying photoactive species in aqueous solution and for intercalating dye molecules.^[181] The adsorption of organic cations by clay minerals has been studied over the past 70 years.^[182] Aqueous dispersions of swelling clay minerals are known for their colloidal and rheological properties and have several industrial applications.^[183] The guest photoactive species, which occupy spaces within the microstructure of the host clay assemblies, are generally organic compounds that are intercalated in the layers of the inorganic substrate. Dye cations are strongly adsorbed on the clay mineral surfaces^[101] and the organisation of the photoactive species within the microstructure is entirely dependent on the host-guest and guest-guest interactions within the microstructure.^[181] Due to the negative charge of their interlayer, the smectites have a suitable host structure for the intercalation of various guests like metals, inorganic complexes and organic cations. Dye intercalated materials are exploited in modern photochemistry and photophysics due to their transparency in the visible wavelength region and their optical activity.^[184-187] The increasing interest in dye/ inorganic nano-composites is focused on changes in optical and thermal^[106, 107] properties during adsorption and / or intercalation of the dye in an inorganic matrix. Intercalation of organic dyes into layered silicates is one method of producing ordered organic-inorganic hybrid materials with interesting photo-functions^[186-188] and thermal properties.^[106, 107] Various dye-clay systems offer an interesting area of research, and spectroscopic techniques have been successfully used to study such systems.^[102, 186-191]

Montmorillonites belong to the dioctahedral smectite group of 2: 1 phyllosilicate class.^[102, 186, 187, 192-194] Smectites are generally nanomaterials with negatively charged elementary platelets of a few nanometre thicknesses; the exact thickness depends on the number of adsorbed water layers. One can transform a clay particle, consisting of a number of more or less well oriented elementary platelets, into an aqueous suspension with randomly moving, elementary clay platelets in which the degree of swelling depends on the charge density of the clay mineral, size and shape of the elementary platelets and particles, the type and charge of the exchangeable cation and the chemical and thermal history of the clay mineral sample.^[195] Smectite group is used as a very convenient host structure for the intercalation of organic dyes.^[102, 184, 186-188, 193]

The blue emission from the K-10 dispersions is important to be discussed as this emission possesses many advantages useful for potential applications since the emission is located partly in the UV-B spectral region.^[196] The novelty of the work is that the dispersions are prepared from the dried dye intercalated samples with same clay amount and different dye concentrations.

2.5.2. Dispersions of dye intercalated montmorillonite:

The aqueous dispersions of the dye adsorbed samples, obtained by the method described in 2.2.2., were prepared by ultra-sonicating 0.1 g of each of the samples in 100 ml water for 10 minutes. To check the absorption behaviour of K-10, 0.1 g was dispersed in 20 ml and the spectrum was taken.

2.5.3. Optical characterization:

The absorption spectra of the aqueous dispersions at room temperature, taken in a 1cm quartz cuvette (Hellma[®], Precision Cells made of Quartz SUPRASIL[®] 300, 100-QX), were noted using a spectrophotometer (JASCO V-570 UV/VIS/NIR) and the fluorescence spectra of all the samples were recorded under the same conditions using a fluorescence spectrophotometer (Varian, Cary Eclipse).

2.5.4. Part A: Rhodamine B intercalated K-10:

D1. Introduction:

Rhodamines, an active medium of dye lasers, have a high absorption coefficient and fluorescent yield. They are convenient dyes for probing heterogeneous systems because of their strong dependence of the absorption and fluorescence capacity on the matrix of the solvent. Similar to other organic dyes with molecules having a flat structure or containing planar chromophore groups, rhodamine dyes form molecular assemblies (aggregates), which are characterised by various types of intermolecular associations and optical properties. The formation of such assemblies is usual in aqueous solutions of higher concentrations. It may be enhanced by the adsorption on solid surfaces.^[100] It is seen that rhodamine dye can be intercalated into clay interlayers and form aggregation states due to the electrostatic intercalation with the cationic charges.^[186] RB has a strong tendency for aggregation, depending on the concentration in the intercalation solution and on the charge distribution in the solvent matrix.^[135, 188]

The goal of the present work is to investigate the optical absorption and fluorescence properties of the RB intercalated K-10 montmorillonites in aqueous dispersions. To

check the dependence on the sample preparation route, one sample is prepared using ultra-sonication and the result is compared. The fluorescence emissions at different wavelengths are also explained.

D2. Experimental- Materials and methods:

Cationic, organic, RB of GR grade was bought from Loba Chemie. Dispersions of RB intercalated K-10 were prepared as described in 2.5.2. The RB intercalation was done as follows

D2.1. Dye adsorption from solution:

These samples were prepared by the methods described earlier in C3. The samples were named as RB-Z, where Z denoted the concentration. The repeatedly adsorbed sample is designated as RB-M.

D2.2. Ultrasonicated dye adsorption:

The sample RB-S was prepared by the method described in C4.5.1., which involved ultrasonicated dye adsorption of 10^{-3} M dye solution by K-10.

D3. Results:

D3.1. Optical absorption studies:

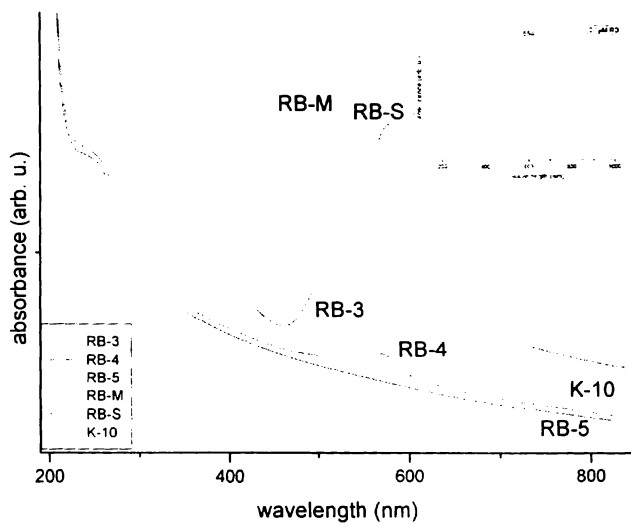


Figure 2.17: Absorption spectra of rhodamine B (RB) intercalated K-10 montmorillonite aqueous dispersions (0.1g sample in 100 ml water). Inset: Absorption spectrum of 0.1μM rhodamine B aqueous solution.

The absorption spectra (*Figure 2.17*) showed that the main absorption peak of RB at 555 nm¹⁵⁾ in all samples was bathochromically shifted. The samples RB-3 and RB-S exhibited maximum intensity at around 580 nm but the intensity of RB-S was higher. The other important peaks (357 nm and 257 nm) of RB appear in the spectra as the RB concentration in the clay mineral increases. The RB-M samples showed broad absorption spectra with peaks at 537, 560, 572 and 590 nm. The absorption spectra of RB-5 and K-10 were similar as the amount of dye loaded was very low in the case of RB-5. It was also observed that K-10 had a shoulder near 250 nm as in the case of all montmorillonites^{197, 198)} and the RB had a peak around the same wavelength.

The highly concentrated K-10 (0.1g in 20ml water) dispersion had small peaks near 371, 421, 521 and 683 nm as seen in *Figure 2.18* and these peaks were not observed in *Figure 2.17* due to the very low concentration of K-10 in the dispersion. These peaks were found to be enhanced in dye intercalated samples under the same conditions which were not shown here as most of the peaks got saturated as the concentration was high.

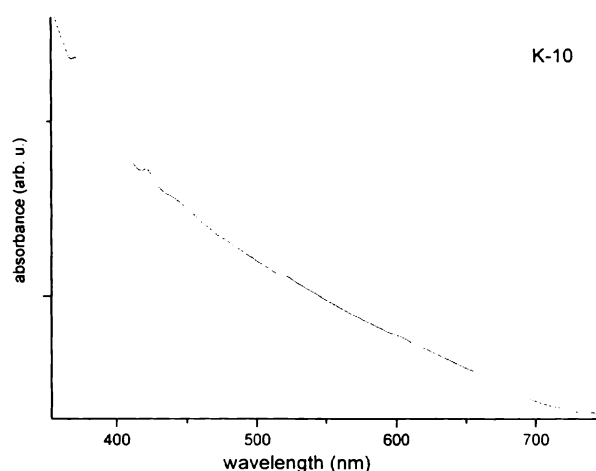


Figure 2.18: Absorption spectrum of K-10 montmorillonite aqueous dispersion (0.1g K-10 in 20 ml water).

D3.2. Fluorescence studies:

The samples showed a fluorescence peak at 421 nm when excited with 371 nm (*Figure 2.19a*). This may be arising from the silica layer. The samples were excited at the same conditions and it was observed that the peak intensity increased for RB-5 than that of K-10. The fluorescence intensity was decreased for all other samples as the dye concentration was increased. *Figure 2.19b* shows the fluorescence emission at

421 nm from samples when they were excited using 250 nm. This figure also showed the same behaviour as in the case of 371 nm excitation.

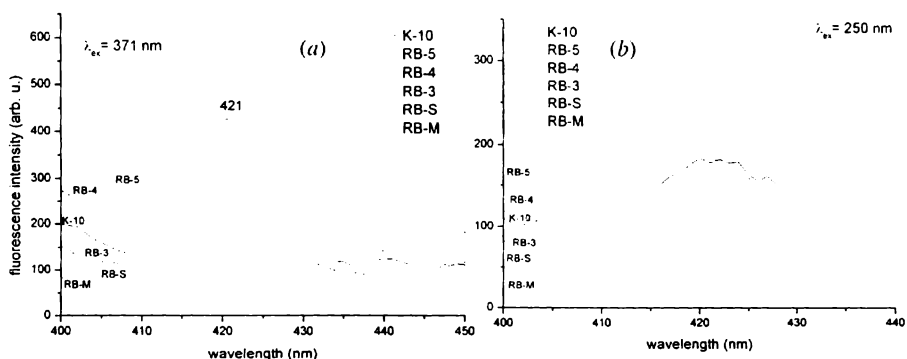


Figure 2.19: Fluorescence spectra of rhodamine B (RB) intercalated K-10 montmorillonite aqueous dispersions (0.1g sample in 100 ml water) peaked at 421 nm when excited using (a) 371 nm (b) 250 nm.

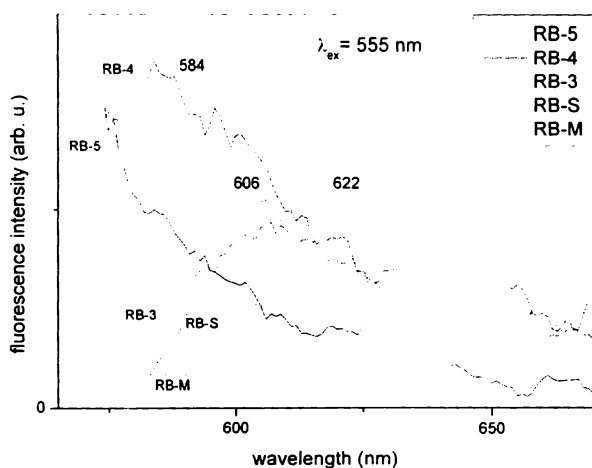


Figure 2.20: Fluorescence spectra of rhodamine B (RB) intercalated K-10 montmorillonite aqueous dispersions (0.1g sample in 100 ml water) when excited using 555 nm.

When the dye intercalated samples were excited using 555 nm, they showed a bathochromic shift as the amount of the intercalated dye increases (Figure 2.20). Since the samples RB-3, RB-S and RB-M were prepared from dye solutions of same molarity, they showed almost same emission intensity, but RB-M peak was bathochromically shifted. The spectrum of sample K-10 is not given as it had no absorption at 555 nm.

The fluorescence peak intensity comparison of RB-3 and RB-S from *Figures 2.19 & 2.20* shows that the emission peak intensity for RB-S is slightly less than that of RB-3. RB-S also shows a broadened nature for fluorescence though both RB-S and RB-3 have the same absorption peak at 580 nm. But, RB-S has a higher absorption.

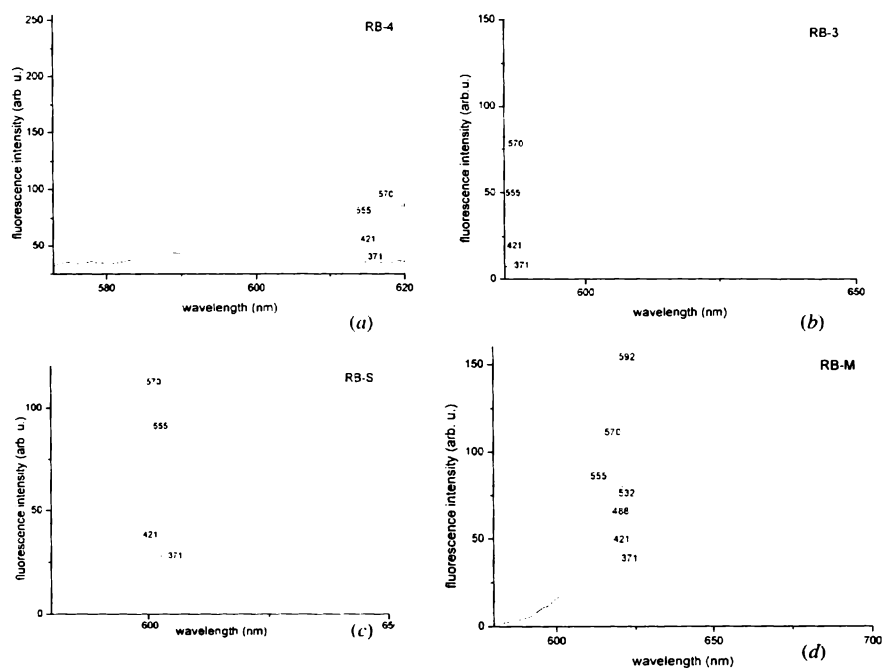


Figure 2.21: Fluorescence spectra of rhodamine B (RB) intercalated K-10 montmorillonite aqueous dispersions (0.1 g sample in 100 ml water) when excited using various wavelengths (a) RB-4, (b) RB-3, (c) RB-S and (d) RB-M

Figure 2.21 shows the fluorescent emissions from RB-4, RB-3, RB-S and RB-M near 600 nm when different excitation wavelengths were used. The fluorescent emission of RB is reported to be near 580 nm when it is excited with 555 nm.^[199] From *Figure 2.21a*, for RB-4, the emission peak near 580 nm was observed when the excitation wavelength was 555 nm. However, in other cases, both absorption and emission peaks of RB were bathochromically shifted and the main fluorescent peak appeared after 600 nm (*Figure 2.21 b-d*). The fluorescent emission from RB-5 was found to be too weak to be presented as it had no absorption peak near 555 nm (*Figure 2.17*).

D4. Discussions:

D4.1. Optical absorption studies:

All the dye intercalated samples showed bathochromic shift which may be due to the formation of J- aggregates.^[116] The greater absorbance shown by RB-S with respect to RB-3 may be due to the more uniformly distributed dye molecules and the minimisation of cluster formation by ultra sonication. Moreover, greater amount of dye can be adsorbed by ultra-sonication.^[180] However, they had the same dye concentration and exhibited the peak at 580 nm.

The RB-M sample showed a broad absorption spectrum due to the dye aggregations. The dye molecular aggregation on the surface of the clay minerals is due to the hydrophobic interactions, which is a general tendency of non-polar molecules to associate physically in aqueous solutions. The molecular exciton model gives a clear-cut explanation for this phenomenon as given by various authors.^[116, 200]

Though montmorillonites are weak absorbers in the visible and NIR spectral range,^[198] the weak peaks of K-10 (*Figure 2.18*) can be attributed to the silica and alumina layers present in their network. The presence of the dye in the network of the RB intercalated K-10 enhances the absorption at these peaks.

The adsorption of rhodamine onto clay samples usually leads to the metachromatic⁸⁸ effect in the absorption spectra, whereby the main absorption band is shifted to higher energies.^[160, 185] The proportion of the dimers to the monomers increases with increasing concentration of the dye. The interaction of dye with the montmorillonite runs on the principle of the ion-exchange reaction. This process is controlled by coulombic and van der Waals interactions, H-bonds, and also non-bond energy contributions between guest and host and between the guest and guest.^[184] In montmorillonite, metachromasy results from π interactions between the adsorbed dye and the oxygen plane of the alumino-silicate.^[201]

The J-aggregates, which are formed more rarely than the H-aggregates, absorb light of lower energies and exhibit luminescent properties. They are assemblies with a head-to-tail association.^[100] However, the present studies showed that the bathochromic shift in the absorption spectra of the samples was due to the formation of J-aggregates. But,

⁸⁸ Relating to the property of certain chemical substances to appear as different colours

RB-M showed the presence of the H-aggregates as evident from the hypsochromic shift and the broadened nature of the main absorption peak of RB.

H-dimers have been observed in polar and low-viscosity solutions. J-dimers may be formed in weakly polar solvents or in the adsorbed state. At the adsorbed state, the electrostatic interaction of the molecule with the polar surface and with other monomer molecules governs the formation of aggregates. The fluorescent character of dimers is due to the allowed transition from the J-dimer level to the ground level.^[200]

D4.2. Fluorescence studies:

Dye molecules are incorporated in the clay mineral network with strong dye and host matrix interactions. When dye molecules are excited, their excitation energy gets transferred to silica in the matrix so that fluorescence of silica at 421 nm is enhanced as shown in *Figure 2.19a*. The 421 nm emission of silica showed fluorescence quenching due to the presence of more dye molecules in the clay network which inhibits the emission from the silica layers. As the concentration of the RB is increased the radiative relaxation of dyes become more predominant resulting in enhancement in 580 nm region (*Figure 2.21*) and decrease in fluorescence intensity at 421 nm. The same intensity of RB-3 and RB-S also confirms the emission from the silicate layer because they are of the same concentration though they are prepared by different methods. It was reported that porous silicon,^[202] silica spheres^[203] and silicon nanoparticles^[196] when excited near 370 nm showed an emission around 420 nm. Since, no peak shift is observed for this emission for all the samples, it may be concluded that the emission arises from the montmorillonite itself. The fluorescence emission of the K-10 colloid also confirms this (2.5.6.). However, the presence of a small amount of dye in the network enhances the fluorescence intensity. Moreover, fluorescence quenching can be observed as the amount of dye in the dispersions increases. The fluorescence quenching is due to the energy transfer from the excited state of the monomers to the aggregated species. This transfer can be via either an electron exchange or coulombic interactions. Dipole-dipole type coulombic interactions are long range and are effective for the systems with a large overlap between the fluorescence spectrum of the donor and absorption spectrum of the acceptor.^[204] Besides dye aggregation, there could also be other effects like light scattering, adsorption by the solid surface,^[189] deformation to a non-planar conformation upon adsorption etc., on the fluorescence of the dye in the adsorbed state, which may significantly reduce the fluorescence yield.^[100, 205] It is reported that montmorillonite intercalated with RB cations showed that the bands corresponding to

the silicate layer remained unchanged after intercalation.^[185] This means that the silicate layers can be treated as rigid bodies during energy minimisation.

The less intense fluorescence behaviour of RB-S compared to RB-3 when excited near 580 nm (*Figure 2.21b* and *Figure 2.21c*) can also be attributed to fluorescence quenching. For RB-3 the aggregation may be more than that of RB-S and the light scattering will be more. The number of photons absorbed by the RB-3 sample will be less due to scattering and hence less absorption. This can cause a lesser fluorescence quenching and can result in more intense fluorescence emission. Thus, the light absorbed is less and quenching of fluorescence will be less and so a slightly higher fluorescence for RB-3. The RB-S had a more uniform distribution and dye intercalation as it was carried out under ultra-sonication and the dye aggregation was less. This may result in absorbing more photons and higher absorption. Consequently, fluorescence quenching becomes more prominent due to the presence of more number of absorbing molecules. Moreover, when two identical fluorescent molecules are in close proximity, their fluorescence emission is quenched due to the intermolecular interaction. Increasing the distance between the two molecules will decrease their interaction and thus increase their fluorescence intensity. Attaching the two fluorophores to a host molecule then allows to sense the conformational change of the host molecule.^[206]

The fluorescence band of the rhodamine-clay system is shifted to higher wavelength compared with that of the rhodamine in aqueous solution.^[188, 189, 207, 208] In addition, the emission band becomes broader as a consequence of the structural inhomogeneity of the rhodamine-clay system, where the surface structure may differ significantly from that in the interlayer space.^[188] The bathochromic shift observed in the case of RB-M (*Figure 2.20*) is due to the clustering and dense packing of the dye molecules which arises from the repeated adsorption. The fluorescence intensity of the RB-M was less compared to RB-3 and RB-S which was attributed to the usual fluorescence quenching in highly concentrated solutions. The changes in fluorescence band profile with increasing RB⁺ concentration reflect the changes in relative proportions of monomers, dimers, and higher aggregates adsorbed on the external surface and intercalated into the interlayer space.^[188]

D5. Conclusions:

The effect of RB on the fluorescence emission of silica layer at 421 nm with two excitation wavelengths at 250 nm and 371 nm showed that the emission intensity of

K-10 montmorillonite can be enhanced by the addition of a small amount of dye in the network. The addition of dye increases the absorption peak intensity of K-10. The increase in dye concentration shows bathochromic shift in peaks due to the formation of J-aggregates. The emission intensity decreases as the amount of the dye increases which is due to the fluorescence quenching. The RB-S sample prepared by ultrasonication method shows more absorption and less fluorescence than the sample RB-3 due to the uniform distribution, increased adsorption and minimised clustering of dye molecules.

2.5.5. Part B: Malachite green intercalated K-10:

E1. Introduction:

The consequence of a fluorescent dye RB intercalated K-10 dispersions are presented in 2.5.4. In this part, the effect of a non-fluorescent^[209] dye MG intercalated K-10 dispersions is discussed.

MG shows strong absorption at the red end of the visible spectrum.^[210] The dye itself is not fluorescent.^[209] Tahir and Naseem^[211] (2006) studied the ability of bentonite to remove MG from aqueous solutions for different adsorbate concentrations by varying the amount of adsorbent, temperature, pH and shaking time. Shivaji et al.^[212] (2004) reviewed the toxicological effect of MG on various fish species and certain mammals. MG can be photocatalytically degraded from textile industry waste-water.^[77] Juraj and Nobuo^[101] investigated the aggregation behaviour of MG in dispersions on montmorillonites. The optical absorbance and fluorescence behaviour of the dispersions prepared from the triphenylmethane (TPM) cationic dye MG adsorbed K-10 montmorillonite is presented.

E2. Dispersions of malachite green intercalated K-10 montmorillonite:

The preparation of the dispersions of the samples, obtained by the method C3, was described in 2.5.2. The samples were designated as KMG-Z and the repeatedly adsorbed sample as KMG-M. The optical characterization was described in 2.5.3.

E3. Results:

E3.1. Optical absorption studies:

The absorption spectra of the dispersions of the samples were as shown in *Figure 2.22*. It is observed that the main peaks of the MG at 426 nm and 616.5 nm are

bathochromically shifted and broadened in KMG-3 and KMG-M due to the aggregation of dye molecules on the clay basal surface.

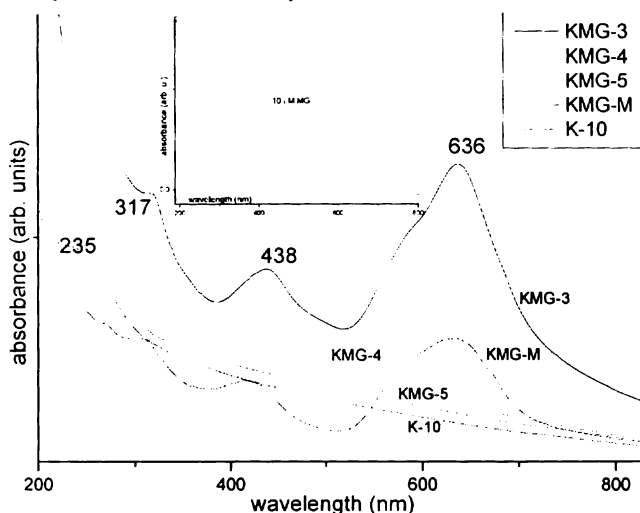


Figure 2.22: Absorption spectra of malachite green (MG) intercalated K-10 dispersions. Inset: Absorption spectra of 10 μ M malachite green aqueous solution.

E3.2. Fluorescence studies:

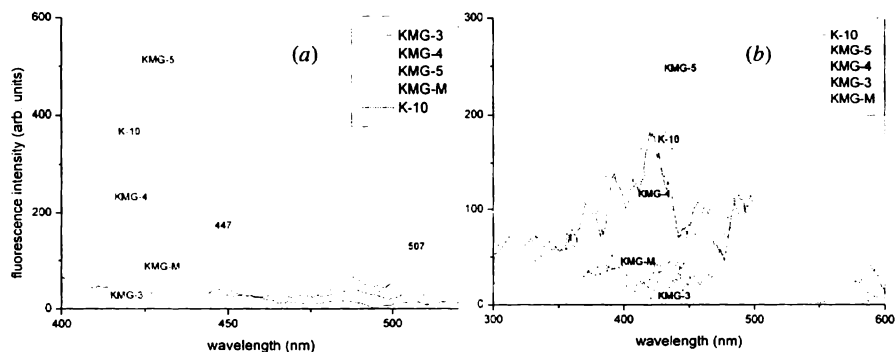


Figure 2.23: Fluorescence spectra of malachite green (MG) intercalated K-10 dispersions at 421 nm when they are excited using (a) 371 nm and (b) 250 nm.

MG is a non-fluorescent dye,^[209] but the presence of a small amount of dye in the clay network enhances the fluorescence behaviour of the K-10 samples at 421 nm when excited using 371 nm as seen in Figure 2.23a. Though noticeable change was not obtained in the absorption of KMG-5, it showed an enhancement in fluorescence at

421 nm. But the fluorescence quenching was observed as the amount of the dye adsorbed was increased. The same phenomenon was observed with RB as described in **D4.2**. The samples also showed fluorescence near 421 nm with vibrational spectrum when they are excited with 250 nm as shown in *Figure 2. 23b*. In this case also the samples have an enhanced fluorescence with a slight amount of dye in the network and the fluorescence is quenched as the amount of dye in the network increases.

E4. Discussions:

The basic change in the absorption and fluorescence spectrum of the dye intercalated montmorillonites arises from the dye aggregation on the clay network. The optical properties of dye/clay reaction systems can also be interpreted assuming charge transfer between the dye cations and the clay surface.^[213] This reaction requires the parallel orientation of dye cations on a clay basal surface. The parallel orientation of triphenylmethane (TPM) dyes like MG would be contrary to their non-flat, propeller-like structures.^[214] Moreover, a triangular plane of the cation center of the TPM dyes is tilted at a large angle to the clay surface.^[210, 214] The parallel orientation and stacking of the cations on top of each other could not lead to stable arrangements in aggregates because the cations would not be able to interact electrostatically with the negatively charged basal surface. However, if the orientation of the cations is sub-perpendicular to the basal surface of the clay, the existence of large, two dimensional dye aggregates on the clay surface is possible.^[101, 125] The more complicated structures of the cations of TPM dyes might cause the absence of the sharp bands formed by the less-ordered J-aggregates.^[101] TPM dye cations have a low degree of freedom to adjust to their shape, in order to fill the space at the clay surface. The only possibilities are a rotation of the phenyl groups.^[101] MG has only a slight change in the cation structure and/or size, such as replacing methyl groups with ethyl groups, which leads to the behaviour of the dye at the surface of clays. The low intense band near 430 nm arises from the lower symmetry in the cations of MG.

The dye aggregation quenches the fluorescence of the silica in clay network. The dye molecules aggregate on the clay network as their concentration increases which in turn inhibits the fluorescence of the silica. Thus, it can be confirmed that the presence of the dye in K-10 undoubtedly affects the fluorescence behaviour of the silica at 421 nm when excited using 371 nm. Hence dye can be used to monitor the fluorescence of clay.

E5. Conclusions:

The intercalation of the non-fluorescent dye MG in K-10 verifies that the 421 nm fluorescence from the K-10 dispersion arises from the silica present in clay network. The result also confirms that the presence of a small amount of dye in the clay enhances this fluorescence. Moreover, the fluorescence intensity can be monitored by the amount of dye added and it does not depend on whether the dye is fluorescent or not.

2.5.6. Part C: Dispersions of KSF and K-10:

F1. Introduction:

Many chemical reactions in soils are affected by their internal surface. In this respect, clay minerals are one of the most reactive species, due to their high SSA. Under the chemical conditions in the soil, the clay mineral particles form large aggregates which contain micropores. Shape, size, and the internal structure of these aggregates depend on the ionic concentration of the dispersion medium.^[215, 216] The colloidal state (stable, coagulated, or gel-like) and the rheological properties of montmorillonite dispersions are strongly influenced by organic cations.^[217] Clay minerals are distinguished from other colloidal materials by the highly anisometric and often irregular particle shape, the broad particle size distribution, the different types of charges (permanent charges on the faces, pH-dependent charges at the edges), the heterogeneity of the layer charges, the pronounced cation exchange capacity, the disarticulation (in case of smectites), the flexibility of the layers, and the different modes of aggregation.^[103, 218] Pure clay mineral dispersions have a tendency to aggregate.^[219]

Light absorption characteristics of clay minerals in the UV and visible range have been studied by several investigators.^[220, 221] Visible absorption spectroscopy has been reported as a useful technique for the estimation of particle size of clays in suspension.^[221] Banin and Lahav^[222] noted that montmorillonite shows a light absorption band in the UV range, at about 245 nm. They proposed a semi-quantitative method for the estimation of the specific light absorption intensity by subtracting the estimated scattered light from the optical density at the absorption band. They further postulated that the absorption band in montmorillonite is caused by compounds which are affecting the tactoid size of the mineral while dispersed in water. This suggestion was based on the fact that a negative correlation was found between the intensity of light absorption and tactoid size.^[223]

Both K-10 and KSF are acid leached commercial montmorillonites. KSF is less acid leached than K-10. From the present study, the change in the absorption and fluorescence of the acid leached montmorillonites can be estimated.

F2. Materials and methods:

To measure the absorption spectrum, 0.1 g of K-10 and KSF were dispersed in 20 ml double distilled water. The fluorescence studies were conducted with dispersions made with 0.1 g montmorillonite in 100 ml double distilled water. The spectral measurements details are given in 2.5.3.

F3. Results and discussions:

F3.1. Optical absorption studies:

The absorption spectrum of the K-10 dispersion is given in *Figure 2.18* and that of KSF is given in *Figure 2.27*. The dispersions show a significant shoulder near 260 nm which is a characteristic of the montmorillonites. The K-10 and KSF dispersions are almost transparent in the visible range with some weak peaks arising from the silica and alumina layers in the clay network. All montmorillonites exhibit either an absorption band or a shoulder at a wavelength near 245 nm.^[223]

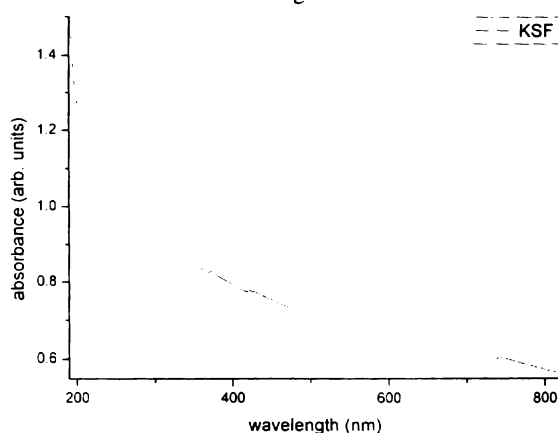


Figure 2.24: Absorption spectrum of KSF montmorillonite aqueous dispersion (0.1g KSF in 20 ml water).

F3.2. Fluorescence studies:

The fluorescence spectra of the K-10 and KSF dispersions are as shown in *Figure 2.25*. These dispersions showed fluorescence at 421 nm when excited using 250 nm and 371 nm. The fluorescence produced by 371 nm is noticeable as it may be arising from

the silica layers of the clay minerals.^[196, 202, 203] The more acid leached K-10 showed higher absorbance near 371 nm and fluorescence at 421 nm. Hence, it may be assumed that the acid leaching enhances the absorbance and fluorescence of montmorillonites. However, more quantitative studies are to be carried out to confirm this. Though the K-10 and KSF dispersions show fluorescence at 421 nm for 250 nm excitation it is weak compared to that originating from the 371 nm excitation.

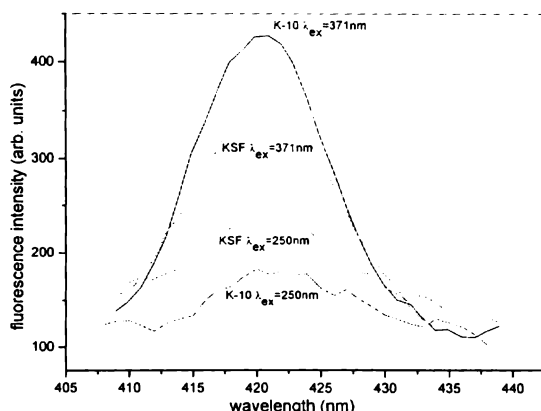


Figure 2. 25: Fluorescence spectrum of KSF montmorillonite aqueous dispersion at 421 nm when excited using 371 nm and 250 nm.

F4. Conclusions:

The optical absorption and fluorescence studies on K-10 and KSF dispersions showed that acid leaching can significantly influence these features. Out of the weak absorption peaks in the visible range arising from the silica and alumina layers of the montmorillonites, only 371 nm excitation was able to produce noteworthy fluorescence.

2.6. Summary:

The PA studies on MB intercalated K-10 and KSF revealed that K-10 is more suitable for obtaining desired TD. The sintered MB intercalated samples showed higher TD in K-10 matrix. As the sintering temperature increases, the TD of the dye intercalated samples tends to that of the non-intercalated sample. It is also noted that the dye adsorbed K-10 samples have different TD values depending on the amount and type of dye adsorbed. The TD studies of the dye adsorbed montmorillonites expose the possibility of these materials for further applications after the industrial waste-water treatment. The repeatedly adsorbed samples showed a low TD compared to the single

adsorbed samples except for MG adsorbed ones. The anomalous behaviour of MG may be arising from the low absorption of MG at 488 nm.

The optical absorption and fluorescence studies of the dye adsorbed montmorillonite dispersions showed that both fluorescent and non-fluorescent dye in a small amount can enhance the fluorescence of the K-10 montmorillonite at 421 nm when the wavelength of excitation is 371 nm. The presence of dye in the clay network can be used to monitor the optical properties of both. Moreover, acid leaching can significantly affect the optical properties of the montmorillonites.

Many cationic dyes and chromophores embedded in inorganic substrates are used in industry, e. g. in photography, in various materials for signal processing and memory storage media, as catalysts, as energy antennas and transducers in photochemical reactions etc. All these applications depend crucially on the optical properties of the employed dye. Therefore, the relationship between dye aggregation and the parameters of inorganic hosts might be very significant in the applied research and engineering of the materials.^[101]

2.7. References:

- [1] S. Venkata Mohan, N. Chandrasekhar Rao, K. Krishna Prasad and J. Karthikeyan (2002). 'Treatment of simulated reactive yellow 22 (Azo) dye effluents using *Spirogyra* species'. *Waste Manage.*; **22** (6), p 575–582. doi:10.1016/S0956-053X(02)00030-2
- [2] A. Alinsafi, F. Evenou, E.M. Abdulkarim, M.N. Pons, O. Zahraa, A. Benhammou, A. Yaacoubi and A. Nejmeddine, (2007). 'Treatment of textile industry wastewater by supported photocatalysis'. *Dyes and Pigments*; **74** (2), p 439- 445. doi:10.1016/j.dyepig.2006.02.024
- [3] F. Ciner, S. K. Akal Solmaz, T. Yonar, and G. E. Ustun (2003). 'Treatability studies on wastewater from textile dyeing factories in Bursa, Turkey'. *Int. J. Environ. Pollut. (IJEP)*; **19** (4), p 403- 407. doi: 10.1504/IJEP.2003.004303
- [4] Mittal A K and Venkobachar C (1989). 'Studies on sorption of dyes by sulfonated coal and *Ganoderma lucidum*'. *Indian J Environ Health.*; **31** (2), p 105-111.
- [5] A. Edwin Vasu (2008). 'Studies on the Removal of Rhodamine B and Malachite Green from Aqueous Solutions by Activated Carbon'. *E-Journal of Chemistry.*; **5** (4), p 844-852. URL: <http://www.e-journals.in/PDF/V5N4/844-852.pdf>
- [6] Takeo Nakamura, Toshimitsu Tokimoto, Takamichi Tamura, Naohito Kawaski and Seiki Tanada (2003). 'Decolorization of Acid dye by Charcoal from coffee grounds'. *J Health Sci.*; **49** (6), p 520-523. URL: [http://jhs.pharm.or.jp/49\(6\)/49_520.pdf](http://jhs.pharm.or.jp/49(6)/49_520.pdf)
- [7] K. Vasanth Kumar, V. Ramamurthi and S. Sivanesan (2006). 'Biosorption of malachite green, a cationic dye onto *Pithophora* sp., a fresh water algae'. *Dyes Pigm.*; **69** (1-2), p 74–79. doi:10.1016/j.dyepig.2005.02.005
- [8] V. K. Gupta, Suhas, Imran Ali and V. K. Saini (2004). 'Removal of Rhodamine B, Fast Green, and Methylene Blue from Wastewater Using Red Mud, an Aluminum Industry Waste'. *Ind. Eng. Chem. Res.*; **43** (7), p 1740–1747. doi: 10.1021/ie034218g

- [9] Tim Robinson, Geoff McMullan, Roger Marchant and Poonam Nigam (2001). 'Remediation of dyes in textile effluent: a critical review on current treatment technologies with a proposal alternative'. *Bioresource Technol.*; **77** (3), p 247–255.
doi:10.1016/S0960-8524(00)00080-8
- [10] Kuo-Cheng Chen, Jane-Yii Wu, Dar-Jen Liou and Sz-Chwun John Hwang (2003). 'Decolorization of the textile dyes by newly isolated bacterial strains'. *J. Biotechnol.*; **101** (1), p 57–68. doi:10.1016/S0168-1656(02)00303-6
- [11] Daneshvar N, Hejazi M. J, Rangarany B. and Khataee A. R(2005). 'Photocatalytic Degradation of an Organophosphorus Pesticide Phosalone in Aqueous Suspensions of Titanium Dioxide'. *J. Environ. Sci. Heal. B*; **39** (2), p 285- 296 doi: 10.1081/PFC-120030242
URL: <http://dx.doi.org/10.1081/PFC-120030242>
- [12] N. Daneshvar, M. Ayazloo, A.R. Khataee and M. Pourhassan (2007). 'Biological decolorization of dye solution containing Malachite Green by microalgae *Cosmarium* sp'. *Bioresource Technol.*; **98** (6), p 1176-1182. doi:10.1016/j.biortech.2006.05.025
- [13] Rabia Köklü and Bülent Şengörür (2004). 'Color removal from textile industry wastewater by polymer resin adsorption'. *Fresenius Environmental Bulletin*; **13** (8), p 700-704.
- [14] Liping Huang, Shaoan Cheng, Farzaneh Rezaei and Bruce E. Logan (2009). 'Reducing organic loads in wastewater effluents from paper recycling plants using microbial fuel cells'. *Environ. Technol.*; **30** (5), p 499-504.
doi: 10.1080/09593330902788244 URL: <http://dx.doi.org/10.1080/09593330902788244>
- [15] Yujie Feng, Xin Wang, Bruce E. Logan and He Lee (2008). 'Brewery wastewater treatment using air-cathode microbial fuel cells'. *Appl Microbiol. Biotechnol.*; **78** (5), p 873-880. doi: 10.1007/s00253-008-1360-2
- [16] S. Sokolovic, R. Secerov-Sokolovic and S. Putnik (1992). 'Some aspects of application of waste polymer materials as a coalescence medium for oily wastewater treatment'. *Environ. Technol.*; **13** (10), p 987 – 994. doi: 10.1080/09593339209385234
- [17] Y. K. K. Koh, T.Y. Chiu, A. Boobis, E. Cartmell, M. D. Scrimshaw and J. N. Lester (2008). 'Treatment and removal strategies for estrogens from wastewater'. *Environ. Technol.*; **29** (3), p 245 – 267. doi: 10.1080/09593330802099122
URL: <http://dx.doi.org/10.1080/09593330802099122>
- [18] J. H. Choi, W. S. Shin, S. H. Lee, D. J. Joo, J. D. Lee and S. J. Choi (2001). 'Application of Synthetic Poly(DADM) Flocculants for Dye Wastewater Treatment'. *Environ. Technol.*; **22** (9), p 1025 – 1033. doi: 10.1080/09593332208618213
- [19] M. Basibuyuk, T. Yilmaz, B. Kayranli, A. Yuceer, and C. F. Forster (2002). 'The Use of Waterworks Sludge for the Treatment of Dye Wastes'. *Environ. Technol.*; **23** (3), p 345 - 351.
doi: 10.1080/09593332508618418 URL: <http://dx.doi.org/10.1080/09593332508618418>
- [20] Sheng H. Lin and Chi F. Peng (1996). 'Continuous treatment of textile wastewater by combined coagulation, electrochemical oxidation and activated sludge'. *Water Res.*; **30** (3), p 587-592. doi:10.1016/0043-1354(95)00210-3
- [21] Sheng H. Lin and Ming L. Chen (1997). 'Purification of textile wastewater effluents by a combined Fenton process and ion exchange'. *Desalination*; **109** (2), p 121-130.
doi:10.1016/S0011-9164(97)00058-1
- [22] S. H. Lin, H. Y. Chan and H. G. Leu (2000). 'Treatment of wastewater effluent from an industrial park for agricultural irrigation'. *Desalination*; **128** (3), p 257-267.
doi:10.1016/S0011-9164(00)00040-0
- [23] Sheng H. Lin and Ming L. Chen (1997). 'Treatment of textile wastewater by chemical methods for reuse'. *Water Res.*; **31** (4), p 868-876. doi:10.1016/S0043-1354(96)00318-1
- [24] Bahadır K. Körbahti and Abdurrahman Tanyolaç (2008). 'Electrochemical treatment of simulated textile wastewater with industrial components and Levafix Blue CA reactive dye: Optimization through response surface methodology'. *J. Hazard. Mater.*; **151** (2-3), p 422-431.
doi:10.1016/j.jhazmat.2007.06.010

- [25] Chen L. Lai and Sheng H. Lin (2003). 'Electrocoagulation of chemical mechanical polishing (CMP) wastewater from semiconductor fabrication'. *Chem. Eng. J.*; **95** (1-3), p 205–211. doi:10.1016/S1385-8947(03)00106-2
- [26] Jiangning Wu and Tingwei Wang (2001). 'Ozonation of aqueous azo dye in a semi-batch reactor'. *Water Res.*; **35** (4), p 1093-1099. doi:10.1016/S0043-1354(00)00330-4
- [27] Gianluca Ciardelli and Nicola Ranieri (2001). 'The treatment and reuse of wastewater in the textile industry by means of ozonation and electroflocculation'. *Water Res.*; **35** (2), p 567-572. doi:10.1016/S0043-1354(00)00286-4
- [28] A. Bottino, G. Capannelli and G. Tocchi, M. Marcucci and G. Ciardelli (2001). 'Membrane separation processes tackle textile waste-water treatment'. *Membrane Technology*; **2001** (130), p 9-11. doi:10.1016/S0958-2118(01)80128-2
- [29] M. Marcucci, G. Ciardelli, A. Matteucci, L. Ranieri and M. Russo (2002). 'Experimental campaigns on textile wastewater for reuse by means of different membrane processes'. *Desalination*; **149** (1-3), p 137-143. doi:10.1016/S0011-9164(02)00745-2
- [30] M. Marcucci, G. Nosenzo, G. Capannelli, I. Ciabatti, D. Corrieri and G. Ciardelli (2001). 'Treatment and reuse of textile effluents based on new ultrafiltration and other membrane technologies'. *Desalination*; **138** (1-3), p 75-82. doi:10.1016/S0011-9164(01)00247-8
- [31] Cheima Fersi and Mahmoud Dhahbi (2008). 'Treatment of textile plant effluent by ultrafiltration and/or nano filtration for water reuse'. *Desalination*; **222** (1-3), p 263-271. doi:10.1016/j.desal.2007.01.171
- [32] A. K. Chakravarti, S. B. Chowdhury, S. Chakrabarty, T Chakrabarty and D. C. Mukherjee (1995). Liquid membrane multiple emulsion process of chromium(VI) separation from waste waters. *Colloids Surf., A*; **103** (1-2), p 59-71. doi:10.1016/0927-7757(95)03201-N
- [33] L. Canet, M. Ilpide, and P. Seta (2002). 'Efficient facilitated transport of lead, cadmium, zinc, and silver across a flat-sheet- supported liquid membrane mediated by lasalocid A'. *Sep. Sci. Technol.*; **37** (8), p1851 - 1860. doi: 10.1081/SS-120003047
URL: <http://dx.doi.org/10.1081/SS-120003047>
- [34] G. Ciardelli, L. Corsi and M. Marcucci (2001). 'Membrane separation for wastewater reuse in the textile industry'. *Resour. Conserv. Recycl.*; **31** (2), p189-197. doi:10.1016/S0921-3449(00)00079-3
- [35] A. Rozzi, M. Antonelli and M. Arcari (1999). 'Membrane Treatment of Secondary Textile Effluents for Direct Reuse'. *Water Sci. Technol.*; **40** (4-5), p 409-416. doi:10.1016/S0273-1223(99)00524-7
- [36] Toraj Mohammadi, Ahmad Moheb, Mohtada Sadrzadeh and Amir Razmi (2005). 'Modeling of metal ion removal from wastewater by electrodialysis'. *Separation and Purification Technology*; **41** (1), p 73-82. doi:10.1016/j.seppur.2004.04.007
- [37] R Aplin and TD Waite (2000). 'Comparison of three advanced oxidation processes for degradation of textile dyes'. *Water Sci. Technol.*; **42** (5-6), p 345–354
- [38] N. Daneshvar, A. Aleboye and A. R. Khataee (2005). 'The evaluation of electrical energy per order (E_{EO}) for photooxidative decolorization of four textile dye solutions by the kinetic model'. *Chemosphere*; **59** (6), p 761-767. doi:10.1016/j.chemosphere.2004.11.012
- [39] N. Daneshvar, D. Salari and A. R. Khataee (2004). 'Photocatalytic degradation of azo dye acid red 14 in water on ZnO as an alternative catalyst to TiO₂'. *Journal of Photochemistry and Photobiology A: Chemistry*; **162** (2-3), p 317-322. doi:10.1016/S1010-6030(03)00378-2
- [40] Stephen J. Allen, Kayed Y. H. Khader and Murad Bino (1995). 'Electrooxidation of dyestuffs in waste waters'. *J. Chem. Technol. Biotechnol.*; **62** (2), p 111–117. doi: 10.1002/jctb.280620202 URL: <http://dx.doi.org/10.1002/jctb.280620202>
- [41] I. A. Balcioglu, and I. Arslan (1997). 'Treatment of textile waste water by heterogenous photocatalytic oxidation processes'. *Environ. Technol.*; **18** (10), p 1053-1059. doi:10.1080/09593331808616625 URL: <http://dx.doi.org/10.1080/09593331808616625>

- [42] Susana Rodríguez Couto and José Luis Toca-Herrera (2006). 'Academic Journals Mini Review Lacasses in the textile industry'. *Biotechnol. Mol. Biol. Rev.*; **1** (4), p 117-122. URL: <http://www.academicjournals.org/bmbr/PDF/Pdf2006/DEC/Couto%20and%20Toca-Herrera.pdf>, <http://www.academicjournals.org/BMBR>
- [43] Allison L. Henderson, Thomas C. Schmitt, Thomas M. Heinze and Carl E. Cerniglia (1997). 'Reduction of Malachite Green to Leucomalachite Green by Intestinal Bacteria'. *Appl Environ Microbiol.*; **63** (10), p 4099-4101 URL: <http://aem.asm.org/cgi/reprint/63/10/4099>
- [44] Jo-Shu Chang, Tai-Shin Kuo, Yun-Peng Chao, Jin-Yen Ho and Ping-Jei Lin (2000). 'Azo dye decolorization with a mutant *Escherichia coli* strain'. *Biotechnol. Lett.*; **22** (9), p807-812. doi: 10.1023/A:1005624707777
- [45] Jo-Shu Chang, Chien Chou and Shan-Yu Chen (2001). 'Decolorization of azo dyes with immobilized *Pseudomonas luteola*'. *Process Biochem.*; **36** (8-9), p 757-763. doi:10.1016/S0032-9592(00)00274-0
- [46] Rajesh Kumar Sani and Utam Chand Banerjee (1999). 'Decolorization of triphenylmethane dyes and textile and dye-stuff effluent by *Kurthia* sp'. *Enzyme Microb. Tech.*; **24** (7), p 433-437. doi:10.1016/S0141-0229(98)00159-8
- [47] Yuzhu Fu and T. Viraraghavan (2002). 'Dye biosorption sites in *Aspergillus niger*'. *Bioresource Technol.*; **82** (2), p 139-145. doi:10.1016/S0960-8524(01)00172-9
- [48] Nirmali Saikia and Madhuban Gopal (2004). 'Biodegradation of β -Cyfluthrin by Fungi'. *J. Agr. Food Chem.*; **52** (5), p 1220-1223. doi: 10.1021/jf0349580
- [49] Diane Fournier, Annamaria Halasz, Sonia Thiboutot, Guy Ampleman, Dominic Manno, and Jalal Hawari (2004). 'Biodegradation of Octahydro-1,3,5,7- tetranitro-1,3,5,7-tetrazocine (HMX) by *Phanerochaete chrysosporium*: New Insight into the Degradation Pathway' *Environ. Sci. Technol.*; **38** (15), p 4130-4133. doi: 10.1021/es049671d
- [50] Zümriye Aksu and Gönül Dönmez (2003). 'A comparative study on the biosorption characteristics of some yeasts for Remazol Blue reactive dye'. *Chemosphere*; **50** (8), p 1075-1083. doi:10.1016/S0045-6535(02)00623-9
- [51] V.K. Gupta, Arshi Rastogi, V.K. Saini and Neeraj Jain (2006). 'Biosorption of copper(II) from aqueous solutions by *Spirogyra* species'. *J. Colloid Interface Sci.*; **296** (1), p 59-63. doi:10.1016/j.jcis.2005.08.033
- [52] E. Acuner and F. B. Dilek (2004). 'Treatment of tectilon yellow 2G by *Chlorella vulgaris*'. *Process Biochem.*; **39** (5), p 623-631. doi:10.1016/S0032-9592(03)00138-9
- [53] Luz E. de-Bashan, Manuel Moreno, Juan-Pablo Hernandez and Yoav Bashan (2002). 'Removal of ammonium and phosphorus ions from synthetic wastewater by the microalgae *Chlorella vulgaris* coimmobilized in alginate beads with the microalgae growth-promoting bacterium *Azospirillum brasilense*'. *Water Res.*; **36** (12), p 2941-2948. doi:10.1016/S0043-1354(01)00522-X
- [54] Luz T. Valderrama, Claudia M. Del Campo, Claudia M. Rodriguez, Luz E. de- Bashan and Yoav Bashan (2002). 'Treatment of recalcitrant wastewater from ethanol and citric acid production using the microalga *Chlorella vulgaris* and the macrophyte *Lemna minuscule*'. *Water Res.*; **36** (17), p 4185-4192. doi:10.1016/S0043-1354(02)00143-4
- [55] Hai Yan and Gang Pan (2004). 'Increase in biodegradation of dimethyl phthalate by *Closterium lunula* using inorganic carbon'. *Chemosphere*; **55** (9), p 1281-1285. doi:10.1016/j.chemosphere.2003.12.019
- [56] Ibrahim M. Banat, Poonam Nigam, Datel Singh and Roger Marchant (1996). 'Microbial decolorization of textile-dye-containing effluents: a review'. *Bioresource Technol.*; **58** (3), p 217-227. doi:10.1016/S0960-8524(96)00113-7
- [57] Das S S, Dey S and Bhattacharyya B C (1995). 'Dye decolorization in a column bioreactor using wood-degrading fungus *Phanerochaete chrysosporium*'. *Indian Chem. Eng. Sect. A*; **37**, p 176-180.

- [58] D. Donnert, and M. Salecker (1999). 'Elimination of Phosphorus from Waste Water by Crystallization'. *Environ. Technol.*; **20** (7), p 735 - 742 doi: 10.1080/09593332008616868 URL: <http://dx.doi.org/10.1080/09593332008616868>
- [59] E. Remoudaki, A. Hatzikioseyan, P. Kousi and M. Tsezos (2003). 'The mechanism of metals precipitation by biologically generated alkalinity in biofilm reactors'. *Water Res.*; **37** (16), p 3843-3854. doi:10.1016/S0043-1354(03)00306-3
- [60] Matthew M. Matlock, Brock S. Howerton and David A. Atwood (2002). 'Chemical precipitation of heavy metals from acid mine drainage'. *Water Res.*; **36** (19), p 4757-4764. doi:10.1016/S0043-1354(02)00149-5
- [61] D. Feng, C. Aldrich and H. Tan (2000). 'Treatment of acid mine water by use of heavy metal precipitation and ion exchange'. *Miner. Eng.*; **13** (6), p 623-642. doi:10.1016/S0892-6875(00)00045-5
- [62] B. Manu and Sanjeev Chaudhari (2002). 'Anaerobic decolorisation of simulated textile wastewater containing azo dyes'. *Bioresour. Technol.*; **82** (3), p 225-231. doi:10.1016/S0960-8524(01)00190-0
- [63] M. Fababuj-Roger, J.A. Mendoza-Roca, M.V. Galiana-Aleixandre, A. Bes-Piá, B. Cuartas-Urbe and A. Iborra-Clar (2007). 'Reuse of tannery wastewaters by combination of ultrafiltration and reverse osmosis after a conventional physical-chemical treatment'. *Desalination*; **204** (1-3), p 219-226. doi:10.1016/j.desal.2006.02.032
- [64] Camille Sagne, Claire Fargues, Richard Lewandowski, Marie-Laure Lameloise and Martine Decloux (2008). 'Screening of reverse osmosis membranes for the treatment and reuse of distillery condensates into alcoholic fermentation'. *Desalination*; **219** (1-3), p 335-347. doi:10.1016/j.desal.2007.05.020
- [65] S. Rengaraj, Kyeong-Ho Yeon and Seung-Hyeon Moon. (2001). 'Removal of chromium from water and wastewater by ion exchange resins'. *J. Hazard. Mater.*; **87** (1-3), p 273-287. doi:10.1016/S0304-3894(01)00291-6
- [66] Viviane de A. Cardoso, Antonio G. de Souza, Patrícia P.C. Sartoratto and Liliane M. Nunes (2004). 'The ionic exchange process of cobalt, nickel and copper(II) in alkaline and acid-layered titanates'. *Colloids Surf., A*; **248** (1-3), p 145-149. doi:10.1016/j.colsurfa.2004.09.012
- [67] I W Nah, K -Y Hwang, Y -G Shul and C Jeon (2008). 'Removal of ammonium ion from aqueous solution using magnetically modified zeolite'. *Environ.l Technol.*; **29** (6), p 633-639. doi: 10.1080/09593330801984514 URL: <http://dx.doi.org/10.1080/09593330801984514>
- [68] Ü G Beker (1999). 'Treatment of geothermal wastewater by ion exchange method'. *Environ. Technol.*; **20** (4), p 437 — 442. doi: 10.1080/09593332008616838 URL: <http://dx.doi.org/10.1080/09593332008616838>
- [69] José M Monteagudo, María J Ortiz (2000). 'Removal of inorganic mercury from mine waste water by ion exchange'. *J. Chem. Technol. Biotechnol.*; **75** (9), p 767-772. doi: 10.1002/1097-4660(200009)75:9<767::AID-JCTB281>3.0.CO;2-1 URL: [http://dx.doi.org/10.1002/1097-4660\(200009\)75:9<767::AID-JCTB281>3.0.CO;2-1](http://dx.doi.org/10.1002/1097-4660(200009)75:9<767::AID-JCTB281>3.0.CO;2-1)
- [70] Elektorowicz M. and Muslat Z.(2008). 'Removal of heavy metals from oil sludge using ion exchange textiles'. *Environ. Technol.*; **29** (4), p 393 – 399. doi: 10.1080/09593330801984290 URL: <http://dx.doi.org/10.1080/09593330801984290>
- [71] Munaf E and Zein R. (1997). 'The Use of Rice Husk for Removal of Toxic Metals from Waste Water' *Environ. Technol.*; **18** (3), p 359 -362. doi: 10.1080/09593331808616549 URL: <http://dx.doi.org/10.1080/09593331808616549>
- [72] Munaf E. Zein R, Kurniadi R and Kurniadi I. (1997). 'The Use of Rice Husk for Removal of Phenol from Waste Water as Studied using 4-Aminoantipyrine Spectrophotometric Method'. *Environ. Technol.*; **18** (3), p 355 – 358. doi: 10.1080/09593331808616548 URL: <http://dx.doi.org/10.1080/09593331808616548>

- [73] J. Paprowicz and S. Ślodeczyk (1988). 'Application of biologically activated sorptive columns for textile waste water treatment' *Environ. Technol.*; **9** (4), p 271 – 280.
doi: 10.1080/0959338809384567
- [74] A. K. Jain, V. K. Gupta, A. Bhatnagar and I. A. Suhas (2003). 'Utilization of industrial waste products as adsorbents for the removal of dyes'. *J. Hazard. Mater.*; **101** (1), p 31–42.
doi:10.1016/S0304-3894(03)00146-8
- [75] Alok Mittal, Lisha Kurup (Krishnan) and Vinod K. Gupta (2005). 'Use of waste materials—Bottom Ash and De-Oiled Soya, as potential adsorbents for the removal of Amaranth from aqueous solutions'. *J. Hazard. Mater.*; **117** (2-3), p 171-178.
doi:10.1016/j.jhazmat.2004.09.016
- [76] Gordon McKay (1982). 'Adsorption of dyestuffs from aqueous solutions with activated carbon I: Equilibrium and batch contact-time studies'. *J. Chem. Technol. Biotechnol.*; **32** (7-12), p 759-772. doi: 10.1002/jctb.5030320712 URL: <http://dx.doi.org/10.1002/jctb.5030320712>
- [77] C. Hachem, F. Bocquillon, O. Zahraa and M. Bouchy (2001). 'Decolourization of textile industry wastewater by the photocatalytic degradation process'. *Dyes Pig.*; **49** (2), p 117-125.
doi:10.1016/S0143-7208(01)00014-6
- [78] S. D. Lambert, N. J. D. Graham, C. J. Sollars and G. D. Fowler (1997). 'Evaluation of inorganic adsorbents for the removal of problematic textile dyes and pesticides'. *Water Science and Technology*; **36** (2-3), p 173–180.
- [79] Cooper P (1995). 'Removing colour from dye house wastewater'. *Asian Text. J.*; **3**, p52-56.
- [80] M. A. Al-Ghouti, M. A. M. Khraish, S. J. Allen and M. N. Ahmad (2003). 'The removal of dyes from textile wastewater: a study of the physical characteristics and adsorption mechanisms of diatomaceous earth'. *J. Environ. Manage.*; **69** (3), p 229-238.
doi:10.1016/j.jenvman.2003.09.005
- [81] Carlos Alberto Policiano Almeida, Clodoaldo Machado and Nito Angelo Debacher (2004). 'Adsorption of methylene blue as a model for the use of Barro Branco as an alternative adsorbent for colour removal'; in "Surface and colloid science". *Prog. Colloid Polym. Sci.*; **128**, p 278- 282. Springer Berlin, Heidelberg. doi: 10.1007/b97109.
- [82] A. N. Fernandes, C. A. P. Almeida, C. T. B. Menezes, N. A. Debacher and M. M. D. Sierra (2007). 'Removal of methylene blue from aqueous solution by peat'. *J. Hazard. Mater.*; **144** (1-2), p 412-419. doi:10.1016/j.jhazmat.2006.10.053
- [83] Grégorio Crini (2006). 'Non-conventional low-cost adsorbents for dye removal: A review'. *Bioresour. Technology*; **97** (9), p 1061-1085. doi:10.1016/j.biortech.2005.05.001
- [84] A. Khenifi, Z. Boubkerka, F. Sekrane, M. Kameche and Z. Derriche (2007). 'Adsorption study on industrial dye by an organic clay'. *Adsorption*; **13** (2), p 149- 158.
doi: 10.1007/s10450-007-9016-6
- [85] Luiz C.A. Oliveira, Maraísa Gonçalves, Diana Q.L. Oliveira, Mário C. Guerreiro, Luiz R.G. Guilherme and Rogério M. Dallago (2007). 'Solid waste from leather industry as adsorbent of organic dyes in aqueous-medium'. *J. Hazard. Mater.*; **141** (1), p 344- 347.
doi:10.1016/j.jhazmat.2006.06.111
- [86] Moreira R. F. P. M, Peruch M. G and Kuhnen N. C (1998). 'Adsorption of textile dyes on alumina: Equilibrium studies and contact time effects'. *Braz. J. Chem. Eng.*; **15** (1).
doi: 10.1590/S0104-66321998000100002
- [87] Soon-An Ong, Eiichi Toorisaka, Makoto Hirata and Tadashi Hano (2007). 'Treatment of methylene blue containing wastewater using microorganisms supported on granular activated carbon under packed column operation'. *Environ. Chem. Lett.*; **5** (2), p 95- 99.
doi: 10.1007/s10311-006-0086-6
- [88] Arun K. Bhattacharya and C. Venkobachar (1984). 'Removal of Cadmium (II) by Low Cost Adsorbents'. *J. Envir. Engrg.*; **110** (1), p 110-122. doi:10.1061/(ASCE)0733-9372(1984)110:1(110) URL: [http://dx.doi.org/10.1061/\(ASCE\)0733-9372\(1984\)110:1\(110\)](http://dx.doi.org/10.1061/(ASCE)0733-9372(1984)110:1(110))

- [89] Binay Kr. Singh and Narendra S. Rawat (1994). 'Comparative sorption equilibrium studies of toxic phenols on flyash and impregnated flyash'. *J. Chem. Technol. Biotechnol.*; **61** (4), p 307-317. doi: 10.1002/jctb.280610405 URL: <http://dx.doi.org/10.1002/jctb.280610405>
- [90] Mamdouh M. Nassar and Mohammad S. El-Geundi (1991). 'Comparative cost of colour removal from textile effluents using natural adsorbents'. *J. Chem. Technol. Biotechnol.*; **50** (2), p 257-264. doi: 10.1002/jctb.280500210 URL: <http://dx.doi.org/10.1002/jctb.280500210>
- [91] Sunil K. Khare, Kamala K. Panday, Ram M. Srivastava and Viswa N. Singh (1987). 'Removal of victoria blue from aqueous solution by fly ash'. *J. Chem. Technol. Biotechnol.*; **38** (2), p 99-104. doi: 10.1002/jctb.280380206 URL: <http://dx.doi.org/10.1002/jctb.280380206>
- [92] G. McKay, G. Ramprasad and P. Pratapa Mowli (1986). 'Equilibrium studies for the adsorption of dyestuffs from aqueous solutions by low-cost materials'. *Water, Air, & Soil Pollution.*; **29** (3), p 273-283. doi: 10.1007/BF00158759
- [93] C. S. Brooks (1964). 'Mechanism of methylene blue dye adsorption on siliceous minerals'. *Colloid. Polym. Sci.*; **199** (1), p 31-36. doi: 10.1007/BF01499689
- [94] J. X. Lin, S. L. Zhan, M. H. Fang and X. Q. Qian (2007). 'The adsorption of dyes from aqueous solution using diatomite'. *J. Porous Mater.*; **14** (4), p 449-455. doi: 10.1007/s10934-006-9039-5
- [95] Saeed B Bukallah, M. A. Rauf, S. S. AlAli, (2007). 'Removal of methylene blue from aqueous solution by adsorption on sand'. *Dyes Pigment.*; **74** (1), p 85-87. doi:10.1016/j.dyepig.2006.01.016
- [96] Yasemin Özdemir, Mehmet Doğan and Mahir Alkan (2006). 'Adsorption of cationic dyes from aqueous solutions by sepiolite'. *Microporous Mesoporous Mater.*; **96** (1-3), p419-427. doi:10.1016/j.micromeso.2006.07.026
- [97] Ceyda Bilgiç (2005). 'Investigation of the factors affecting organic cation adsorption on some silicate minerals'. *J. Colloid Interface Sci.*; **281** (1), p 33-38. doi:10.1016/j.jcis.2004.08.038
- [98] Juang R. S, Wu F. C and Tseng R. L (1997). 'The Ability of Activated Clay for the Adsorption of Dyes from Aqueous Solutions'. *Environmental Technology*, **18** (5), p 525-531. doi: 10.1080/09593331808616568 URL: <http://dx.doi.org/10.1080/09593331808616568>
- [99] B. K. G. Theng and N. Wells (1995). 'Assessing the capacity of some New Zealand clays for decolourizing vegetable oil and butter'. *Applied Clay Science*; **9** (5), p 321-326. doi:10.1016/0169-1317(94)00031-K
- [100] Juraj Bujdák, Nobuo Iyi and Ryo Sasai (2004). 'Spectral Properties, Formation of Dye Molecular Aggregates, and Reactions in Rhodamine 6G/Layered Silicate Dispersions'. *J. Phys. Chem. B*; **108** (14), p 4470-4477. doi: 10.1021/jp037607x
- [101] Juraj Bujdák and Nobuo Iyi (2002). 'Visible spectroscopy of cationic dyes in dispersions with reduced-charge montmorillonites'. *Clays and Clay Minerals*; **50** (4), p 446-454.
- [102] F. Bergaya, B.K.G. Theng and G. Lagaly (Ed.) (2006). 'Handbook of Clay Science'. Elsevier. 1224pp. Developments in Clay Science, Vol. 1. Elsevier Science, Amsterdam.
- [103] H van Olphen (1977). 'An Introduction to Clay Colloid Chemistry: For Clay Technologists, Geologists and Soil Scientists' 2nd Edition. Wiley Interscience Publication, John-Wiley & Sons. Toronto. 318pp.
- [104] D. A. Morgan, D. B. Shaw, M. J. Sidebottom, T. C. Soon and R. S. Taylor (1985). 'The function of bleaching earths in the processing of palm, palm kernel and coconut oils'. *J. Am. Oil Chem. Soc. (JAOCs)*; **62** (2), p 292 - 299. doi:10.1007/BF02541394
- [105] Prakash Kumar, Raksh V. Jasra and Thirumaleshwara S. G. Bhat (1995). 'Evolution of Porosity and Surface Acidity in Montmorillonite Clay on Acid Activation'. *Ind. Eng. Chem. Res.*; **34** (4), p 1440-1448. doi: 10.1021/ie00043a053.
- [106] Lyjo K Joseph, H Suja, G Sanjay, S Sugunan, V P N Nampoori and P Radhakrishnan (2009). 'Thermal characterization of methylene blue intercalated montmorillonites by photoacoustic technique'. *Appl. Clay. Sci.*; **42** (3-4), p 483-487. doi:10.1016/j.clay.2008.06.006

- [107] Lyjo K Joseph, Sanjay G, Suja H, Sugunan S, Nampoori V P N and Radhakrishnan P (2009). 'Thermal characterization of dye intercalated K-10 montmorillonite ceramics using photoacoustic technique'. *Philos. Mag.*; **89** (10), p 895-905. doi: 10.1080/14786430902806652
- [108] Nélida Gimeno, Xiaoe Li, James R. Durrant and Ramón Vilar (2008). 'Cyanide Sensing with Organic Dyes: Studies in Solution and on Nanostructured Al₂O₃ Surfaces'. *Chemistry - A European Journal*; **14** (10), p 3006 – 3012. doi: 10.1002/chem.200700412
- [109] Jonathan Maserc and John A. Pojman (1998). 'Free radical-scavenging dyes as indicators of frontal polymerization dynamics'. *J. Chem. Soc., Faraday Trans.*; **94** (7), p 919-922. doi: 10.1039/a707270h.
- [110] Juan Pablo Padilla Martínez, Imelda Santiago Núñez, Georgina Beltrán Pérez, Juan Castillo Mixcoatl, Severino Muñoz Aguirre and Rodolfo Palomino Merino (2007). 'Optical fiber sensor for the measurement of the pH level using organic dyes deposited by the sol-gel process'. *Proc. SPIE*; **6422**, 64220Z. 7p. Sixth Symposium Optics in Industry. Monterrey, Mexico, 8th March 2007 doi:10.1117/12.742279 URL: <http://dx.doi.org/10.1117/12.742279>
- [111] I. R. Nasimova, E. E. Makhaeva and A. R. Khokhlov (2001). 'Poly(N-vinylcaprolactam) gel/organic dye complexes as sensors for metal ions in aqueous salt solutions'. *Journal of Applied Polymer Science*; **81** (13), p 3238 – 3243. doi: 10.1002/app.1778
- [112] Takashi Ohyama, Yasuko Yamada Maruo, Tohru Tanaka and Takayoshi Hayashi (1999). 'Fluorescence-intensity changes in organic dyes impregnated in porous glass on exposure to NO₂'. *Sens. Actuators, B*; **59** (1), p16-20. doi:10.1016/S0925-4005(99)00037-4
- [113] Pascale Lacan, P. Legall, Jeannine Rigola, Christian L. Lurin, D. Wettling, Christian Guizard and L. Cot (1992). 'Sol-gel-derived optical pH sensors'. *Proc. SPIE*; **1758**, p 464-475. Sol-Gel Optics II, 20th July. doi:10.1117/12.132038 URL:<http://dx.doi.org/10.1117/12.132038>
- [114] Hiromu Kashida, Hiroyuki Asanuma and Makoto Komiyama (2003). 'Development of a probe DNA which accompanies color change on hybridization'. *Nucleic Acids Research Supplement*; No. **3**, p 143-144 URL: <http://nass.oxfordjournals.org/cgi/reprint/3/1/143.pdf>
- [115] Shmuel Yariv (2002). 'Staining of clay minerals and visible absorption spectroscopy of dye-clay complexes'; in: "Organo-Clay Complexes and Interactions". Shmuel Yariv and Harold Cross (Eds.), 688pp. Marcel Dekker, Inc., New York, p. 463.
- [116] Juraj Bujdák (2006). 'Effect of the layer charge of clay minerals on optical properties of organic dyes. A review'. *Appl. Clay Sci.*; **34** (1-4), p 58–73. and the references therein doi:10.1016/j.clay.2006.02.011
- [117a] A S Davydov (1964). 'The theory of molecular excitons'. *Sov. Phys. Usp.*; **7** (2), p 145-178. doi: 10.1070/PU1964v007n02ABEH003659
- [117b] M. Kasha, H. R. Rawls and M. Ashraf El-Bayoumi. 'The exciton model in molecular spectroscopy'. URL: <http://media.iupac.org/publications/pac/1965/pdf/1103x0371.pdf>.
- [118] L. Antonov, G. Gergov, V. Petrov, M. Kubista and J. Nygren (1999). 'UV-Vis spectroscopic and chemometric study on the aggregation of ionic dyes in water'. *Talanta* **49** (1), p 99-106. doi:10.1016/S0039-9140(98)00348-8
- [119] A. Eisfeld and J. S. Briggs (2006). 'The J- and H-bands of organic dye aggregates'. *Chem. Phys.*; **324** (2-3), p 376-384. doi:10.1016/j.chemphys.2005.11.015
- [120a] Edwin E. Jelley (1936). 'Spectral Absorption and Fluorescence of Dyes in the Molecular State'. *Nature*; **138** (3502), p 1009-1010. doi:10.1038/1381009a0
- [120b] G. Scheibe (1937). 'About the variability of the absorption spectra in solutions and the secondary valences as their cause': 'Über die Veränderlichkeit der Absorptionsspektren in Lösungen und die Nebenvalenzen als ihre Ursache' (original in German). *Angewandte Chemie*; **50** (11), p 212- 219. doi: 10.1002/ange.19370501103 URL: <http://dx.doi.org/10.1002/ange.19370501103>

- [121] Zhen Zhao and Frank C. Spano (2005). 'Vibronic fine structure in the absorption spectrum of oligothiophene thin films'. *J. Chem. Phys.*: **122** (11), 114701, 11p. doi: 10.1063/1.1861456 URL: <http://link.aip.org/link/JCPSA6/122/114701/1>
- [122] E. W. Knapp, P. O. J. Scherer and S. F. Fischer (1984). 'On the lineshapes of vibronically resolved molecular aggregate spectra. application to pseudoisocyanin (PIC)'. *Chem. Phys. Lett.*: **111** (4-5), p 481-486. doi:10.1016/0009-2614(84)85544-X
- [123] P. O. J. Scherer and Sighart F. Fischer (1984). 'On the theory of vibronic structure of linear aggregates. Application to pseudoisocyanin (PIC)'. *Chem. Phys.*: **86** (3), p 269-283. doi:10.1016/0301-0104(84)80015-4
- [124] F. C. Spano and S. Siddiqui (1999). 'Exciton-vibrational coupling in pinwheel aggregates of π -conjugated molecules'. *Chem. Phys. Lett.*: **314** (5-6), p 481-487. doi:10.1016/S0009-2614(99)01078-7
- [125] Juraj Bujdák and Peter Komadel (1997). 'Interaction of Methylene Blue with Reduced Charge Montmorillonite'. *J. Phys. Chem. B*: **101** (44), p 9065-9068. doi: 10.1021/jp9718515
- [126] Kobayashi T (1996). 'J-Aggregates'. World Scientific. Singapore. 240pp.
- [127] Hiroshi Yao, Mayumi Omizo and Noboru Kitamura (2000). 'Mesoscopic string structures of thiacyanine J aggregates in solution'. *Chem. Commun.*: **9**, p 739 - 740. doi: 10.1039/b000548g
- [128] Miaomiao Wang, Gloria L. Silva and Bruce A. Armitage (2000). 'DNA-Templated Formation of a Helical Cyanine Dye J-Aggregate'. *J. Am. Chem. Soc.*: **122** (41), p 9977-9986. doi: 10.1021/ja002184n
- [129] Hiroshi Yao, Kaori Domoto, Takeshi Isohashi, and Keisaku Kimura (2005). 'In Situ Detection of Birefringent Mesoscopic H and J Aggregates of Thiacyanine Dye in Solution'. *Langmuir*: **21** (3), p 1067-1073. doi: 10.1021/la0479004
- [130] Francisco del Monte and David Levy (1999). 'Identification of *Oblique* and *Coplanar Inclined* Fluorescent J-Dimers in Rhodamine 110 Doped Sol-Gel-Glasses'. *J. Physical Chem. B*: **103** (38), p 8080-8086. doi: 10.1021/jp991491g
- [131] Adriana Czímerová, Luboš Jankovič and Juraj Bujdák (2004). 'Effect of the exchangeable cations on the spectral properties of methylene blue in clay dispersions'. *Journal of Colloid and Interface Science.*: **274** (1), p 126-132. doi:10.1016/j.jcis.2003.10.025
- [132] Juraj Bujdák, Marián Janek, Jana Madejová and Peter Komadel (1998). 'Influence of the layer charge density of smectites on the interaction with methylene blue'. *J. Chem. Soc., Faraday Trans.*: **94** (23), p 3487-3492. doi: 10.1039/a805341c
- [133] Juraj Bujdák, Marián Janek, Jana Madejová and Peter Komadel (2001). 'Methylene blue interactions with reduced-charge smectites'. *Clays and Clay Minerals*: **49** (3), p 244-254.
- [134] Adriana Czímerová, Alexander Čeklovský and Juraj Bujdák (2009). 'Interaction of montmorillonite with phenothiazine dyes and pyronin in aqueous dispersions: A visible spectroscopy study'. *Cent. Eur. J. Chem.*: **7** (3), p 343-353. doi: 10.2478/s11532-009-0035-x
- [135] Darryl P Almond and Pravin M Patel (1996). 'Photothermal Science and Techniques'. Chapman & Hall, London. 241pp.
- [136] Sajan D George, Rajesh Kombar, K G K Warriar, P Radhakrishnan, V P N Nampoori and C P G Vallabhan (2007). 'Photoacoustic thermal characterization of porous rare-earth phosphate ceramics'. *Int. J. Thermophys.*: **28** (1), p 123-132. doi: 10.1007/s10765-007-0153-7
- [137] Sajan D. George, Aji A. Anappara, P. R. S. Warriar, K. G. K. Warriar, P. Radhakrishnan, V. P. N. Nampoori and C. P. G. Vallabhan (2008). 'Photoacoustic thermal characterization of Al₂O₃-Ag ceramic nanocomposites'. *Mater. Chem. Phys.*: **111** (1), p 38-41. doi:10.1016/j.matchemphys.2008.03.009
- [138] Annieta Philip K, Lyjo K. Joseph, Litty Mathew Irimpan, Radhakrishnan P and Nampoori V. P. N (2005). 'Photoacoustic study on the photostability of polymethyl methacrylate films doped with Rhodamine 6G- Rhodamine B dye mixture system'. *J. Phys. D: Appl. Phys.*: **38** (6), p 2904-2909. doi: 10.1088/0022-3727/38/16/024

- [139] Annieta Philip K, Lyjo K. Joseph, Litty M. Irimpan, Bindu Krishnan, P. Radhakrishnan, V. P. N. Nampoori and Raghu Natarajan (2007). 'Thermal characterization of ceramic tapes using photoacoustic effect'. *Phys. Stat. Sol. (A)*; **204** (3), p 737-744.
doi: 10.1002/pssa.200622287 URL: <http://dx.doi.org/10.1002/pssa.200622287>
- [140] J. A. Balderas-López (2006). 'Photoacoustic methodology to measure thermal and optical properties of dye solutions'. *Rev. Sci. Instrum.*; **77** (8), 086104 [4pp].
doi:10.1063/1.2336206. URL: <http://link.aip.org/link/?RSINAK/77/086104/1>
- [141] J. L. Jiménez Pérez, J. F. Sánchez Ramírez, R. Gutiérrez Fuentes, A. Cruz-Orea and J. L. Herrera Pérez (2006). 'Enhanced of the R6G thermal diffusivity on aggregated small gold particles'. *Braz. J. Phys.*; **36** (3B), p 1025- 1028.
URL: http://www.sbfisica.org.br/bjp/files/v36_1025.pdf
- [142] Sajad D. George, Aji A Anapara, K. G. K Warriar, P. Radhakrishnan, C. P. G. Vallabhan and V. P. N. Nampoori (2003). 'Laser-induced thermal characterization of nano Ag metal dispersed ceramic alumina matrix'. *Proc. SPIE*; **5118**, p 207-212. Proceedings of SPIE on New Characterization Techniques for Nanotechnology. doi:10.1117/12.499026
- [143] S. Sankara Raman, V. P. N. Nampoori, C. P. G. Vallabhan, G. Ambadas and S. Sugunan (1995). 'Photoacoustic study of the effect of degassing temperature on thermal diffusivity of hydroxyl loaded alumina'. *Appl. Phys. Lett.*; **67** (20), p 2939- 2941. doi:10.1063/1.114818
URL:<http://link.aip.org/link/?APPLAB/67/2939/1>
- [144] J. Alexandre, F. Saboya, B. C. Marques, M. L. P. Ribeiro, C. Salles, M. G. da Silva, M. S. Stihel, L. T. Auler and H. Vargas (1999). 'Photoacoustic thermal characterization of kaolinite clays'. *Analyst*; **124** (8), p 1209- 1214. doi: 10.1039/a902601k
- [145] M.F. Rodrigues, M.S. Stihel, H. Vargas, J.N.F. Holanda (2005). 'Thermal characterization of sintered clay-petroleum waste mix by the photoacoustic technique'. *Mater. Sci. Forum*; **498-9**, p 512- 516. Advanced Powder Technology IV, Lucio Salgado and Francisco Ambrozio Filho (Ed.). doi:10.4028/www.scientific.net/MSF.498-499.512
- [146] A. Rosencwaig (1980). 'Photoacoustics and Photoacoustic Spectroscopy' John Wiley, New York. 309pp.
- [147] Allan Rosencwaig and Allen Gersho (1976). 'Theory of the photoacoustic effect with solids'. *J. Appl. Phys.*; **47** (1), p 64-69. URL: <http://link.aip.org/link/?JAPIAU/47/64/1>
- [148] Y H Pao (Ed.) (1977). 'Optoacoustic spectroscopy and detection'. Academic press, Inc. New York USA, 244pp.
- [149] Piyamaporn Jaruwong, Jakrit Aumpush, Ratanawan (Wibulswas) Kiattikomol (2005). 'Uptake of cationic and azo dyes by montmorillonite in batch and column systems'. *Thammasat Int. J. Sc. Tech.*; **10** (1), p 47-56. Thammasat International Journal of Science and Technology (TIJSAT). URL: http://www.tijsat.tu.ac.th/issues/2005/no1/2005_V10_No1_6.PDF
- [150] G. Rytwo, S. Nir, M. Crespin and L. Margulies (2000). 'Adsorption and Interactions of Methyl Green with Montmorillonite and Sepiolite'. *J. Colloid Interface Sci.*; **222** (1), p 12-19. doi:10.1006/jcis.1999.6595
- [151] F. Alan McDonald and Grover C. Wetsel Jr. (1978). 'Generalized theory of the photoacoustic effect'. *J. Appl. Phys.*; **49** (4), p 2313-2322. doi:10.1063/1.325116
URL:<http://link.aip.org/link/?JAPIAU/49/2313/1>
- [152a] F. Alan McDonald (1980). 'Three-dimensional heat flow in the photoacoustic effect'. *Appl. Phys. Lett.*; **36** (2), p 123-125. doi:10.1063/1.91402
URL:<http://link.aip.org/link/?APPLAB/36/123/1>
- [152b] idem. Erratum: 36 (9), p 782
doi:10.1063/1.91672 URL: <http://link.aip.org/link/?APPLAB/36/782/1>
- [153] P. Charpentier, F. Lepoutre and L. Bertrand (1982). 'Photoacoustic measurements of thermal diffusivity description of the "drum effect"'. *J. Appl. Phys.*; **53** (1), p 608- 614. doi:10.1063/1.329966 URL:<http://link.aip.org/link/?JAPIAU/53/608/1>

- [154] G. Rousset, F. Lepoutre and L. Bertrand (1983). 'Influence of thermoelastic bending on photoacoustic experiments related to measurements of thermal diffusivity of metals'. *J. Appl. Phys.*: **54** (5), p 2383-2391. doi:10.1063/1.332352
URL: <http://link.aip.org/link/?JAPIAU/54/2383/1>
- [155] P. K. Kuo, E. D. Sandler, L. D. Favro, and R. L. Thomas (1986). 'Mirage-effect measurement of thermal diffusivity. Part II: theory'. *Can. J. Phys.*: **64** (9), p 1168-1171. doi:10.1139/p86-203
- [156] Katrien Y Jacobs and Robert A Schoonheydt (2001). 'Time dependence of the spectra of methylene blue- clay mineral suspensions'. *Langmuir*; **17** (17), p 5150-5155. doi: 10.1021/la010141u
- [157] Schoonheydt R. A and Heughebaert L (1992). 'Clay adsorbed dyes: methylene blue in laponite'. *Clay Minerals*.; **27** (1), p 91-100.
URL: http://www.minersoc.org/pages/Archive-CM/Volume_27/27-1-91.pdf
- [158] Young Sun MOK, Hyun Tae AHN and Joeng Tai KIM (2007). 'Treatment of dyeing wastewater by using positive pulsed corona discharge to water surface'. *Plasma Sci. Technol.*: **9** (1), p 71- 75. doi: 10.1088/1009-0630/9/1/15
- [159] James D. Lindberg and David G. Snyder (1972). 'Diffuse reflectance spectra of several clay minerals'. *Am. Mineral.*; **57** (3-4), p 485-493.
URL: http://www.minsocam.org/ammin/AM57/AM57_485.pdf
- [160] Katrien Y Jacobs and Robert A Schoonheydt (1999). 'Spectroscopy of Methylene Blue-Smectite Suspensions'. *J. Colloid Interface Sci.*:**220** (1), p103-111. doi:10.1006/jcis.1999.6513
- [161] J. B. Baldo and W. N. dos Santos (2002). 'Phase transitions and their effects on the thermal diffusivity behaviour of some SiO₂ polymorphs'. *Ceramica*; **48** (307), p 172- 177. URL: <http://www.scielo.br/pdf/ce/v48n307/13835.pdf>
- [162] Donn G DeCoursey (1988). 'Environmental features important in nonpoint source models- Microclimatology': in: "The proceedings of the NATO advanced study institute on recent advances in the modelling of hydrologic systems". David S Bowles and P Enda O'Connell (Eds). Sintra, Portugal, July 10-23. chapter 11.
- [163] Hong X, Leach M. J and Raman S. Vegetation forcing and thermally induced generation of mesoscale circulation. ARM Science Meeting. Four-Dimensional Data Assimilation. p 163-169. URL: http://www.arm.gov/publications/proceedings/conf03/extended_abs/hong_x.pdf
- [164] Nidal H. Abu-Hamdeh (2003). 'Thermal Properties of Soils as affected by Density and Water Content'. *Biosystems Eng.*: **86** (1), p 97-102. doi:10.1016/S1537-5110(03)00112-0
- [165] William M. Chirdon, Wilkins Aquino and Kenneth C. Hover (2007). 'A method for measuring transient thermal diffusivity in hydrating Portland cement mortars using an oscillating boundary temperature'. *Cem. Concr. Res.*; **37** (5), p 680-690. doi:10.1016/j.cemconres.2007.01.010
- [166] R. C. Patil, S. Radhakrishnan, Sushama Pethkar and K. Vijaymohan (2001). 'Piezoresistivity of conducting polyaniline/BaTiO₃ composites'. *J. Mater. Res. (JMR)*; **16** (7), p 1982-1988. doi: 10.1557/JMR.2001.0271
- [167] Harold E. McGannon, J M Camp and C B Francis (1964). 'The Making, Shaping and Treating of Steel'. USS Pub., Pittsburgh. p195.
- [168] T. Sharma, R. C. Gupta and T. Prakash (1992). 'Swelling of Iron Ore Pellets by Statistical Design of Experiment'. *ISIJ Int.*; **32** (12), p 1268-1275. doi:10.2355/isijinternational.32.1268
- [169] Kouki Nishioka, Takeaki Murayama and Yoichi Ono (1996). 'Estimation of Effective Thermal Diffusivity of Porous Solid Using Data for Image Processing'. *ISIJ Int.*: **36** (2), p150-155. doi:10.2355/isijinternational.36.150
- [170] N. S. Sundarmurti and Vandana Rao (2002). 'Thermal Conductivity and Diffusivity of Iron Ore Pellet Having Low Porosity'. *ISIJ Int.*: **42** (7), p 800-802. doi:10.2355/isijinternational.42.800

- [171] W. M. Lima, W. R. Weinand, V. Biondo, E. S. Nogueira, A. N. Medina, M. L. Baesso and A. C. Bento (2003). 'Microstructure effects on the thermal properties of vacuum sintered AISI 316L stainless steel' *Rev. Sci. Instrum.*; **74** (1), p 716-718. doi: 10.1063/1.1512981 URL: <http://link.aip.org/link/?RSINAK/74/716/1>
- [172] S. Bailliez and A. Nzihou (2004). 'The kinetics of surface area reduction during isothermal sintering of hydroxyapatite adsorbent'. *Chem. Eng. J.*; **98** (1-2), p 141-152. doi:10.1016/j.cej.2003.07.001
- [173] Anurag Jain, Svetlana Rogojevic, Shom Ponoht, William N. Gill, Joel L. Plawsky, Eva Simonyi, Shyng-Tsong Chen and P. S. Ho (2002). 'Processing dependent thermal conductivity of nanoporous silica xerogel films'. *J. Appl. Phys.*; **91** (5), p 3275- 3281. doi:10.1063/1.1448407 URL:<http://link.aip.org/link/?JAPIAU/91/3275/1>
- [174] Xiang XIONG, Hong-chao SHENG, Jie CHEN and Ping-ping YAO (2007). 'Effects of sintering pressure and temperature on microstructure and tribological characteristic of Cu-based aircraft brake material'. *Trans. Nonferrous Met. Soc. China*; **17** (4), p 669-675. doi:10.1016/S1003-6326(07)60154-X
- [175] Regien G Stomphorst, Gert van der Zwan, Marc A M J van Zandvoort, Alexander B Sieval, Han Zuilhof, Frank J Vergeldt and Tjeerd J Schaafsma (2001). 'Spectroscopic Study of Erythrosin B in PVA Films'. *J. Phys. Chem. A*; **105**(17), p4235-4240. doi: 10.1021/jp0041813
- [176] Masumi Takeshima and Atsuo H. Matsui (1999). 'Suppression and enhancement of the exciton-phonon interaction in optical absorption spectra of Frenkel exciton microcrystallites'. *J. Lumin.*; **82** (3), p 195-204. doi:10.1016/S0022-2313(99)00053-8
- [177] Satoru Sugano and Norimichi Kojima (Ed.)(1999). 'Magneto-Optics'. Springer, NY 334p
- [178] Ramaier Narayanaswamy and Otto S. Wolfbeis (Ed.) (2004). 'Optical Sensors: Industrial, Environmental and Diagnostic Applications'. Springer. New York. 456pp.
- [179] Loubna Nouri and Oualid Hamdaoui (2007). 'Ultrasonication-Assisted Sorption of Cadmium from Aqueous Phase by Wheat Bran'. *J. Phys. Chem. A*; **111** (34), p 8456-8463. doi: 10.1021/jp0721393 and the references therein.
- [180] İlknur Küncek and Savaş Şener (2010). 'Adsorption of methylene blue onto sonicated sepiolite from aqueous solutions'. *Ultrason. Sonochem.*; **17** (1), p 250-257. doi:10.1016/j.ulsonch.2009.05.012
- [181] J. Cenens and R. A. Schoonheydt (1988). Visible spectroscopy of methylene blue on hectorite, laponite B, and barasym in aqueous suspension'. *Clays Clay Miner.* **36**(3), p214-224.
- [182] Shmuel Yariv and Harold Cross (Eds.) (2002). 'Organo-Clay Complexes and Interactions'. Marcel Dekker, Inc., New York, 688pp.
- [183] Jiří Konta (1995). 'Clay and man: Clay raw materials in the service of man'. *Applied Clay Science*; **10** (4), p 275-335. doi:10.1016/0169-1317(95)00029-4
- [184] Z. Klika, H. Weissmannová, P. Čapková and M. Pospíšil (2004). 'The rhodamine B intercalation of montmorillonite'. *J. Colloid Interface Sci.*; **275** (1), p 243-250. doi:10.1016/j.jcis.2004.02.040
- [185] Miroslav Pospíšil, Pavla Čapková, Helena Weissmannová, Zdeněk Klika, Miroslava Trchová, Marta Chmielová and Zdeněk Weiss (2003). 'Structure analysis of montmorillonite intercalated with rhodamine B: modeling and experiment'. *J. Mol. Model.*; **9** (1), p 39-46. doi: 10.1007/s00894-002-0107-8
- [186] Tetsuya Shichi and Katsuhiko Takagi (2000). 'Clay minerals as photochemical reaction fields'. *J. Photochem. Photobiol. C: Photochem. Rev.*; **1** (2), p 113-130. doi:10.1016/S1389-5567(00)00008-3
- [187] Makoto Ogawa and Kazuyuki Kuroda (1995). 'Photofunctions of intercalation compounds'. *Chem. Rev.*; **95** (2), p 399-438. doi: 10.1021/cr00034a005
- [188] Pavla Čapková, Petr Malý, Miroslav Pospíšil, Zdeněk Klika, Helena Weissmannová and Zdeněk Weiss (2004). 'Effect of surface and interlayer structure on the fluorescence of

- rhodamine B–montmorillonite: modeling and experiment'. *J. Colloid Interface Sci.*: **277** (1), p 128-137. doi:10.1016/j.jcis.2004.03.035
- [189] R. Chaudhuri, F. López Arbeloa and I. López Arbeloa (2000). 'Spectroscopic Characterization of the Adsorption of Rhodamine 3B in Hectorite'. *Langmuir*: **16** (3), p 1285–1291. doi: 10.1021/la990772c
- [190] Fendler J. H (1981). 'Membrane Mimetic Chemistry'. John Wiley & Sons, NY. 522pp
- [191] Kuppuswamy Kalyanasundaram (1987). 'Photochemistry in Microheterogeneous Systems'. Academic Press, New York. 388pp.
- [192] Zoltán Adamis and Richard B Williams (2005). 'Environmental health criteria 231. Bentonite, Kaolin, and Selected Clay Minerals'. World Health Organization, Geneva. 175pp.
- [193] Alain Meunier (2005). 'Clays'. Springer, Berlin, Germany. 472pp.
- [194] Charles Edward Weaver and Lin Davis Pollard (1975); 'The chemistry of clay minerals'. Elsevier Scientific Publishing Company, Amsterdam. 213pp.
- [195] Robert A. Schoonheydt (2002). 'Smectite-type clay minerals as nanomaterials'. *Clays and Clay Minerals*; **50** (4), p 411-420
- [196] J Valenta, A Fucikova, I Pelant, K Kúsová, K Dohnalová, A Aleknavičius, O Cibulka, A Fojtík and G Kada (2008). 'On the origin of the fast photoluminescence band in small silicon nanoparticles'. *New J. Phys.*; **10**, 073022 [6pp]. doi: 10.1088/1367-2630/10/7/073022
- [197] Laurier L. Schramm and Jan C. T. Kwak (1982). 'Influence of exchangeable cation composition on the size and shape of montmorillonite particles in dilute suspension'. *Clays Clay Miner.*; **30** (1), p 40-48.
- [198] James B. Gillespie, James D. Lindberg, and Michael S. Smith (1974). 'Visible and Near-Infrared Absorption Coefficients of Montmorillonite and Related Clays'. *Am. Mineral.*; **59** (9-10), p 1113-1116. URL: http://www.minsocam.org/ammin/AM59/AM59_1113.pdf
- [199] URL: <http://www.anaspec.com/products/product.asp?id=28769>
- [200] Francisco del Monte, Maria L. Ferrer and David Levy (2001). 'Preferred Formation of Coplanar Inclined Fluorescent J-Dimers in Rhodamine 101 Doped Silica Gels'. *Langmuir*; **17** (16), pp 4812–4817. doi: 10.1021/la010357w and the references therein
- [201] C. Dobrogowska, L. G. Hepler, D. K Ghosh and Sh. Yariv (1991). 'Metachromasy in clay mineral systems'. *J. Therm. Anal. Calorim.*; **37**(6), p1347-1356. doi: 10.1007/BF01913866
- [202] Yue Zhao, Dongsheng Li, Deren Yang and Minghua Jiang (2005). 'Blue emission of porous silicon intensified by boron deposition'. *J. Mater. Sci.*: **40** (18), p 5071-5073. doi: 10.1007/s10853-005-1621-8
- [203] Adam M. Jakob and Thomas A. Schmedake (2006). 'A Novel Approach to Monodisperse, Luminescent Silica Spheres'. *Chem. Mater.*; **18** (14), p 3173–3175. doi: 10.1021/cm060664t
- [204] Fernando López Arbeloa, Pilar Ruiz Ojeda and Iñigo López Arbeloa (1988). 'Dimerization and trimerization of rhodamine 6G in aqueous solution. Effect on the fluorescence quantum yield'. *J. Chem. Soc., Faraday Trans. 2*; **84** (12), p 1903 – 1912. doi: 10.1039/F29888401903.
- [205] L. F. Vieira Ferreira, M. J. Lemos, M. J. Reis and A. M. Botelho do Rego (2000). 'UV–Vis Absorption, Luminescence, and X-ray Photoelectron Spectroscopic Studies of Rhodamine Dyes Adsorbed onto Different Pore Size Silicas'. *Langmuir*: **16** (13), pp 5673–5680. doi: 10.1021/la9908182
- [206] Xiaowei Zhuang, Taekjip Ha, Harold D. Kim, Thomas Centner, Siegfried Labeit and Steven Chu (2000). 'Fluorescence quenching: A tool for single-molecule protein-folding study'. *Proceedings of the National Academy of Sciences (PNAS)*: **97** (26), p 14241–14244. URL: <http://www.pnas.org/content/97/26/14241.full.pdf+html>
- [207] T. Endo, N. Nakada, T. Sato and M. Shimada (1988). 'Fluorescence of clay-intercalated xanthene dyes'. *J. Phys. Chem. Solids*; **49** (12), p 1423-1428. doi:10.1016/0022-3697(88)90115-1

- [208] M. J. Tapia Estévez, F. López Arbeloa, T. López Arbeloa and I. López Arbeloa (1995). 'Characterization of Rhodamine 6G Adsorbed onto Hectorite by Electronic Spectroscopy'. *J. Colloid Interface Sci.*; **171** (2), p 439-445. doi:10.1006/jcis.1995.1200
- [209] Michael Famulok (2004). 'Chemical biology: Green fluorescent RNA'. *Nature*; **430** (7003), p 976-977. doi: 10.1038/430976a.
- [210] Kiwamu Yamaoka and Ryo Sasai (2000). 'Pulsed Electric Linear Dichroism of Triphenylmethane Dyes Adsorbed on Montmorillonite K10 in Aqueous Media'. *J. Colloid. Interf. Sci.*; **225** (1), p 82-93. doi:10.1006/jcis.2000.6738
- [211] S. S. Tahir and Naseem Rauf (2006). 'Removal of a cationic dye from aqueous solutions by adsorption onto bentonite clay'. *Chemosphere*; **63** (11), p 1842-1848. doi:10.1016/j.chemosphere.2005.10.033
- [212] Shivaji Srivastava, Ranjana Sinha and D. Roy (2004). 'Toxicological effects of malachite green'. *Aquatic Toxicology*; **66** (3), p 319-329. doi:10.1016/j.aquatox.2003.09.008
- [213] R. Cohen and S. Yariv (1984). 'Metachromasy in clay minerals. Sorption of acridine orange by montmorillonite'. *J. Chem. Soc., Faraday Trans. 1*; **80** (7), p 1705 - 1715. doi: 10.1039/F19848001705
- [214] Dorothee Fischer, Walter R. Caseri and Georg Hähner (1998). 'Orientation and electronic structure of ion exchanged dye molecules on mica: An X-Ray absorption study'. *J. Colloid. Interface Sci.*; **198** (2), p 337-346. doi:10.1006/jcis.1997.5296 and the references therein.
- [215] Karl Jasmund and Gerhard Lagaly (1993). 'Clay minerals and clays: structure, properties, applications and use in industry and environment'; Tonminerale und Tone: Struktur, Eigenschaften, Anwendungen und Einsatz in Industrie und Umwelt (Original in German). Steinkopff Verlag: Darmstadt, 490pp.
- [216] T. Preis and J. Thieme (1996). 'Dynamical Studies of Aqueous Clay Mineral Dispersions by X-ray Microscopy'. *Langmuir*; **12** (4), p 1105-1106. doi: 10.1021/la950775z
- [217] D. Penner and G. Lagaly (2000). 'Influence of organic and inorganic salts on the coagulation of montmorillonite dispersions'. *Clays and Clay Minerals*; **48** (2), p 246-255.
- [218] G. Lagaly (2006). 'Colloid clay science'; in: "Handbook of clay science". F. Bergaya, B. K. G. Theng and G. Lagaly (Ed.). Developments in Clay Science, Vol.1. Chapter 5. Elsevier Science, Amsterdam. doi: 10.1016/S1572-4352(05)01005-6 and the references therein.
- [219] S. Holzheu and H. Hoffmann (2002). 'Mechanistic Origin of Transient Electric Birefringence Anomaly of Clay Mineral Dispersion'. *J. Phys. Chem. B*; **106** (17), p 4412-4418. doi: 10.1021/jp012531v
- [220] G. H. Faye (1968). 'The optical absorption spectra of iron in six-coordinate sites in chlorite, biotite, phlogopite and vivianite: some aspects of pleochroism in the sheet silicates'. *Can. Mineral.*; **9** (3), p 403-425 .
- [221] A. Banin and N. Lahav (1968). 'Optical Study of Particle Size of Montmorillonite with Various Adsorbed Cations'. *Nature*; **217** (5134), p 1146-1147. doi:10.1038/2171146a0
- [222] A. Banin and N. Lahav (1968). 'Particle size and optical properties of montmorillonite in suspension'. *Israel J. Chem.*; **6**, p 235-250.
- [223] Y. Chen, D. Shaked and A. Banin (1979). 'The role of structural iron (III) in the UV absorption by smectites'. *Clay Minerals*; **14** (2), p 93-102.

Chapter 3

Photoluminescence and photothermal studies on rare earth titanates prepared by self propagating high temperature synthesis method

Abstract

The laser induced luminescence studies of the rare earth titanates (RETs, $R_2Ti_2O_7$, $R=La, Pr, Nd, Sm, Gd, Dy$ and Y), using 355 nm radiation from an Nd: YAG laser, are presented. These samples with nanometre size were prepared by the self propagating high temperature synthesis (SHS) method. There is no known fluorescence shown by $La_2Ti_2O_7$ in the visible region. Hence, the luminescence transitions shown by the $La_2Ti_2O_7$ near 610 nm are interesting to notice. Though La^{3+} ions without 4f electrons have no electronic energy levels that can induce excitation and luminescence processes in the visible region, the presence of the Ti^{3+} ions leads to luminescence. The luminescence spectra of all other RETs are also presented, but there is no significant luminescence observed in the visible region. The photoacoustic spectra of these samples are also given. The frequency up-conversion study on $La_2Ti_2O_7$ was also carried out. The approximate thermal diffusivity values of these RETs are obtained using photothermal deflection studies and an attempt is made to describe the possible fractal nature of the samples. Finally, an effort is made to find out the thermal effusivity values of these RETs using photoacoustic technique.

3.1. Prologue	153
3.2. Sample preparation	154
3.3. Experimental details	155
3.4. Section I- Optical studies of rare earth titanates	158
3.4.1. Part A: Photoluminescence studies	158
3.4.2. Part B: Photoacoustic spectroscopy	168
3.4.3. Part C: Frequency up-conversion in $\text{La}_2\text{Ti}_2\text{O}_7$	172
3.5. Section II- Photothermal studies of rare earth titanates	175
3.5.1. Part A: Thermal characterization using photothermal deflection	175
3.5.2. Part B: Photoacoustic thermal characterization – Fractal approach	181
3.5.3. Part C: Thermal effusivity measurement using photoacoustics	185
3.6. Summary	187
3.7. References	188



Lyjo K Joseph, K R Dayas, Soniya Damodar, Bindu Krishnan, K Krishnankutty, V P N Nampoori and P Radhakrishnan; "Photoluminescence studies on rare earth titanates prepared by self propagating high temperature synthesis method" *Spectrochimica Acta Part A: Molecular and Biomolecular Spectroscopy* **71(4)**, pp1281-1285 (2008).

[doi:10.1016/j.saa.2008.03.030](https://doi.org/10.1016/j.saa.2008.03.030)

3.1. Prologue:

The rare-earth (RE) doped laser crystals, glasses and ceramics, which possess trivalent RE ions, are popular solid state gain media. RE ions are also used as co-dopants for quenching the population in certain energy levels by the energy transfer processes, or for realising saturable absorbers, or as optically passive constituents of laser crystals.¹¹ In the realisation of photonic devices based on RE doped solid state materials, the optical, mechanical, and thermal properties of the lanthanide (Ln) play a major role and require a very careful consideration.¹² The photoluminescence (PL) and decay times in nano-structured xerogel and annealed sol gel silica glasses doped with RE ions, transition metal ions, metal complexes and semiconductor nano-crystals are investigated previously to study the excitation energy transfer processes, which reflect the optical properties of these confined nano-porous networks.¹³⁻⁵ RE metal compounds, especially their oxides, have become increasingly important in recent years because of their special PL and catalytic properties.^{16, 7} RE based phosphors play a critical and indispensable role as luminescent materials in the display industry. Synthesis of high quality RE based phosphor materials in the nano-region is thus important. With the growing interest in nano-scale RE activated phosphors for display applications, many efforts have been made to develop these phosphor materials because of their good luminescence characteristics, stability in high vacuum, and absence of corrosive gas emission under electron bombardment.^{18, 9} The possibilities for continuously tuning the stimulated emission (SE) wavelength of crystalline lasers based on the compounds using both lanthanide and transition metal were demonstrated.¹¹⁰ A broad-band tuneable SE can be excited with trivalent Ln^{3+} activators both at $4f^N - 4f^N$ and $4f^{N-1}5d^1 - 4f^N$ transitions.

RE titanates ($\text{R}_2\text{Ti}_2\text{O}_7$, RET) have interesting dielectric, piezoelectric and ferroelectric properties.¹¹¹⁻¹³ These materials usually possess a cubic pyrochlore structure¹¹⁴⁻¹⁷ for the ions with small R^{3+} (Sm^{3+} - Lu^{3+}), while the larger R^{3+} (La^{3+} - Nd^{3+}) exhibit a monoclinic structure.^{112, 18} The lanthanide pyrochlores are more susceptible to amorphization and have higher critical temperatures than Y-pyrochlore.¹¹⁹ Compounds with the pyrochlore structure have the formula $\text{A}_2^{3+}\text{B}_2^{4+}\text{O}_7$, where A can be the RE cation and B is Ti or any transition metal ions.¹²⁰

Pyrochlore RETs and zirconates find numerous applications such as hosts for fluorescence centres, high temperature pigments, catalysts, thermal barrier coatings, ionic/ electronic conductors, host phase in nuclear waste control etc.^{113, 21-23} Some of

the pyrochlores exhibit good catalytic activity, high melting point, low thermal conductivity, high thermal and phase stability, which make them promising for the catalytic combustion applications and thermal barrier coatings.^[24, 25] The RETs have a number of applications like photocurrent conductors in the UV region,^[26-28] thin film optical waveguides,^[28, 29] high temperature piezoelectric materials,^[29] multilayer ceramic chip capacitors^[30] etc. The RETs are found to have low dielectric constant values, which remain almost constant at different temperatures. This peculiar property makes the RETs and their doped compositions to be attractive candidates for microwave applications as resonators etc.^[31-33]

The RETs for the present studies are prepared by self propagating high temperature synthesis (SHS) method, which is also known as the self ignition synthesis or combustion synthesis. The titanates and oxides prepared by SHS method are superior to those prepared by conventional methods. The salient feature of SHS method is that it utilises reaction heat, instead of electric power. The SHS products are good quality nanometre sized powders with non-agglomerated nature. It can be synthesised to phase pure and sintered to high density at relatively lower temperatures.^[34-38] The SHS process involves the propagation of the reaction interface in the form of a combustion wave which is sustained by the large enthalpy release in the reaction front. The nature of this process, its general characteristics and its advantages and limitations have been described in ample detail in recent publications.^[34-38]

RETs are generally prepared by sintering the constituent oxides at high temperatures.^[39] But phase pure materials are seldom obtained even by the SHS method using organic fuels such as urea, glycine, etc. Therefore, development of new methods are essential for the synthesis of phase pure crystalline RETs having desired physico-chemical properties. The RETs used in the present study were prepared using ammonium acetate as fuel for the SHS reaction. The product obtained on characterization revealed that the method is very effective in the synthesis of phase pure RETs.^[40]

3.2. Sample preparation:

The RE oxides (0.02 mol, assay > 99 %), procured from Indian Rare Earths Limited, Kerala, were dissolved in hot HNO₃ (assay: 69.00 %. Merck India). This solution was slowly heated on a boiling water bath to remove the excess acid, if any, and evaporated to get the dry RE nitrate. To this, TiO₂ (0.04 mol, assay = 99.00 %, Merck

India Limited) and urea (0.16 mol, assay: 99.00 %, Qualigens, India) were added and slowly heated on an electric Bunsen and the contents in the beaker were thoroughly mixed by stirring. Urea acts as the solid fuel in the reaction and its molar ratio is very crucial. As the temperature increased to around 300 °C, urea melted and started decomposing with the evolution of ammonia. When the temperature reached ~350 °C, copious brown fumes of oxides of nitrogen started evolving. At this stage a spontaneous incandescent reaction took place vigorously and the mixture self ignited at about 400 °C along with evolution of large amount of gases. The content of the vessel frothed up to a highly porous network of foam-like structure, which almost filled the reaction vessel and gradually the flame subsided. The highly porous network of the fine crystallites of the RET formed was cooled to room temperature. The powder was calcined, pelletised and sintered at 1350 °C to 1550 °C.^[40, 41]

3.3. Experimental details:

3.3.1. Instrumental:

The relative reflectance spectra (*Figure 3.1*) of the pelletised samples were taken using a JASCO V-570 UV/ VIS/ NIR spectrophotometer with the model SLM-468 single reflection attachment. The surface area of the samples was measured using the Quanta chrome Nova model 1200 BET analyser and from the data on density of the SHS powders, their average particle size can be calculated (*Table 3.1*). The Bruker AXS 5005 XRD machine with Cu K α ($\lambda = 1.5418\text{\AA}$) radiation was used for evaluating the products synthesised in this study. The SEM microstructure measurements were done using A JEOL JSM-840A SEM.

Table 3.1: The details of the rare earth titanates (RETs) prepared by self propagating high temperature synthesis (SHS).^[40]

$R_2Ti_2O_7$ (R =)	Density (g/cc)	Surface area (m^2/g)	Average Particle Size (nm)
Gd	6.56	13.67	67
La	5.78	11.40	91
Nd	6.11	16.01	61
Pr	5.95	3.24	169
Sm	6.31	11.71	81
Dy	6.86	2.88	303
Y	4.98	4.64	259

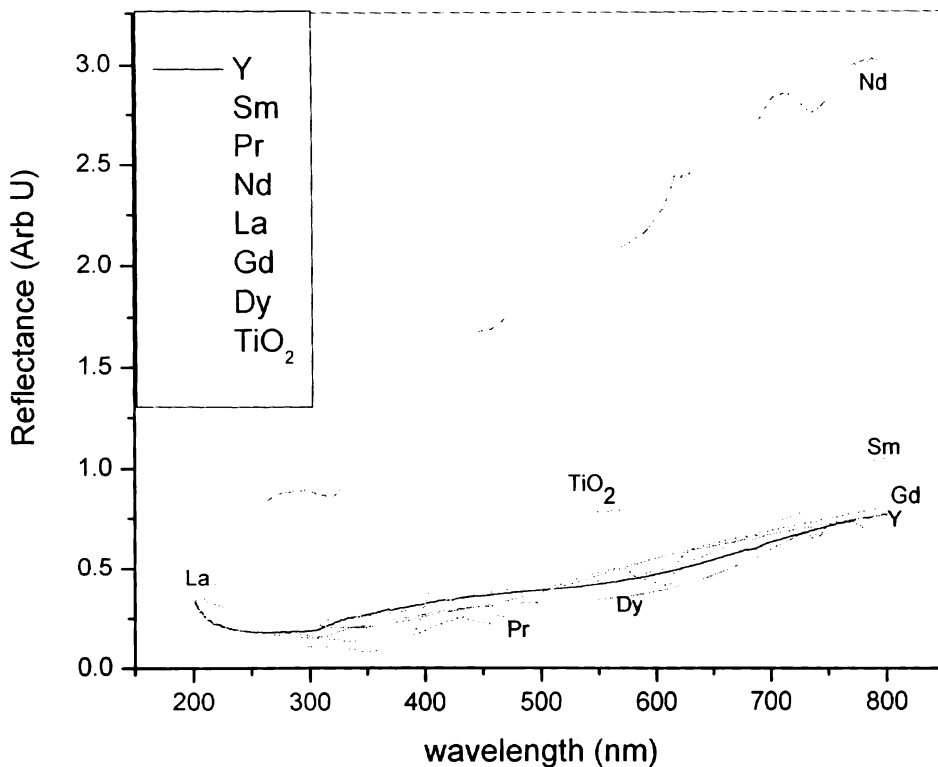


Figure 3.1: Reflectance spectra of the rare earth titanates (RETs).

3.3.2. XRD and SEM measurements:

The XRD of these SHS powders showed the amorphous or microcrystalline nature of the products. However, the crystallinity gradually improved on calcination at different temperatures and at 1200 °C, transformed to 100% phase pure crystalline material. Typical XRD and SEM photograph of a cubic and monoclinic RET pyrochlore are shown in Figure 3.2- 3.4 to get an idea about their structure. The detailed structural studies and salient features of these RETs were given in ref.^[40,41] The peaks in the spectra of $R_2Ti_2O_7$ ($R = La, Pr$ and Nd) synthesised by SHS method and calcined at 1200 °C (Figure 3.2), matched exactly with the peaks of the standard monoclinic $R_2Ti_2O_7$; whereas the spectra of $R = Gd, Sm, Dy$ and Y agreed well with standard cubic $R_2Ti_2O_7$.

The SEM photographs show very fine sizes of the order of nanometre ranges for the powders. The $La_2Ti_2O_7$ (Figure 3.3a) and $Nd_2Ti_2O_7$ powders appear to be free in nature with fewer inter-connections of the powder particles.

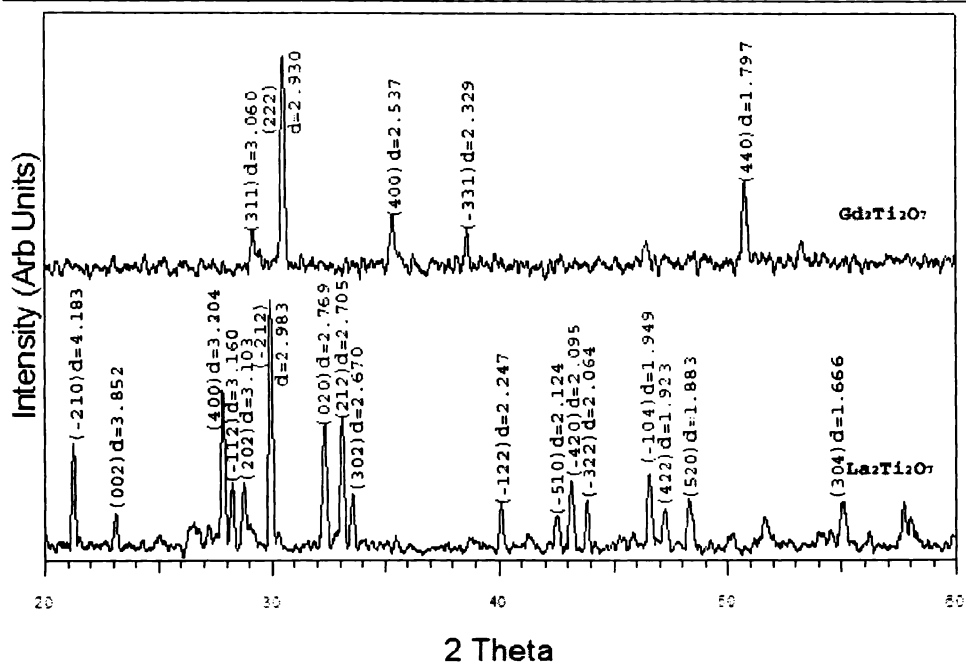


Figure 3.2: Typical XRD spectra of $Gd_2Ti_2O_7$ (Match JCPDS-ICDD 23-0259 cubic $Gd_2Ti_2O_7$) and $La_2Ti_2O_7$ (Match JCPDS-ICDD 28-0517 monoclinic $La_2Ti_2O_7$) synthesised by SHS method and calcined at $1200\text{ }^\circ\text{C}$.

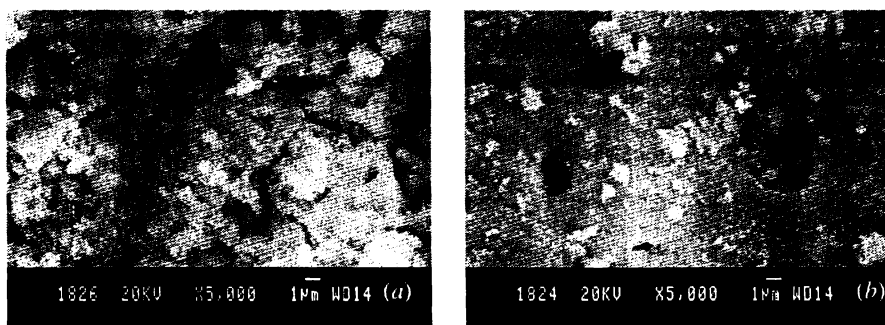


Figure 3.3: SEM microstructure of SHS powders of (a) monoclinic $La_2Ti_2O_7$ and (b) cubic $Gd_2Ti_2O_7$.

The SEM microstructure of the sintered (at $1450\text{ }^\circ\text{C}$) monoclinic RETs exhibit a well sintered physical appearance for the broken cross-sectional structure of the discs. The grains are smoothly inter-connected with almost zero porosity and appear to be single domain in structure. The SEM microstructure of the cross sectional surfaces of the $La_2Ti_2O_7$ discs sintered at $1450\text{ }^\circ\text{C}$ is given in *Figure 3.4a*.

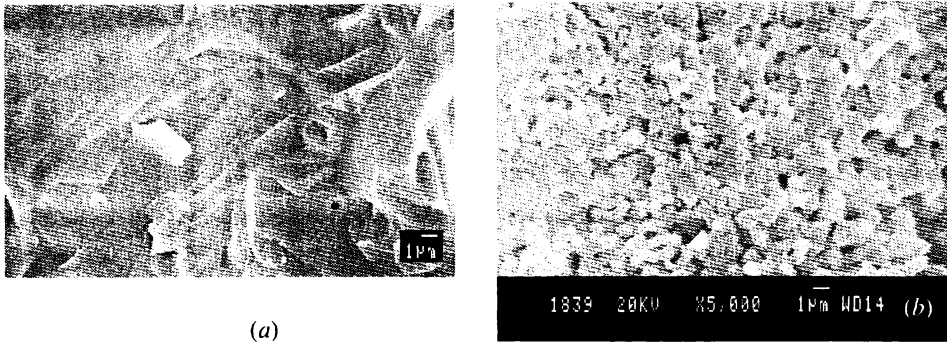


Figure 3.4: SEM of the cross section of sintered discs (at 1450 °C) of (a) monoclinic $\text{La}_2\text{Ti}_2\text{O}_7$ and (b) cubic $\text{Gd}_2\text{Ti}_2\text{O}_7$ made from SHS powders.

The SEM of $\text{Gd}_2\text{Ti}_2\text{O}_7$ in Figure 3.3b shows loosely packed powders along with some particles in a free state. SEM of cross section of the sintered $\text{Gd}_2\text{Ti}_2\text{O}_7$ (1450 °C) discs made from SHS powders of cubic crystalline RETs is shown in Figure 3.4b. A comparison with SEM structure of sintered monoclinic titanates reveals that the cubic form is not well sintered even at temperatures of 1450 °C to 1500 °C, unlike the monoclinic material.

3.4. Section I- Optical studies of rare earth titanates:

Many solid state systems containing lanthanides are very important for technological applications. Often these have to be studied in complex systems, without disturbing the physical and chemical environments within it. Laser induced fluorescence (LIF) and laser photoacoustic spectroscopy (PAS) are ideally suited for such applications. An important requirement for many of these studies is to get precise information on the structural environment of the Ln atom. Room temperature fluorescence spectra of molecules doped in solid matrices normally consist of broad bands corresponding to overlapping vibrational bands of electronic transitions. This broad fluorescence arises from inhomogeneous broadening arising from a distribution of the fluorescing species at different sites, and actually consists of several fine structure peaks.^[42]

3.4.1. Part A: Photoluminescence (PL) studies:

PL is a non-destructive and highly sensitive method commonly used to study the photo-physical and photo-chemical properties in photo assisted reactions. It is closely related to the surface stoichiometry and the nature of surface states, which can usually be changed by the annealing process.^[43] Investigations have shown that the

luminescence efficiency of materials can be improved by appropriate impurity addition.^[44, 45]

A1. Laser induced fluorescence (LIF):

The LIF technique is one of the most sensitive approaches, which is used widely in research for a variety of analytical applications, from interrogation of plasma plumes in laser induced breakdown spectroscopy (LIBS), to determination of cancerous tissues, to fluorescence spectroscopy of single molecules. It is relatively easy to implement, phenomenologically straightforward and well investigated, and largely non-invasive which can be imperative for biomedical application.^[46] LIF can be used for high resolution atomic and molecular spectroscopy of lanthanides for various applications, like ultra trace analysis, precision atomic and molecular structural parameter determination, molecular dynamics, chemical kinetics etc.

Fluorescence spectra due to the presence of RE ions in solids give information about the crystal field exerted on the respective elements in the compounds. The characteristic fluorescence spectra of different RE ions arise from the electronic transitions in the partially filled 4f orbitals. Electrons present in the occupied 4f shells can be transferred by light absorption, into unoccupied levels of higher energies. The 4f orbitals are well shielded by the fully filled or partially filled 5s and 5p outer shells. As a result, emission lines are relatively narrow and the energy level structure varies only slightly from one host to another. The effect of the crystal field is normally treated as a perturbation on the free-ion levels. The perturbation is small compared to spin-orbit and electrostatic interactions among the 4f electrons. Since the splittings are small, the terms and their levels remain easily identifiable for the REs. The primary change in the energy levels due to a splitting of the free ion levels is caused by the Stark effect of the crystal field. In crystals the free-ion levels are then referred to as manifolds. The trivalent Ln ions show efficient extrinsic localised type luminescence of the characteristic line spectra owing to $f \leftarrow f$ forbidden type transition in the visible to near-infrared region. When atoms and ions are incorporated in crystals, the forbidden character of the electric dipole transition is altered by the perturbation of the crystal electric field, so that the forbidden transition becomes allowed to some degree.^[47] Energy transfer from a light gathering meso-structured host lattice to an appropriate RE ion generates selected PL in the region 600- 1540 nm. Exciting the titania in its band gap results in the energy transfer and it is possible to observe PL from the crystal field states of the RE ions.^[48]

A2. Experimental details:

Using the pellets sintered at 1350 °C the luminescence studies were carried out at room temperature with the third harmonic of an Nd:YAG laser (355 nm, 7 ns Spectra Physics Quanta Ray). The luminescence spectrum was recorded at a pump power of 100 mW using 0.5 m triple grating spectrograph/ monochromator assembly (Spectrapro 500i Acton Research) attached with a CCD camera (Roper Scientific NTE/CCD 1340/100-EM). The experimental set up is as shown in *Figure 3.5*.

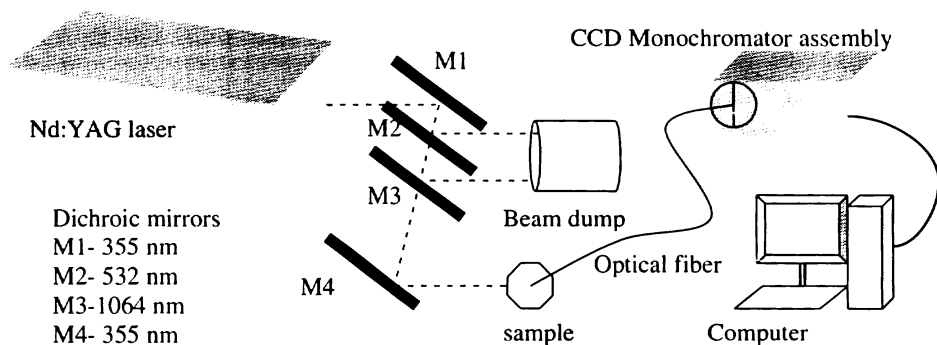


Figure 3.5: Schematic diagram of the experimental setup for measuring the photoluminescence (PL) of rare earth titanates (RETs).

A3. Results and discussions:

From the reflectance spectrum, shown in *Figure 3.1*, it is clear that the samples have absorption at around 355 nm. The details of PL spectra of the samples are given below. For a comparison, PL of TiO_2 is also given in *Figure 3.6a*. It has been reported earlier that the transition metal activator Ti^{3+} ions in insulating laser crystals have spectral SE channel ${}^2\text{E} \rightarrow {}^2\text{T}_2$. This leads to emission near 611 nm and within the range 660-1180 nm (*Figure 3.6b*) for operating temperature 300 K and at laser pumping conditions.^[49] A broad spectrum near 1000 nm is also seen, which is produced by the TiO_6 octahedra centre that is common in all the RETs used for the present study. There are a number of less intense peaks which are present in between 600 -1200 nm in the PL spectra of all RETs. These peaks may be arising from the TiO_6 octahedra in which the SE channel ${}^2\text{E} \rightarrow {}^2\text{T}_2$ of Ti^{3+} ions gives rise to the emission. In the PL spectra of all RETs presented here a peak near 1095 nm is also observed which can be attributed to the Ti^{3+} ions as mentioned earlier. The spectra of the lanthanide RETs presented here are compared with the Dieke diagram,^[50, 51] since RE spectra do not vary much with different hosts. However, the presence and absence of certain prominent lines may be attributed to the method of preparation and to the host matrix. In many of the RETs presented here, only certain transitions which are producing luminescence are shown.

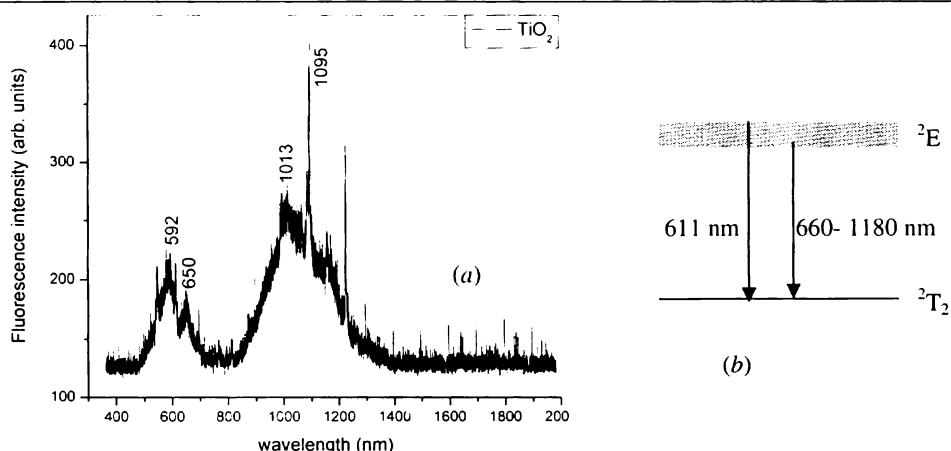


Figure 3.6: (a) Luminescence spectrum of TiO₂ when excited using 100 mW laser pulse of 355nm. (b) Energy level diagram of Ti³⁺[49].

A3.1. La₂Ti₂O₇:

The excited ions of the La₂Ti₂O₇ sample are observed to luminesce with peak emission within the range 608- 612 nm and also at 1221 nm which is the next harmonic (Figure 3.7). The La₂Ti₂O₇ is reported to have direct band gap and act as a good photo-catalyst for different light absorption.^[12, 18] La₂Ti₂O₇ has a monoclinic structure with a space group of P2₁ at room temperature. La³⁺ ion has inert gas [Xe] 4f⁰ configuration leading to a ¹S₀ ground state. Excited states can arise from a p-d transition leading to the electronic configuration 5s² 5p⁵ 5d¹ which gives rise to the singlet ¹P₁, ¹D₂ and ¹F₃ and the triplet ³P₁, ³D₂ and ³F₃ states.^[52]

Ions without 4f electrons are reported to have no electronic energy levels that can induce excitation and luminescence processes in or near the visible region.^[47] However, in the case of La₂Ti₂O₇ a transition close to 611 nm is observed in the present studies. The luminescent peaks observed at 610.5 and 1221.6 nm are sharp and it can be credited to the unfilled 4f orbital of the RE (La) added. An enhancement in the emission at around 611 nm is due to the presence of the unfilled 4f orbital of the La³⁺ ions present in the TiO₆ octahedra centres.^[53] Transition of the La³⁺ from the excited ³F₄ state to the ground state ¹S₀ enhances the Ti³⁺ SE channel near 611 nm to give rise to the observed luminescence for the La₂Ti₂O₇. The La³⁺ with the unfilled 4f orbital acts as a sensitizer and enhances the SE of the Ti³⁺. The lowest energy transition of La³⁺ is ¹S₀→¹D₂ (~318 nm) and the next transition arise from ¹S₀→¹F₃ (~285 nm). The excited states of the La³⁺ ion result from a p-d transition and the crystal field surrounding the ion is approximated by an O_h field.^[52] The electronic absorption spectra of RE ions in a crystal field are classified by Van Vleck^[54] to result

from: (1) electric-quadrupole transition, (2) magnetic dipole transition, (3) vibronic electric transitions and (4) electric dipole transitions. Only the last transition is allowed.^[52] The crystal field splitting can also be observed in the resolved spectrum which is shown in the inset of *Figure 3.7*. Internal 4f transitions are observed at wavelengths shorter than the absorption edges. There is no contribution from the La to the valence band.^[12] The various Russell-Saunders states arising from the 4fⁿ configurations are split by the crystal field, but the splitting is about 100 cm⁻¹. The extremely small splitting makes the f-f absorption bands very sharp giving rise to line-like spectra.

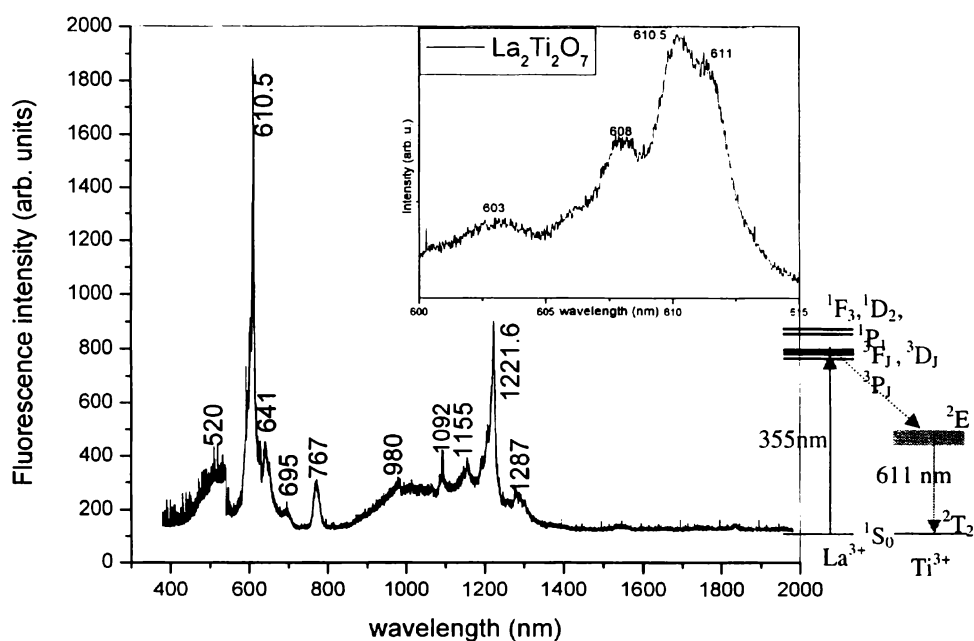


Figure 3.7: Luminescence spectrum of the $\text{La}_2\text{Ti}_2\text{O}_7$ when excited using 100 mW laser pulse of 355 nm. The energy level of La^{3+} is also shown with the possible emission from Ti^{3+} ion due to energy transfer. Inset: Crystal field splitting shown by $\text{La}_2\text{Ti}_2\text{O}_7$.

The observed luminescence property may be attributed to Ti^{3+} centre in the nano-sized $\text{La}_2\text{Ti}_2\text{O}_7$ which is enhanced by the presence of La^{3+} ions, whereas for the other titanates it may be attributed alone to TiO_6 octahedra centres. Thus nano-sized $\text{La}_2\text{Ti}_2\text{O}_7$ is a promising red phosphor for display applications.^[53]

A3.2. $\text{Gd}_2\text{Ti}_2\text{O}_7$:

Gd^{3+} has a 4f⁷ configuration and a ground state of $^8\text{S}_{7/2}$.^[17, 51, 55, 56] The $\text{Gd}_2\text{Ti}_2\text{O}_7$ has peaks at 767 nm and 1536 nm (*Figure 3.8*). The second peak is observed to be the

multiple of the first and hence can be considered as the harmonic. The 6G_J to 6I_J transitions give rise to the 767 nm emission from the Gd^{3+} ions. The R 4f level in $R_2Ti_2O_7$ is shifted to lower energy as the number of R 4f electrons increases. This red shift of the R 4f band decreases the band gap energy of the $R_2Ti_2O_7$.^[12] Thus a red shift in the luminescence to Gd^{3+} ions with respect to La^{3+} ions is also observed as the R^{3+} ion radius is decreased due to lanthanide contraction. This explains the red shift exhibited by Gd^{3+} ions which has a smaller ionic radius with respect to La^{3+} ions.^[53]

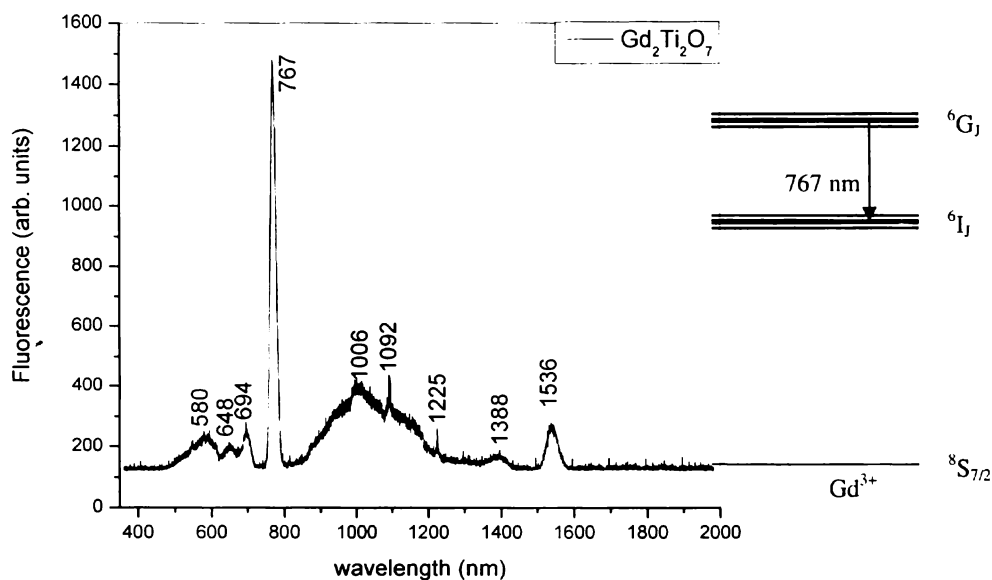


Figure 3.8: Luminescence spectrum of the $Gd_2Ti_2O_7$ when excited using 100 mW laser pulse of 355nm. The energy level of Gd^{3+} , along with the possible emission transitions, is also given.

A3.3. $Nd_2Ti_2O_7$:

In the case of $Nd_2Ti_2O_7$ the spectrum (Figure 3.9) is more prominent in the region 850-1150 nm and can be associated with the emission due to the Nd^{3+} ions arising from ${}^4F_{3/2}$ to the 4I_J (${}^4I_{9/2}$: 900 nm, ${}^4I_{11/2}$: 1060 nm, ${}^4I_{13/2}$: 1350 nm) transitions. The luminescence spectrum in the 860-940 nm spectral range, corresponds to ${}^4F_{3/2}$ - ${}^4I_{9/2}$ transition, contains 6 peaks and ${}^4F_{3/2}$ - ${}^4I_{11/2}$ transition has 5 peaks. Here all these peaks are combined to give a broad spectrum. The decay time of IR luminescence of Nd^{3+} in titanate is reported to be the shortest one in the known systems activated by Nd^{3+} arising from the energy level quenching by the host matrix material. Another group of lines was detected in the titanate luminescence spectrum, which was considered to be connected with the Nd^{3+} emission. These lines at 589, 658, 743 and 846 nm are arising from the electron transitions from ${}^2G_{7/2}$ level to ${}^4I_{9/2}$, ${}^4I_{11/2}$, ${}^4I_{13/2}$ and ${}^4I_{15/2}$ levels. Such a

combination of emission lines with relatively short decay times is very unusual for minerals and may not be easily connected to any RE element traditional for luminescence in the visible range. The above mentioned luminescent lines were reported to be strong in the PL spectra when excited by 532 nm.^[57] But, in the present case the 589 nm and 658 nm lines were observed with 355 nm excitation, whereas the other peaks at 743 and 846 nm were combined with ${}^4F_{3/2} \rightarrow {}^4I_J$ transitions. These transitions may be producing the peaks at 984 nm and 1094 nm along with those of the Ti^{3+} SE channel. The SE in the 1037-1123 nm range from the ${}^4F_{3/2} \rightarrow {}^4I_{11/2}$ is also observed. Additionally, Nd^{3+} has another emission near 1300 nm due to ${}^4F_{3/2} \rightarrow {}^4I_{13/2}$ transition.^[49]

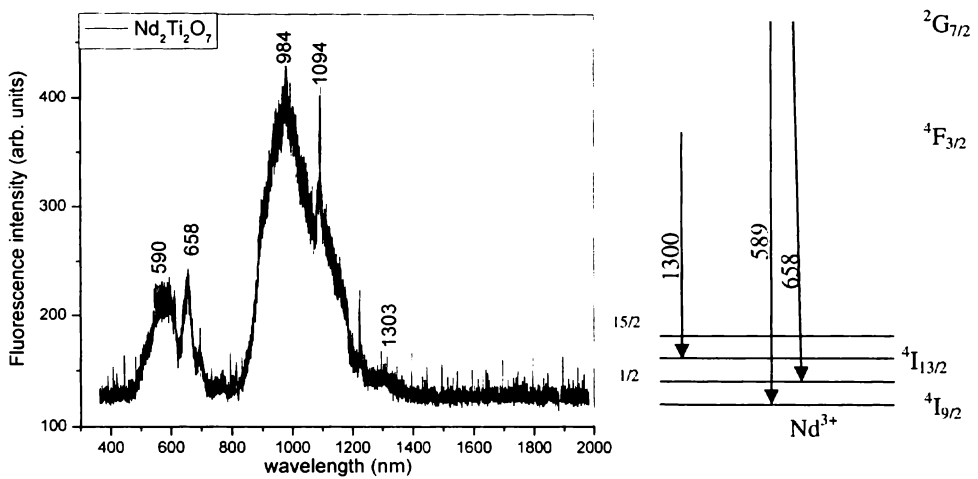


Figure 3.9: Luminescence spectrum of the $Nd_2Ti_2O_7$ when excited using 100 mW laser pulse of 355 nm. The schematic Nd^{3+} energy level diagram is given on the right side along with the possible emission transitions.

A3.4. $Pr_2Ti_2O_7$:

Figure 3.10 shows the PL spectra of $Pr_2Ti_2O_7$. It was reported that the visible lines of the Pr^{3+} PL arise from the 3P_0 excited state. The ${}^3P_0-{}^3H_4$ and ${}^3P_0-{}^3F_1$ transitions give rise to the prominent peaks in the visible region. There are many SE channels for Pr^{3+} in the visible and NIR region at room temperature. The line near 657 nm is ascribed to ${}^3P_0-{}^3F_2$ and/or ${}^1D_2-{}^3H_J$ transitions in Pr^{3+} . It was also reported that the transition ${}^3P_0-{}^3H_6$ causes the orange emission from Pr^{3+} in 598-622 nm range. There are SE at 996nm and 1056 nm for Pr^{3+} ions which arises from ${}^1D_2 \rightarrow {}^3F_3, {}^3F_4$ transitions.^[49] This SE is combined to with the SE channel of Ti^{3+} to form the broad spectrum.

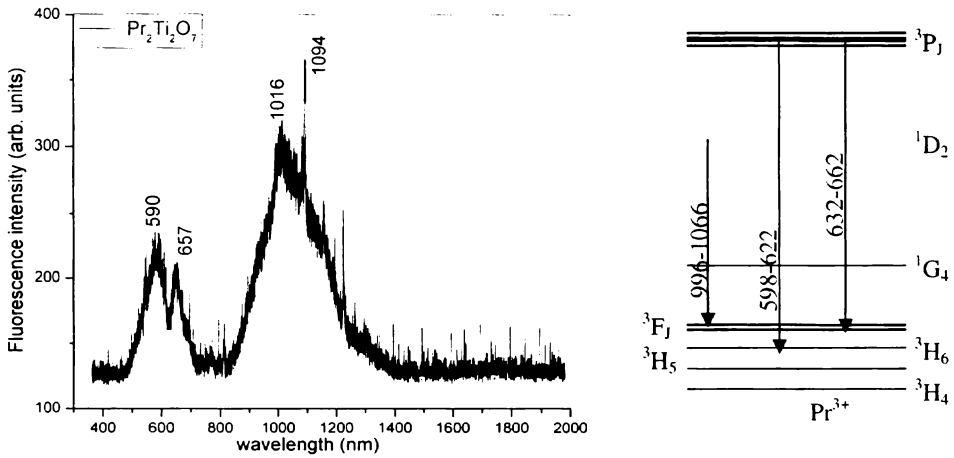


Figure 3.10: Luminescence spectrum of the $\text{Pr}_2\text{Ti}_2\text{O}_7$ when excited using 100 mW laser pulse of 355 nm. On right: Schematic representation of Pr^{3+} energy levels with possible emission transitions.

A3.5. $\text{Dy}_2\text{Ti}_2\text{O}_7$:

The PL spectrum of Dy^{3+} and the schematic representation of Dy^{3+} energy levels are given in Figure 3.11. Dy^{3+} has narrow characteristic lines near 490 and 572-575 nm^[57] arising from the $^4\text{F}_{9/2}$ to $^6\text{H}_{15/2}$ and $^6\text{H}_{13/2}$ transitions. The peak near 580 nm can be attributed to Dy^{3+} with these transitions and it is merged with that of Ti^{3+} . The other $^6\text{F}_J$ to $^6\text{H}_J$ transitions give rise to the spectrum around 900-1100 nm which is appearing along with the SE channel of Ti^{3+} in this region. The peak near 648 nm may be originating from Ti^{3+} .

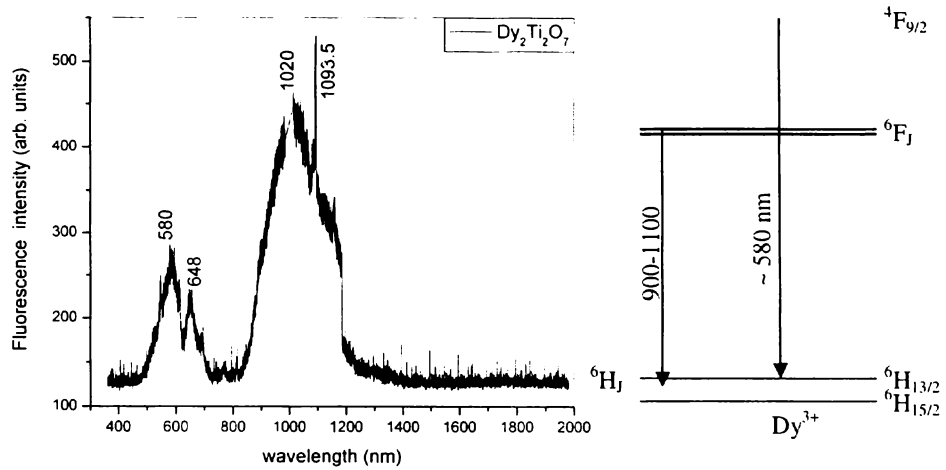


Figure 3.11: Luminescence spectrum of the $\text{Dy}_2\text{Ti}_2\text{O}_7$ when excited using 100mW laser pulse of 355 nm. The energy levels of Dy^{3+} are given on right with possible emission transitions.

A3.6. $\text{Sm}_2\text{Ti}_2\text{O}_7$:

Glasses containing Sm^{3+} ions have stimulated extensive interest due to their potential application for high-density optical memory devices.^[58, 59] The emitting $^4\text{G}_{5/2}$ level of Sm^{3+} ions in the visible region exhibits relatively high quantum efficiency and shows different quenching emission channels, which make Sm^{3+} ions an interesting case to analyse the energy transfer process.^[60-64]

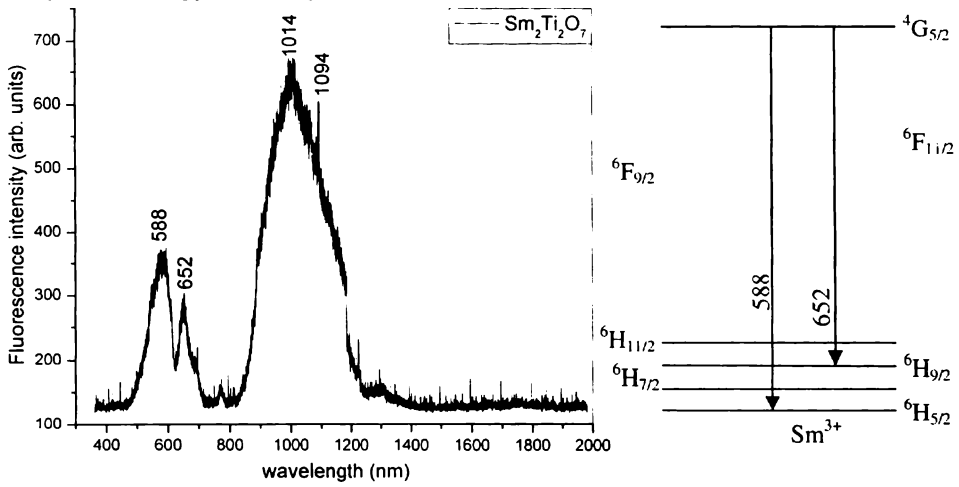


Figure 3.12: Luminescence spectrum of the $\text{Sm}_2\text{Ti}_2\text{O}_7$ when excited using 100 mW laser pulse of 355 nm. The energy levels of Sm^{3+} are shown on right with possible emission transitions.

Figure 3.12 represents the PL spectrum of $\text{Sm}_2\text{Ti}_2\text{O}_7$. It was reported that broad emission peak near 652 nm appeared in the PL spectra of Sm^{3+} doped BaAl_2Se_4 due to donor-acceptor pair recombinations.^[65] Such a recombination may be occurring in the present case also to produce the PL peak near 652 nm. Sm^{3+} activated minerals usually display an intense luminescence spectrum with a distinct line structure in the red-orange part of the spectrum. The radiating term $^4\text{G}_{5/2}$ is separated from the nearest lower level $^6\text{F}_{11/2}$ by an energy interval of $\sim 7500 \text{ cm}^{-1}$. This distance is too large compared to the energy of phonons capable to accomplish an effective non-radiative relaxation of excited levels and these processes do not significantly affect the nature of their spectra in minerals. Thus all detected lines of the Sm^{3+} luminescence take place from one excited level and usually are characterised by a long decay time. The line near 600 nm has a long decay time of 1 ms. It is the strongest one in the titanate luminescence spectrum under 266, 355 and 532 nm excitations, but its relative intensity is much lower under 514 nm excitation. A combination of luminescence lines is very typical for Sm^{3+} . Thus the emission spectrum of Sm^{3+} in titanate exhibits three peaks corresponding to $^4\text{G}_{5/2} \rightarrow ^6\text{H}_{5/2}$, $^6\text{H}_{7/2}$ and $^6\text{H}_{9/2}$. The intensity of the SE channel

${}^4G_{5/2} - {}^6H_{7/2}$ (~600 nm) transition^[49] is much stronger than the other emission transitions, which is in accordance with the Sm^{3+} behaviour in glasses. The little difference in spectral position and half width of the line at 600 nm under different excitations shows that several Sm^{3+} centers may present.^[57] The emission near 900-1100 nm range^[57] is united with that of the Ti^{3+} . The other peaks may also be originating from Ti^{3+} ions.

A3.7. $\text{Y}_2\text{Ti}_2\text{O}_7$:

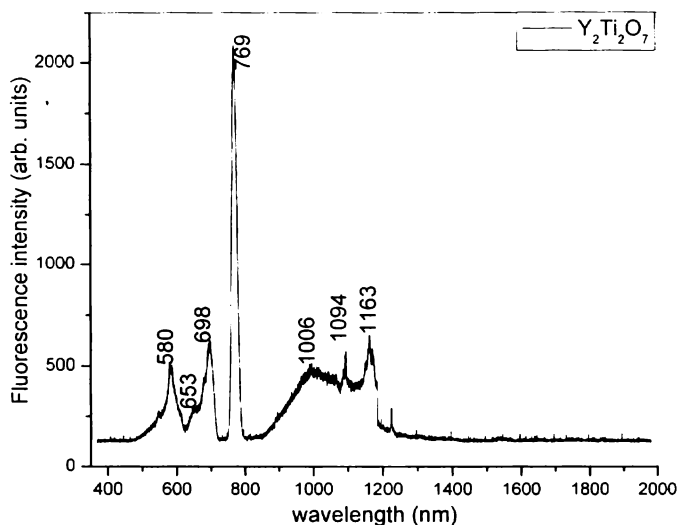


Figure 3.13: Luminescence spectrum of the $\text{Y}_2\text{Ti}_2\text{O}_7$ when excited using 100 mW laser pulse of 355 nm. The energy level diagram is not given as Y does not belong to lanthanides.

Y does not have energy levels that can cause excitation and luminescence in or near the visible region due to the absence of 4f electrons.^[47] It was reported that Ti: YAG showed intense fluorescence near 775 nm and 770 nm when excited using 532 nm and 512 nm laser lines respectively.^[66, 67] Analogous to Ti: sapphire, the band at 770 nm in Ti: YAG crystal is directly attributed to the Stokes-shift $E_g \rightarrow T_{2g}$ optical relaxation of Ti^{3+} in most publications. Admittedly, there have been no experimental data to prove the peak at about 770 nm to be attributed to Ti^{3+} . If Ti^{3+} ion indeed contribute to the peak, the two peaks of Ti: YAG excited at 532 nm should be attributed to the optical relaxation from non-degenerate $E_{g(+)}$ and $E_{g(-)}$ to T_{2g} , respectively. But 769 nm emission (Figure 3.13) from the $\text{Y}_2\text{Ti}_2\text{O}_7$ confirms that the emission arises from the Y itself. No other RET samples except $\text{Gd}_2\text{Ti}_2\text{O}_7$ showed the fluorescence near 770 nm. All other peaks may be arising from the SE channel of Ti^{3+} . The energy level diagram of Y^{3+} is not given as it does not belong to the lanthanide RE.

A4. Conclusions:

The luminescence shown by the nano-sized $\text{La}_2\text{Ti}_2\text{O}_7$ in the visible region is due to the presence of the unfilled 4f orbital of the La^{3+} ions in the TiO_6 octahedral centres even though ions with no 4f electrons do not have such emission in this region. The SE of transition metal activator Ti^{3+} ions in insulating laser crystals near 611 nm can be enhanced by the sensitiser La^{3+} ions and it is sharp due to the presence of the 4f orbitals. In other RETs, this SE is inhibited by the presence of R^{3+} ions in 4f orbital. In the case of $\text{Nd}_2\text{Ti}_2\text{O}_7$ the luminescence emission of the Nd^{3+} ions is overlapped by the presence of the Ti^{3+} SE channels. A red shift in the luminescence of Gd^{3+} ions with respect to La^{3+} ions is observed as the R^{3+} ion radius is decreased due to Ln contraction. The observed luminescence of nano-sized $\text{La}_2\text{Ti}_2\text{O}_7$ near 610 nm makes it suitable for display applications after further characterizations. The sharp peak of $\text{Y}_2\text{Ti}_2\text{O}_7$ near 769 nm is attributed to the Y^{3+} . Samples with no 4f or half filled 4f electron showed sharp intense luminescence.

3.4.2. Part B: Photoacoustic spectroscopy (PAS):

PAS and related photothermal (PT) techniques have become well established due to a number of facts like provision of direct absorption spectra, depth profile analysis, characterization of thermal properties as well as investigation of non-radiative relaxation processes. The PA signal arises from the non-radiative de-excitation of the energy absorbed in an optical transition and hence can be correlated with the optical absorption of the sample. Thus PAS can be used for measuring non-radiative transitions in materials. Further, PAS can be applied to materials with large optical densities where optical absorption spectroscopy cannot be used as the transmitted light is weak. PAS measures the absorbed energy directly and hence can be used to probe spectroscopic information in such cases.

PAS is a well-known technique which is very useful for spectral studies of difficult samples (highly absorbing or scattering), as well as samples which may not give a fluorescence spectrum because of rapid non-radiative relaxation processes.^[68] It is extremely sensitive, can be applied to solids, liquids or gases and is simple to carry out.^[42] PAS does not require highly reflecting surfaces which is essential in conventional reflection spectroscopy. Furthermore, the need for ultra-clean surfaces and thus the need for elaborate high-vacuum equipment so necessary for conventional reflection studies is not required for PAS.^[69]

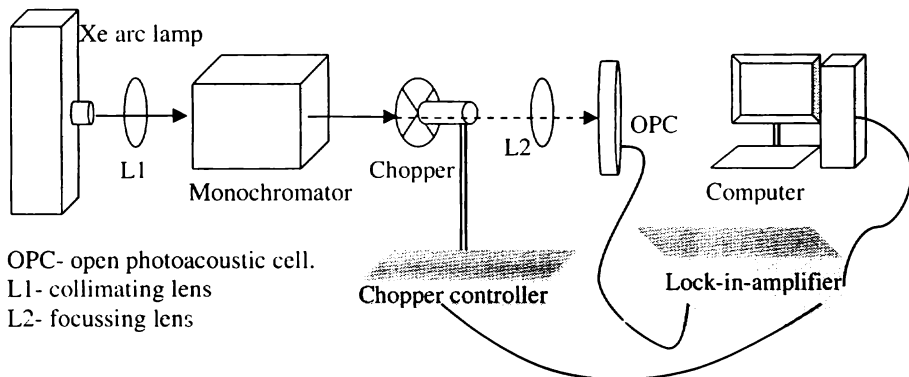
B1. Experimental setup:

Figure 3.14: Schematic representation of photoacoustic spectroscopy experimental setup.

The schematic representation of the experimental set up is given in Figure 3.14. Optical radiation from a 1000W Xe arc lamp (ozone free Newport model 6271) was used as the source of excitation. The output was given to a monochromator (ORIEL compact 77250 1/8 meter monochromator with model 77298 grating) to select the wavelength between 350 nm and 790 nm at an interval of 5 nm. It was intensity modulated at 40 Hz using a mechanical chopper (Stanford Research Systems SR 540) before it reached the sample. Detection of the PA signal was made using a sensitive electret microphone (Knowles BT 1834). The amplitude of the PA signal was measured by means of a dual phase lock-in-amplifier (Stanford Research Systems SR 830). The lock-in-amplifier output was interfaced to a computer using LabVIEW 7 Express (National Instruments). The reflection mode geometry (Figure 2.4) of the open cell PA technique was used in this experiment. Prior to the experiment the monochromator was calibrated using a mercury lamp. The PA cell was calibrated using carbon black. The samples were placed at the open end of the PA cell.

B2. Results and discussions:

Figure 3.15 shows the PA spectrum obtained for carbon black and $\text{Nd}_2\text{Ti}_2\text{O}_7$ using LabVIEW. Figure 3.16 shows the PA spectrum of RETs. The absorption spectrum of Nd^{3+} titanates usually have peaks at 583 nm ($^4\text{I}_{9/2}$ - $^4\text{G}_{5/2}$, $^2\text{G}_{7/2}$); 723, 751, 762 nm ($^4\text{I}_{9/2}$ - $^4\text{F}_{7/2}$); 796, 806, 820 nm ($^4\text{I}_{9/2}$ - $^4\text{F}_{5/2}$) and 855 nm ($^4\text{I}_{9/2}$ - $^4\text{F}_{3/2}$).^{157]}For Sm^{3+} titanates have peaks at 971 nm ($^6\text{H}_{5/2}$ - $^6\text{F}_{11/2}$) and 1061 nm ($^6\text{H}_{5/2}$ - $^6\text{F}_{9/2}$).^{157]}In Y^{3+} and La^{3+} the core electronic structure comprises completely filled shells. In such cases, no electronic absorption spectra at >200 nm is expected because the corresponding process of promoting an electron out of a filled shell requires much higher energies.^{170]}

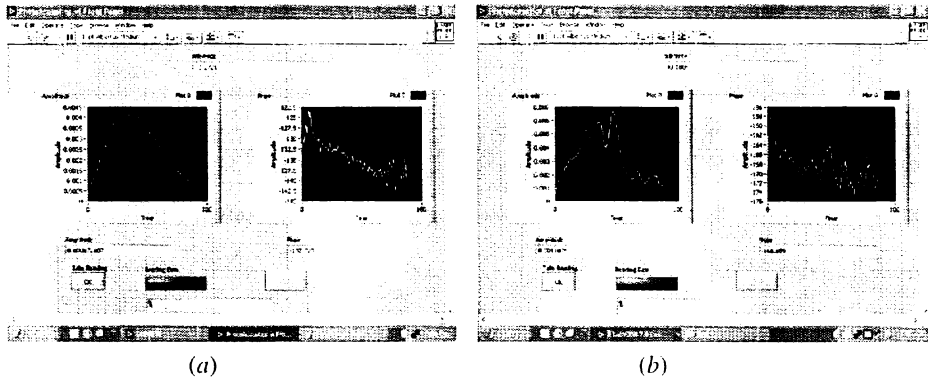


Figure 3.15: Photoacoustic (PA) spectrum of (a) carbon black and (b) $Nd_2Ti_2O_7$, obtained in the computer.

The absorption transitions of the Nd^{3+} samples arise from the conversion processes and the corresponding peaks are assigned in Figure 3.16a. Pr^{3+} has absorption transitions arising from the 3H_4 to 3P_2 (454 nm), 3P_1 (477nm), 3P_0 (491nm) and 1D_2 (601 nm) shifts.^[71] Most of these characteristic peaks are observed in the present PA spectrum which is denoted in Figure 3.16. The energy level transitions for the RE in the visible region, which are obtained from the Dieke diagram,^[50, 51] are also given alongside. La^{3+} , Gd^{3+} and Y^{3+} do not have absorption peaks in the visible region and hence, their energy level diagrams are not shown. The minor peaks in these samples may be arising from noises and the TiO_6 octahedra.

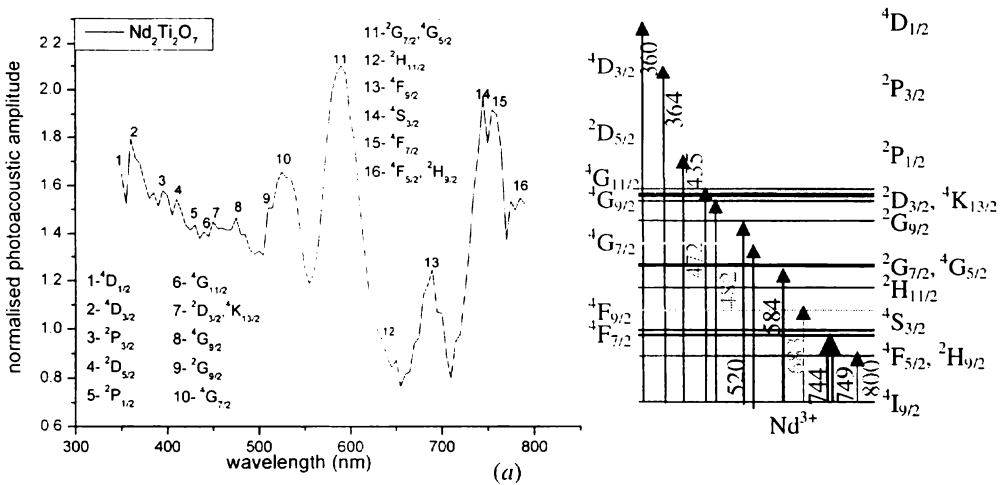


Figure 3.16a: Photoacoustic (PA) spectrum of $Nd_2Ti_2O_7$ along with the energy level diagram and absorption transitions in Nd^{3+} .

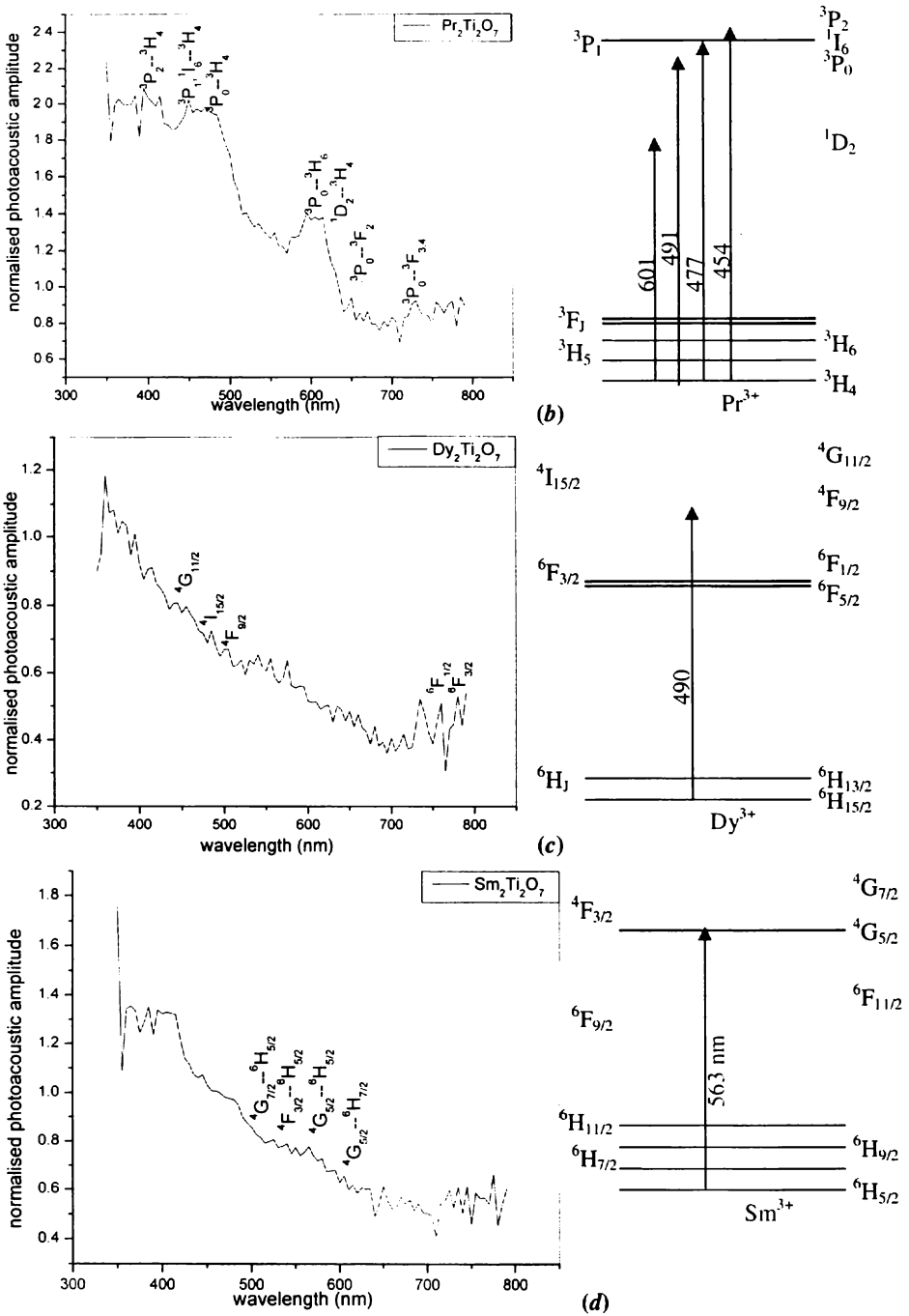


Figure 3.16: Photoacoustic (PA) spectrum of (b) $Pr_2Ti_2O_7$, (c) $Dy_2Ti_2O_7$ and (d) $Sm_2Ti_2O_7$ along with the energy level diagrams and the main absorption transitions.

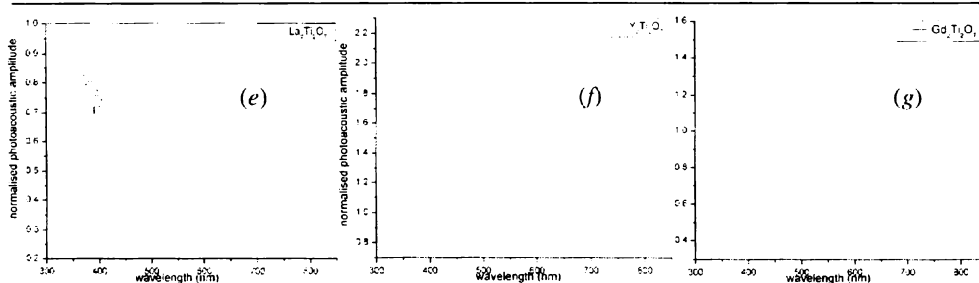


Figure 3.16: Photoacoustic (PA) spectrum of (e) $\text{La}_2\text{Ti}_2\text{O}_7$, (f) $\text{Y}_2\text{Ti}_2\text{O}_7$ and (g) $\text{Gd}_2\text{Ti}_2\text{O}_7$.

B3. Conclusions:

Since, the direct measurement of absorption spectra of the opaque samples is not possible, approximate absorption behaviour of the samples can be obtained from their reflectance spectra. However, their PAS gives directly, an excellent absorption characterization of opaque materials. Thus the present study gives the absorption performance of the RETs prepared by SHS method.

3.4.3. Part C: Frequency up-conversion studies on lanthanum titanate:

Intensive research has recently been devoted to the conversion of the NIR radiation into visible light exploiting frequency up-conversion in RE doped solid state materials^[72, 73] for a variety of applications including optical data storage,^[74] lasers,^[75] tri-dimensional colour displays,^[76] remote optical temperature sensors,^[77, 78] biomedical diagnostics,^[79] and under-sea optical communications amongst many. The frequency up-conversion process is a nonlinear non-parametric mechanism in which photons are generated with energy higher than the excitation photons. This is in general accomplished by sequential or multi-photon stepwise excitation, successive and /or cooperative energy transfer between pairs or triads of RE ions in solids, and subsequent radiative de-population of the excited levels with the emission of photons with energy higher than that of the excitation photons.^[72, 73] In these up-conversion excitation mechanisms, one can have either the creation or annihilation of optical phonons in order to compensate for energy mismatches between the excitation photon and/or energy transfer processes, and the pertinent energy levels of the activated RE ion.^[51, 72, 73, 80, 81]

Frequency up-conversion of IR radiation into visible light was first reported by Bloembergen (1959) as a noiseless technique for IR detection.^[82] There exist numerous schemes for the realisation of up-conversion excitation of RE ions implanted into different materials. In addition to the classical sequential or multi-photon absorption

(resonant or phonon- assisted), in which excited state absorption (ESA) takes place, there exists the very efficient sequential energy-transfer, which is distinguished from the process named cooperative up-conversion involving either two RE ions or a pair of ions and a third one.^[80] There is also the photon avalanche effect which involves down-conversion sequential energy (cross-relaxation), and the up-conversion step itself is due to excited state absorption.^[83] In the process of up-conversion, the excited ions play a role of energy acceptors.^[49]

The present work is based on the up-conversion study on $\text{La}_2\text{Ti}_2\text{O}_7$. Among the RETs prepared by SHS method, only $\text{La}_2\text{Ti}_2\text{O}_7$ showed luminescence in the visible region and so the current study is conducted for $\text{La}_2\text{Ti}_2\text{O}_7$. Moreover, changes in the visible region are observed in the case of $\text{La}_2\text{Ti}_2\text{O}_7$.

C1. Experimental setup:

Figure 3.17 shows the experimental arrangement for recording the up-conversion emission from $\text{La}_2\text{Ti}_2\text{O}_7$. The samples were excited at 300 mW using a 180 fs Ti: sapphire (Spectra Physics, *Tsunami*®) laser at 800 nm. The up-conversion emission from the sample was collected using an optical fiber and was fed to the CCD-monochromator assembly (Spectrapro 500i Acton Research, Roper Scientific NTE/CCD 1340/100-EM) to record the spectrum.

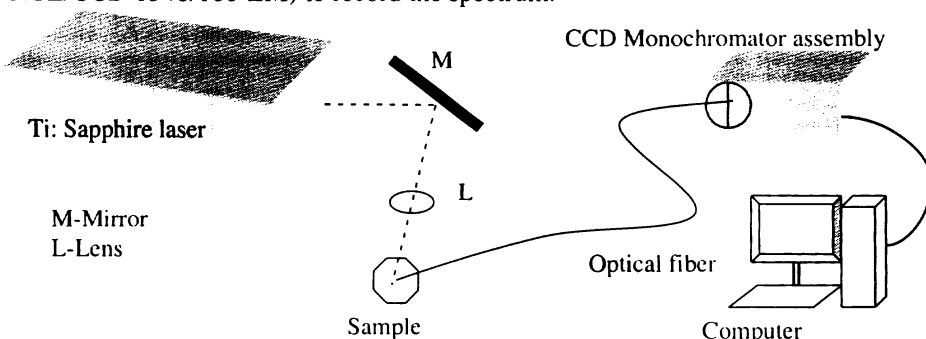


Figure 3.17: Schematic representation of the experimental arrangement for frequency up-conversion studies.

C2. Results and discussions:

In the sequential or multi-step up-conversion excitation process which is considered as a one ion process, with the referred ion interacting with external electrical fields, a first pump photon populates an intermediate state and a second pump photon excites the ion to an upper excited state level via excited state absorption. If the absorption is non-resonant, optical phonons can be either absorbed or emitted in order to

compensate for the energy mismatch between the pump photon energy and the pertinent transition energy. For sufficiently intense pump sources as in the present case, the first absorption step may take place through a nonlinear multi-photon absorption. From the upper excited state, the excited ion relaxes either radiatively to generate up-conversion emission signals or non-radiatively through a multi-phonon relaxation process^[81] and a lower lying excited state is populated.^[2]

When the active ions are located at a sufficiently short distance from one another, interaction between them may occur, and new types of up-conversion processes take place, where two or even more ions can contribute to one absorption or emission process. Energy transfer mechanism is the most important among them in which an excited ion, usually called a donor or sensitiser, transfers its excitation energy to a neighbour, which is called the acceptor or activator. There exists also the possibility of two interacting ions combine together either to absorb or to emit one photon.^[2]

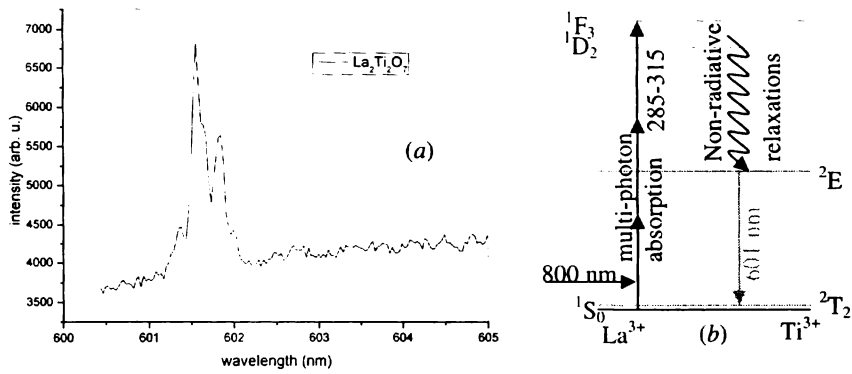


Figure 3.18: (a) Frequency up-conversion emission from $\text{La}_2\text{Ti}_2\text{O}_7$. (b) Schematic representation of multi-photon absorption and frequency up-conversion emission.

The Figure 3.18 shows the up-conversion emission from $\text{La}_2\text{Ti}_2\text{O}_7$. Here, the SE channel of Ti^{3+} ions^[49] due to the transition $^2E \rightarrow ^2T_2$ can be the reason for the up-conversion emission. The multi-photon absorption by the La^{3+} ions followed by the energy transfer mechanism may populate the upper excited state of Ti^{3+} ions. This in turn results in the emission near 601 nm.

C3. Conclusions:

The NIR excited frequency up-conversion emission spectrum of $\text{La}_2\text{Ti}_2\text{O}_7$ is explained by the SE channel of Ti^{3+} ions. The light emission properties of this novel RET prepared by SHS method is to be investigated further for the potential applications in photonic devices.

3.5. Section II- Photothermal studies of rare earth titanates:

The present section includes the PT characterization of the RETs prepared by the SHS method. Though PAS is also a class of PT phenomena, the complementary nature of PAS to fluorescence spectroscopy^[84, 85] prompted us to present in the previous section. The estimation of the TD values of the RETs is made using photothermal deflection (PTD) and the result is used to interpret the possible fractal nature of the samples.

3.5.1. Part A: Thermal characterization using photothermal deflection:

PTD was proved to be an effective method for finding the TDs of ceramic materials. Neither the finite duration of the laser pulse nor optical transmission through the sample obviously affects PTD.^[86] In PTD, the absorption of the exciting optical beam (pump beam) causes a corresponding change in the refractive index of the optically heated region. The absorption also causes an index-of-refraction gradient in a thin layer adjacent to the sample surface. By probing the gradient of the varying index of refraction with a probe beam, one can relate its deflection to the optical absorption of the sample. *Figure 3.19* shows a schematic diagram of the passage of a probe-beam through a refractive index profile. One can use two methods for PTD^[87]

- (i) **Collinear PTD**, where the gradient of the refractive index is both created and probed within the sample.
- (ii) **Transverse PTD**, where the probing of the refractive index gradient is accomplished in the thin layer adjacent to the sample- an approach most suited for opaque samples and for materials of poor optical quality.

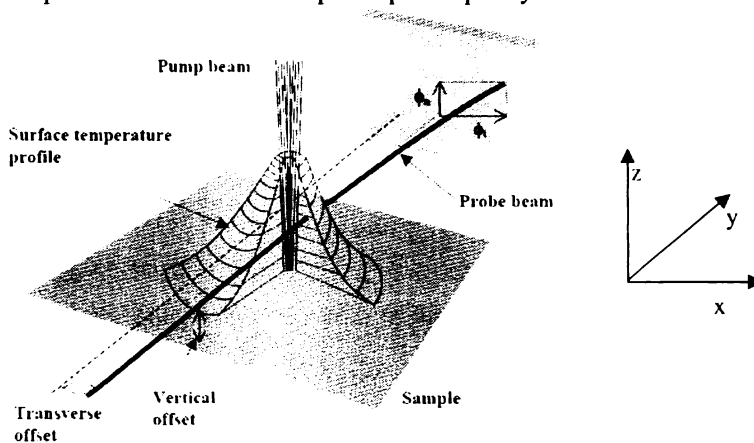


Figure 3.19: A schematic diagram of the passage of a probe-beam through a refractive index profile and the resulting normal and transverse components of the photothermal deflection (PTD) signal.

PTD has high sensitivity and versatility^[87] for measuring in situ small absorptions in thin films, solids, liquids and gases.^[88-90] Its potential for imaging and scanning microscopy has been demonstrated.^[91] PTD provides simple, direct, non-destructive measurement of TD with neither contact with the sample nor thermometry.^[92, 93] Moreover, only one surface of the sample needs to be accessible and the measurement is inherently local so that the measurement of non-uniform or small samples can be made. Also, the diffusivity can be measured in different orientations on anisotropic materials simply by rotating the probe beam direction.^[89, 92, 93] In addition, the mirage effect or PTD allow measurements of the TD of the materials in global scales.^[94]

D1. Theory:

The beam parameters of a Gaussian beam propagating through an inhomogeneous medium can be deduced from the analysis of Casperson.^[95] From Fermat's principle, the propagation of light beam through a spatially varying refractive index is governed

by the equation^[96, 97]

$$\frac{d}{ds} \left(n_0 \frac{d\delta}{ds} \right) = \nabla_{\perp} n(r, t) \tag{3.1}$$

where n_0 is the uniform (unperturbed) refractive index of the medium,

δ is the perpendicular displacement of the beam from its original direction.

$\nabla_{\perp} n(r, t)$ is the gradient of the refractive index perpendicular to the beam path.

The above expression is justified because any variations of n along s will not deflect the beam. The refractive index $n(r, t)$ is related to the unperturbed refractive index

n_0 by

$$n(r, t) = n_0 + \left. \frac{\partial n}{\partial T} \right|_{T_A} T(r, t) \tag{3.2}$$

where T_A stands for the ambient temperature.

Thus (3.1) is rewritten using (3.2) as,

$$\frac{d\delta}{ds} = \frac{1}{n_0} \frac{\partial n}{\partial T} \int_{\text{path}} \nabla_{\perp} T(r, t) ds \tag{3.3}$$

where the integration is carried out over the path of the probe beam. For small deflections, the angular deviation ϕ from the ray path s , is given by

$$\frac{d\delta}{ds} \equiv \phi = \frac{1}{n_0} \frac{\partial n}{\partial T} \int_{\text{path}} \nabla_{\perp} T(r, t) ds \tag{3.4}$$

For the refractive index gradient set up at a sample surface by a modulated Gaussian

profile heating (pump) laser beam, the deflection angle in the x-direction is

$$\phi(x, y, t) = \frac{1}{n_0} \frac{\partial n}{\partial T} \int_{\rho_{\text{psh}}} \frac{\partial T(x, y, t)}{\partial x} ds \quad (3.5)$$

Again, considering the cases of transverse PTD (the probe beam propagating in the y-direction) and collinear PTD (the probe beam propagating in the z-direction), both have a deflection of the probe beam in the x-direction. Hence the transverse and collinear PTD's probe beam deflections, considering the probe beam as infinitesimally small, respectively are

$$\phi_t(x, t) = \frac{1}{n_0} \frac{\partial n}{\partial T} \int \frac{\partial T(x, y, t)}{\partial x} dy \quad (3.6)$$

$$\phi_L(x, y, t) = \frac{1}{n_0} \frac{\partial n}{\partial T} \int \frac{\partial T(x, y, t)}{\partial x} dz \quad (3.7)$$

Again, the transverse PTD can be resolved into two.^[98]

1. Normal deflection, parallel to z, $\phi_n = \frac{1}{n_0} \frac{dn}{dT} \int_{-\infty}^{+\infty} \frac{\partial T}{\partial z} dy$ (3.8)

2. Transverse deflection, parallel to x, $\phi_r = \frac{1}{n_0} \frac{dn}{dT} \int_{-\infty}^{+\infty} \sin \alpha \frac{\partial T}{\partial r} dy$ (3.9)

The point to be noted that ϕ_n is related to the heat diffusion processes perpendicular to the surface, whereas ϕ_r describes the heat diffusion processes parallel to the sample surface. These two measurements are particularly useful for non-destructive investigation^[99] and for TD measurements.^[92]

The heat diffusion equation treatment of Salzar et al.,^[100] has arrived at a linear relationship between the phase of the PTD signal and pump-probe offset with various experimental and theoretical conditions. The slope of the plot connecting the phase of the PTD signal and the pump-probe offset is given by

$$m = \frac{1}{\mu_s} = \sqrt{\frac{\pi f}{\alpha_s}} \quad (3.10)$$

where α_s is the TD of the sample under investigation, f is the chopping frequency and μ_s is the thermal diffusion length of the sample.

Sánchez-Lavega (1997) et al. have defined two lengths L and L_{th} , assumed to be characteristic of the heterogeneous nature of the material, and of the spatial range of

the thermal disturbance, respectively. For a granular ceramic, L might be the typical size of the grains or the mean of the distribution of the sizes when this distribution is broad. The thermal diffusion length μ is related to the natural scale length L_{th} , by

$$L_{th} \approx 2\pi\mu \quad (3.11)$$

When the scale length L_{th} of the thermal disturbance is large, compared to the scale length L of the material, the thermal disturbance does not notice the heterogeneity of the material. Diffusivity measurements then yield a 'global effective diffusivity' of the material.^[94, 101] Under these conditions the relation (3.10) holds for the linear dependence of the phase of the transverse component of the PTD on the pump-probe separation.^[94]

D2. Experimental:

The *Figure 3.20* shows the schematic representation of the PTD experimental setup. The pump beam used was 488 nm optical radiation from an Argon ion laser with a Gaussian profile of diameter 1.2 mm, set at a power 25mW (cw, Liconix 5300) with a stability of $\pm 0.5\%$. It was intensity modulated at 10 Hz using a mechanical chopper (Stanford Research Systems SR 540) and focussed using a convex lens (Melles Griot) of focal length 10 cm, before it reached the sample. The probe beam was 633 nm output from a He-Ne laser (4mW, cw, Uniphase). It was focussed using another convex lens of focal length 5 cm (Melles Griot). The probe beam was arranged such that it just skimmed along the sample surface, and it propagated along the y-direction, which was orthogonal to the direction of propagation of the pump axis (z-axis). All the samples under investigation were opaque at the incident wavelength and the sample was placed at the bottom of a quartz cuvette having dimensions 1x 1x 4 cm containing CCl_4 . In most of the PT experiments, CCl_4 is chosen as a coupling medium due to its low thermal conductivity, specific heat capacity and TD. Additionally, CCl_4 has high rate of change of refractive index with temperature.^[102-104] Moreover, it offers the highest gain in signal amplitude by a factor of 1000 with respect to air.^[105] A position sensitive quadrant detector was used to measure the probe beam deflection. The output of the quadrant detector was given to an I to V converter and the output voltage was given to a dual phase lock-in amplifier (Stanford Research Systems SR 830). The use of a differential position sensor like quadrant cell allows elimination of the probe laser intensity fluctuations.^[98] The entire setup was placed on a vibration isolated table to protect the system from ambient vibrations. In the present arrangement, the distance between the probe and the sample surface was kept as small as possible so as to get a

non-diffracted beam at the detector. The lock-in amplifier was interfaced to a computer through LabVIEW software.

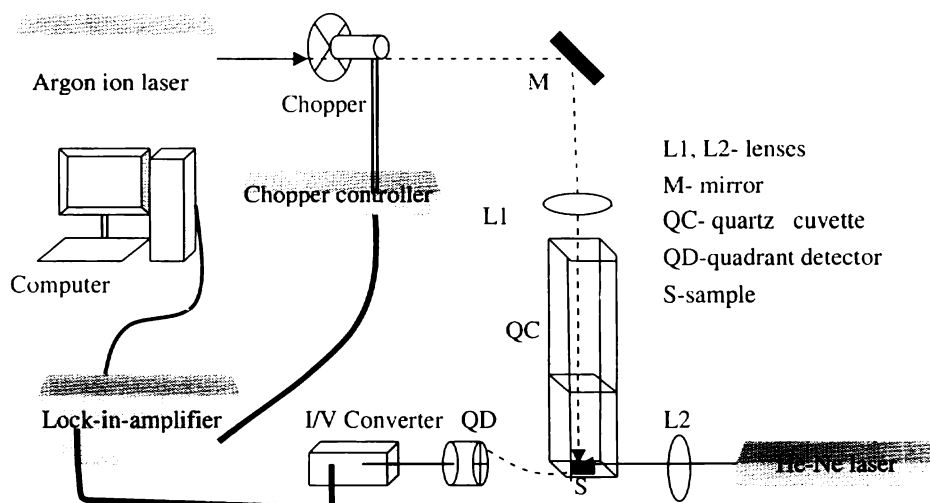


Figure 3.20: Schematic diagram of dual-beam photothermal deflection (PTD) set-up.

D3. Results and discussions:

The approximate TD of the samples is obtained (Table 3.2) using the above expression (3.10) as used by various authors.^[94, 104, 106-108] The PTD signal phase variation as a function of the pump-probe offset for the samples is given in Figure 3.21. The TD values are evaluated from the slope of these plots and are given along with the plots. The discrepancies in the plots can be attributed to the non-homogeneous nature of the samples. However, the above relation is applied to obtain the approximate TD values which are very close to those obtained by the PA studies conducted earlier.^[40] The TD values of some RE doped single crystals^[106, 109] and pyrochlores^[110] were similar to the RETs presented here. $\text{Sm}_2\text{Ti}_2\text{O}_7$ has found to have a higher TD than other RETs. This may be because of the variation in the pyrochlore structure.^[110] The RETs change their structure from monoclinic to cubic with the change in the ionic radius of the R^{3+} .^[12, 14-18] Factors like particle size,^[111, 112] hardness^[113] etc. may also be affecting the TD values.

Table 3.2: The effective thermal diffusivity (TD) values of the rare earth titanates (RETs) obtained using photothermal deflection (PTD) study.

RET (R=)	TD $\times 10^{-4} \text{ m}^2\text{s}^{-1}$
Dy	0.006
La	0.012
Sm	0.041
Y	0.005
Gd	0.009
Nd	0.018
Pr	0.011

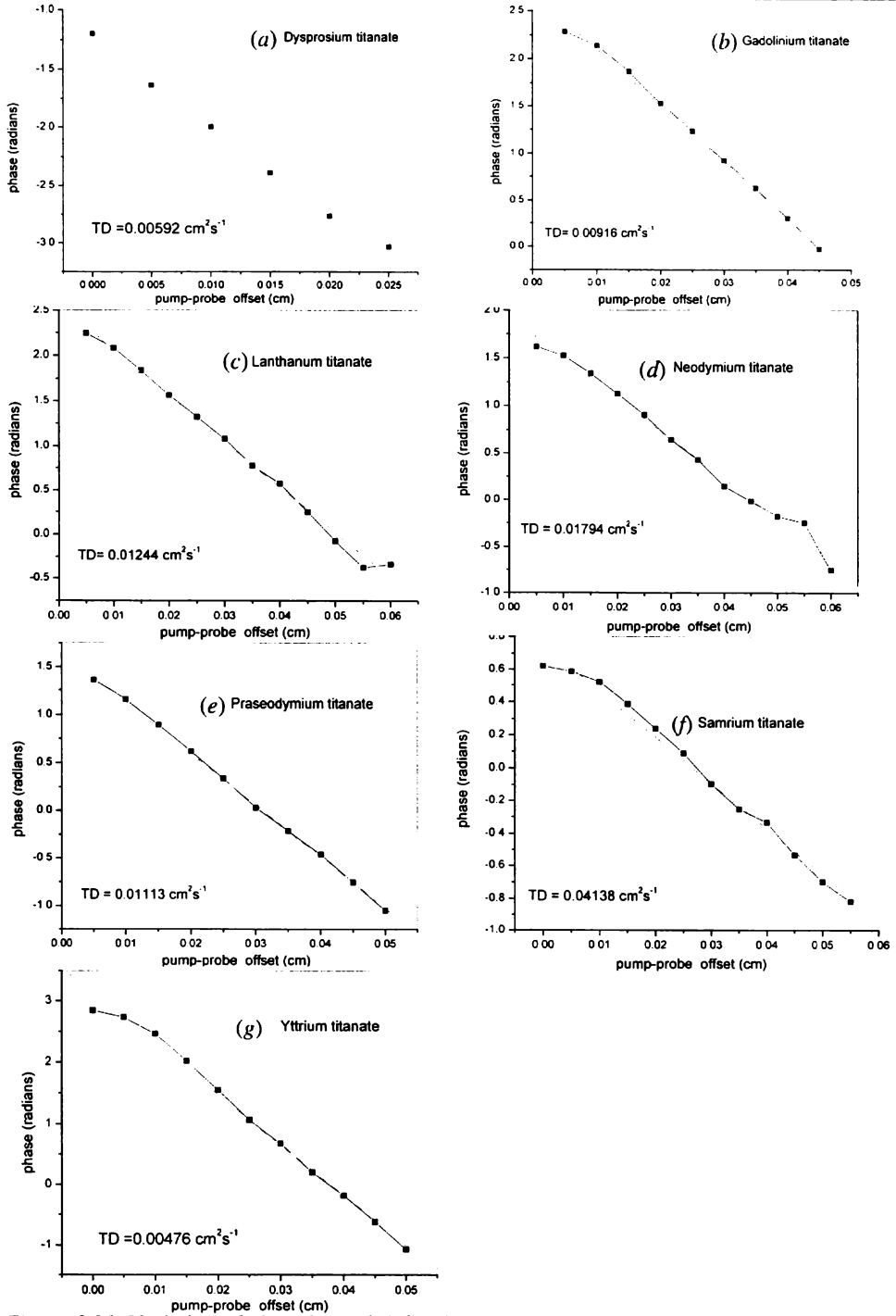


Figure 3.21: Variation of photothermal deflection signal phase with pump-probe offset for (a) Dy₂Ti₂O₇, (b) Gd₂Ti₂O₇, (c) La₂Ti₂O₇, (d) Nd₂Ti₂O₇, (e) Pr₂Ti₂O₇, (f) Sm₂Ti₂O₇ and (g) Y₂Ti₂O₇.

The TD measurement gives an indirect way to investigate the structural aspects of the RET ceramics. The local measurement of thermo-physical parameters of the ceramics using PT techniques are an effective tool to measure some of the inherent properties of ceramics, which are hard to measure using conventional methods. A recent investigation shows the effectiveness of non-destructive PT technique for profiling the hardness of the material, which has tremendous applications in the industrial area, especially in device fabrication.^[113] The thermal properties of ceramics are basically determined by the composition, the structure and arrangement of the phases.^[94] In the present study the material is regarded as ‘thermally homogeneous’ with a TD given by the ‘global’ values.^[101]

The heat diffusion, like other diffusion processes is related to the mean square displacement of the diffusers. Due to phonon-phonon or phonon-electron collisions the heat diffusers (phonons or electrons) exhibit a random walk and the diffusion coefficient is constant. If the diffusing medium is not homogeneous but random, the diffusion coefficient is then no more a constant.^[114] A similar situation may be assumed in the present case also, which can be explained by the fractal approach.

It is known that the propagation of phonons and hence the TD value are greatly influenced by the structural variations arising due to variation in sintering temperature, preparation procedure etc.^[104] From the *Table 3.1*, it is clear that the samples have a non-uniform change in the particle size and surface area. Random media transport properties exhibit special behaviours.^[115] This may be the reason for the non-uniformity in the TD values. It is also considered that these TD values are only an approximation to check the fractal nature of these RETs.

D4. Conclusions:

The PTD characterization of the RET samples gave a rough estimation of the TD values. Appropriately managed use of modulated PT method is well suited to measure the effective TD at global scales.^[94] Their low TD values indicate the possibility of using them as thermal barrier coatings.

3.5.2. Part B: Photoacoustic thermal characterization – Fractal approach:

Since the rediscovery of the PA in the seventies it has been commonly assumed that this experimental technique is a valuable tool for the investigation of the samples.^[116,117] It has been shown earlier, that thermal diffusion in assemblies of

spheres can be treated similar to diffusion in percolation system.^[118, 119] In disordered systems the diffusion coefficient becomes time or frequency dependent.^[120] The macroscopic self-similar objects have been considered in the framework of fractal theory developed by Mandelbrot.^[121] Fournier and Boccara made an approach to understand the thermal behaviour of rough surfaces and heterogeneous samples using this theory.^[98] These problems are of great interest both from a fundamental point of view (physics of disordered systems) and for practical applications to characterise materials of high technological interest (ceramics, sintered materials). Fournier and Boccara had studied the heat diffusion temporal behaviour, using fractal structures.^[114] Aleksic et al. have used the fractal structure approach for analysing the PA amplitude spectrum of NTC* layers.^[122]

E1. Theoretical background:

Korpiun and Osiander has obtained the frequency dependence of TD as

$$\alpha \propto (i\omega)^{-d_w} \quad (3.12)$$

with $d_w = \frac{d_s}{d_f}$ where d_s is the spectral dimension^[119] and d_f is the fractal dimension.

The introduction of the dimension of random walk d_w , in the case of a percolating network, is to account for the peculiar diffusion process.^[114] When the sample has an anomalous diffusion, the diffusion coefficient is time dependent. One can solve the problem analytically, if one assumes that the sample has a fractal structure.^[118, 119, 123] The amplitude of the temperature oscillation at the sample to gas boundary becomes

$$\Theta(\omega) \propto (i\omega)^{-\frac{\{2+d_w(2-d_f)\}}{2}} \quad (3.13)$$

The amplitude of the pressure variation in the gas depends on frequency as^[124]

$$p_0 \propto (i\omega)^{-\frac{\{3+d_w(2-d_f)\}}{2}} \quad (3.14)$$

The amplitude of the microphone output is proportional to this pressure variation.

E2. Experimental setup:

The schematic representation of the experimental set up (*Figure 3.22*) is similar to that given in *Figure 2.3*. Optical radiation from an Argon ion laser at 488 nm, with a power output of 25 mW (cw, Liconix 5300) and a stability of $\pm 0.5\%$ was used as the source of excitation. It was intensity modulated using a mechanical chopper (HMS

* Negative temperature coefficient

Light Beam Chopper 230) before it reached the sample. Detection of the PA signal was made using a sensitive electret microphone (Knowles BT 1834). The amplitude of the PA signal was measured by means of a dual phase lock-in-amplifier (Stanford Research Systems SR 830). The lock-in-amplifier was interfaced to a computer using LabVIEW. The reflection mode geometry of the open cell PA technique was used in this experiment (*Figure 2.4*).

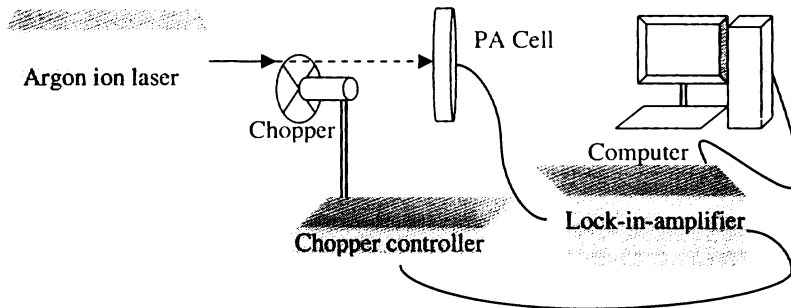


Figure 3.22: Schematic representation of photoacoustic (PA) experimental setup.

E3. Results and discussions:

The PA amplitude spectra of the samples are given in *Figure 3.23*. The theoretical fitting on these plots are done. The fitting parameters are compared with (3.14). The TD values obtained using the PTD studies, are employed in (3.12). Making use of these two relations, the fractal dimension of the RETs can be evaluated.

The calculated fractal dimensions of the samples are given along with the plots. From these values, it is obvious that all the samples prepared by SHS method have the same fractal dimension. PA spectra may behave differently for sintered materials. Random sample structure has an influence on the transport of heat. The fractal concept has been used to characterise random structures by a non-integer mass scaling exponent, the fractal dimension.^[119] The diffusion processes are strongly affected in random structures, which can be described by the time dependent diffusion constant.^[125] It was reported that for large grains of micrometer size, there are only a few direct contacts, and the system appears to be percolative. For small grains, there are also contacts between the spheres across the pores, as now the thermal resistance of the small gas filled pores becomes smaller and the distribution of thermal resistance increases. As the spectral dimension increases, the power of the frequency dependence of the magnitude comes closer to -1, as observed for the samples with small grains. A similar behaviour is observed in the present study since the samples have small particle sizes as evident from the *Table 3.1*. The amplitude of the microphone output, used as the

PA detector depends on the fractal dimension^[122] by the relation (3.14). Thus PA amplitude diagram is suitable for checking the validity of the fractal concept regarding the RET samples.

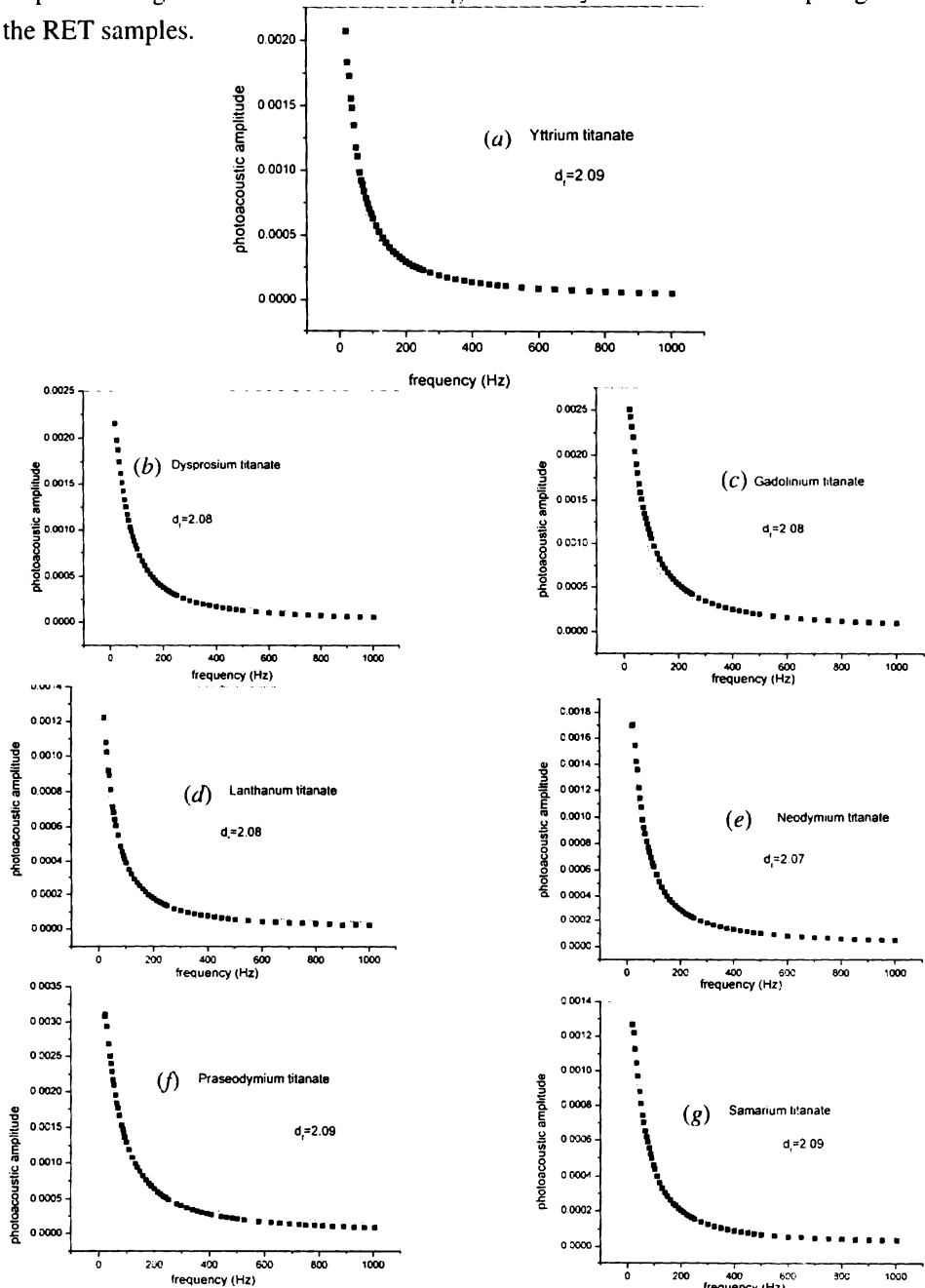


Figure 3.23: Photoacoustic (PA) amplitude plots for (a) $Y_2Ti_2O_7$, (b) $Dy_2Ti_2O_7$, (c) $Gd_2Ti_2O_7$, (d) $La_2Ti_2O_7$, (e) $Nd_2Ti_2O_7$, (f) $Pr_2Ti_2O_7$ and (g) $Sm_2Ti_2O_7$.

E4. Conclusions:

An attempt is made to explain the possibility of fractal nature of RETs using PTD and PA. The PA amplitude spectrum shows frequency dependence near to -1 which is a natural behaviour of samples with small grains.

3.5.3. Part C: Thermal effusivity measurement using photoacoustics:

Thermal effusivity (TE) is the ability of the sample to exchange heat with the environment and hence it is an important parameter for surface heating and cooling processes. TE, also known as 'contact coefficient',^[126] measures the thermal impedance of the material. In the present section an effort is done to establish a rough calculation on TE of the RETs using PA.

F1. Theory:

The TE is defined as $e_s = \frac{k_s}{\sqrt{\alpha_s}} = \sqrt{k_s \rho C}$ (3.15)

The PA method was successfully used for the simultaneous measurement of thermal conductivity and heat capacity.^[127] When the sample is kept in contact with a thermally thin absorbing layer, the acoustic pressure in the microphone chamber is given by the relation

$$\delta Q_1 = \frac{\gamma P_0 I_0 (\alpha_g \alpha_s)^{1/2} e^{j(\omega t - \frac{\pi}{2})}}{2\pi T_0 l_g k_s f} \quad (3.16)$$

where γ is the ratio of specific heat capacities of air, P_0 and T_0 respectively are the ambient pressure and temperature, I_0 is the radiation intensity, and l_i , k_i & α_i are length, thermal conductivity & TD of the medium. Here $i = g, 0, s$ refers to gas inside the chamber, the ambient and the solid sample. $\omega = 2\pi f$ where f is the modulation frequency. l_g is the length of the gas column inside the cavity. The acoustic signal varies as $1/f$ and is proportional to the ratio $\sqrt{\alpha_s}/k_s$, the inverse of the TE of the sample. In the absence of the sample (i.e. only the absorbing layer is present) the pressure fluctuation inside the cavity is given by

$$\delta Q_2 = \frac{\gamma P_0 I_0 (\alpha_g)^{1/2} \alpha_o e^{j(\omega t - \frac{3\pi}{4})}}{(2\pi)^3 T_0 l_g l_o k_o f^{3/2}} \quad (3.17)$$

The PA signal varies as $f^{-3/2}$ and depends on the ratio α_o/k_o of the absorbing layer.

$$\text{Now, } \frac{\delta Q_1}{\delta Q_2} \propto \frac{l_o k_o \sqrt{\alpha_s}}{\alpha_o k_s} f^{1/2} \quad (3.18)$$

This facilitates the normalisation of the instrumental factor. The TE of the sample can be evaluated by measuring the signal amplitude as a function of the modulation frequency from the absorbing layer– sample composite and that from the absorbing layer alone; provided the thickness (l_o), density and specific heat capacity of the thin absorbing layer are known.^[128]

F2. Experimental setup:

The experimental setup is same as in *Figure 3.22*. The measurements were done as given in **E2**. with the following modifications. The entire experiment was carried out at a power of 50 mW. An aluminium foil of 10 μm thickness was used as absorbing layer, which was commercially available. The samples were pasted on this thermally thin foil using a thermal paste. The sample-aluminium foil combination is mounted on the PA cell using vacuum grease at the edges so that the free surface of the sample faces the ambient. Irradiation is made through the front glass window and thermal waves are generated from the aluminium–gas interface. The front surface illumination or the reflection mode (*Figure 2.4*) geometry was used for TE studies.

F3. Results and discussions:

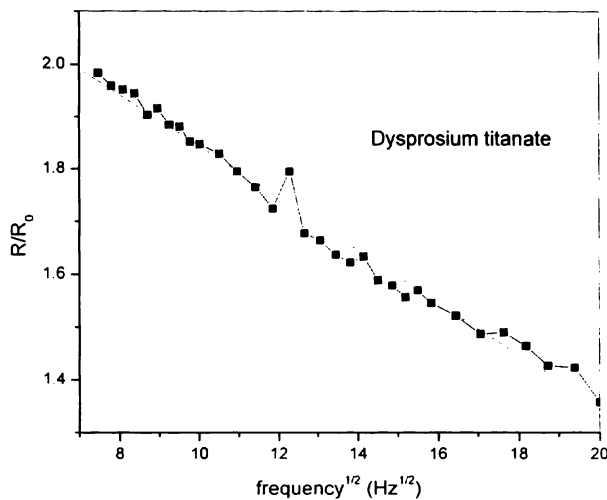


Figure 3.24: Variation of the ratio of photoacoustic (PA) amplitude as a function of modulation frequency for dysprosium titanate.

A typical plot of the variation of the ratio of PA amplitude as a function of modulation frequency is given in *Figure 3.24*. All other samples show similar characteristics. The TE and thermal conductivity values of the samples are tabulated in *Table 3.3*. The effective thermal conductivity values the RETs obtained from these studies is very close to those of ceramics.^[129] For non-homogeneous materials like composites, all the thermal properties are discontinuous functions. Hence, the concept of effective properties appears to be useful.^[130]

Table 3.3: The thermal parameters of the rare earth titanates (RETs) obtained using photoacoustic (PA) method.

$R_2Ti_2O_7$ (R =)	Density ($\times 10^3 \text{kgm}^{-3}$)	Effusivity ($\text{Ws}^{-1/2}\text{m}^{-2}\text{K}^{-1}$)	Conductivity ($\text{Wm}^{-1}\text{K}^{-1}$)	Sp. heat capacity ($\text{Jkg}^{-1}\text{K}^{-1}$)
Y	4.98	487 \pm 1	0.34	140 \pm 1
La	5.78	330 \pm 1	0.37	51 \pm 1
Pr	5.95	581 \pm 1	0.61	93 \pm 1
Nd	6.11	578 \pm 1	0.77	71 \pm 1
Sm	6.31	689 \pm 1	1.40	54 \pm 1
Gd	6.56	507 \pm 1	0.49	80 \pm 1
Dy	6.86	500 \pm 1	0.38	96 \pm 1

F4. Conclusions:

PA method provides an easy method to measure the TE of the RETs and thus gives information about the thermal properties of these samples. The TD and TE values, obtained using PTD and PA studies respectively, are used to calculate the thermal conductivity of the samples which are found to be very close to that of the ceramics.

3.6. Summary:

The LIF studies on RETs revealed the possibility of new fluorophores prepared by SHS method. SHS method provides the production of good quality RETs of nanometre sizes. The fluorescence emission enhancement of Ti^{3+} ions near 610 nm in the presence of La^{3+} ions in the $La_2Ti_2O_7$ opens the door for the development of novel fluorescent materials. The presence of the unfilled 4f orbitals in La^{3+} is supposed to be the reason for the PL. The opacity of the samples has made PAS a better option to study the absorption behaviour of these RETs. The widespread interest in novel lanthanide doped optical materials as IR to visible up-converters is due to the fact that they can find applications in solid state three dimensional colour displays. blue-green

laser media utilised for writing and reading in high density optical data storage, high resolution printing, biomedical diagnostics, biological fluorescence labelling, remote thermometry, nano-sized temperature sensors, and under-sea optical communications. The wide variety of potential applications led to a renaissance in the study of the luminescence properties of RE doped materials. Envisioning that objective, novel host materials for lanthanide ions implantation is demanded in order to produce high IR to visible up-conversion efficiencies and allow suitable combinations of RE luminescence centers which can diversify the visible emission wavelengths as seen in $\text{La}_2\text{Ti}_2\text{O}_7$. PTD measurements of RETs give a notion about the effective TD values of RETs prepared by SHS process. These values are used to furnish the probable fractal nature of these RETs. The TE values obtained by PA method are useful in obtaining the thermal conductivity and specific heat capacity of the RETs prepared by SHS method. The thermal conductivity values thus obtained are found to be in agreement with those of the ceramics.

3.7. References:

- [1] J. C. Krupa (2006). 'Optical excitation of f- electrons in lanthanide and actinide solid compounds'; in: "Recent developments in spectroscopy of lanthanides and actinides". B. N. Jagatap and A. Venugopalan (Eds.), R V Enterprises, Mumbai, p 41-53. 235pp.
- [2] Artur da Silva Gouveia-Neto (2007). 'Light emission properties of lanthanide doped novel optical glasses for application in photonic devices'; in: "New research on optical materials". p 185-216. Sherman J. Litchitika (Ed.). Nova Science Publishers, Inc. New York. 255pp.
- [3] M. Morita, S. Buddhudu, D. Rau and S. Murakami (2004). 'Photoluminescence and excitation energy transfer of rare earth ions in nanoporous xerogel and sol-gel SiO_2 glasses'; in: "Optical spectra and chemical bonding in transition metal complexes". Springer, Berlin. *Struct. Bond.*; **107**, p 115- 143. doi:10.1007/b83927
- [4] S. Buddhudu, M. Morita, S. Murakami and D. Rau (1999). 'Temperature dependent luminescence and energy transfer in europium and rare earth codoped nano-structured xerogel and sol-gel silica glasses'. *J. Lumin.*; **83-84**, p199- 203. doi:10.1016/S0022-2313(99)00098-8
- [5] M. Morita, D. Rau, S. Kajiyama, T. Sakurai, M. Baba and M. Iwamura (2004). 'Luminescence properties of nano-phosphors: metal-ion doped sol-gel silica glasses'. *Materials Science- Poland*; **22** (1), p 5- 15.
URL: http://www.materialsscience.pwr.wroc.pl/bi/vol22no1/articles/ms_2003_998.pdf
- [6] Yuhong Zhang, Huaxing Zhang, Yongxi Xu and Yanguang Wang (2003). 'Europium doped nanocrystalline titanium dioxide: preparation, phase transformation and photocatalytic properties'. *J. Mater. Chem.*; **13** (9), p 2261- 2265. doi: 10.1039/b305538h
- [7] Zili Xu, Qiuqing Yang, Chao Xie, Weijun Yan, Yaoguo Du, Zhongmin Gao and Jiahua Zhang (2005). 'Structure, luminescence properties and photocatalytic activity of europium doped TiO_2 nanoparticles'. *J. Mater. Sci.*; **40** (6), p 1539- 541. doi:10.1007/s10853-005-0599-6
- [8] Jong- Ho Park, Min-Gi Kwak, Chung Sik Kim, Dae-Hwang Yoo, Ho-Soon Yang, Byung Kee Moon, Byung-Chun Choi, Hyo Jin Seo, E. D. Jeong and K. S. Hong (2006). 'Synthesis and Spectral Properties of Rare-Earth Ions-Doped Nano-Sized Y_2O_3 Phosphors'. *J. Korean Phys. Soc. (JKPS)*; **48** (6), p 1369- 1373.

- URL:http://www.kps.or.kr/home/kor/journal/library/abstract_view.asp?articleid={DE7F7959-BE7D-4801-8405-ABF452FA3C2F}
- [9] Jong- Ho Park, Nam Gwon Back, Kyong- Soo Hong, Chung-Sik Kim, Dae-Hwang Yoo, Min Gee Kwak, Jeong-In Han, Jei-Hong Sung, Byung Kee Moon, Hyo-Jin Seo and Byung-Chun Choi (2005). 'Annealing Effect on Photoluminescence Intensity of Eu-Doped Y2O3 Nanocrystals'. *J. Korean Phys. Soc. (JKPS)*; **47 (92)**, p S368-S371.
URL:http://www.kps.or.kr/home/kor/journal/library/abstract_view.asp?articleid={FD4CE4A6-4364-4230-8064-48B4F934A615}
- [10] L. F. Johnson, H. J. Guggenheim and R. A. Thomas (1966). 'Phonon-terminated optical masers'. *Phys. Rev.*; **49 (1)**, p 179 -185. URL: <http://link.aps.org/doi/10.1103/PhysRev.149.179> doi: 10.1103/PhysRev.149.179
- [11] I. Burn and S. Neirman (1982). 'Dielectric properties of donor- doped polycrystalline SrTiO₃'. *J. Mater. Sci.*; **17 (12)**, p 3510- 3524. doi: 10.1007/BF00752196
- [12] Dong Won Hwang, Jae Sung Lee, Wei Li and Se Hyuk Oh (2003). 'Electronic band structure and Photocatalytic activity of Ln₂Ti₂O₇ (Ln = La, Pr, Nd)'. *J. Phys. Chem. B*; **107 (21)**, p 4963- 4970. doi: 10.1021/jp034229n
- [13] M. A. Subramanian, G. Aravamudan and G. V. Subba Rao (1983). 'Oxide pyrochlores- a review'. *Prog. Solid State Chem.* **15 (2)**, p 55- 143. doi:10.1016/0079-6786(83)90001-8
- [14] K. B. Helean, S. V. Ushakov, C. E. Brown, A. Navrotsky, J. Lian, R. C. Ewing, J. M. Farmer and L. A. Boatner (2004). 'Formation enthalpies of rare earth titanate pyrochlores'. *J. Solid State Chem.*; **177 (6)**, p 1858-1866. doi:10.1016/j.jssc.2004.01.009
- [15] F. X. Zhang and S. K. Saxena (2005). 'Structural changes and pressure induced amorphization in rare earth titanates RE₂Ti₂O₇ (RE= Gd, Sm) with pyrochlore structure'. *Chem. Phys. Lett.*; **413 (1-3)**, p 248- 251. doi:10.1016/j.cplett.2005.07.094
- [16] Ni Zhong, Ping-hua Xiang, Da-zhi Sun and Xian-lin Dong (2005). 'Effect of rare earth additives on the microstructure and dielectric properties of 0.67Pb(Mg_{1/3}Nb_{2/3})O₃-0.33PbTiO₃ ceramics'. *Mater. Sci. Eng., B*; **116 (2)**, p 140-145. doi:10.1016/j.mseb.2004.09.030
- [17] S. T. Bramwell, M. N. Field, M. J. Harris and I. P. Parkin (2000). 'Bulk magnetization of the heavy rare earth titanate pyrochlores- a series of model frustrated magnets'. *J. Phys. Condens. Matter.*; **12 (4)**, p 483- 495. doi: 10.1088/0953-8984/12/4/308
- [18] Ryu Abe, Masanobu Higashi, Kazuhiro Sayama, Yoshimoto Abe and Hideki Sugihara (2006). 'Photocatalytic Activity of R₃MO₇ and R₂Ti₂O₇ (R= Y, Gd, La; M= Nb, Ta) for Water Splitting into H₂ and O₂'. *J. Phys. Chem. B.*; **110 (5)**, p 2219-2226. doi: 10.1021/jp0552933
- [19] S. X. Wang, L. M. Wang, R. C. Ewing and K. V. Govindan Kutty (2000). 'Ion irradiation of rare-earth- and yttrium-titanate-pyrochlores'. *Nucl. Instrum. Methods Phys. Res., Sect. B*; **169 (1-4)**, p 135-140. doi:10.1016/S0168-583X(00)00030-6
- [20] Arthur W. Sleight (1969). 'Rare earth plumbates with the pyrochlore structure'. *Inorg. Chem.*; **8 (8)**, p 1807-1808. doi: 10.1021/ic50078a060
- [21] K. E. Sickafus, L. Minervini, R. W. Grimes, J. A. Valdez, M. Ishimaru, F. Li, K. J. McClellan and T. Hartmann (2000). 'Radiation Tolerance of Complex Oxides'. *Science*; **289 (5480)**, p 748-751. doi: 10.1126/science.289.5480.748
- [22] Jie Wu, Xuezheng Wei, Nitin P. Padture, Paul G. Klemens, Maurice Gell, Eugenio Garcia, Pilar Miranzo and Maria I. Osendi (2003). 'Low thermal conductivity rare earth zirconates for Potential thermal barrier coating applications'. *ChemInform*; **34 (10)**, doi: 10.1002/chin.200310007 URL: <http://dx.doi.org/10.1002/chin.200310007>
- [23] Rodney C. Ewing, William J. Weber and Jie Lian (2004). 'Nuclear waste disposal-pyrochlore (A₂B₂O₇): Nuclear waste form for the immobilization of plutonium and minor actinides'. *J. Appl. Phys.*; **95 (11)**, p 5949- 5971. doi:10.1063/1.1707213
URL: <http://link.aip.org/link/?JAPIAU/95/5949/1>
- [24] Yasutake Teraoka, Ken-ichiro Torigoshi, Hidetoshi Yamaguchi, Takashi Ikeda and Shuichi Kagawa (2000). 'Direct decomposition of nitric oxide over stagnate pyrochlore oxides:

- relation between solid state chemistry and catalytic activity'. *J. Mol. Catal. A: Chem.*; **155** (1-2), p 73- 80. doi:10.1016/S1381-1169(99)00320-9
- [25] Henry Lehmann, Dieter Pitzer, Gerhard Pracht, Robert Vassen and Detlef Stöver (2003). 'Thermal conductivity and thermal expansion coefficients of the lanthanum rare earth element zirconate system'. *J. Am. Ceram. Soc.*; **86** (8), p 1338- 1344.
doi:10.1111/j.1151-2916.2003.tb03473.x URL: <http://dx.doi.org/10.1111/j.1151-2916.2003.tb03473.x>
- [26] Masakazu Kimura, Satoshi Nanamatsu, Kikuo Doi, Shigeo Matsushita and Masao Takahashi (1972). 'Electrooptic and piezoelectric properties of $\text{La}_2\text{Ti}_2\text{O}_7$ single crystal'. *Jpn. J. Appl. Phys.*; **11** (6), p 904. URL:<http://jjap.ipap.jp/link?JJAP/11/904/> doi: 10.1143/JJAP.11.904
- [27] K. Scheunemann and H. K. Müller-Buschbaum (1975). 'The crystal structure of $\text{La}_2\text{Ti}_2\text{O}_7$ '; Zur kristallstruktur von $\text{La}_2\text{Ti}_2\text{O}_7$ (in German). *J. Inorg. Nucl. Chem.*; **37** (9), p 1879-1881. doi:10.1016/0022-1902(75)80906-7
- [28] S. B. Xiong, W. P. Ding, Z. G. Liu, X. Y. Chen, X. L. Guo, T. Yu, Y. Y. Zhu, and W. S. Hu (1996). 'Layered defective lanthanum titanate thin films prepared by pulsed laser ablation of potassium lanthanum titanate ceramics'. *Appl. Phys. Lett.*; **69** (2), p 191-193. doi:10.1063/1.117368 URL: <http://link.aip.org/link/APPLAB/69/191/1>
- [29] Hiroaki Takeda, Hideki Sako, Hiroyuki Shimizu, Kaoru Kodama, Masahiro Nishida, Hiroshi Nakao, Takashi Nishida, Soichiro Okamura, Takashi Shikida and Tadashi Shiosaki (2003). 'Growth and Characterization of Lanthanum Calcium Oxoborate $\text{LaCa}_4\text{O}(\text{BO}_3)_3$ Single Crystals'. *Jpn. J. Appl. Phys.*; **42** (9B), p 6081-6085. doi: 10.1143/JJAP.42.6081
URL:<http://jjap.ipap.jp/link?JJAP/42/6081/>
- [30] Xiao Qiang Liu and Xiang Ming Chen (2005). 'Toughening of 8Y-FSZ Ceramics by Neodymium Titanate Secondary Phase'. *J. Am. Ceram. Soc.*; **88** (2), p 456-458.
doi: 10.1111/j.1551-2916.2005.00065.x URL: <http://dx.doi.org/10.1111/j.1551-2916.2005.00065.x>
- [31] Hyung J. Jung, Hyun J. Kim, Kyong Y. Kim, Seok J. Yoon, Sang O. Yoon, Tetsuro Nakamura, Mitsuru Itoh and Yoshiyuki Inaguma (1996). 'Compositions of High Frequency Dielectrics'. US Patent 5569632
- [32] Mailadil T. Sebastian, Sam Solomon, Ravindran Ratheesh, Jacob George and Pezholil Mohanan (2001). 'Preparation, characterization, and microwave properties of RETiNbO_6 (RE = Ce, Pr, Nd, Sm, Eu, Gd, Tb, Dy, Y, and Yb) dielectric ceramics'. *J. Am. Cer. Soc.*; **84** (7), p 1487-1489. doi: 10.1111/j.1151-2916.2001.tb00865.x
URL: <http://dx.doi.org/10.1111/j.1151-2916.2001.tb00865.x>
- [33] C. W. A. Paschoal, R. L. Moreira, C. Fantini, M. A. Pimenta, K. P. Surendran and M. T. Sebastian (2003). 'Raman scattering study of RETiTaO_6 dielectric ceramics'. *Journal of the European Ceramic Society.*; **23** (14), p 2661-2666. doi:10.1016/S0955-2219(03)00141-9
- [34] Hlavacek V(1991). 'Combustion synthesis: a historical perspective'. *Am. Cer. Soc. Bull.*; **70** (2), p 240-243.
- [35] H. C. Yi and J. J. Moore (1990). 'Self-propagating high-temperature (combustion) synthesis (SHS) of powder-compacted materials'. *J. Mater. Sci.*; **25** (2), p 1159- 1168.
doi: 10.1007/BF00585421
- [36] Zuhair A. Munir and Umberto Anselmi-Tamburini (1989). 'Self-propagating exothermic reactions: The synthesis of high-temperature materials by combustion'. *Materials Science Reports*; **3** (7-8), p 277-365. doi:10.1016/0920-2307(89)90001-7
- [37] Alexander G. Merzhanov (2004). 'The chemistry of self-propagating high-temperature synthesis'. *J. Mater. Chem.*; **14** (12), p 1779 – 1786. doi: 10.1039/b401358c
- [38] Kashinath C Patil, Singanahally T Aruna and Sambandan Ekambaram (1997). 'Combustion synthesis'. *Curr. Opin. Solid State Mater. Sci.*; **2** (2), p 158-165.
doi:10.1016/S1359-0286(97)80060-5
- [39] Michael Kestigian and Roland Ward (1955). 'The Lanthanum-Titanium-Oxygen System'. *J. Am. Chem. Soc.*; **77** (23), p 6199-6200. doi: 10.1021/ja01628a035

- [40] K. R. Dayas (2006). 'Self propagated high temperature synthesis of electroceramic rare earth titanates and its characterization'. Ph.D. Thesis, Calicut University, Calicut, India.
- [41] K Krishnankutty and K R Dayas (2008). 'Synthesis and characterization of monoclinic rare earth titanates, RE₂Ti₂O₇ (RE = La, Pr, Nd), by a modified SHS method using inorganic activator'. *Bulletin of Materials Science.*; **31** (6), p 907–918. doi: 10.1007/s12034-008-0145-7
- [42] V B Kartha (2006). 'Laser spectroscopy of lanthanides and actinides: structural, analytical and molecular dynamics applications'; in: "Recent developments in spectroscopy of lanthanides and actinides". B. N. Jagatap and A. Venugopalan (Eds.), R V Enterprises, Mumbai, p 84-97. 235pp.
- [43] Jianying Shi, Jun Chen, Zhaochi Feng, Tao Chen, Yuxiang Lian, Xiuli Wang and Can Li (2007). 'Photoluminescence Characteristics of TiO₂ and Their Relationship to the Photoassisted Reaction of Water/Methanol Mixture'. *J. Phys. Chem. C*; **111** (2), p 693- 699. doi: 10.1021/jp065744z
- [44] Haijme Yamamoto, Shinji Okamoto and Hiroshi Kobayashi (2002). 'Luminescence of rare earth ions in perovskite type oxides: from basic research to applications'. *J. Lumin.*; **100** (1-4), p 325- 332. doi:10.1016/S0022-2313(02)00432-5
- [45] Shinji Okamoto and Haijme Yamamoto (2003). 'Luminescent properties of praseodymium doped alkaline earth titanates'. *J. Lumin.*; **102-3**, p 586- 589. doi:10.1016/S0022-2313(02)00591-4
- [46] Claes af Klinteberg, Markus Andreasson, Ola Sandström, Stefan Andersson-Engels and Sune Svanberg. 'Compact System for Clinical Recordings of Laser-Induced Fluorescence Spectra'. URL: http://www.lot-oriel.com/site/site_down/cc_appexlifs_deen.pdf
- [47] Shigeo Shionoya (1998). 'Photoluminescence'; in: 'Luminescence of Solids'. 1st ed. D. R. Vij (Ed.), Plenum Press, New York, p 95-134. 446pp
- [48] Karen L. Frindell, Michael H. Bartl, Matthew R. Robinson, Guillermo C. Bazan, Alois Popitsch and Galen D. Stucky (2003). 'Visible and near-IR luminescence via energy transfer in rare earth doped mesoporous titania thin films with nanocrystalline walls'. *J. Solid State. Chem.*; **172** (1), p 81- 88. doi:10.1016/S0022-4596(02)00126-3
- [49] Alexander Aleksandrovich Kaminskii (1996). 'Crystalline Lasers: physical processes and operating schemes'. CRC Press, USA, 561pp.
- [50] Gerhard Heinrich Dieke (1968). 'Spectra and energy levels of rare earth ions in crystals'. H M Crosswhite and Hannah Crosswhite (Eds.). Interscience Publishers, John Wiley & Sons New York, USA. 401pp.
- [51] G. H. Dieke and H. M. Crosswhite (1963). 'The spectra of the doubly and triply ionized rare earths'. *Appl. Opt.*; **2** (7), p 675-686. doi:10.1364/AO.2.000675
URL: <http://www.opticsinfobase.org/ao/abstract.cfm?URI=ao-2-7-675>
- [52] Rafie H. Abu-Eittah, Sayed A. Marie and Marbrouka B. Salem (2004). 'The electronic absorption spectra of Lanthanum (III) Cerium (III) and Thorium (IV) ions in different solvents'. *Can. J. Anal. Sci. Spectrosc.*; **49** (4), p 248-257.
URL: <http://www.cjass.ca/v49n4p248.pdf>
- [53] Lyjo K Joseph, K R Dayas, Soniya Damodar, Bindu Krishnan, K Krishnankutty, V P N Nampoori and P Radhakrishnan (2008). 'Photoluminescence studies on rare earth titanates prepared by self propagating high temperature synthesis method'. *Spectrochimica Acta Part A: Molecular and Biomolecular Spectroscopy*; **71** (4), p1281-1285 doi:10.1016/j.saa.2008.03.030
- [54] J. H. Van. Vleck (1937). 'The Puzzle of Rare-earth Spectra in Solids'. *J. Phys. Chem.*; **41** (1), p 67–80. doi: 10.1021/j150379a006
- [55] Sambhu N. Datta (2006). 'Theoretical aspects of electronic excitations in lanthanide and actinide complexes'; in: "Recent developments in spectroscopy of lanthanides and actinides". B. N. Jagatap and A. Venugopalan (Eds.), R V Enterprises, Mumbai, p 17-35. 235pp.
- [56] Walter Koechner and Michael Bass (2003). 'Solid State Lasers'. Springer. NY. 440pp

- [57] Michael Gaft, Renata Reisfeld and Gérard Panczer (2005). 'Modern luminescence spectroscopy of minerals and materials'. Springer-Verlag, Germany. 356pp.
- [58] M. Nogami and K. Suzuki (2002). 'Fast Spectral Hole Burning in Sm^{3+} -Doped Al_2O_3 - SiO_2 Glasses'. *Adv. Mater.*; **14** (12), p 923-926.
doi: 10.1002/1521-4095(20020618)14:12<923::AID-ADMA923>3.0.CO;2-D
URL:[http://dx.doi.org/10.1002/1521-4095\(20020618\)14:12<923::AID-ADMA923>3.0.CO;2-D](http://dx.doi.org/10.1002/1521-4095(20020618)14:12<923::AID-ADMA923>3.0.CO;2-D)
- [59] Jianrong Qiu, K. Miura, T. Suzuki, T. Mitsuyu and K. Hirao (1999). 'Permanent photoreduction of Sm^{3+} to Sm^{2+} inside a sodium aluminoborate glass by an infrared femtosecond pulsed laser'. *Appl. Phys. Lett.*; **74** (1), p 10-12. doi:10.1063/1.123117
URL: <http://link.aip.org/link/?APPLAB/74/10/1>
- [60] V. Lavín, I. R. Martín, C. K. Jayasankar and Th. Tröster (2002). 'Pressure-induced energy transfer processes between Sm^{3+} ions in lithium fluoroborate glasses'. *Phys. Rev. B*; **66** (6), 064207 [7pp] doi: 10.1103/PhysRevB.66.064207
URL:<http://link.aps.org/doi/10.1103/PhysRevB.66.064207>
- [61] Christiane GÖRLLER-WALRAND and Koen BINNEMANS (1998). 'Spectral intensities of f-f transitions'; in: "Handbook on the Physics and Chemistry of Rare Earths". vol **25**, Karl A Gschneidner Jr and LeRoy Eyring (Eds.) (New York: Elsevier) chapter 167. p 101-264.
- [62] C. K. Jayasankar and P. Babu (2000). 'Optical properties of Sm^{3+} ions in lithium borate and lithium fluoroborate glasses'. *J. Alloys Compounds*; **307** (1-2), p 82-95. doi:10.1016/S0925-8388(00)00888-4
- [63] L. M. Lacha, R. Balda, J. Fernández and J. L. Adam (2004). 'Time-resolved fluorescence line narrowing spectroscopy and fluorescence quenching in Nd^{3+} -doped fluoroarsenate glasses'. *Opt. Mater.* **25** (2), p 193-200. doi:10.1016/S0925-3467(03)00269-6
- [64] R Praveena, V Venkatramu, P Babu, C K Jayasankar, Th Tröster, W Sievers and G Wortmann (2009). 'Luminescence properties of Sm^{3+} -doped P_2O_5 - PbO - Nb_2O_5 glass under high Pressure'. *J. Phys.: Condens. Matter*; **21** (3), 035108 [9pp].
doi:10.1088/0953-8984/21/3/035108
- [65] Moon-Seog Jin, Choong-Il Lee, Chang-Sun Yoon, Chang-Dae Kim, Jae-Mo Goh and Wha-Tek Kim (2001). 'Photoluminescence spectra of undoped and Sm^{3+} -doped BaAl_2S_4 and BaAl_2Se_4 single crystals'. *J. Mater. Res.*; **16** (5), p 1520-1524. doi: 10.1557/JMR.2001.0211
- [66] Tongde Huang, Benxue Jiang, Yusong Wu, Jiang Li, Yun Shi, Wenbin Liu, Yubai Pan and Jingkun Guo (2009). 'Fabrication, microstructure and optical properties of titanium doped YAG transparent ceramic'. *J. Alloys Compounds*; **478** (1-2), p L16-L20. doi:10.1016/j.jallcom.2008.11.157
- [67] F. Bantien, P. Albers and G. Huber (1987). 'Optical transitions in titanium-doped YAG'. *J. Lumin.*; **36** (6), p 363-367. doi:10.1016/0022-2313(87)90153-0
- [68] Tetsuo Ikari, Hirosumi Yokoyama, Shigeru Shigetomi and Koji Futagami (1990). 'Near Band Edge Photoacoustic Spectra of p-Si Single Crystals'. *Jpn. J. Appl. Phys.*; **29** (5), part 1, p 887-890. URL:<http://jjap.ipap.jp/link?JJAP/29/887/> doi: 10.1143/JJAP.29.887
- [69] Allan Rosenzweig (1977). 'Solid state photoacoustic spectroscopy'; in: "Optoacoustic spectroscopy and detection". 244pp. Yoh Han Pao (Ed.), Academic press, Inc. New York USA, p 193-239.
- [70] William T. CARNALL (1979). 'The absorption and fluorescence spectra of rare earth ions in solution'; in: "Handbook on the Physics and Chemistry of Rare Earths". vol **3**, Karl A Gschneidner Jr and LeRoy Eyring (Eds.) (North-Holland Publishing Company) Chapter 24.
- [71] Zhang Yugeng, Su Qinde and Zhao Guiwen (1993). 'Photoacoustic Spectra of Pr^{3+} , Nd^{3+} , Gd^{3+} Acetate Complexes'. *Cryst. Res. Technol.*; **28** (7), p 995-999.
doi: 10.1002/crat.2170280723 URL: <http://dx.doi.org/10.1002/crat.2170280723>
- [72] Auzel F.E (1973). 'Materials and devices using double-pumped-phosphors with energy transfer'. *Proc. IEEE.*; **61** (6), p 758-786.

- [73] J C Wright (1976). 'Up-conversion and excited state energy transfer in rare-earth doped materials'; in: "Radiationless Processes in Molecules and Condensed Phases". *Top. Appl. Phys.*; Springer, New York. **15**, p 239-295. doi:10.1007/BFb0111143
- [74] David Lande, Sergei S. Orlov, Annapoorna Akella, Lambertus Hesselink, and R. R. Neurgaonkar (1997). 'Digital holographic storage system incorporating optical fixing'. *Opt. Lett.*; **22** (22), p 1722-1724.
doi:10.1364/OL.22.001722 URL:<http://www.opticsinfobase.org/ol/abstract.cfm?URI=ol-22-22-1722>
- [75] Ping Xie and T. R. Gosnell (1995). 'Room-temperature upconversion fiber laser tunable in the red, orange, green, and blue spectral regions'. *Opt. Lett.*; **20** (9), p 1014-1016.
doi: 10.1364/OL.20.001014 URL:<http://www.opticsinfobase.org/ol/abstract.cfm?URI=ol-20-9-1014>
- [76] Elizabeth Downing, Lambertus Hesselink, John Ralston and Roger Macfarlane (1996). 'A Three-Color, Solid-State, Three-Dimensional Display'. *Science*; **273** (5279), p 1185-1189.
doi: 10.1126/science.273.5279.1185
- [77] S F Collins, G W Baxter, S A Wade, T Sun, K T V Grattan, Z Y Zhang and A M Palmer (1998). 'Comparison of fluorescence-based temperature sensor schemes: Theoretical analysis and experimental validation'. *J. Appl. Phys.*; **84** (9), p 4649-4654. doi:10.1063/1.368705
URL: <http://link.aip.org/link/?JAPIAU/84/4649/1>
- [78] P. V. dos Santos, M. T. de Araujo, A. S. Gouveia-Neto, J. A. Medeiros-Neto and A. S. B. Sombra (1999). 'Optical thermometry through infrared excited upconversion fluorescence emission in Er³⁺- and Er³⁺-Yb³⁺-doped chalcogenide glasses'. *IEEE J. Quant. Elect.*; **35** (3), p 395-399. doi: 10.1109/3.748846
- [79a] Paras N. Prasad (2004). 'Nanophotonics'. Wiley Interscience, NJ; 415pp.
- [79b] *idem* (2003). 'Introduction to biophotonics' John Wiley and Sons, Hoboken, NJ, 622pp.
- [80] François Auzel (2004). 'Upconversion and Anti-Stokes Processes with f and d Ions in Solids'. *Chem. Rev.*; **104** (1), p 139-174. doi: 10.1021/cr020357g
- [81] S. Hufner (1978). 'Optical spectra of transparent rare earth compounds'. Academic Press. London. 237pp.
- [82] N. Bloembergen (1959). 'Solid State Infrared Quantum Counters'. *Phys. Rev. Lett.*; **2** (3), p 84-85. doi:10.1103/PhysRevLett.2.84 URL:<http://link.aps.org/doi/10.1103/PhysRevLett.2.84>
- [83] Jay S. Chivian, W. E. Case, and D. D. Eden (1979). 'The photon avalanche: A new phenomenon in Pr³⁺-based infrared quantum counters'. *Appl. Phys. Lett.*; **35** (2), p124-125.
doi:10.1063/1.91044 URL: <http://link.aip.org/link/?APPLAB/35/124/1>
- [84] A. Rosencwaig (1980). 'Photoacoustics and Photoacoustic Spectroscopy' John Wiley, New York. 309pp.
- [85] David W Ball (2006). 'Photoacoustic Spectroscopy'. *Spectroscopy*; **21** (9), p 14-16.
URL:<http://spectroscopyonline.findanalyticchem.com/spectroscopy/data/articlestandard/spectroscopy/382006/373853/article.pdf>
- [86] Giovanna Suber, Mario Bertolotti, Concita Sibilila and Aldo Ferrari (1988). 'Test measurements of the photothermal deflection method to determine the thermal diffusivity of solids'. *Appl. Opt.*; **27** (9), p 1807-1810. doi:10.1364/AO.27.001807
URL:<http://www.opticsinfobase.org/ao/abstract.cfm?URI=ao-27-9-1807>
- [87] W B Jackson, N M Amer, A C Boccara and D Fournier (1981). 'Photothermal deflection spectroscopy and detection'. *Appl. Opt.*; **20** (8), p 1333-1344. doi:10.1364/AO.20.001333
URL:<http://www.opticsinfobase.org/ao/abstract.cfm?URI=ao-20-8-1333>
- [88] A. C. Boccara, D. Fournier, Warren Jackson and Nabil M. Amer (1980). 'Sensitive photothermal deflection technique for measuring absorption in optically thin media'. *Opt. Lett.*; **5** (9), p 377- 379. URL: <http://www.opticsinfobase.org/ol/abstract.cfm?URI=ol-5-9-377>
doi:10.1364/OL.5.000377
- [89] A C Boccara, D Fournier and J Badoz (1979). 'Thermo-optical spectroscopy: Detection by the "mirage effect"'. *Appl. Phys. Lett.*; **36** (2), p 130-132. doi:10.1063/1.91395
URL: <http://link.aip.org/link/?APPLAB/36/130/1>

- [90] D. Fournier, A. C. Boccara, Nabil M. Amer and Robert Gerlach (1980). 'Sensitive *in situ* trace-gas detection by photothermal deflection spectroscopy'. *Appl. Phys. Lett.*; **37** (6), p 519-521. doi:10.1063/1.91970 URL: <http://link.aip.org/link/?APPLAB/37/519/1>
- [91] D Fournier and A C Boccara. (1980). 'Scanned imaging microscopy'. Eric A Ash (Ed.) Academic Press, London. 461pp
- [92] P. K. Kuo, M. J. Lin, C. B. Reyes, L. D. Favro, R. L. Thomas, D. S. Kim, Shu-Yi Zhang, L. J. Inglehart, D. Fournier, A. C. Boccara and N. Yacoubi (1986). 'Mirage-effect measurement of thermal diffusivity. Part I: experiment'. *Can. J. Phys.*; **64** (9), p 1165–1167. doi:10.1139/p86-202
- [93] P K Kuo, E D Sendler, L D Favro, and R. L. Thomas (1986). Mirage-effect measurement of thermal diffusivity. Part II: theory'. *ibid*; p 1168–1171. doi: 10.1139/p86-203
- [94] A Sánchez-Lavega, A Salazar, A Ocariz, L Pottier, E Gomez, L M Villar and E Macho (1997). 'Thermal diffusivity measurements in porous ceramics by photothermal methods'. *Appl. Phys. A.*; **65** (1), p 15-22. doi:10.1007/s003390050534 and the references therein.
- [95] Lee W. Casperson (1973). 'Gaussian Light Beams in Inhomogeneous Media'. *Appl. Opt.*; **12** (10), p 2434-2441.
URL:<http://www.opticsinfobase.org/ao/abstract.cfm?URI=ao-12-10-2434> doi:10.1364/AO.12.002434
- [96] Max Born and Emil Wolf. (1970). 'Principles of Optics; electromagnetic theory of propagation, interference and diffraction of light'. 4th ed. Pergamon Press, Oxford. 808pp.
- [97] R Gupta (1989). 'The theory of photothermal effect in fluids'; in: "Photothermal Investigations of Solids and Fluids" Jeffrey A Sell (Ed.). p 81-126. Academic Press, Inc. San Diego, CA. 346 pp
- [98] D Fournier and A C Boccara 'Photothermal investigation of solids: basic physical principles'; *ibid* p 35-79.
- [99] F. Lepoutre, D. Fournier and A. C. Boccara (1985). 'Nondestructive control of weldings using the mirage detection'. *J. Appl. Phys.*; **57** (4), p 1009-1015. doi:10.1063/1.334540 URL: <http://link.aip.org/link/?JAPIAU/57/1009/1>
- [100] A. Salazar and A. Sánchez-Lavega (1994). 'Thermal diffusivity measurements using linear relations from photothermal wave experiments'. *Rev. Sci. Instrum.*; **65** (9), p 2896-2900. doi:10.1063/1.1144635 URL: <http://link.aip.org/link/?RSINAK/65/2896/1>
- [101] Jerry F. Kerrisk (1971). 'Thermal diffusivity of heterogeneous materials'. *J. Appl. Phys.*; **42** (1), p 267-271. doi:10.1063/1.1659581 URL: <http://link.aip.org/link/?JAPIAU/42/267/1>
- [102] Stephen E. Bialkowski (1996). 'Photothermal Spectroscopy Methods for Chemical Analysis'. Vol. **134** "Chemical analysis: a series of monographs on analytical chemistry and its applications". J. D. Winefordner (Ed.). John Wiley & Sons, Inc., New York, 1st ed. 584pp.
- [103] David R. Lide (1999). 'CRC Handbook of Chemistry and Physics'. CRC press, Boca Raton. 80th ed. 2504pp.
- [104] Sajan D George (2003). 'Laser induced photothermal investigations on thermal and transport properties of certain selected photonic materials'. Ph. D. Thesis. CUSAT. Kochi. 172p
- [105] Darryl P Almond and Pravin M Patel (1996). 'Photothermal Science and Techniques'. Chapman & Hall, London. 241pp.
- [106] J. Bodzenta, A. Kaźmierczak-Bałata, T. Łukasiewicz and M. Pyka (2008). 'Correlation between the thermal diffusivity and the velocity of ultrasound in YVO₄ single crystals'. *Eur. Phys. J. Special Topics*; **154** (1), p 313–317. doi: 10.1140/epjst/e2008-00567-4
- [107] J. Bodzenta, A. Kaźmierczak-Bałata, T. Łukasiewicz, B. Hofman and J. Kucytowski (2008). 'Thermal Wave Measurements with a Mirage Detection for Investigation of Thermal Diffusivity of GdCa₄O(BO₃)₃ Single Crystals'. *Acta Physica Polonica A*; **114** (6-A). p A-27-A-32. URL: <http://prz.yrbwn.icm.edu.pl/APP/PDF/114/a114zA05.pdf>
- [108] M. Bertolotti, V. Dorogan, G. Liakhou, R. Li Voti, S. Paoloni and C. Sibilìa (1997). 'New photothermal deflection method for thermal diffusivity measurement of semiconductor

- wafers'. *Rev. Sci. Instrum.*; **68** (3), p 1521-1526. doi:10.1063/1.1147589 URL: <http://link.aip.org/link/?RSINAK/68/1521/1>
- [109] A. Stanimirovic, N. M. Balzaretta, A. Feldman and J. E. Graebner (2001). 'Thermal conductivity and thermal diffusivity of selected oxide single crystals'. *J. Mater. Res.*; **16** (3), p 678-682. doi: 10.1557/JMR.2001.0090
- [110] C. X. Zhao, A. H. Luo, X. J. Liu, S. Y. Zhang and S. Y. Zhang (2005). 'Doping effect on thermal diffusivity of pyrochlore $\text{Sm}_{2-x}\text{Sr}_x\text{Mo}_2\text{O}_7$ '. *J. Phys. IV France*; **125**, p 257-259. doi: 10.1051/jp4:2005125061
- [111] Noor Jawad Ridha, W. Mahmood Mat Yunus, S.A. Halim, Z.A. Talib, Firas K. Mohamad Al-Asfoor and Walter C. Primus (2009). 'Effect of Sr Substitution on Structure and Thermal Diffusivity of $\text{Ba}_{1-x}\text{Sr}_x\text{TiO}_3$ Ceramic'. *Am. J. Engg. & Applied Sci.*; **2** (4), p 661-664. URL: <http://www.scipub.org/fulltext/ajeas/ajeas24661-664.pdf>
- [112] M Haydari, M M Moksini, A E Abdeirahman, M Deraman, W M M Yunus, and I V Grozescu (2008). 'Thermal Diffusivity of Carbon Pellets (CPs) Treated with KOH'. *Am. J. Applied Sci.*; **5** (2), p 165-168. URL: <http://scipub.org/fulltext/ajas/ajas52165-168.pdf> and the references therein
- [113] D. Fournier, J. P. Roger, A. Bellouati, C. Boué, H. Stamm and F. Lakestani (2001). 'Correlation between Hardness and Thermal Diffusivity'; in: "Proceedings of 11th International Conference of Photoacoustic and Photothermal Phenomena". *Anal. Sci.*; **17**, p s158- s160. URL: http://www.jstage.jst.go.jp/article/analscisp/17icpp/0/s158/_pdf
- [114] D. Fournier and A.C. Boccara (1989). 'Heterogeneous media and rough surfaces: A fractal approach for heat diffusion studies'. *Physica A*; **157** (1), p 587-592. doi:10.1016/0378-4371(89)90367-1 and the references therein.
- [115] Horatio Scott Carslaw and J C Jaeger (1986). 'Conduction of heat in solids'. Clarendon, Oxford. 520pp.
- [116] Allan Rosencwaig and Allen Gersho (1976). 'Theory of the photoacoustic effect with solids'. *J. Appl. Phys.*; **47** (1), p 64-69. URL: <http://link.aip.org/link/?JAPIAU/47/64/1> doi:10.1063/1.322296
- [117] E. M. Monahan Jr. and A. W. Nolle (1977). 'Quantitative study of a photoacoustic system for powdered samples'. *J. Appl. Phys.* **48** (8), p 3519- 3523. doi:10.1063/1.324148 URL:<http://link.aip.org/link/?JAPIAU/48/3519/1>
- [118] A Boccara and D Fournier (1988). 'Heat diffusion and fractals: heterogeneous media and rough surfaces'; in: "Photoacoustic and photothermal phenomena I". P Hess and J Pelzl (Eds.), Springer series in Optical sciences, vol. **58**, Springer. p302.
- [119] R Osiander, R Haberkern, P Korpiun and W Schirmacher (1990). 'The Photoacoustic Signal of Fractal Structures'; in: "Photoacoustic and photothermal phenomena II". J C Murphy, J W Maclachlan Spicer, L C Aamodt and B S H Royce (Eds.) Springer series in Optical sciences, vol. **62**, Springer, Berlin, Germany. p 309-312.
- [120] Dietrich Stauffer and Amnon Aharony (1994). 'Introduction to Percolation Theory'. Taylor and Francis. London. 192pp.
- [121] Benoit B Mandelbrot(1983). 'The fractal geometry of nature'. W H Freeman. NY.500pp.
- [122] O. A. Aleksić, P. M. Nikolić, D. Luković, K. Radulović, D. Vasiljević Radović and S. Savić (2004). 'Thermal diffusivity of NTC layers obtained with photoacoustic technique'. *Microelectronic international*; **21** (1), p 10-14. doi: 10.1108/13565360410517120
- [123] P Korpiun and R Osiander (1992). 'Photothermal study of heat conduction, diffusion and sorption in thin films and porous materials': in "Photoacoustic and photothermal phenomena III". p 619-627. Springer Series in Optical Sciences, Vol. **69**. Dane Bićanić (Ed.), Springer-Verlag, Berlin, Heidelberg, Germany. 731pp. and the references therein.
- [124] R Osiander, J Lobermeier and P Korpiun. (1992). 'Anomalous thermal waves in powdered samples'. *Ibid*, p 725-727. and the references therein.

- [125] Yuval Gefen , Amnon Aharony and Shlomo Alexander (1983). 'Anomalous Diffusion on Percolating Clusters'. *Phys. Rev. Lett.*; **50** (1), p 77 – 80. doi: 10.1103/PhysRevLett.50.77
URL: <http://link.aps.org/doi/10.1103/PhysRevLett.50.77>
- [126] E. Marín (2006). 'Thermal Physics Concepts: The Role of the Thermal Effusivity'. *Phys. Teach.*; **44** (7), p 432-434. doi: 10.1119/1.2353583
URL: <http://dx.doi.org/10.1119/1.2353583>
- [127] U Zammit, M Marinelli, R Pizzoferrato, F Scudieri and S Martellucci (1988). 'Photoacoustics as a technique for simultaneous measurement of thermal conductivity and heat capacity'. *J. Phys. E: Sci. Instrum.*; **21** (10), p 935-937 doi: 10.1088/0022-3735/21/10/004
- [128a] Nibu A. George, C. P. G. Vallabhan, V. P. N. Nampoori, A. K. George and Periasamy Radhakrishnan (2001). 'Open-cell photoacoustic investigation of the thermal effusivity of liquid crystals'. *Opt. Eng.*; **40** (07), p 1343-1347. doi: 10.1117/12.427305
- [128b] Annieta Philip K, Lyjo K. Joseph, Litty M. Irimpan, Bindu Krishnan, P. Radhakrishnan, V. P. N. Nampoori and Raghu Natarajan (2007). 'Thermal characterization of ceramic tapes using photoacoustic effect'. *phys. stat. sol. (a)*; **204** (3), p 737–744.
doi: 10.1002/pssa.200622287 URL: <http://dx.doi.org/10.1002/pssa.200622287>
- [129] Clark's tables, Science data book (1992). Oliver & Boyd, Edinburgh. 105pp
- [130] Agustín Salazar (2003). 'On thermal diffusivity'. *Eur. J. Phys.*; **24** (4), p 351-358.
doi: 10.1088/0143-0807/24/4/353

Optical and thermal characterization of rare earth doped sol gel silica glasses

Abstract

Rare earth (RE=Y, La, Dy, Nd, Tb, Er and Yb) doped silica glasses were prepared by sol gel technique with various weight percentage of the RE in the silica matrix. The glasses were sintered at three different temperatures and their optical absorption and fluorescence spectra were obtained. The fluorescence spectra of the samples also showed an emission near 421 nm under UV excitation, arising from silica, as seen in the case of dye intercalated montmorillonites. Photoacoustic method was used for the thermal characterization of these glasses. By this method, the thermal effusivity and diffusivity values were evaluated.

4.1. Prologue	199
4.2. Theoretical background	203
4.2.1. Crystalline field theory of rare earth ions	204
4.2.2. Weak crystalline field	204
4.3. Rare earth doped sol gel glasses- preparation	205
4.3.1. General trends	205
4.3.2. Sample preparation details	208
4.4. Section I- Optical studies	209
4.4.1. Preamble	209
4.4.2. Energy level diagram of the rare earth ions	209
4.4.3. Absorption studies	210
4.4.4. Excitation and emission studies	211
4.4.5. Results and discussions	212
4.4.6. Concluding remarks	216
4.5. Section II- Thermal characterization using photoacoustics	216
4.5.1. Preamble	216
4.5.2. Part A: Thermal effusivity measurement	217
4.5.3. Part B: Thermal diffusivity of erbium doped glasses	220
4.5.4. Conclusions	224
4.6. Summary	224
4.7. References	224

4.1. Prologue:

Novel optical materials suitable for the development of solid-state photonic devices based on lanthanide (Ln) doped crystal or vitreous hosts have attracted significant scientific and technological interest.^[1-3] The most remarkable feature of the Ln or rare earth (RE) ions in solid-state host is the sharpness of many absorption and emission spectral lines which are as narrow as the spectra of free atoms. This is due to their electronic configuration ($4f^N 5s^2 5p^6$) both for divalent and trivalent ion. The optical active electrons are in the 4f shell such that they are not the outermost ones. They are shielded from external fields by two atomic shells with larger radial extension ($5s^2 5p^6$), which explains the atomic-like behaviour of their spectra. Thus, the 4f electrons are weakly perturbed by the static crystal field of the surrounding medium. The RE ions in solids are good light emitters in the spectral region covering visible, NIR and IR up to $3\mu\text{m}$. A characteristic property of the trivalent RE ions is that their electronic transitions usually occur within the 4f shell, which is somewhat shielded from the host lattice by the optically passive outer electron orbits. (Ce^{3+} with its 5d-4f transitions is an exception.). This reduces the influence of the host lattice on the wavelengths, bandwidths and cross sections of the relevant optical transitions. Trivalent RE ions have taken a dominant position as laser crystal activators responsible for stimulated emission in a variety of crystalline matrices.^[4]

Glasses offer a medium for the production of devices that are both small and efficient. For photonic device applications glassy hosts are advantageous because they exhibit better mechanical strength, chemical durability, and thermal stability^[5] and are suitable for developing low-loss, high strength, and low cost optical fibers. In addition, the glassy host matrices possess the durability and mechanical properties of an oxide host. The advent of high optical quality transparent nano-structured glasses, the so-called transparent glass ceramics or vitroceramics disclosed the possibility of producing nano-sized photonic devices based on RE doped up-converters. Transparent glass ceramics have been investigated as hosts for Ln ions envisioning the production of materials with high performances that are easy to shape for photonic applications.^[6, 7]

RE doped glasses have been extensively studied with great interest due to their potential applications in optical devices^[8], such as solid-state lasers^[9- 11] and optical fibers. These systems can be easily prepared in different shapes and sizes with uniform distribution of RE concentrations, accept RE ions without inducing crystallisation, and exhibit large optical transparency window covering UV, visible and IR regions. The

knowledge of the optical properties of RE ions in glass is very important in order to optimise the best ion-host configuration.^[12] RE doped glasses have many uses as amplifiers in optical communication systems and as optical sources. Glass wave-guide lasers are another interesting subject for the development of compact laser sources and amplifier devices.^[13] Silica glass is a highly attractive material as RE host matrix as silica glass has high glass transition temperature, low thermal expansion coefficient and low non-linear index of refraction.^[10, 11]

Thermodynamically, REs have a low solubility in silica glass,^[10] and thus a doping concentration higher than the equilibrium solubility will lead to formation of RE clusters, which is detrimental to the optical properties of laser glasses. In traditional melt casting and chemical vapour deposition (CVD), the doping concentration is limited to the equilibrium solubility of RE ions in the host matrix.^[10] To achieve a high doping level of RE ions in silica glass, a non-equilibrium low temperature approach is required to kinetically trap RE ions in host matrix with an atomic level homogeneity.^[10, 11]

The sol gel method for preparing optical materials attracted renewed interest due to their advantages.^[14] The sol gel process, characterised by low-temperature reaction, has been proved to be a very promising route for preparing host materials for encapsulating optically active species.^[5, 15] Doped glasses obtained via thermal densification of the gels show similar properties with that of the melt route glasses.^[16] The optical absorption and luminescence properties of several RE ions incorporated into sol gel silica have been reported.^[17]

A high doping level of RE ions in silica glass with minimal formation of clusters of RE ions can be achieved by sol gel process.^[11] With a high doping concentration, RE and other metal ions have a strong tendency to form clusters in sol gel silica as well.^[11, 18-21] At low concentrations, the RE ions can be distributed homogeneously in a tetrahedral network with the formation of Si-O-RE structure. However, with an increasing concentration, due to strong interaction between the RE ions and oxygen ions, RE-O-RE clusters may form, and eventually lead to phase separation.^[11, 22-24]

Sol gel glass preparation has been extensively studied since Dislich^[25] reported the formation of borosilicate glass by hot-pressing granules of dehydrated gel.^[13] Glasses synthesised by the sol gel method are promising matrices for the formation of optical nano-composites. The use of these nano-composites in optoelectronics, photonics, and

fiber optics has opened up a new way for the development of unique information systems with tuneable characteristics over a wide frequency range.^[26] Sol gel glasses allow much higher dopant concentrations than melt glasses and couple better with broad-band pumping sources than crystals due to their amorphous structure, which make them attractive alternate hosts. The structure of sol gel glasses depends on several manufacturing factors with main parameters as pH and temperature during preparation. This structure ultimately affects the dopant distribution in the material and consequently the dopant fluorescence by encouraging certain energy transfer processes. Additionally, because of their nano-porous properties, sol gels are susceptible to diffusion of environmental molecules, which may interact with the dopants. Sol gel glasses are nano-porous silica glass monoliths made by the sol gel process. The annealing process removes any excess water and organic molecules as well as creating a dense, amorphous product - the sol gel glass.^[27] This final material features a narrow pore size distribution, a high degree of pore connectivity and optical quality, and a relatively uniform distribution of the ions throughout the material when compared to traditional melt-glasses.^[28]

Two fluorescence quenching processes that are characteristic problems of using sol gel glasses in research^[29] are concentration quenching via cross-relaxation and non-radiative vibrational excitation of hydroxyl (-OH) groups^[28] limit their luminescence efficiency.^[30] Dopant clustering is the tendency of a luminescent species to aggregate with itself through oxygen linkages. RE ions clustering^[31] results in fluorescence quenching due to the interaction of neighbouring RE ions. It leads to concentration quenching of luminescence through cross relaxation and energy transfer processes which depends on the glass type and composition.^[13] The high concentration of hydroxyl groups that remain in sol gel glasses decreases the fluorescence efficiencies and shortens luminescent level lifetimes of dopant ions in glasses,^[32] adversely affecting optical device performance.^[33, 34] Hydroxyl quenching arises from the residual water solvents and silanol group present in sol gel glasses. This leads to an enhancement in the non-radiative decay of the RE ions^[35] because of the coupling between the RE states and the high energy (3200 cm^{-1}) vibrations of -OH.^[36] Its contribution to non-radiative decay is considered to be larger than that of the multi-phonon process because of the higher vibration energy.^[13]

The sol gel route allows powder-less processing of glasses and ceramics. Sol gel chemistry provides mild conditions so that organic species can be mixed with the inorganic precursors, leading to the formation of hybrid organic-inorganic systems.^[37]

Rare earth doped sol gel glass

Glasses containing refractory materials like SiO_2 , TiO_2 etc. with ultra high purity can be prepared by sol gel technique.^[13] Sol gel approaches^[14] to photonic materials can be considered as inorganic structure formation by self-assembly on multiple nanometre length scales. The outstanding features of these silicas include

- very high homogeneity and purity,
- superior refractory nature,
- thermal shock resistance,^[38]
- optical transparency in both the UV and visible regions,^[39]
- high chemical durability,
- low non-linear refractive index coefficient,
- low strain birefringence,
- thermal expansion coefficient close to zero,
- low temperature dependence of expansion coefficient,
- low optical loss,
- ease of chemical doping, and
- near net shape casting.^[13, 33]

These features make sol gel silicas potentially applicable to a wide range of optical products, host materials lasers etc.^[40] The potential advantages of the sol gel technology like the possibility of structural manipulation on an extremely fine scale, i.e. within the nanometre range, and the prevention of impurity pick-up due to the lower processing temperatures have resulted in the practical realisation of photonic crystals^[41, 42] like inverse opals^[43] and slab waveguides.^[44]

The preparation of materials with optical properties is currently of the outmost relevance due to their technological applications.^[45] Recently, the sol gel process has been used extensively to obtain optical materials with luminescent properties^[17] by incorporating different cations or molecules in a silica host.^[46, 47] Sol gel glasses doped with RE ions are of interest for various applications including solid-state lasers, optical waveguides and fiber amplifiers.^[48] Thermal treatment of the doped gels changes the local environment of the metal ions,^[49] which results in changes in the fluorescence spectra. The main characteristics of spectroscopic transition involving RE ions are long lifetime of metastable states (ranging from tens of microsec to a few millisec) and narrow absorption and emission lines in the NIR regions. It is to be mentioned that it is very difficult to prepare REs doped silica glass by the conventional technique involving the quenching of an oxide melt due to the high melting temperature of SiO_2 . But silica based glasses show excellent durability and optical quality.^[13] The sol gel process offers an attractive method for preparing these

materials at relatively lower temperature without melting,^[50] and it provides an opportunity of having a control over the micro-structure and composition of the host matrix.^[14, 29] A sol gel derived glass contains neither oxide nor chlorine impurity but does contain water. The glass shows a good transparency in the UV region.^[13, 51]

4.2. Theoretical background:

The 4f shell energy levels of the lanthanides arise from spin-spin and spin-orbit interactions which are denoted by the Russel-Saunders notation $^{2s+1}L_J$. All the energy levels of a particular RE ion have the same electronic configuration and consequently all of them have the same parity. Since the electric dipole matrix elements between the two states of the same parity are identically zero, electric dipole transition between any two levels of the ions is totally forbidden. However, in a solid, the slight mixing with odd parity wave-functions makes the transition slightly allowed.^[52] In a crystal or glass matrix with crystal fields which lack inversion symmetry at the active ion, however, the slight, crystal field induced admixture of other wave-functions with the 4f wave-functions creates a small probability for electric dipole transitions. Magnetic dipole and electric quadrupole transitions are allowed by the selection rule but their contributions to radiative decay are generally small or negligible.^[13, 53-56]

The optical transitions in RE ions also have been found to be predominantly electric dipole in nature.^[13] In crystals, the optical properties of trivalent 4f ions in the visible and NIR region are well understood in terms of the weak crystal field approximation.^[57, 58] The crystal fields have two important effects on the energy levels of the RE ions:

1. The previously $(2J+1)$ degenerate LSJ levels are split into a number of Stark levels. Due to the shielding of the 4f valence electrons by the $5s^2 5p^6$ electrons, these Stark shifts are quite small only around a few 100 cm^{-1} .
2. The crystal field breaks the inversion symmetry of the ions environment and this permits electric dipole transition to occur between Stark levels in different LSJ multiplets. The oscillator strength of these transitions is very small of the order of 10^{-6} , which reflects the weak nature of the interaction of the 4f electrons with the crystal field.

The magnetic dipole transitions, which are of many orders weaker magnitude than fully allowed electric dipole transitions, may nevertheless take place. Broadening of the RE ion fluorescence and absorption bands in glass is necessarily more complicated than in crystals, since glasses have a random structure with each RE ion seeing a

different electric field and therefore having a different set of stark levels. For a first approximation it is considered that at room temperature the broadening of the absorption and fluorescence bands of RE doped glasses is homogeneous in nature.^[52]

4.2.1. Crystalline field theory of rare earth ions:^[59]

In crystalline field theory, the valence electrons belong to the RE ion and the effect of the lattice is considered through the electrostatic field created by the surrounding ligand ions at the RE position. This electrostatic field is called the '*crystalline field*'. It is assumed that the valence electrons are localised in RE ion and that the charge of the ligand ions does not penetrate into the region occupied by these valence electrons. The Hamiltonian can be written as^[59]

$$H=H_{FI} + H_{CF} \quad (4.1)$$

where H_{FI} is the Hamiltonian related to the free ion (RE) which is an ideal situation in which the RE ions are isolated and H_{CF} is the crystal field Hamiltonian, which accounts for the interaction of the valence electrons of RE with the electrostatic crystal field created by the ligand ions.

In order to apply quantum mechanical perturbation theory, the free ion term is usually written as^[59]

$$H_{FI} = H_O + H_{ee} + H_{SO} \quad (4.2)$$

where H_O is the central field Hamiltonian which reflects the electric field acting on the valence electrons due to the nucleus and the inner- and outer-shell electrons, H_{ee} takes into account any perturbation due to the Coulomb interactions among the valence electrons, and H_{SO} represents the spin-orbit interaction summed over these electrons.

Depending on the size of the crystal field term H_{CF} in comparison to these three free ion terms, different approaches can be considered of which the weak crystalline field approach describes the energy levels of the trivalent RE ions.

4.2.2. Weak crystalline field:^[59]

$H_{CF} \ll H_{SO}, H_{ee} \text{ \& } H_O$. The energy levels of the free ion RE are only slightly perturbed (shifted and split) by the crystalline field. The free ion wave-functions are then used as basis functions to apply perturbation theory, H_{CF} being the perturbation Hamiltonian over the $^{2S+1}L_J$ states. The shielding of the 4f valence electrons is considered to describe the energy levels of the RE ions using this approach. Consequently, the spin – orbit interaction term of the free ion Hamiltonian is dominant over the crystalline field Hamiltonian term. This causes the $^{2S+1}L_J$ states of the RE ions to be slightly perturbed when these ions are incorporated in crystals. The effect of the crystal field is to produce a slight shift in the energy of these states and to cause additional level

splitting. However, the amount of this shift and the splitting energy are much smaller than the spin-orbit splitting, and thus, the optical spectra of RE^{3+} ions are fairly similar to those expected for free ions. Moreover, this implies that the main features of a RE^{3+} ion spectrum are similar from one crystal to another.^[59]

4.3. Rare earth doped sol gel glasses- preparation:

4.3.1. General trends:

The most important reagent in sol gel process is a metal alkoxide, $M(OR)_x$, where OR is an alkoxy^{*} group. Tetraethyl orthosilicate ($Si(OC_2H_5)_4$ or tetraethoxysilane, or silicon tetraethoxide, TEOS) is an alkoxide precursor commonly used for preparing sol gel materials. The basic chemical reactions contain the following steps:

1. hydrolysis of the alkoxide precursor

Metal alkoxides are popular precursors because they react readily with water. The reaction is called hydrolysis, because a hydroxyl ion becomes attached to the metal atom, as in the following reaction:^[14]



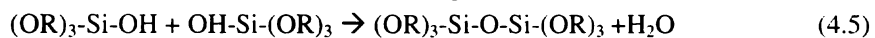
R is an alkyl[†] group and $R(OH)$ is an alcohol[‡]. Depending on the amount of water and catalysts present, hydrolysis may go to completion,



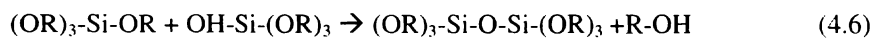
or stop while it is only partially hydrolysed, $Si(OR)_{4-n}(OH)_n$.

2. condensation reaction:

Two partially hydrolysed molecules can link together in a condensation reaction such as,



or



3. polymerisation:

The condensation liberates water or alcohol. This condensation reaction grows, and more Si-O-Si bonds are formed. As polymerisation continues, the viscosity of the solution increases until a solid gel is formed.

Silicate gels are most often synthesised by hydrolysing monomeric, tetrafunctional alkoxide precursors employing a mineral acid (e.g., HCl) or base (e.g., NH_3) as a catalyst. At the functional group level three reactions are generally used to describe the sol gel process:

* A ligand formed by removing a proton from the hydroxyl on an alcohol.

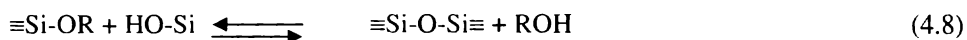
† An alkyl is a ligand formed by removing one hydrogen (proton) from an alkane (molecule containing only carbon and hydrogen linked exclusively by single bonds) molecule.

‡ An alcohol is a molecule formed by adding a hydroxyl (OH) group to an alkyl (or other) molecule.



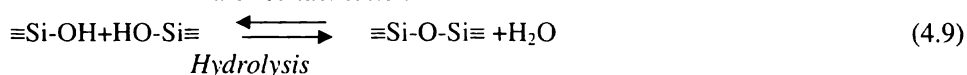
Esterification

Alcohol condensation



Alcoholysis

Water condensation



Hydrolysis

where R is an alkyl group, $\text{C}_x\text{H}_{2x+1}$. The hydrolysis reaction (4.7) replaces alkoxide groups (OR) with hydroxyl group (OH). Subsequent condensation reactions involving the silanol groups produce siloxane bonds (Si-O-Si) plus the by-products, alcohol (ROH) or water. Under most conditions, condensation commences before hydrolysis is complete. Because water and alkoxysilanes are immiscible, a mutual solvent such as alcohol is normally used as a homogenising agent. However, gels can be prepared from silicon alkoxide- water mixtures without added solvent,^[60] since alcohol produced as the by-product of the hydrolysis reaction is sufficient to homogenise the initially phase separated system. As indicated in (4.7& 4.8), alcohol can also participate in esterification and alcoholysis reactions.^[14]

Numerous investigations have shown that variations in the synthesis conditions, for e.g., the value of the $\text{H}_2\text{O}:\text{Si}$ molar ratio, the catalyst type and concentration, the solvent, temperature, and pressure, cause modifications in the structure and properties of the polysilicate products.^[14] The higher values of $\text{H}_2\text{O}:\text{Si}$ molar ratio cause more complete hydrolysis of the monomers before significant condensation occurs. The increased values of $\text{H}_2\text{O}:\text{Si}$ molar ratio generally promote hydrolysis. When $\text{H}_2\text{O}:\text{Si}$ molar ratio is increased while maintaining a constant solvent: silicate ratio, the silicate concentration is reduced. This in turn reduces the hydrolysis and condensation rates, causing an increase in the gel time.^[14] Large values of $\text{H}_2\text{O}:\text{Si}$ molar ratio cause liquid-liquid immiscibility. However, both alcohol produced as the by-product of the hydrolysis reaction and partial hydrolysis of the TEOS precursor lead to homogenisation. Because water is the by-product of the condensation reaction (4.9), large values of $\text{H}_2\text{O}:\text{Si}$ molar ratio promote siloxane bond hydrolysis.^[14]

Solvents are added to prevent liquid-liquid phase separation during the initial stages of the hydrolysis reaction and to control the concentrations of silicate and water that influence the gelation kinetics. More polar solvents are used to solvate polar, tetra-

functional silicate species used in the sol gel processing.^[14] Under acidic conditions, an alkoxide group may be rapidly protonated. Electron density is withdrawn from silicon, making it more electrophilic and thus more susceptible to attack by water.^[14]

Polymerisation to form siloxane bonds occurs by either an alcohol-producing (4.8) or a water-producing (4.9) condensation reaction. When gelation occurs, a solution suddenly loses its fluidity and takes on the appearance of an elastic solid.^[14]

The processes of change during ageing after gelation are categorised as polymerisation, coarsening and phase transformation. Polymerisation is the increase in connectivity of the network produced by condensation reactions. Coarsening or ripening is a process of dissolution and re-precipitation. The condensation in silica gels continues long after gelation, because of the large concentration of the hydroxyl groups. By creating new bridging bonds, such reactions stiffen and strengthen the network. In addition to condensation, ageing can result in further hydrolysis or in the reverse reaction, re-esterification.^[14]

The drying process of a porous material is divided into several stages. First, the body shrinks by an amount equal to the volume of the liquid that evaporates, and the liquid-vapour interface remains at the exterior surface of the body. Then the body becomes too stiff to shrink and the liquid recedes into the interior, leaving air-filled pores near the surface. Even as air invades the pores, a continuous liquid film supports flow to the exterior, so evaporation continues to occur from the surface of the body. Eventually, the liquid becomes isolated into pockets and drying can proceed only by evaporation of the liquid within the body and the diffusion of the vapour to the outside.^[14]

Although homogeneity is frequently cited as a feature of sol gel processing, it is often not achieved until the gel is sintered[§] or even melted. Generally the scale of heterogeneity is small enough so that homogeneous ceramics are readily prepared at relatively low temperatures and short firing times. Low processing temperature may permit fabrication of homogeneous glasses that cannot be made by melting.^[14] The properties of a glass depend on thermal history (e.g. cooling rate, annealing time) and

[§] Sintering is a process of densification driven by interfacial energy. Material moves by viscous flow or diffusion in such a way as to eliminate porosity and thereby reduce the solid-vapour interfacial area.^[14]

can vary over a wide range. *Figure 4.1* shows the schematic representation of sol gel process for glass preparation.^[13] The highest temperature required to obtain a silica glass prepared by sol gel method is about 1000 °C, which is lower by about 1000 °C compared to the temperature required for the melt-quenching process.^[13]

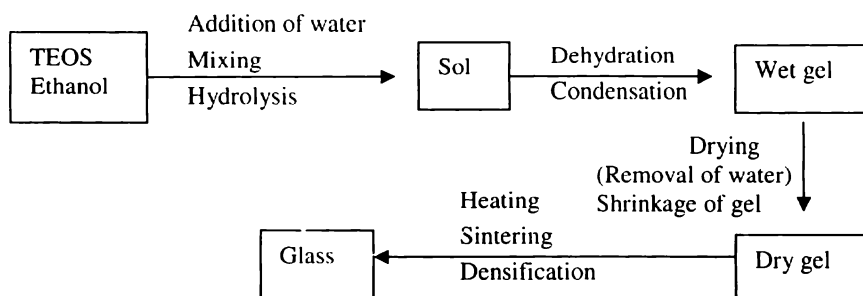


Figure 4.1: Schematic illustration of sol gel process for glass preparation.

4.3.2. Sample preparation details:

The preparation of the RE doped sol gel glasses is similar to the method given by Vinoy et al.^[49] The RE doped silica glasses of different weight percentage were prepared. Water soluble acetates (the Indian Rare Earths Ltd, 99.9%) of the REs (RE= La, Y, Dy, Tb and Nd) and nitrates of Er and Yb (Aldrich, 99.9%) were taken for obtaining the weight percentages of 0.1, 0.5, 1.0, 1.5 and 2.0 in the glass. The sol gel glasses were prepared by mixing TEOS (Fluka, assay \geq 99.0%), ethanol (Hayman Ltd. AR grade 99.9%), double distilled water and HCl (Nice chemicals) in the ratio 1: 4: 14: 0.01 respectively. TEOS and ethanol were magnetically stirred thoroughly till both were in well-mixed state. To this, a part of water, in which the RE was dissolved, was added and magnetic stirring was done again. To this well-mixed solution the remaining water was added in which the desired acid was mixed. Again the solution was magnetically stirred to get a clear solution. The sols were cast in polypropylene dishes and were sealed to avoid intercalation of external impurity. The gels were aged for one month at room temperature to obtain the RE doped sol gel.

Fluorescence decay may occur at high concentrations of REs due to the formation of clusters. Lifetime may be shortened if the water content is not reduced to very low concentrations during drying and densification processes.^[17] Hence, the samples taken in silica crucibles were sintered at three temperatures 500, 600 and 700 °C for 3hrs. The furnace was programmed (Eurotherm, 902-904 Controller/ Programmer) to raise the temperature at a rate of 1°C per minute and the samples were kept at the desired temperature for 3 hrs and then the furnace was cooled to room temperature at a rate of

0.5 °C per minute. The removal of the residual organics can be achieved by thermal treatment in an oxidising atmosphere in the temperature range 300 to 500 °C.^[52]

When gel powders were heated to obtain dense glass, independently of whether or not monolithic formation takes place, this could result in a lower crystallisation temperature and faster nucleation and crystallisation rates relative to melted glasses.^[61] These differences have been attributed to the lower viscosity of the gel powder caused by the higher hydroxyl content^[62] and to the excess free energy due to the larger interior surface and structural differences.^[63, 64]

4.4. Section I- Optical studies:

4.4.1. Preamble:

Atomic spectroscopic techniques provide useful and specific means for the determination of the RE elements at the trace, minor, and major constituent levels. Even though the chemical properties of the elements may be remarkably similar, the energy states within each atomic system are just as uniquely different for the individual RE elements as they are for other elements. As a consequence, the spectra produced by energy transitions between these states are also highly specific.^[65]

Optical properties of RE doped glasses are widely investigated for potential photonic applications.^[66] Glass hosts activated with REs have much wider emission bands and hence provide better opportunities for tuning and Q switching.^[8, 67] Since optical spectroscopy provides an excellent tool to obtain information on the electronic structure of the absorbing/emitting centers, their lattice locations, and their environments; it allows to 'look inside' samples by analysing the emerging light.^[59]

In the present section, the optical absorption and luminescence studies carried out on the samples under investigation are described. As these studies are strongly correlated, they are presented together. Since, there are already a lot of works in this regard, only a few of the spectra of the samples are provided to give an insight into the status of the samples in the present study.

4.4.2. Energy level diagram of the rare earth ions:

The energy level diagrams of the lanthanide REs under the present study are given in *Figure 4.2*. Some of the major peaks observed are denoted by the transitions and the corresponding wavelengths are also given. This diagram is derived from the original Dieke diagram^[68] to give an idea of the energy levels involved in the present studies.

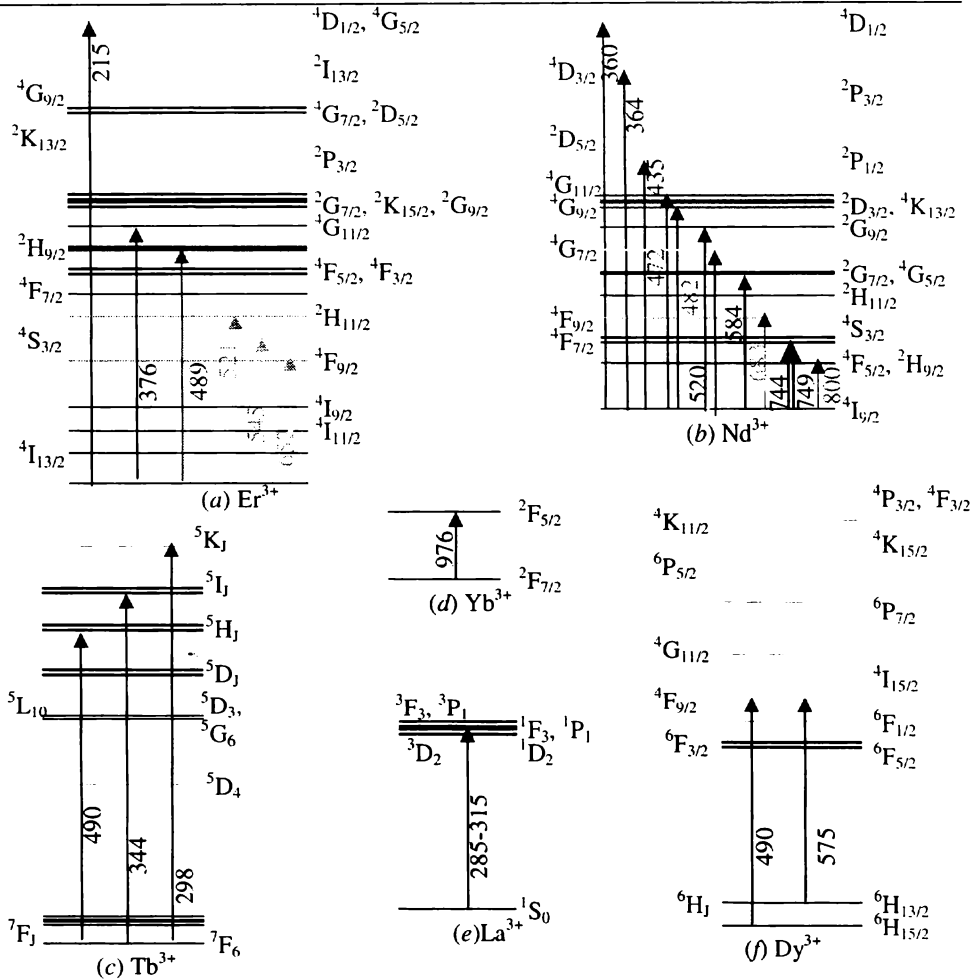


Figure 4.2: Energy level diagram and the main absorption transitions of the lanthanide rare earths (REs) used in the present study. (a) Er³⁺, (b) Nd³⁺, (c) Tb³⁺, (d) Yb³⁺, (e) La³⁺ and (f) Dy³⁺. The energy level diagram of Y³⁺ is not given as it does not belong to lanthanides.

4.4.3. Absorption studies:

The absorption spectra of the RE doped sol gel glasses shown in figures were recorded using JASCO V570 UV/VIS/NIR spectrophotometer. Significant peaks of the REs are observed in their corresponding spectra.

Figure 4.3 shows the absorption spectra of the 2.0% Er doped glasses sintered at three temperatures. They show major peaks of Er which are already reported. The absorption spectra of other RE doped glasses with 2.0%, sintered at 700 °C are as shown in Figure 4.4 and Figure 4.5. The spectrum of silica is also shown in Figure

4.4. However, major peaks of Tb and Dy in the visible region are not observed in their absorption spectra which may be due to the insufficiency of the concentration of their ions in the silica matrices.

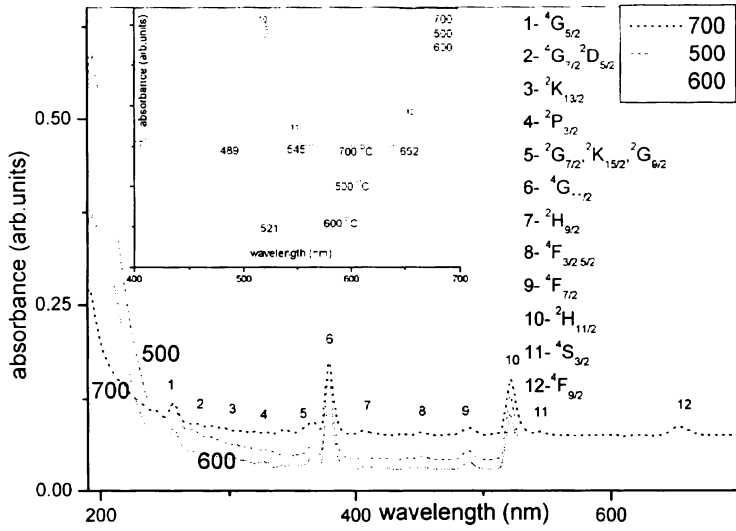


Figure 4.3: Absorption spectra of 2.0% Er doped sol gel silica glasses sintered at 500 °C, 600 °C and 700 °C. Inset: Spectra in the visible range.

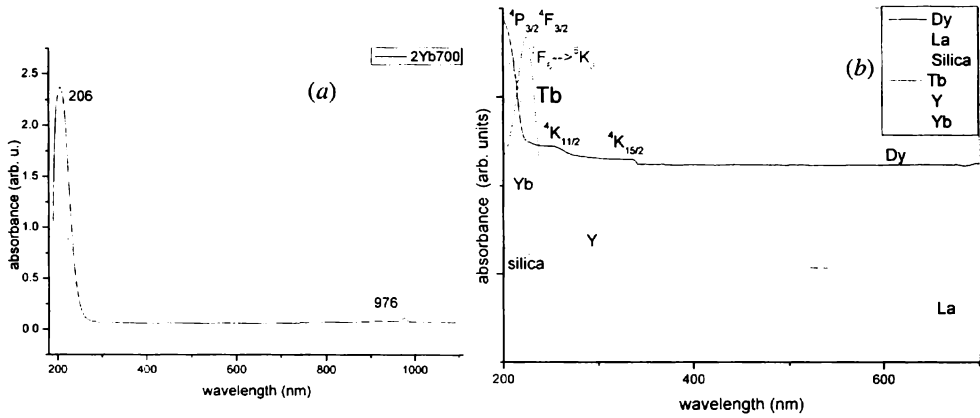


Figure 4.4: Absorption spectra of rare earth (RE) doped sol gel glass samples with RE weight percentage 2.0 and sintered at 700 °C. (a) Yb³⁺ (b) RE= Dy, La, Tb, Y, Yb and pure silica.

4.4.4. Excitation and emission studies:

Luminescence is, in some ways, the inverse process to absorption. The photoluminescence (PL) spectra are usually recorded using a spectrofluorimeter.^[59] Varian Cary Eclipse spectrofluorimeter was used to register the emission and excitation spectra of the samples in the present investigation. The excitation spectrum

of Dy and Tb showed some of the prominent peaks which were not observed in their absorption spectra (Figure 4.4b). Figure 4.6 shows the excitation spectra of 2.0% Tb doped sol gel glass with two emission wavelength peaks 421 nm and 545 nm which are in good agreement the previous studies.^[69] The PL spectra of 2.0% all RE samples doped sol gel glasses with 255 nm excitation (Figure 4.7) show PL near 421 nm as in the case of montmorillonite dispersions. The absorption peak near 370 nm as observed in the case of montmorillonites is not seen in the absorption spectra of the samples, but all the samples have absorption at 255 nm. Moreover, the excitation spectra of many of the samples with 421 nm emission line have shown the excitation peak near 375 nm similar to montmorillonite dispersions. However, a quantitative study as in the case of montmorillonites was not done as the samples were of various thicknesses and there were alignment difficulties in the spectrofluorimeter for the solid samples.

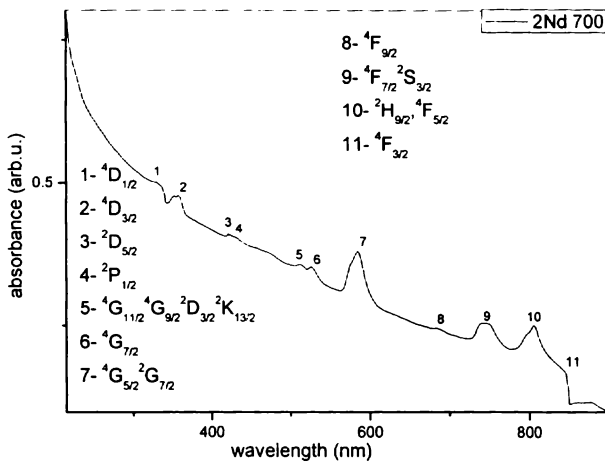


Figure 4.5: Absorption spectra of 2.0% Nd doped sol gel silica glass sintered at 700 °C.

4.4.5. Results and discussions:

The absorption and fluorescence studies verified the REs used in the present study. These spectra showed the prominent peaks of the corresponding REs which are discussed in detail in the following sub-sections. However, all these samples showed luminescence near 421 nm for the excitation wavelength at 255 nm (Figure 4.7). But, their quantitative measurement was not done as their thickness was non-uniform. The excitation spectrum of these samples showed a peak near 375 nm with the fixed emission line near 421 nm. These peaks are attributed to the silica in the network as in the case of montmorillonite. However, it was reported by many researchers that UV excitation on silica produced blue luminescence in the 400-500 nm range.^[70-73] The luminescence intensity variations in the RE doped glasses as observed here is

attributed to the change in the environment of the defect centers due to the incorporation of RE ions and the superposition of 4f-f transitions of REs.^[70]

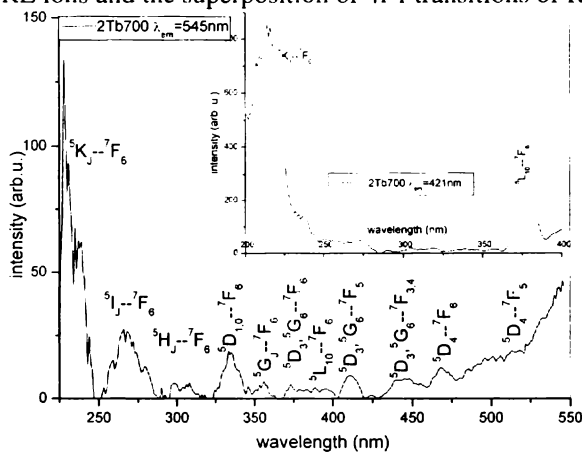


Figure 4.6: Excitation spectra of 2.0% Tb doped sol gel silica glass sintered at 700 °C with emission wavelength fixed at 545 nm and (in inset :) at 421 nm.

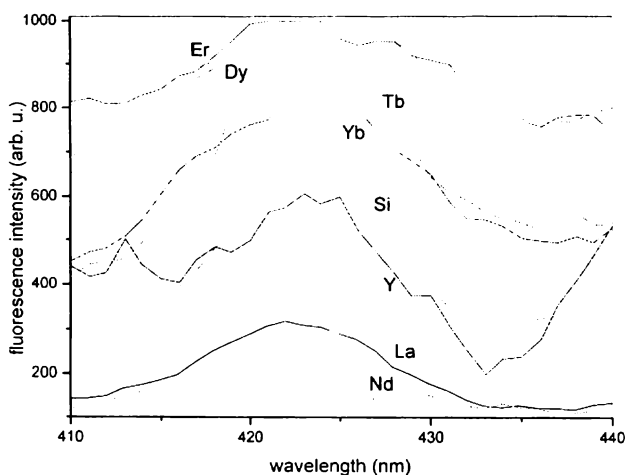


Figure 4.7: Emission spectra of 2.0% RE doped sol gel silica glasses sintered at 700 °C with 255 nm excitation.

4.4.5.1. La³⁺ and Y³⁺:

Both La³⁺ and Y³⁺ have no electrons in their 4f orbitals and have the ground state as ¹S₀. There is no known absorption peaks for them in the visible region.^[74] However, the excited states of lanthanum can arise from a p-d transition leading to the electronic configuration: 5s²5p⁵5d¹ which gives rise to the singlet ¹P₁, ¹D₂ and ¹F₃ and the triplet ³P₁, ³D₂ and ³F₃ states. These states are responsible for the peaks in the UV region in the spectrum^[75] as observed in *Figure 4.4b*.

4.4.5.2. Yb³⁺:

The direct excitation of the Yb³⁺ is difficult since it requires a comparatively short wavelength UV radiation. Interest in Yb doped silicate optical fibers is significant because of their use in high power fiber lasers with higher energy conversion efficiency compared to Nd. However, a clear relation is observed when the glass is exposed to radiation resonant with the f–f transitions of the RE ion. The Yb ion is known to be multivalent in several host materials, and there have been suggestions that a changed valence state of the RE ion could be part of the photo-darkening process in RE doped materials.^[76, 77] The valence state of Yb has been extensively studied in various crystal hosts.^[78, 79] The Yb³⁺ ion has only one f–f transition located near 10,000 cm⁻¹, and 4f¹³→4f¹² 5d transitions are usually located well above 50,000cm⁻¹.^[80, 81] This appears as a broad absorption band near the UV region^[81] as in *Figure 4.4a* and *Figure 4.8*. The 376 nm excitation peak of the silica is also observed as is evident from *Figure 4.8*.

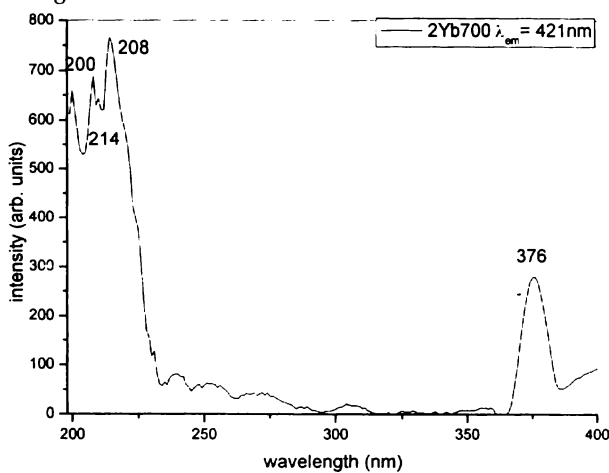


Figure 4.8: Excitation spectra of 2.0% Yb doped sol gel silica glass sintered at 700 °C with emission wavelength fixed at 421 nm.

4.4.5.3. Tb³⁺:

Typical Tb activated phosphors always show strong 4f-5d transition band absorption around 200-300 nm.^[82] The luminescence of Tb activated silicate glasses was already studied.^[69] Tb doped samples have an absorption band near 252 nm.^[83] This band is assigned to the 4f⁸→4f⁷5d transition.^[84] Other low intensity bands are assigned as 7F₆→5H₆, 5H₇, 5D₂, 5L₁₀ and 5D₃ transitions.^[83, 85] All these bands are observed in the excitation and absorption spectra of the Tb doped glass (*Figure 4.4b* & *4.6*).

4.4.5.4. Er³⁺:

The major transition levels of Er³⁺ are presented in *Figure 4.2a* and are observed in the absorption (*Figure 4.3*), emission and excitation spectra (*Figure 4.9*) of the 2.0% samples. Here also an excitation peak is observed at 376 nm for the fixed emission line 421 nm which is again attributed to the silica matrix. The transition peaks are also assigned in the corresponding graphs.

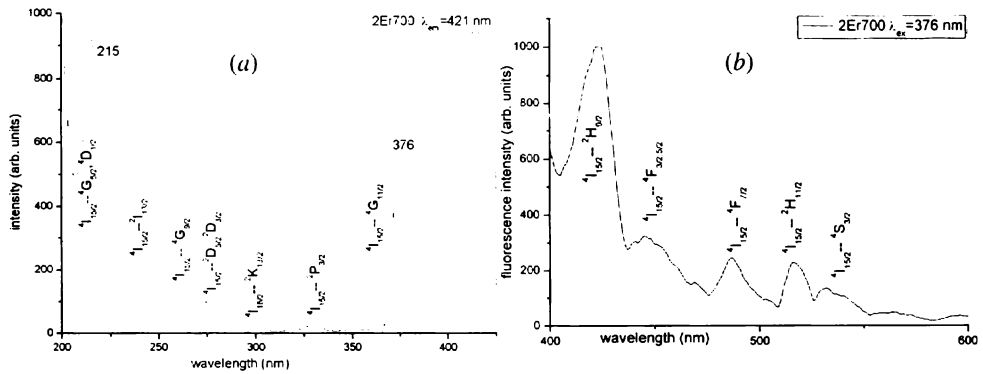


Figure 4.9: (a) the excitation spectrum with 421 nm emission and (b) the emission spectrum with 376 nm excitation for 2.0% Er³⁺ doped sol gel silica glass sintered at 700 °C.

4.4.5.5. Nd³⁺:

Neodymium-doped silica glass possesses many properties ideal for high-power laser applications. These include low thermal expansion coefficient, high temperature stability, and low nonlinear index of refraction. Silica has a high softening temperature, high thermal shock resistance, low thermal expansion coefficient, and low nonlinear index of refraction, and Nd doped silica is an ideal candidate for high-power laser applications.^[86] The absorption spectra of the Nd doped glass are given in *Figure 4.5* and the peaks are assigned according to the available literature.^[68]

4.4.5.6. Dy³⁺:

Dysprosium has the well-known strong fluorescence in the visible spectral range around 480 and 570 nm,^[87] which is also observed in the present study, but not presented here. Dy offers a rather dense energy level scheme in the IR region.^[88] However, in the absorption spectrum, only some peaks near UV region are obtained (*Figure 4.4b*), which may be due to the insufficiency of the concentration of Dy³⁺ ions in the sol gel silica matrix.

4.4.6. Concluding remarks:

All the samples show fluorescence near 421 nm as in the case of montmorillonites which is described in the second chapter and is attributed to the silica present in the sol gel glasses. The samples excited with UV radiation near 255 nm and 376 nm has fluorescence near 421 nm. Moreover, most of the REs used in the present study have transitions near 421 nm and 376 nm. However, slight differences from the spectra of montmorillonite dispersions are observed because in the present case the host matrix is solid while in montmorillonites the spectra arise from their aqueous dispersions. Hence, a detailed experimental work is necessary to quantify the exact efficiency of the luminescence and how the various REs are affecting this luminescence. Thus, further characterizations are essential to use them as potential blue phosphors.

4.5. Section II- Thermal characterization using photoacoustics:

4.5.1. Preamble:

Determination of thermal properties is a useful tool in the study of materials and processes.^[89] The photoacoustic (PA) technique has proven to be a valuable method for the thermal characterization of a wide range of materials as described in the previous chapters.

Dry gels have high porosity and silica gels have good transparency. This is related to their texture which is composed of solid colloidal particles and pores which have a size smaller than the visible light wavelengths. The high proportion of non-bridging bonds in gels produces a very high coefficient of thermal expansion.^[90, 91] The glasses prepared by sol gel process differed from fused silica only in that it had higher OH content and hence higher non-radiative decay.^[13] Yamane et al.^[92] observed that silica gels heated only to 900 °C were identical to silica in density, refractive index, hardness, thermal expansion, and modulus.^[14] The properties of glasses prepared by the sol gel method are very much dependent on the precursors, reaction conditions and subsequent heat treatment.^[27, 93]

Usually, molecular and chemical variations of the solution depend on the following factors:^[94]

- ∞ Structure and chemical reactivities and sequence adding reactants.
- ∞ Nature of solvents and solubility of reactants in the solvents.
- ∞ Concentration of water and sequence of addition.
- ∞ pH of the reaction medium or presence of catalysts.
- ∞ Time and temperature of reactions.

In the present section an attempt is made to evaluate the thermal properties of the samples prepared by sol gel method and sintered at temperatures 500, 600 and 700 °C. Prior to the experiment the cell was calibrated using copper and aluminium samples.

4.5.2. Part A: Thermal effusivity (TE) measurement:

The detailed theoretical treatment for the effusivity measurement is given in detail in *chapter 3*. The signal with and without the sample is used to plot the normalised signal versus various chopping frequencies. The relation 3.18,

$\frac{\delta Q_1}{\delta Q_2} \propto \frac{l_o k_o}{\alpha_o} \frac{\sqrt{\alpha_s}}{k_s} f^{1/2}$, can be used to obtain the TE of the samples. $\frac{\sqrt{\alpha_s}}{k_s}$ is the inverse of TE of the sample.^[95]

4.5.2.1. Experimental:

The experimental set up for measuring the TE of the samples was similar to that given in *chapter 3*, F2, with an exception that the source of excitation was a CW DPSS laser (BWT-50) emitting radiations at 532 nm with a power of 50 mW. All the samples have a thickness less than 1 mm.

4.5.2.2. Results and discussions:

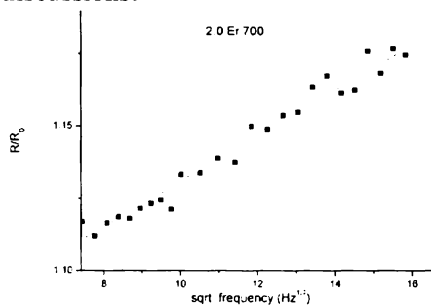


Figure 4.10: The normalised photoacoustic (PA) amplitude plot in respective of 2.0% Er doped sol gel silica glass sintered at 700 °C for thermal effusivity (TE) measurement.

Figure 4.10 shows a typical representation of the normalised amplitude plot of PA signal for the measurement of TE of Er doped sol gel glass samples. All the other samples show a similar trend. The TE values of the samples, which are obtained using the relation (3.18), are given in tables (Table 4.1- Table 4.8). TE values did not give any specific trend with regard to the doping level or sintering temperature. This may be due to the fact that the measurements were carried out on samples which were not completely transformed to glass. The samples may be in a state in between the xerogel

Rare earth doped sol gel glass

and glass because the gels heated to 900 °C are usually similar to silica.¹⁹²¹ Moreover, the thermal values of the samples are extremely dependent on the conditions and method of preparation. Hence, the present investigation can provide only some general idea about the TE values of the RE doped sol gel silica glasses. More precise experimental works have to be carried out to characterise these samples to get the exact values and explain their observed behaviour.

Table 4.1: Thermal effusivity (TE) values ($Ws^{-1/2}m^{-2}K^{-1}$) obtained for the Er doped sol gel glasses with various Er weight percentages and sintering temperatures using photoacoustics.

Wt percentage →	0.1 Er	0.5 Er	1.0 Er	1.5 Er	2.0 Er
Sintering temp ↓					
500 °C	1031	1237	853	950	4123
600 °C	3534	728	990	853	1302
700 °C	3534	2249	4123	2062	3093

Table 4.2: Thermal effusivity (TE) values ($Ws^{-1/2}m^{-2}K^{-1}$) of the Dy doped sol gel glasses for various Dy weight percentages and sintering temperatures using photoacoustics.

Wt percentage →	0.1 Dy	0.5 Dy	1.0 Dy	1.5 Dy	2.0 Dy
Sintering temp ↓					
500 °C	6185	2749	2474	3534	884
600 °C	2749	3534	2474	4123	3093
700 °C	3093	634	2749	2062	1302

Table 4.3: Thermal effusivity (TE) values ($Ws^{-1/2}m^{-2}K^{-1}$) of the Yb doped sol gel glasses for various Yb weight percentages and sintering temperatures using photoacoustics.

Wt percentage →	0.1 Yb	0.5 Yb	1.0 Yb	1.5 Yb	2.0 Yb
Sintering temp ↓					
500 °C	2062	2474	1649	2474	505
600 °C	990	990	1374	990	884
700 °C	1076	884	575	1031	773

Table 4.4: Thermal effusivity (TE) values ($Ws^{-1/2}m^{-2}K^{-1}$) of the Y doped sol gel glasses for various Y weight percentages and sintering temperatures using photoacoustics.

Wt percentage →	0.1 Y	0.5 Y	1.0 Y	1.5 Y	2.0 Y
Sintering temp ↓					
500 °C	1031	1237	1124	8247	1546
600 °C	1767	2749	2474	728	853
700 °C	4123	798	1455	884	1302

Table 4.5: Thermal effusivity (TE) values ($Ws^{-1/2}m^{-2}K^{-1}$) of the Tb doped sol gel glasses for various Tb weight percentages and sintering temperatures using photoacoustics.

Wt percentage →	0.1 Tb	0.5 Tb	1.0 Tb	1.5 Tb	2.0 Tb
Sintering temp ↓					
500 °C	916	1031	687	1125	1767
600 °C	1076	1178	2749	1178	916
700 °C	651	1178	4948	8264	526

Table 4.6: Thermal effusivity (TE) values ($Ws^{-1/2}m^{-2}K^{-1}$) of the Nd doped sol gel glasses for various Nd weight percentages and sintering temperatures using photoacoustics.

Wt percentage →	0.1 Nd	0.5 Nd	1.0 Nd	1.5 Nd	2.0 Nd
Sintering temp ↓					
500 °C	3534	1302	798	1455	651
600 °C	3092	1767	1076	1767	3534
700 °C	1546	1455	1903	1546	2748

Table 4.7: Thermal effusivity values ($Ws^{-1/2}m^{-2}K^{-1}$) of the La doped sol gel glasses for various La weight percentages and sintering temperatures using photoacoustics.

Wt percentage →	0.1 La	0.5 La	1.0 La	1.5 La	2.0 La
Sintering temp ↓					
500 °C	1767	2749	1546	1649	1649
600 °C	1546	1076	4948	2062	1767
700 °C	1903	2249	1374	1649	990

Table 4.8: Thermal effusivity (TE) values ($Ws^{-1/2}m^{-2}K^{-1}$) of the pure sol gel glasses for various sintering temperatures using photoacoustics.

Sintering temp ↓	silica
500 °C	4124
600 °C	8247
700 °C	6185

It is evident from these tables that almost all lanthanide doped sol gel glasses presented here have lower TE than the undoped sol gel silica glass. From the TE values obtained for these samples, it may be difficult to give a solid conclusion. However, the variations in TE values may be arising due to the strong dependence of the samples on the various preparation stages, preparation conditions, thermal history and doping levels.

4.5.3. Part B: Thermal diffusivity (TD) of erbium doped glasses:

Er^{3+} doped silica glass is of particular interest because the electronic transition of Er^{3+} from $^4\text{I}_{13/2}$ to $^4\text{I}_{15/2}$ emits light at a wavelength of 1.53 μm , which is outside the range of wavelengths focused on the retina of the human eye,^[96, 97] and is close to the wavelength of minimum loss window of silica glass.^[96, 98] This wavelength is used in the application of optical fibers and fiber amplifiers for optical communications.^[99] In addition, Yb^{3+} codoped Er^{3+} doped silica glasses are used as active elements providing laser wavelengths in the blue and green regions.^[96, 100] Er^{3+} doped silica fibers, fiber amplifiers and wave-guides have wide commercial uses due to their superior qualities. Optical fibers have demonstrated to be efficient with a low Er^{3+} doping.^[101] For planar optical wave-guide amplifiers, however, due to a short optical interaction path, a high Er^{3+} doping concentration is needed to obtain sufficient optical amplification gains.^[111]

The thermal diffusivity (TD) measurement of Er doped sol gel glasses is presented. These glasses have absorption near 488 nm and 532 nm, which are the wavelengths used in the present study. The innumerable applications of the Er doped materials have prompted us to consider the measurement of the TD values of the sintered Er doped samples with different weight percentages.

4.5.3.1. Experimental:

The TD measurements were carried out using argon ion laser (Liconix 5300) and DPSS laser (BWT-50, 50mW, CW, 532nm), the details of which were given earlier in *chapter 3, E2*. Both reflection and transmission mode geometry of the PA set up were used to obtain the TD values.

4.5.3.2. Results and discussions:

A typical representation of the amplitude plot for TD measurement in the reflection mode geometry using argon ion laser is shown in *Figure 4.11*. The TD values are obtained using the characteristic frequency obtained from the plot and the relation $\alpha = l^2 f_c$. The TD values are tabulated in *Table 4.9*. In this case, an absorbing Al layer of thickness 10 μm was used as backing as it is commonly available.

The experiments were repeated for samples using DPSS laser both in reflection and transmission geometry without any absorbing layer as backing. The typical amplitude and phase plots of the samples are given in *Figure 4.12*. The TD values are obtained

using the relation^[102] $\alpha = l^2 \pi / \text{slope}^2$, and are tabulated in *Table 4.10*, where l represents the sample thickness. From these TD values, it can be concluded that there is not much variation in TD values with and without an absorbing layer. All methods used for TD measurement give the TD values of the same order. The TD values of the Er doped sol gel glass samples do not have a common trend as it is observed from the *Table 4.9* and *Table 4.10*. The only exception observed is in *Table 4.9* with the samples sintered at 500 °C, where the TD values increase with the increase in weight percentage of the Er added.

Table 4.9: Thermal diffusivity (TD) values of the pure and Er doped sol gel glasses for various Er weight percentages and sintering temperatures using the reflection mode geometry of the photoacoustics technique with **argon ion laser** as source of excitation.

Sintering temperature →	500 °C		600 °C		700 °C	
Sample ↓	Thickness* (×10 ⁻⁴ m)	TD×10 ⁻⁵ (m ² s ⁻¹)	Thickness* (×10 ⁻⁴ m)	TD×10 ⁻⁵ (m ² s ⁻¹)	Thickness* (×10 ⁻⁴ m)	TD×10 ⁻⁵ (m ² s ⁻¹)
Silica	5.53	1.87	9.54	9.41	8.65	7.04
0.1 Er	4.36	1.00	5.52	2.00	5.19	1.88
0.5 Er	4.91	1.40	6.49	3.05	4.35	1.50
1.0 Er	6.59	2.95	6.52	2.76	6.02	2.50
1.5 Er	8.13	4.39	8.42	4.08	5.08	3.01
2.0 Er	10.87	8.45	5.70	2.38	5.75	1.72

*The sample thickness has an accuracy of 0.01×10⁻⁴ m

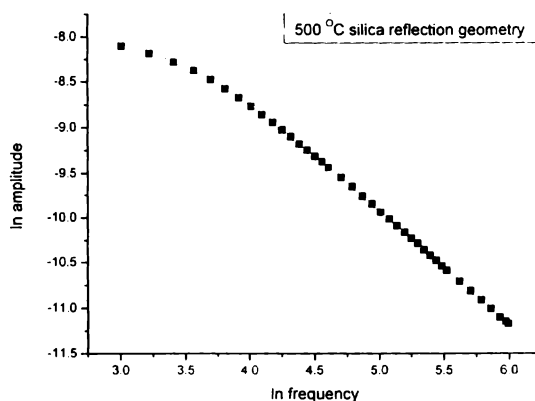


Figure 4.11: Photoacoustic (PA) amplitude plot for the thermal diffusivity (TD) measurement of pure silica samples sintered at 500 °C in the reflection geometry.

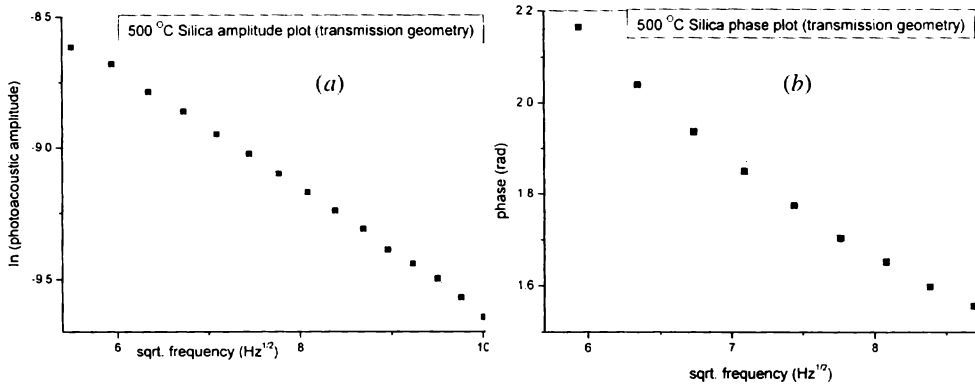


Figure 4.12: Photoacoustic (PA) (a) amplitude (b) phase plot for the thermal diffusivity (TD) measurement of pure silica samples sintered at 500 °C in the transmission geometry.

Table 4.10: Thermal diffusivity (TD) values of the pure and Er doped sol gel glasses for various Er weight percentages and sintering temperatures using photoacoustics with DPSS laser as source of excitation.

temperature →	500 °C				600 °C				700 °C			
Samples ↓	Thickness* ($\times 10^{-4}$ m)	TD $\times 10^{-5}$ ($m^2 s^{-1}$)			Thickness* ($\times 10^{-4}$ m)	TD $\times 10^{-5}$ ($m^2 s^{-1}$)			Thickness* ($\times 10^{-4}$ m)	TD $\times 10^{-5}$ ($m^2 s^{-1}$)		
		TG [#] (amp)	TG [#] (phase)	RG ⁺ (amp)		TG [#] (amp)	TG [#] (phase)	RG ⁺ (amp)		TG [#] (amp)	TG [#] (phase)	RG ⁺ (amp)
Silica	6.16	2.25	2.63	2.21	9.97	6.63	3.13	7.47	9.92	7.01	2.58	6.29
0.1 Er	4.87	1.42	0.80	1.41	4.93	1.59	0.97	1.75	5.33	1.27	0.76	1.03
0.5 Er	5.20	1.63	0.91	1.60	7.42	4.59	2.46	4.03	4.31	1.36	0.77	1.44
1.0 Er	6.43	3.41	1.26	2.22	6.11	3.15	1.85	2.01	7.49	3.27	2.30	4.13
1.5 Er	5.33	1.34	1.83	1.55	8.85	4.31	2.61	5.04	5.36	1.80	1.07	2.62
2.0 Er	13.06	8.85	11.80	11.04	7.57	15.43	3.07	3.48	6.24	2.42	1.39	2.63

*The sample thickness has an accuracy of 0.01×10^{-4} m.

⁺RG- Reflection Geometry, [#]TG- Transmission Geometry.

The TD values of some of the other samples are also tabulated in Table 4.11 and Table 4.12. All samples have reasonably high TD values. The thermal conductivity values obtained for the 2.0% RE doped samples are also calculated and tabulated in Table 4.13. The TD values of Er and Nd doped sol gel glass samples are given separately as they are the most commonly used REs in many photonic applications. From Table 4.10-4.12, it may be concluded that the sol gel glass samples sintered at 700 °C with 2.0% weight of the dopant RE have a decrease in TD as their ionic radius decreases

due to 'lanthanide contraction'. It was reported earlier that the particle size of the samples can affect the TD and thermal conductivity values.^{1103, 1041}

Table 4.11: Thermal diffusivity (TD) values of the 2.0% rare earth doped sol gel glasses for various sintering temperatures using photoacoustics with **DPSS laser** as source of excitation.

Sintering temperature →	500 °C		600 °C		700 °C	
Sample ↓	Thickness* (×10 ⁻⁴ m)	TD×10 ⁻³ (m ² s ⁻¹)	Thickness* (×10 ⁻⁴ m)	TD×10 ⁻³ (m ² s ⁻¹)	Thickness* (×10 ⁻⁴ m)	TD×10 ⁻³ (m ² s ⁻¹)
2.0 Y	10.25	6.46	11.04	6.70	12.14	12.05
2.0 La	7.06	3.99	11.53	9.56	12.87	13.13
2.0 Dy	5.06	1.84	12.10	10.4	8.45	4.39
2.0 Tb	12.15	11.25	13.38	10.63	8.57	4.56
2.0 Yb	7.64	4.77	4.34	1.37	4.28	1.30

*The sample thickness has an accuracy of 0.01×10⁻⁴ m

The TD values are somewhat higher than the values available in the literature.^{1105]} However, the thermal conductivity values of some of the samples are close to that of glasses prepared by other methods. This discrepancy in the thermal properties may be due to the strong dependence on the environmental and experimental conditions for preparing the samples.^{114]} However, more precise and deep characterizations are necessary to give the exact reason for this behaviour.

Table 4.12: Thermal diffusivity (TD) values of the Nd doped sol gel glasses sintered at 700 °C for various weight percentages using photoacoustics with DPSS laser as source of excitation.

Sintering temperature →	700 °C	
Sample ↓	Thickness* (×10 ⁻⁴ m)	TD×10 ⁻³ (m ² s ⁻¹)
0.1 Nd	7.53	3.40
0.5 Nd	10.91	6.71
1.0 Nd	11.75	11.40
1.5 Nd	10.91	6.43
2.0 Nd	8.04	4.72

*The sample thickness has an accuracy of 0.01×10⁻⁴ m.

Table 4.13: Thermal conductivity values of 2.0% rare earth (RE) doped and pure sol gel glasses sintered at 700 °C using photoacoustics.

Sample	Thermal conductivity (Wm ⁻¹ K ⁻¹)
2.0 Y	14.29
2.0 La	11.34
2.0 Nd	17.96
2.0 Tb	3.55
2.0 Dy	8.63
2.0 Er	15.22
2.0 Yb	2.79
silica	51.78

4.5.4. Conclusions:

The TD and TE values of some of the RE doped sol gel silica samples sintered at different temperatures are obtained using PA method. The TD values of the samples obtained by various geometries are almost equal. All these values are higher than the previously reported ones. This is attributed to the preparation conditions and procedures though the exact reason for this needs further characterizations. Moreover, the proper glass transition temperature of the sol gel materials is about 900 °C.^[92] Here the present samples may be in a state in between the xerogel and pure glass.

4.6. Summary:

Sol gel method provides a low temperature route to glass preparation. RE doped glasses with various weight percentages are prepared and sintered at different temperatures. These glasses show blue luminescence under UV irradiation which is attributed to the silica matrix. The higher TD and TE values of these glasses may be due to the changes in the preparation procedures and conditions, which require further characterization.

4.7. References:

- [1] William J Miniscalco (2001). 'Optical and electronic properties of rare earth ions in glasses'; in: "Rare earth doped fiber lasers and amplifiers". Michel J F Dignonnet (Ed). 2nd ed. Marcel Dekker, Inc. New York, USA. Chapter 2.
- [2] Paras N Prasad (2003) 'Introduction to biophotonics'. J Wiley & Sons, Hoboken, NJ, 622pp.
- [3] François Auzel (2004). 'Upconversion and Anti-Stokes Processes with f and d Ions in Solids'. *Chem. Rev.*; **104** (1), p 139-174. doi: 10.1021/cr020357g
- [4] A Elizebeth, V Thomas, G Jose, G Jose, N V Unnikrishnan, C Joseph and M A Ittyachen (2004). 'Studies on the growth and optical characterization of dysprosium gadolinium oxalate single crystals'. *Cryst. Res. Technol.*; **39** (2), p 105-110. doi: 10.1002/crat.200310156
- [5] H. J. Zhang, L. S. Fu, S. B. Wang, Q. G. Meng, K. Y. Yang and J. Z. Ni (1999). 'Luminescence characteristics of europium and terbium complexes with 1,10-phenanthroline in-situ synthesized in a silica matrix by a two-step sol-gel process'. *Mater. Lett.*; **38** (4), p 260-264. doi:10.1016/S0167-577X(98)00169-4
- [6] M J Dejneka (1998). 'Transparent oxyfluoride glass ceramics'. *MRS Bull.*; **23** (11), p 57-62.
- [7] Artur da Silva Gouveia-Neto (2007). 'Light emission properties of lanthanide doped novel optical glasses for application in photonic devices'; in: "New research on optical materials". p 185-216. Sherman J. Litchitika (Ed.). Nova Science Publishers, Inc. New York. 255pp.
- [8] P Babu and C K Jayasankar (2000). 'Spectroscopic properties of Dy³⁺ ions in lithium borate and lithium fluoroborate glasses'. *Opt.Mater.* **15**(1), p65-79. doi:10.1016/S0925-3467(00)00015-X
- [9] Jean-Luc Adam, Jacques Lucas and Shilin Jiang (1997). 'Recent developments on rare-earth-doped glasses' in: "Rare-Earth-Doped Devices". Seppo Honkanen (Ed.). *Proc. SPIE*: Vol. **2996**, p 8-19. doi:10.1117/12.271163 URL: <http://dx.doi.org/10.1117/12.271163>
- [10] M.J. Weber (1990). 'Science and technology of laser glass'. *J. Non-Cryst. Solids*; **123** (1-3), p 208-222. doi:10.1016/0022-3093(90)90786-L

- [11] Xiuhong Han, Guozhong Cao, Tom Pratum, Daniel T. Schwartz and Barry Lutz (2001). 'Synthesis and properties of Er³⁺-doped silica glass by sol-gel processing with organic complexation'. *J. Mater. Sci.*; **36** (4), p 985–993. doi:10.1023/A:1004836225856
- [12] A. G. Souza Filho, P. T. C. Freire, I. Guedes, F. E. A. Melo, J. Mendes Filho, M. C. C. Custódio, R. Lebullenger and A. C. Hernandez (2000). 'High-pressure dependence of Sm³⁺ emission in PbO–PbF₂–B₂O₃ glasses'. *J. Mater. Sci. Lett.*; **19** (2), p 135–137. doi: 10.1023/A:1006655632032
- [13] Masayuki Yamane and Yoshiyuki Asahara (2000). 'Glasses for photonics'. Cambridge University Press, Cambridge, UK. 271pp.
- [14] C Jeffrey Brinker and George W Scherer (1990). 'Sol-gel science: The physics and chemistry of sol-gel processing'. Academic Press: London, 908 pp.
- [15] Sumio Sakka (1992). 'Current status of the preparation of optical solids by the sol-gel method'; in: "Sol-Gel Optics II". John D. Mackenzie (Ed.). *Proc. SPIE*; Vol. **1758**, p 2–13. doi:10.1117/12.131995 URL: <http://dx.doi.org/10.1117/12.131995>
- [16] A Patra, D Kundu and D Ganguli (1997) 'A study of the structural evolution of the sol-gel derived Sm³⁺-doped silica glass'. *Mater. Lett.* **32**(1), p43–47. doi:10.1016/S0167-577X(97)00005-0
- [17] Vinoy Thomas (2002). 'Spectroscopic Studies of Certain doped Melt and Sol-gel Glasses'. Ph. D Thesis, Mahatma Gandhi University, Kottayam. and the references therein
- [18] Natalia I. Koslova, Bruno Viana and Clément Sanchez (1993). 'Rare-earth-doped hybrid siloxane–oxide coatings with luminescent properties'. *J. Mater.Chem.*; **3** (1), p 111–112. doi: 10.1039/JM9930300111
- [19] Ian M Thomas, Stephen A Payne and Gary D Wilke (1992). 'Optical properties and laser demonstrations of Nd-doped sol-gel silica glasses'. *J. Non-Cryst.Solids.*; **151** (3), p 183–194. doi:10.1016/0022-3093(92)90028-1
- [20] William V. Moreshead, Jean-Luc R. Noguès and Robert H. Krabill (1990). 'Preparation, processing, and fluorescence characteristics of neodymium-doped silica glass prepared by the sol-gel process'. *J. Non-Cryst. Solids*; **121** (1–3), p 267–272. doi:10.1016/0022-3093(90)90142-9
- [21] Lang-Luen Lee and Dah-Shyang Tsai (1994). 'Ion clustering and crystallization of sol-gel-derived erbium silicate glass'. *J. Mater. Sci. Lett.* **13** (8), p 615–617. doi:10.1007/BF00592626
- [22] P. C. Hess (1991). 'The role of high field strength cations in silicate melts'; in: "Physical Chemistry of Magmas, Advances in Physical Geochemistry". Vol 9, p. 152–191. L. L. Perchuk and I. Kushireo (Eds.). Springer, New York. 341pp
- [23] Vincent McGahay and Minoru Tomozawa (1993). 'Phase separation in rare-earth-doped SiO₂ glasses'. *J. Non-Cryst. Solids*; **159** (3), p 246–252. doi:10.1016/0022-3093(93)90230-U
- [24] J. Wang, W. S. Brocklesby, J. R. Lincoln, J. E. Townsend and D. N. Payne (1993). 'Local structures of rare-earth ions in glasses: the 'crystal-chemistry' approach'. *J. Non-Cryst. Solids*; **163** (3), p 261–267. doi:10.1016/0022-3093(93)91303-K
- [25] H. Dislich (1971). 'Preparation of multicomponent glasses without fluid melts'. *Glastech. Ber.* **44** (1), p 1–8.
- [26] N. N. Khimich, G. M. Berdichevskii, E. N. Poddenezhnyi, V. V. Golubkov, A. A. Boiko, V. M. Ken'ko, O. B. Evreinov and L.A. Koptelova (2007). 'Sol–Gel Synthesis of an Optical Silica Glass Doped with Rare-Earth Elements'. *Glass Phys. Chem.*: (original in Russian *Fizika i Khimiya Stekla*). **33** (2), p 152–155. doi: 10.1134/S1087659607020095
- [27] J. Sahu, A. Biswas and H. N. Acharya (1995). 'Effect of neodymium oxide dopant on the structure of alkoxide gel'. *Mater. Lett.*: **24** (1–3), p 31–34. doi:10.1016/0167-577X(95)00083-6
- [28] Carlos P Ortiz (2007). 'Spectroscopy of terbium doped sol-gel glasses'. Davidson College. URL: http://www.phy.davidson.edu/honors_theses/COrtiz.2007.thesis.pdf

- [29] Dipankar Mandal, H D Banerjee, M L N Goswami and H N Acharya (2004). 'Synthesis of Er³⁺ and Er³⁺: Yb₃₊ doped sol-gel derived silica glass and studies on their optical properties'. *Bull. Mater. Sci.*; **27** (4), p 367-372. doi:10.1007/BF02704774
- [30] Vilma C. Costa, Michael J. Lochhead and Kevin L. Bray (1996). 'Fluorescence Line-Narrowing Study of Eu³⁺-Doped Sol-Gel Silica: Effect of Modifying Cations on the Clustering of Eu³⁺'. *Chem. Mater.*; **8** (3), p 783-790. doi: 10.1021/cm9504910
- [31] Takeshi Fujiyama, Makoto Hori and Minoru Sasaki (1990). 'Preparation of Nd-doped silica glasses by the sol-gel method'. *J. Non-Cryst. Solids*; **121** (1-3), p 273- 278. doi:10.1016/0022-3093(90)90143-A
- [32] S. S. Wang, Y. Zhou, Y. L. Lam, C. H. Kam, Y. C. Chan and X. Yao (1997). 'Fabrication and characterisation of neodymium-doped silica glass by sol-gel process'. *Mat Res Innovat.*; **1** (2), p 92-96. doi: 10.1007/s100190050026
- [33] A J Berry and T A King (1989). 'Characterisation of doped sol-gel derived silica hosts for use in tunable glass lasers'. *J. Phys. D: Appl. Phys.*; **22** (10), p 1419-1422. doi: 10.1088/0022-3727/22/10/001
- [34] Phalippou J, Woigneur T and Zarzycki J (1984). 'Behavior of Monolithic Silica Aerogels at Temperatures Above 1000° C'; in: "Ultrastructure processing of ceramics, glasses and composites". Chapter 7, p 70- 87. L Larry Hench and D Ronald Ulrich (Eds.). Wiley Interscience, New York. 582pp.
- [35] Long Zhang and Hefang Hu (2002). 'The effect of OH⁻ on IR emission of Nd³⁺, Yb³⁺ and Er³⁺ doped tetraphosphate glasses'. *J. Phys. Chem. Solids*; **63** (4), p 575-579. doi:10.1016/S0022-3697(01)00196-2
- [36] S E Stokowski (1985). *CRC Handbook of laser science and technology. Vol.1 . Lasers and masers.* Marvin J Weber (Ed.). CRC Press Inc., Boca Raton FL. p 215.
- [37] J Livage (1999). 'Sol gel synthesis of hybrid materials'. *Bull. Mater. Sci.*; **22**(3), p201-205. doi: 10.1007/BF02749920
- [38] Ivan Fanderlik (Ed.) (1991). 'Silica glass and its application'. *Glass science and technology*; vol. **11**, p 15. Elsevier, Amsterdam. 304pp.
- [39] G H Sigel Jr. (1977). 'Optical Absorption of Glasses'; in: " Glass I: Interaction with electromagnetic radiation". *Treatise on materials science and technology*; Vol **12**. p 5-89. Minoru Tomozawa and Robert H. Doremus (Ed.). Academic Press, New York. 349pp.
- [40] Hench L. L and Wang S. H (1990). 'The sol-gel glass transformation of silica'. *Phase Transitions*; **24** (2), p 785 -834. doi: 10.1080/01411599008210251
URL: <http://dx.doi.org/10.1080/01411599008210251>
- [41] M. Schmidt, G. Boettger, M. Eich, W. Morgenroth, U. Huebner, R. Boucher, H. G. Meyer, D. Konjhdzic, H. Bretinger, and F. Marlow (2004). 'Ultralow refractive index substrates—a base for photonic crystal slab waveguides'. *Appl. Phys. Lett.*; **85** (1), p 16-18. doi:10.1063/1.1767962 URL: <http://link.aip.org/link/?APPLAB/85/16/1>
- [42] Frank Marlow, Denan Konjhdzic, Helmut Bretinger and Hongliang Li (2006). 'Sol gel approaches to photonic crystal systems' in: "Advances in Solid State Physics". Vol **45**. p 149-161. Bernhard Kramer (Ed.). Springer Verlag, Berlin Heidelberg, Germany. 425pp. doi:10.1007/11423256_12
- [43] Judith E G J Wijnhoven and Willem L Vos (1998). 'Preparation of photonic crystals made of air spheres in titania'. *Science*; **281** (5378), p 802-804. doi:10.1126/science.281.5378.802
- [44] Thomas F. Krauss, Richard M. De La Rue and Stuart Brand (1996). 'Two-dimensional photonic-bandgap structures operating at near-infrared wavelengths'. *Nature*; **383** (6602), p 699-702. doi:10.1038/383699a0
- [45] V. K. Tikhomirov, A. B. Seddon, D. Furniss and M. Ferrari (2003). 'Intrinsic defects and glass stability in Er³⁺ doped TeO₂ glasses and the implications for Er³⁺-doped tellurite fiber amplifiers'. *J. Non-Cryst. Solids*; **326-327**, p 296-300. doi:10.1016/S0022-3093(03)00415-0

- [46] Donald R. Ulrich (1988). 'Prospects of sol-gel processes'. *J. Non-Cryst Solids*; **100 (1-3)**, p 174-193. doi:10.1016/0022-3093(88)90015-4
- [47] Lisa C Klein (1994). 'Sol gel optics: Processing and applications'. Springer. 605pp.
- [48] A J Kenyon (2002). 'Recent developments in rare-earth doped materials for optoelectronics'. *Prog. Quantum Electron.*; **26 (4-5)**, p 225-284. doi:10.1016/S0079-6727(02)00014-9
- [49] Vinoy Thomas, Gijo Jose, Gin Jose, P. R. Biju, S. Rajagopal and N. V. Unnikrishnan (2005). 'Structural Evolution and Fluorescence Properties of Dy³⁺: Silica Matrix'. *Journal of Sol-Gel Science and Technology*; **33 (3)**, p 269-274. doi: 10.1007/s10971-005-6376-9
- [50] Masumi Ito, Tatsuhiko Saitoh and Hiroshi Yokota (1996). 'Method for producing rare earth element-doped glass by sol-gel process'. European Patent EP0433643. URL: <http://www.freepatentsonline.com/EP0433643B1.html>
- [51] Shuyuan Liu and Larry L. Hench (1992). 'Control of the texture of gel-silica monoliths by aging treatments'; in "Sol-Gel Optics II". John D. Mackenzie (Ed.). *Proc. SPIE*; Vol. **1758**, p 14-25. doi:10.1117/12.131996 URL: <http://dx.doi.org/10.1117/12.131996>
- [52] Gin Jose (2001). 'Spectroscopic investigations of rare earth doped glasses and sol-gel thin films'. PhD. Thesis. M G University, Kottayam, Kerala. 131pp.
- [53] Renata Reisfeld and Christian K Jørgensen (1987). 'Excited state phenomena in vitreous materials'; in "Handbook on the physics and chemistry of rare earth". Vol **9**. Chapter 58. Karl A Gschneidner Jr. and LeRoy Eyring (Ed.). North Holland, Amsterdam. p 1-90.
- [54] Renata Reisfeld (1975). 'Radiative and non-radiative transitions of rare-earth ions in glasses' *Structure & Bonding*; **22**, p 123-175. doi: 10.1007/BFb0116557
- [55] Robert D. Peacock (1975). 'The intensities of lanthanide $f \leftrightarrow f$ transitions'; in "Rare Earths". *Structure & Bonding*; **22**, p 83-122. doi: 10.1007/BFb0116556
- [56] Renata Reisfeld and Christian Klixbüll Jørgensen (1977). 'Lasers and excited states of rare earths'. Springer Verlag, Berlin. 226pp.
- [57] Gerhard Heinrich Dieke (1968). 'Spectra and energy levels of rare earth ions in crystals'. H M Crosswhite and Hannah Crosswhite (Eds.). Interscience Publishers, John Wiley & Sons New York, USA. 401pp.
- [58] Alexander Aleksandrovich Kaminskii (1990). 'Laser Crystals: Their Physics and Properties'. Springer Verlag, Berlin. 446pp.
- [59] J García Solé, L E Bausá and D Jaque (2005). 'An introduction to the optical spectroscopy of inorganic solids'. John Wiley & Sons, Ltd. New Delhi, India. 283pp.
- [60] D. Avnir and V. R. Kaufman (1987). 'Alcohol is an unnecessary additive in the silicon alkoxide sol-gel process'. *J. Non-Cryst. Solids.*; **92 (1)**, p 180-182. doi:10.1016/S0022-3093(87)80368-X
- [61] G. F. Neilson and M. C. Weinberg (1984). 'Crystallization of Na₂O---SiO₂ gel and glass'. *J. Non-Cryst. Solids*; **63 (3)**, p 365-374. doi:10.1016/0022-3093(84)90104-2
- [62] M. C. Weinberg (1986). In: "Better Ceramics Through Chemistry, II" C. Jeffrey Brinker (Ed.). Symposium Held April 15-19, 1986 Palo Alto, California, U.S.A. (Materials Research Society Symposium Proceedings). North Holland, New York, p 431.
- [63] D. R. Uhlmann, M. C. Weinberg and G. Teowee (1988). 'Crystallization of gel-derived glasses'. *J. Non-Cryst. Solids*; **100 (1-3)**, p 154-161. doi:10.1016/0022-3093(88)90012-9
- [64] M. Sales and J. Alarcón (1994). 'Crystallization of sol-gel-derived glass ceramic powders in the CaO-MgO-Al₂O₃-SiO₂ system'. *J. Mater. Sci.*; **29 (19)**, p 5153-5157. doi: 10.1007/BF01151110
- [65] E. L. DeKALB and V. A. FASSEL (1979). 'Optical atomic emission and absorption methods'; in "Handbook on the physics and chemistry of rare earth". Vol **4**. Chapter 37D. p 405- 440. Karl A Gschneidner Jr. and LeRoy Eyring (Ed.). North Holland, Amsterdam.

- [66] Yoh Mita, Masahiro Togashi and Hajime Yamamoto (2000). 'Energy transfer processes in rare-earth-ion-doped materials'. *J. Lumin.*; **87–89**, p 1026- 1028. doi:10.1016/S0022-2313(99)00518-9
- [67] K Itoh, N Kamata, T Shimazu, C Satoh, K Tonooka and K Yamada (2000). 'An improved emission characteristics of Tb³⁺-doped sol-gel glasses by utilizing high solubility of terbium nitrate'. *J. Lumin.*; **87–89**, p 676- 678. doi:10.1016/S0022-2313(99)00354-3
- [68] G. H. Dieke and H. M. Crosswhite (1963). 'The spectra of the doubly and triply ionized rare earths'. *Appl. Opt.*; **2 (7)**, p 675-686. doi:10.1364/AO.2.000675
URL: <http://www.opticsinfobase.org/ao/abstract.cfm?URI=ao-2-7-675>
- [69] G. O. Karapetyan and S. G. Lunter (1966). 'The luminescence of glasses activated with terbium'. *J. Appl. Spectroscopy.*; **5 (3)**, p 232-236. doi: 10.1007/BF00605833
- [70] M. N. Muralidharan, C. A. Rasmitha and R. Ratheesh (2009). 'Photoluminescence and FTIR studies of pure and rare earth doped silica xerogels and aerogels'. *J Porous Mater.*; **16 (6)**, p 635-640. doi: 10.1007/s10934-008-9243-6
- [71] Michael R. Ayers and Arlon J. Hunt (1997). 'Visibly photoluminescent silica aerogels'. *J. Non-Cryst. Solids.*; **217 (2-3)**, p 229-235. doi:10.1016/S0022-3093(97)00126-9
- [72] Yinhua Han, Jun Lin and Hongjie Zhang (2002). 'Photoluminescence of organic-inorganic hybrid SiO₂ xerogels'. *Mater. Lett.*; **54 (5-6)**, p 389-396. doi:10.1016/S0167-577X(01)00599-7
- [73] J. M. García, M. A. Mondragón, C. S. Téllez, A. Campero and V. M. Castaño (1995). 'Blue emission in tetraethoxysilane and silica gels'. *Mater. Chem. Phys.*; **41 (1)**, p 15-17. doi:10.1016/0254-0584(95)01498-5
- [74] William M. Yen, Shigeo Shionoya and Hajime Yamamoto (2007). 'Phosphor handbook'. CRC Press. 2nd edition. 1051pp.
- [75] Raffie H. Abu-Eittah, Sayed A. Marie and Marbrouka B. Salem (2004). 'The electronic absorption spectra of Lanthanum (III) Cerium (III) and Thorium (IV) ions in different solvents'. *Can. J. Anal. Sci. Spectrosc.*; **49 (4)**, p 248-257. URL: <http://www.cjass.ca/v49n4p248.pdf>
- [76] M. M. Broer, D. M. Krol, and D. J. DiGiovanni (1993). 'Highly nonlinear near-resonant photodarkening in a thulium-doped aluminosilicate glass fiber'. *Opt. Lett.*; **18 (10)**, p 799-801. doi:10.1364/OL.18.000799 URL: <http://www.opticsinfobase.org/ol/abstract.cfm?URI=ol-18-10-799>
- [77] Yasutaka Suemune (1983). 'Effects of Rare Earth Impurities on Photochromic Characteristics of Rare Earth Orthoniobates'. *Jpn. J. Appl. Phys.*; **22 (11)**, part 1, p 1669-1674. doi: 10.1143/JJAP.22.1669 URL: <http://jjap.ipap.jp/link?JJAP/22/1669/>
- [78] S. Lizzo, A. Meijerink and G. Blasse (1994). 'Luminescence of divalent ytterbium in alkaline earth sulphates'. *J. Lumin.*; **59 (3)**, p 185-194. doi:10.1016/0022-2313(94)90040-X
- [79] P. Dorenbos (2005). 'Valence Stability of Lanthanide Ions in Inorganic Compounds'. *Chem. Mater.*, **17 (25)**, p 6452–6456. doi: 10.1021/cm051456o
- [80] Eugene Loh (1968). '4fⁿ→4fⁿ⁻¹5d spectra of rare-earth ions in crystals'. *Phys. Rev.*; **175 (2)**, p 533- 536. URL:<http://link.aps.org/doi/10.1103/PhysRev.175.533>
doi:10.1103/PhysRev.175.533
- [81] M. Engholm, L. Norin and D. Åberg (2007). 'Strong UV absorption and visible luminescence in ytterbium-doped aluminosilicate glass under UV excitation'. *Opt. Lett.*; **32 (22)**, p 3352-3354. URL:<http://www.opticsinfobase.org/ol/abstract.cfm?URI=ol-32-22-3352>
doi:10.1364/OL.32.003352
- [82] Yu-Chun Li, Yen-Hwei Chang, Yee-Shin Chang, Yi-Jing Lin and Chih-Hao Laing (2007). 'Luminescence and Energy Transfer Properties of Gd³⁺ and Tb³⁺ in LaAlGe₂O₇'. *J.Phys. Chem. C.*; **111 (28)**, p 10682 –10688. doi: 10.1021/jp0719107
- [83] I. Hernández, G. Córdoba, J. Padilla, J. Méndez-Vivar and R. Arroyo (2008). 'Photoluminescence properties of silica monoliths codoped with terbium and germanium'. *Mater. Lett.*; **62 (12-13)**, p 1945-1948. doi:10.1016/j.matlet.2007.10.047

- [84a] G. Wakefield, H. A. Keron, P. J. Dobson and J. L. Hutchison (1999). 'Structural and optical properties of terbium oxide nanoparticles'. *J. Phys. Chem. Solids.*; **60** (4), p 503-508. doi:10.1016/S0022-3697(98)00307-2
- [84b] Hong-Mei Yang, Jian-Xin Shi, Hong-Bin Liang and Meng-Lian Gong (2006). 'A novel green emitting phosphor $\text{Ca}_2\text{GeO}_4:\text{Tb}^{3+}$ '. *Mater. Res. Bull.*; **41** (4), p 867-872. doi:10.1016/j.materresbull.2005.09.026
- [84c] Fei Zhao, Peimin Guo, Guobao Li, Fuhui Liao, Shujian Tian and Xiping Jing (2003). 'Luminescent properties of Eu^{3+} , Tb^{3+} or Bi^{3+} activated yttrium germanates'. *ibid.* **38** (6), p 931-940. doi:10.1016/S0025-5408(03)00086-2
- [85a] M. Flores, U. Caldiño and R. Arroyo (2006). 'Luminescence properties of terbium doped poly(acrylic acid) containing 1,10-phenanthroline and 2,2-bipyridine'. *Opt. Mater.*; **28** (5), p 514-518. doi:10.1016/j.optmat.2005.03.013
- [85b] M. E. Villafuerte-Castrejon, M. E. Alvarez, U. Caldiño and Julio Gonzolo (2001). 'Emission spectra of $\text{Cs}_2\text{KTbCl}_6$ and $\text{Cs}_2\text{KEuCl}_6$, and $\text{Tb}^{3+} \rightarrow \text{Eu}^{3+}$ non-radiative energy transfer in $\text{Cs}_2\text{KTb}_{0.9}\text{Eu}_{0.1}\text{Cl}_6$ '. *Ferroelectr. Lett.*; **28** (3&4), p 103-113. doi: 10.1080/07315170108202954 URL: <http://dx.doi.org/10.1080/07315170108202954>
- [86] S. S. Wang, Y. Zhou, Y.L. Lam, C.H. Kam, Y.C. Chan and X. Yao (1997). 'Fabrication and characterisation of neodymium-doped silica glass by sol-gel process'. *Mat. Res. Innovat.*; **1** (2), p 92-96. doi: 10.1007/s100190050026
- [87] P. V. Jyothy, K. A. Amrutha, Joseph Xavier and N. V. Unnikrishnan (2009). 'Fluorescence characteristics of $\text{Dy}^{3+}/\text{CdS}$ nanocrystals doped silica xerogel'. *J. Phys. Chem. Solids*; **70** (6), p 927-930. doi:10.1016/j.jpics.2009.04.017
- [88] Frank Träger (Ed.) (2007). 'Springer handbook of lasers and optics'. Springer, NY. 1332pp
- [89] T. López, M. Picquart, G. Aguirre, G. Arriola, Y. Freile, D. H. Aguilar, P. Quintana and J. J. Alvarado-Gil and F. M. Vargas-Luna. 'Thermal characterization of agar encapsulated in TiO_2 sol-gel'. URL: <http://symp15.nist.gov/pdf/p195.pdf>
- [90] N. Tohge, G. S. Moore and J. D. Mackenzie (1984). 'Structural developments during the gel to glass transition'. *J. Non-Cryst. Solids.*; **63** (1-2), p 95-103. doi:10.1016/0022-3093(84)90389-2
- [91] T. Kawaguchi, J. Iura, N. Taneda, H. Hishikura and Y. Kokubu (1986). 'Structural changes of monolithic silica gel during the gel-to-glass transition'. *J. Non-Cryst. Solids.*; **82** (1-3), p 50-56. doi:10.1016/0022-3093(86)90110-9
- [92] Masayuki Yamane, Shinji Aso, Seitarō Okano and Teruo Sakaino (1979). 'Low temperature synthesis of a monolithic silica glass by the pyrolysis of a silica gel'. *J. Mater. Sci.*; **14** (3), p 607-611. doi: 10.1007/BF00772720
- [93a] S. Chakrabarti, J. Sahu, M. Chakraborty and H. N. Acharya (1994). 'Monophasic silica glasses with large neodymia concentration'. *J. Non-Cryst. Solids*; **180** (1), p 96-101. doi:10.1016/0022-3093(94)90403-0
- [93b] J. Sahu, A. Biswas and H. N. Acharya (1996). 'Photoluminescence study of Nd-doped sol-gel silica glasses'. *Mater. Lett.*; **28** (4-6), p 347-351. doi:10.1016/0167-577X(96)00078-X
- [94] Shyama P. Mukherjee (1984). 'Homogeneity of gels and gel-derived glasses'. *J. Non-Cryst. Solids*; **63** (1-2), p 35-43. doi:10.1016/0022-3093(84)90384-3
- [95a] Nibu A. George, C. P. G. Vallabhan, V. P. N. Nampoori, A. K. George and Periasamy Radhakrishnan (2001). 'Open-cell photoacoustic investigation of the thermal effusivity of liquid crystals'. *Opt. Eng.*; **40** (07), p 1343-1347. doi: 10.1117/12.427305
- [95b] Annieta Philip K. Lyjo K. Joseph, Litty M. Irimpan, Bindu Krishnan, P. Radhakrishnan, V. P. N. Nampoori and Raghu Natarajan (2007). 'Thermal characterization of ceramic tapes using photoacoustic effect'. *phys. stat. sol. (a)*; **204** (3), p 737-744. doi: 10.1002/pssa.200622287 URL: <http://dx.doi.org/10.1002/pssa.200622287>
- [96] Brandon T. Stone and Kevin L. Bray (1996). 'Fluorescence properties of Er^{3+} -doped sol-gel glasses'. *J. Non-Cryst. Solids*; **197** (2-3), p 136-144. doi:10.1016/0022-3093(95)00514-5

- [97] D. C. Winburn (1989). 'Practical Laser Safety'. 2nd edition. Marcel Dekker, NY. 256pp.
- [98] T. Miya, Y. Terunuma, T. Hosaka and T. Miyashita (1979). 'Ultimate low-loss single-mode fibre at 1.55 μm '. *Electron. Lett.*; **15** (4), p 106–108. doi:10.1049/el:19790077 URL: <http://dx.doi.org/10.1049/el:19790077>
- [99] B. James Ainslie (1991). 'A review of the fabrication and properties of erbium-doped fibers for optical amplifiers'. *J. Lightwave Tech.*; **9** (2), p 220-227. doi: 10.1109/50.65880
- [100] J. L. Jackel, A. Yi-Yan, E. M. Vogel, A. Von Lehmen, J. J. Johnson and E. Snitzer (1992). 'Guided blue and green upconversion fluorescence in an erbium-ytterbium-containing silicate glass'. *Appl. Opt.*; **31** (18), p 3390-3392. doi:10.1364/AO.31.003390 URL:<http://www.opticsinfobase.org/ao/abstract.cfm?URI=ao-31-18-3390>
- [101] Nobuyuki Kagi, Aura Oyobe and Kazunori Nakamura (1990). 'Efficient optical amplifier using a low-concentration erbium-doped fiber'. *IEEE Photo. Technol. Lett.*; **2** (8), p 559-561. doi: 10.1109/68.58048
- [102] L F Perondi and L C M Miranda (1987). 'Minimal volume photoacoustic cell measurement of thermal diffusivity: Effect of the thermoelastic sample bending'. *J. Appl. Phys.*; **62** (7), p 2955- 2959. URL: <http://link.aip.org/link/?JAPIAU/62/2955/1> doi:10.1063/1.339380
- [103] Noor Jawad Ridha, W. Mahmood Mat Yunus, S.A. Halim, Z.A. Talib, Firas K. Mohamad Al-Asfoor and Walter C. Primus (2009). 'Effect of Sr Substitution on Structure and Thermal Diffusivity of Ba_{1-x}Sr_xTiO₃ Ceramic'. *Am. J. Engg. & Applied Sci.*; **2** (4), p 661-664. URL: <http://www.scipub.org/fulltext/ajeas/ajeas24661-664.pdf>
- [104] M Haydari, M M Moksini, A E Abdelrahman, M Deraman, W M M Yunus and I V Grozescu (2008). 'Thermal Diffusivity of Carbon Pellets (CPs) Treated with KOH'. *Am. J. Applied Sci.*; **5** (2), p 165-168. URL: <http://scipub.org/fulltext/ajas/ajas52165-168.pdf> and the references therein
- [105] Clark's tables, Science data book (1992). Oliver & Boyd, Edinburgh. 105pp

Conclusions and future prospects in a nutshell

This chapter summarises the general conclusions and findings of the present work. Non-destructive photothermal methods as well as optical absorption and fluorescence spectroscopy are utilised to characterise three different materials, both thermally and optically. The possibility of using montmorillonite clay minerals, after textile wastewater treatment, is investigated for further applications. The laser induced luminescence studies and thermal characterization of certain rare earth titanates, prepared by self propagating high temperature synthesis method, are also presented. Moreover, effort is made to characterise rare earth doped sol gel silica glasses with the help of these non-destructive techniques. An outline of the works, which can be carried out in future, is also presented.

5.1. Major findings:

- The presence of dye in the montmorillonites changes their thermal diffusivity values depending on the concentration of the dye adsorbed.
 - The sample in which the dye is repeatedly adsorbed has less thermal diffusivity value than the sample that has adsorbed once.
 - The sintered methylene blue adsorbed K-10 montmorillonite samples show a higher thermal diffusivity.
 - K-10 montmorillonite which is more acid leached than KSF shows significant thermal diffusivity changes on dye adsorption.
 - The ultrasonicated dye adsorbed sample showed a low thermal diffusivity compared to the sample prepared by the direct dye adsorption from solution
 - Dye intercalation in montmorillonites affects the fluorescence at 421 nm arising from the silica matrix. A slight amount of dye in the clay network can enhance this fluorescence.
 - Acid leaching can considerably affect the fluorescence emission of montmorillonites near 421 nm.
- ¶ The presence of La^{3+} ions in the lanthanum titanate enhances the luminescence of Ti^{3+} near 610 nm.
- ¶ The lanthanum titanate, prepared by SHS method, exhibits frequency up-conversion.

Conclusions

- ¶ The approximate thermal diffusivity and thermal effusivity values of the rare earth titanates prepared by SHS method are evaluated using photothermal techniques and the possible fractal nature of the samples has been established.
- * Rare earth doped sol gel glasses also show fluorescence near 421 nm on UV excitation, which arises from the silica host.
 - * The thermal diffusivity and thermal effusivity values of rare earth doped sol gel silica glasses are obtained using photoacoustic method.
 - * The higher thermal diffusivity values of these materials indicate that the preparation procedure highly influence the properties of these materials.

5.2. Scenario for future:

5.2.1. Dye intercalated clay minerals:

Construction of hybrid clay nano-films gives the opportunity to look at clay minerals from a material scientist's point of view. Research could progress along two lines: (1) optimisation of the preparation of films towards a particular property (e.g. second harmonic light generation) or a device (e.g. sensor); (2) fundamental understanding of the film-forming process, the organisation of the molecules, and the elementary clay mineral platelets and of the stability of the films. The outcome will certainly be a better knowledge of smectites and their surface properties. This will be an advantage to clay scientists and the clay industry. This kind of research can result in new industrial applications of clay minerals with high technological value. There is also room for theoretical work to better understand the magnitude of the various interaction forces and their relative importance in the organisation of organic cations at the clay surface in the aqueous suspensions.

The formation of semiconductor nanoparticles with different layered inorganic solids is useful to construct novel layered nano-hybrid materials with controlled functions and microstructures.

Many cationic dyes and chromophores embedded in inorganic substrates are used in industry. e. g. in photography, in various materials for signal processing and memory storage media, as catalysts, as energy antennas and transducers in photochemical reactions etc. All these applications depend crucially on the optical properties of dye. Therefore, the relationship between dye aggregation and the parameters of inorganic

hosts might be very significant in the applied research and engineering of the materials.

Moreover the following works can also be taken up in future:

- ① Verification of the thermal diffusivity values of some commonly available dye intercalated clay minerals.
- ① Effect of preparation methods on clay mineral properties.
- ① Use of more fluorescent and non-fluorescent dyes for intercalation in clay minerals and hence to study the fluorescence near 421 nm.
- ① The sintering effects on the fluorescence of dye intercalated clay mineral dispersions.
- ▶ studies and photoacoustic spectroscopy of dye intercalated clay minerals.
- ① Time dependent studies to understand the dynamics of light induced processes.

5.2.2. Sol gel:

It is important to consider the industrial investment in the area of sol gel technology and seeking perspectives on future applications and markets. Future prospects for scientists in this field depend greatly on the economic prospects for the development of successful commercial products which use sol gel processes and materials to a great extent to support a thriving future research activity. Future prospects for successful new applications of sol gel technology depend on the availability of skilled researchers who are able to find solutions to outstanding obstacles to successful commercial applications and to develop innovative new high-performance materials which will in turn create new markets. To develop new functional sol gel materials, improved mechanistic understanding, a wider range of precursors and new processing methods are all desirable.

5.2.3. Rare earth doped materials:

Numerous experimental and theoretical works can be performed on rare earth doped materials due to their possible applications in the visible range of the electromagnetic spectrum. Some of the works which can be carried out based on the present experimental studies are listed below.

- ① High power laser studies of rare earth titanates prepared by SHS method.
- ① Effect of rare earth combinations on thermal and optical properties.
- ① Photoacoustic spectroscopy and frequency up-conversion studies using laser.
- ① Quantitative studies of rare earth titanate luminescence.

Conclusions

- ⊗ Thermal lens and nonlinear optical studies of rare earth doped glasses.
- ⊗ Thermal and optical properties of combination of rare earths in sol gel glasses.
- ⊗ Effect of sintering rate on glass properties.
- ⊗ Thermal and optical properties of rare earth doped polymers using non-destructive photothermal methods.